ISSN 2708-6437(Online)
2708-6429(Print)

Journal of Engineering Advancements

Editor-in-Chief:
Prof. Dr. Mohammad Mashud

Volume 01 Issue 04

Published by:
SciEn Publishing Group

Journal of Engineering Advancements
Apt. # 6 C-D, House # 191
Road # 9/A, Dhanmondi R/A
Dhaka-1209, Bangladesh
Email: jea@scienpg.com Website: www.scienpg.com/jea/

Published in: December 2020
Published by: SciEnPG

Price: Each Issue BDT 200.00 (US$ 15) **ISSN:** 2708-6437 (Online) 2708-6429 (Print)

Journal of Engineering Advancements

Volume 01, Issue 04 December 2020

CONTENTS

Original Articles

This page is intentionally left blank.

Journal of Engineering Advancements

Published by: SciEn Publishing Group

Apt. # 6 C-D, House # 191, Road # 9/A
Dhanmondi, Dhaka-1209, Bangladesh
Email Address: jea@scienpg.com

www.scienpg.com/jea/

This page is left intentionally blank

SciEn
Journal of Engineering Advancements Vol. 01(04) 2020, pp 111-115 https://doi.org/10.38032/jea.2020.04.001

Flexural Behavior of Sandwich Composite Made of JFRP Honeycomb as Core and GFRP as Skin

Md. Rakibul Islam, Md. Arifuzzaman, Asif Karim Neon, Md. Shahe Duzzaman and Md. Rafiul Islam*

Department of Mechanical Engineering, Khulna University of Engineering & Technology, Khulna-9203, BANGLADESH

Received: September 23, 2020, Revised: November 21, 2020, Accepted: November 25, 2020, Available Online: November 29, 2020

ABSTRACT

The increasing demand of lightweight, strong and sustainable materials in aerospace, automobile and marine sectors is leading towards the development of new materials and structures. The sandwich composite is one of them which is well-known for their high strength to weight ratio and the fiber based sandwich structures with cellular core show comparatively good mechanical, acoustic, thermal and energy absorption properties than metallic cellular structure. The purpose of this work is to fabricate a sandwich structure with jute fiber reinforced polymer composite (JFRP) as core and glass fiber reinforced polymer composite (GFRP) as face sheet and to investigate bending properties of the fabricated structures for varying face sheet thicknesses. Skin and core honeycomb strips of the sandwich composites were manufactured using hand layup method and steel mold was used to obtain honeycomb shape. Flexural test results show that face sheet thickness has significant effect on the flexural behavior such as peak load, flexural strength and energy absorption. The failure mechanism during bending tests were also identified which would serve as a basis for future improvement of manufactured composites. The delamination at the interface between the core and the face sheet was the first catastrophic failure during bending. The presented sandwich structures are able to carry a significant amount of load even after failure.

Keywords: Sandwich composite; JFRP; GFRP; Honeycomb; Flexural properties; Energy absorption.

1. Introduction

A sandwich composite structure is constructed by fastening two thin but resilient face sheets to a thick but lightweight core. Core materials provide high flexural stiffness with overall low density the composite material. The separation of thin face sheets with a light weight core significantly increase the second moment of area thus the flexural stiffness of the material cross section increases through a small increase in weight. Various types of cores are used in sandwich structures i.e. honeycomb, corrugated, cellular etc. By varying the core types, geometry, thickness and material it is possible to achieve a wide range of properties and anticipated performances. Now a days honeycomb sandwich structures are widely used in damping and weight sensitive structures. In automobile, marine and aerospace industries, these materials are being used extensively due to their excellent weight saving characteristics without compromising the strength [1]. In a honeycomb sandwich structure, flexural loads are carried by forming force couple by the face sheets and shear loads are carried by lightweight core materials [2]. So, the honeycomb sandwich panels are highly efficient for carrying bending loads. Under flexural loading, one laminate is subjected to compression and the other one is subjected to tension which forming a force couple as face sheets acts together [3]. Many researchers have worked to develop honeycomb core based sandwich structure using either metals or fiber reinforced polymer composites. However, the composite honeycomb performs much better than metallic honeycombs under both quasi static and dynamic condition although the cost of composite honeycomb was higher than metallic honeycombs [4]. Thomas et al. [4] studied the influence of cell wall thickness, node length, cell size and loading on the bending and crushing responses of honeycomb structure in both out-of-plane and in-plane loading conditions. They concluded that the geometrical core configuration and geometric property like cell size, cell wall thickness and node length etc. play a crucial role in administrating potential of honeycomb. Thomas et. al. [4] also found that the face sheet material and their thickness affects the energy absorption capability. Hussain et al. [5] explored the static failure behavior of wood based sandwich panels using wood-based core and face sheets made of glass fiber reinforced polymer. It was found that, the load carrying ability of sandwich structures with plywood and solid MDF cores was higher compared to sandwich structures with honeycomb cores, but honeycomb sandwich panels can carry significant amount of loads even after the failure. The hexagonal honeycomb core shape has high strength and load carrying capacity along with minimum material and space requirement [4]. Most of the cellular sandwich structures are made of metals or polymers because of the complexity of manufacturing cellular cores using fiber reinforced composite. For core material using natural fiber like jute is cheaper, eco-friendly, lower mass per unit area, bio-degradable, recyclable and offer good acoustic insulating properties as well [6]. As face sheet material glass fiber reinforced composites show good mechanical performance and water resistance properties [7], [8]. A combination of natural and synthetic fibers may provide an improved performance as a hybrid sandwich structure.

Therefore, in this paper a hybrid sandwich composite is introduced in which the natural jute fiber is used to fabricate the honeycomb core and the synthetic glass fiber reinforced epoxy as a face sheet. The manufacturing and flexural behavior of the fabricated sandwich structure is investigated in terms of peak load, bending strength, interfacial shear stress, energy absorption and failure mechanism.

*Corresponding Author Email Address: arif48@me.kuet.ac.bd Published by: SciEn Publishing Group

2. Experimental details

2.1 Constituent materials

The constituent materials used for manufacturing the sandwich composites are E-glass fiber mat, jute fiber mat, and epoxy resin with hardener. E-glass fiber mat of 0.45 mm thickness was used as reinforcement on epoxy to manufacture sandwich face sheet. Jute fiber mat of 0.85 mm thickness was used in epoxy matrix for making honeycomb core strips.

2.2 Specimen manufacturing

2.2.1 Mold making

A steel mold is modelled and manufactured in CNC machine to provide the required shape of the jute fiber reinforced epoxy composite strips for making honeycomb core. The CAD model of the mold is given in Fig. 1.

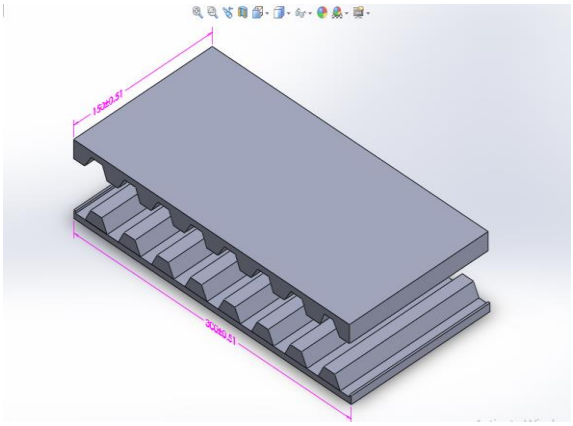

Fig. 1 CAD model of the mold with dimensions 300 mm × 150 mm

2.2.2 Face sheet making

At first, the resin and hardener was blended in a pot according to the ratio of resin to hardener (10:1) provided by the manufacturer. On top of a plastic sheet a layer of epoxy was placed first and the reinforcing glass fiber mat was laid then another layer of epoxy was poured over the mat. Then the layup has been rolled with a wooden roller in order to remove any bubbles and to ensure proper epoxy distribution. The layup was kept between two metal plates with approximately 10 kg weight of top metal plate and cured for 24 hours. Similar method was adopted to manufacture double and triple layer face sheets. Finally the manufactured face sheets were cut to the required size.

2.2.3 Core strip making

At first, the resin and hardener was mixed at 10:1 ratio given by the manufacturer. Then the jute fiber mat was wetted by the epoxy using a hand layup method. The layup was kept on top of the lower mold part and the upper part of the mold was placed. The whole setup was kept under pressure with a 10 kg load on the top plate for 24hours for curing. The desired size of the core strips was cut from the manufactured panel.

2.2.4 Sandwich preparation

The core of the sandwich structure was made by joining the core strips together using epoxy adhesive in such a way that they form hexagonal cells as shown in Fig. 2 (a). The face sheets were then attached (see Fig. 2(b)) with the core using epoxy to obtain the finished composite beams (see Fig. 2(c)). The width of the bending specimens were b = 46.5mm for all samples.

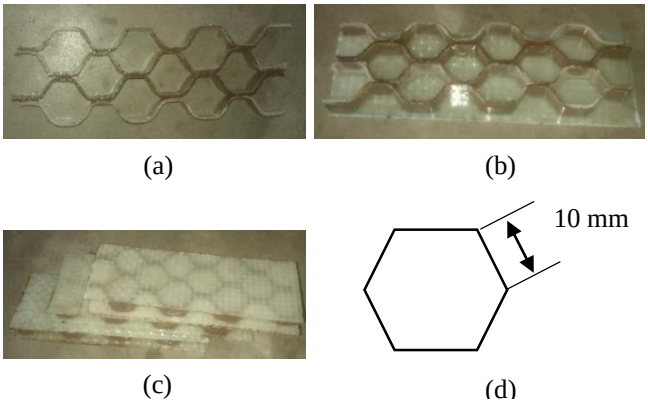

Fig. 2 (a) The hexagonal honeycomb core made using core strips; (b) the core was attached with face sheet; (c) the fabricated sandwich structure; and (d) schematic diagram of cell size.

2.3 Mechanical tests

Flexural test was conducted in the Universal Testing Machine (UTM) with digital data acquisition system for the load and the displacements at a cross head speed of approximately 5mm/min. At least three specimens for each category were tested to obtain the average values of flexural properties. International standard ASTM D790-03 [9] and ASTM C393/C393M-11 [10] were used as a guide for flexural test and the calculation of bending properties.

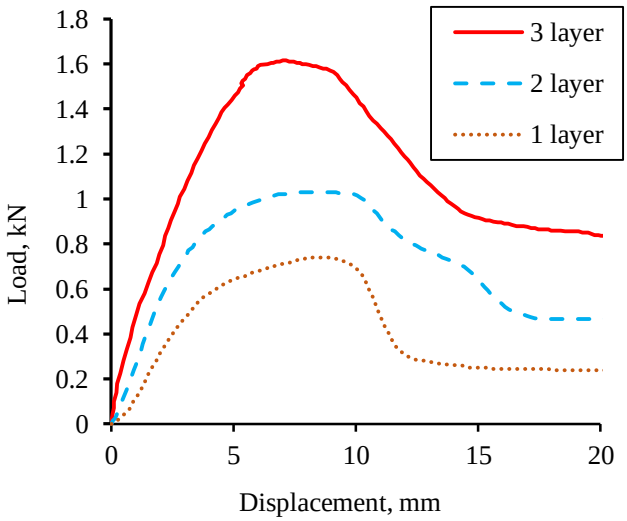

Fig. 3 Typical load – displacement curves for sandwich composite under three point bending for 1, 2 and 3 layers of glass fiber mat in the face sheet.

3. Results and discussion

3.1 Flexural properties

Typical load-displacement curves obtained from three point bend test of three different sandwich composites with different layers in the face sheet (i.e. 1, 2 and 3 layers of glass fiber mats in the face sheet) are given in Fig. 3. All curves show similar trends i.e. the load increases linearly with the displacement then

the rate of increase of load with displacement starts to decrease at some point and a pseudo-plateau region is seen. After that load starts to decrease gradually until another plateau is noticed. The failure of the composite actually starts and completes in the pseudo-plateau region. It can also be observed from Fig. 3 that the linear elastic line becomes stiffer for the higher thickness of the face sheet but the trend of the load-displacement curve remains the same.

The peak load and the bending strength with the mass of fabricated sandwich composite are plotted in Fig. 4 for three different face sheet thicknesses with standard deviations as error bar. The peak load and the bending strength both increased with increasing face sheet thickness. Sandwich structures reported in literature also revealed similar observations [11]-[12][14]. However the increase in peak load/bending strength is obtained with the cost of the weight of the composites.

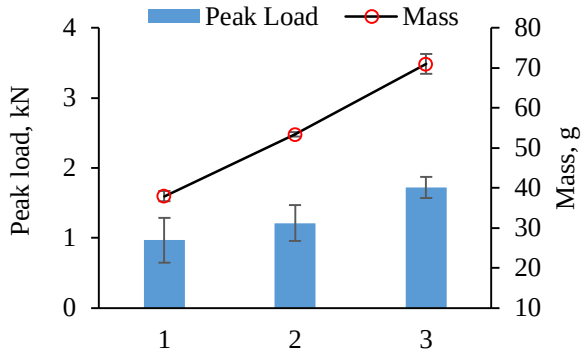

(a)

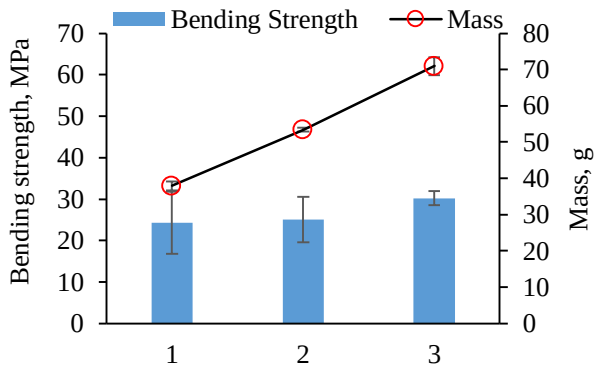

(b)

Fig. 4 (a) Peak load and (b) bending strength as a function of the number of glass fiber layers in the face sheet.

When the glass fiber layer in the face sheet was increased to two the peak load and bending strength were increased by 25.32% and 3.29% respectively but the mass of sandwich structure was increased by 40.61%. In the case of three layer glass fiber in the face sheet the peak load and bending strength was increased by 77.48% and 24.58% while the mass was increased by 86.91%. The specific strength is a key indicator for a material to be assumed as a lightweight material. The specific bending strength of the manufactured sandwich structures were found to be 639.13, 469.51 and 426.00 MPa/g for 1 layer, 2 layers and 3 layers of glass fiber in the face sheet respectively. This clearly shows that the thicker face sheet makes the sandwich structure heavier with higher bending strength.

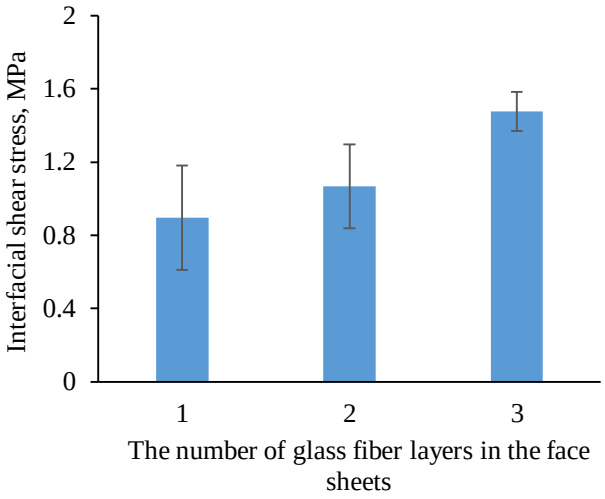

Fig. 5 Shear stress at the core/face sheet interface as a function of the number of glass fiber layers in the face sheet.

The shear stress calculated at the core/face sheet interface is given in Fig. 5 for various face sheets used in this study. It is seen that the shear stress also increased with increasing the number of glass fiber layers in the sandwich skin alike the peak load and the bending strength. The interfacial shear stress = $\frac{P}{(d+c)*b}$ where, P, d, c and b are the peak load, sandwich height, core height and beam width of the sandwich structure [10]. According to this formula, the shear stress at the interface between the skin and the core increases with the increase in peak load but decreases with the increase in sandwich height. When the number of layer was increased in the face sheet without changing the core height there is a slight increase in sandwich height but the peak load increased considerably as shown in Fig. 4 (a) and this is the reason for the increase in shear stress in the interface between the core and skin when the face sheet thickness increased. The shear stress was increased by 19.16% and 64.67% when the number of layers in the face sheet was increased to two and three respectively.

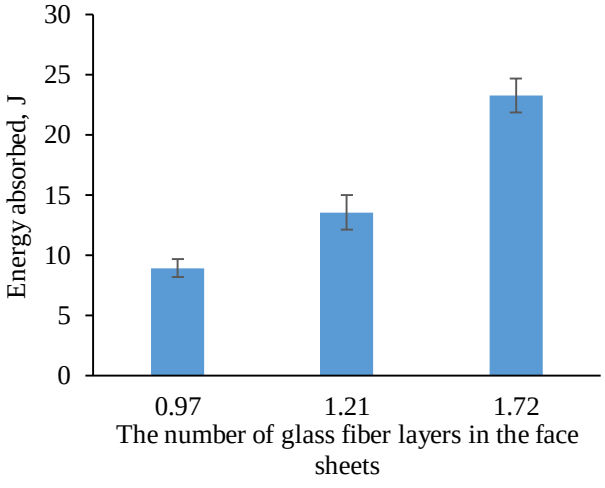

Fig. 6 Energy absorbed by the sandwich composite for a cross head displacement of 20 mm.

The energy absorbed by the sandwich structure during bending was calculated from the area under the load-displacement curve up to a cross head displacement of 20mm. The energy absorption is plotted for various face sheet thicknesses in Fig. 6. The bending energy absorption increased with increasing the face sheet thickness as expected. Since the load bearing capacity was increased with the increase in face sheet thickness, the energy absorption must increase with increasing face sheet thickness. From Fig. 3 , it is seen that the load-displacement curves are stiffer for the thicker face sheet thickness and the plateau region is also higher for thicker face sheets. Again the energy absorption is the area under the curve of load-displacement. Therefore the energy absorption must increase with the increase in face sheet thickness. The energy absorption during bending was increased by 51.84% and 160.73% when the number of glass fiber layers increased to two and three respectively. The specific energy absorption is found to be 0.23, 0.25 and 0.33 J/g for the number of glass fiber layers in face sheet 1, 2 and 3 respectively. The specific energy absorption increased with increasing face sheet thickness which indicates that the thicker face sheet provides not only higher strength but also better energy absorption. However this is not always the case as reported by Yan et. al. [14] that the density of core material plays an important role. They have found that for high density foam core the energy absorption capacity of the sandwich decreases with the increase in face sheet thickness.

3.3 Failure Mechanism

The photographs of failed specimens and the load versus displacement curves are given in Fig. 7, Fig. 8 and Fig. 9 for sandwich specimens made with a single, double and triple layers of glass fiber mats respectively. For the specimens with a single layer face sheet, it is observed that the delamination started on the top side but either left or right side of the middle load pin. The whole face sheet was not delaminated but a small portion as shown in Fig. 7 (a). The delamination continued until the load became steady again indicating a flat line. The flat line of the load versus displacement curve represents the load carrying capacity of sandwich after failure with the contribution from the lower face sheet and honeycomb core together. In the case of specimens with the double and triple layer face sheets the whole top face sheet was delaminated in one side of the middle load pin as shown in Fig. 8 (a) and Fig. 9 (a) respectively. The load carrying capacity of the sandwich after failure is also seen in the case of specimens with double and triple layer face sheets. No failure has been noticed in both face sheets for the cross head displacement studied in the case of double and triple layer face sheets. But the buckling of the delaminated top face sheet in the case of single layer face sheet specimens was noticed. The face sheet delamination is a very common type of failure for sandwich structures because of the weak bonding between the face sheet and the core. A clear difference in delamination behavior between thin and thick face sheets is seen in this study. That is the thick face sheet causes catastrophic delamination while the thin face sheet causes localized delamination.

(a)

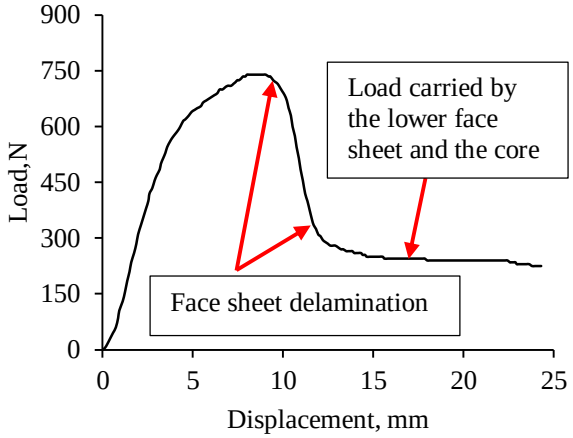

(b)

Fig. 7 A photograph of face sheet delamination and (b) a typical load - displacement curve for specimens with face sheet made of single layer of glass fiber mat.

(a)

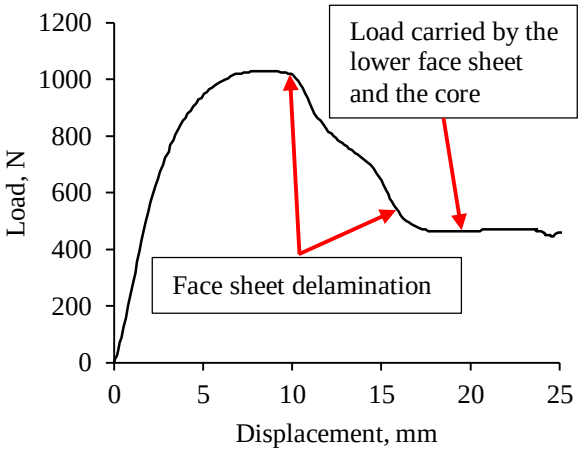

(b)

Fig. 8 (a) A photograph of face sheet delamination and (b) a typical load - displacement curve for specimens with face sheet made of double layer of glass fiber mats.

(a)

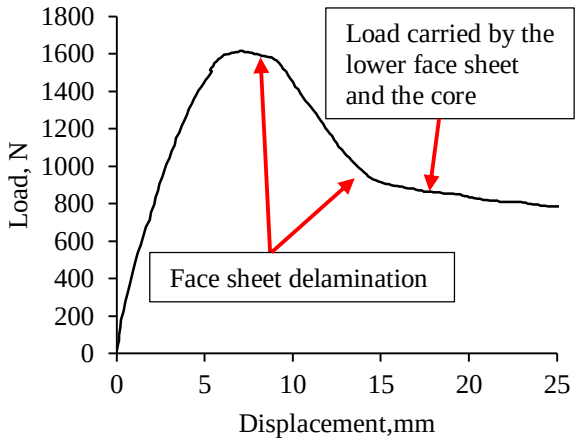

(b)

Fig. 9 A photograph of face sheet delamination and (b) a typical load - displacement curve for specimens with face sheet made of triple layer of glass fiber mats.

4. Conclusions

In this work, the sandwich composites with glass fiber/epoxy face sheet and jute fiber/epoxy honeycomb core were fabricated. Three point bending tests were conducted to investigate the bending properties and failure mechanism of the fabricated structure for various face sheet thicknesses. It was observed that face sheet thickness plays an important role on the flexural properties of the manufactured honeycomb sandwich structure. The peak load, flexural strength and core shear stress and energy absorption increased with increasing the thickness of face sheets but keeping the core height constant. All specimens showed failure due to the delamination of the upper face sheet during flexural tests and it is also observed that the fabricated sandwich structure is capable of carrying a substantial amount of load after failure. The load carrying capacity after failure is higher for thicker face sheets.

Acknowledgements

Authors acknowledge the partial funding and laboratory facilities provided for this work by Khulna University of Engineering & Technology.

References

[1] Yang, Y., Li, B., Chen, Z., Sui, N., Chen, Z., Saeed, M.U., Li, Y., Fu, R., Wu, C. and Jing, Y., 2016. Acoustic properties of glass fiber assembly-filled honeycomb sandwich panels. *Composites Part B: Engineering*, 96, pp.281-286.

[2] Nguyen, M.Q., Jacombs, S.S., Thomson, R.S., Hachenberg, D. and Scott, M.L., 2005. Simulation of impact on sandwich structures. *Composite structures*, 67(2), pp.217-227.

[3] Ali, M.X.M., 2016. Performance of Honeycomb Sandwich Structure with Natural Fibres Fabric Reinforced Facesheets (*Doctoral dissertation*, Universiti Teknologi Malaysia).

[4] Thomas, T. and Tiwari, G., 2019. Crushing behavior of honeycomb structure: a review. *International Journal of Crashworthiness*, 24(5), pp.555-579.

[5] Hussain, M., Abbas, N., Zahra, N., Sajjad, U. and Awan, M.B., 2019. Investigating the performance of GFRP/wood-based honeycomb sandwich panels for sustainable prefab building construction. *SN Applied Sciences*, 1(8), p.875.

[6] Du, Y., Yan, N. and Kortschot, M.T., 2012. Light-weight honeycomb core sandwich panels containing biofiber-reinforced thermoset polymer composite skins: Fabrication and evaluation. *Composites Part B: Engineering*, 43(7), pp.2875-2882.

[7] Wambua, P., Ivens, J. and Verpoest, I., 2003. Natural fibres: can they replace glass in fibre reinforced plastics?. *Composites science and technology*, 63(9), pp.1259-1264.

[8] Mohammed R., Ahmed A., Elgalib M. A., Ali A. H. M., Ahmed H. A., 2016. Damage Behaviors of Glass Fabric Honeycomb Sandwich Composite Materials Under Static Loading. *International Journal of Mechanical And Production Engineering*, 4(5), pp. 35-40,.

[9] ASTM D 790-03, "Standard Test Methods for Flexural Properties of Unreinforced and Reinforced Plastic and Electrical Insulating Material," PA, USA.

[10] ASTM C393/C393M-11, "Standard Test Method for Core Shear Properties of Sandwich Construction by Beam Flexure," PA, USA, 2012.

[11] Zu, G.Y., Lu, R.H., Li, X.B., Zhong, Z.Y., HAN, M.B. and YAO, G.C., 2013. Three-point bending behavior of aluminum foam sandwich with steel panel. *Transactions of Nonferrous Metals Society of China*, 23(9), pp.2491-2495.

[12] Wang, N.Z., Xiang, C.H.E.N., Ao, L.I., Li, Y.X., Zhang, H.W. and Yuan, L.I.U., 2016. Three-point bending performance of a new aluminum foam composite structure. *Transactions of Nonferrous Metals Society of China*, 26(2), pp.359-368.

[13] Zu, G., Song, B., Zhong, Z., Li, X., Mu, Y. and Yao, G., 2012. Static three-point bending behavior of aluminum foam sandwich. *Journal of alloys and compounds*, 540, pp.275-278.

[14] Yan, C., Song, X., Zhu, H., Jing, C. and Feng, S., 2018. Flexural response of carbon fiber reinforced aluminum foam sandwich. *Journal of Composite Materials*, 52(14), pp.1887-1897.

SciEn
Journal of Engineering Advancements Vol. 01(04) 2020, pp 116-122 https://doi.org/10.38032/jea.2020.04.002

Computer Vision Based Industrial Robotic Arm for Sorting Objects by Color and Height

Abu Salman Shaikat, Suraiya Akter, Umme Salma*

Department of Mechatronics Engineering, World University of Bangladesh, Dhaka - 1205, Bangladesh

Received: October 1, 2020, Revised: December 02, 2020, Accepted: December 04, 2020, Available Online: December 09, 2020

ABSTRACT

In industrial production systems, manufacturers often face difficulties in sorting different types of objects. Color and height-based sorting which is done manually by human is quite a tedious task and its needs countless time as well. For manual sorting, many workers are required, which can be quite expensive. Moreover, robots that can sort only color or height can't be effective when there is a need of products with same color with different heights and vice versa. In this paper, a computer vision based robotic sorter is proposed, which is capable of detecting and sorting objects by their colors and heights at the same time. This work isn't done before as height sorting of same shapes is a new technique, which is done with color sorting techniques by computer vision. It is equipped with a robotic arm having 6 degree of freedom (DOF), by which it picks up and then place objects according to its color and height, to a predetermined place as per the production system requirement. A camera with the computer vision software detects various colors and heights. Haar Cascade algorithm has been used to sort the products. This multi-DOF robotic sorter can be a remarkably useful tool for automating the production process completely, where multiple conveyor belts are used, which can reduce time complexity as well. In the proposed system, the efficiency of color and height sorting is around 99%, which proves the efficiency of our system. The overall improvement in the efficiency of the production process can be significantly enhanced by using this system.

Keywords: Color and Height Detection, Sorting, Computer Vision, Degree of Freedom, Robotic Arm, Efficiency.

1. Introduction

For over two decades, industrial automation has transformed itself into a more adaptable and programmable automation from its earlier fixed self with the recent technological advancement. The combined field of electrical, electronics, mechanical, and computer vision-based control system has substituted the manual workers, i.e. human beings. Intelligent machines have enhanced both productivity as well as comfort. Usually, industrial robot is used to carry out the monotonous and recurring pick and place tasks; for example, placing the parts from and to a conveyor belt, managing Computerized Numerical Control (CNC) machineries, stowing the parts to and offloading these from the machines. It is extensively used in the industrial assembly line. Industrial robot has proven its worth in this regard within the past few decades. In addition, it sets the tempo of the operations up for boosting the production rate. Robots have been used for quite a long time to automate the flexible product manufacturing system. Robots are turning into more than just machines by using Artificial Intelligence (AI), thus are in great demand in recent years. Robots have solved the expensive labor issues. They also satisfy and fulfill rapidly increasing demands from the customers. Although the expense of assembling a robotic system has relatively increased, performing the intricate, hazardous and insecure tasks competitively has made the robots preferable than their human competitors. Robotic automation not only enhances the production capability, but also offers efficient and improved solutions in numerous scenarios.

In this paper, an autonomous robotic arm is proposed, which can identify objects from the conveyor belt and transfer these to the desired location based on their colors. In an industry dealing with a large number of products, this autonomous robotic sorter can be used in the production system for keeping the expenses below the margin. The robot has been designed stationary around its platform. It uses camera to collect information regarding the colors and heights of the objects. The robot has the capability of identifying objects' colors and heights by placing those in front of its camera as well as sorting out based on color. After sorting, it relocates objects to the destined location.

OpenCV and .NET framework are used as software tools to sort the products in accordance with color and height. Haar Cascade algorithm has been used for Computer Vision (CV) methods. Furthermore, Arduino Nano has been employed for moving or picking the products from specific areas and placing into different locations taking help from CV method.

2. Literature Review

In recent years, researchers and engineers have developed and assembled various types of pick and place robots for carrying out industrial operation. Among them, Dhayalini et al. 0 presented a method for separating deterioration & non-deterioration waste by utilizing a pick and place robot. A simple CV technique for robotics had been implemented in their work which is Android mobile phones based. It solved the issue of separating degradable and non-degradable wastes in streets, which are separated by human beings with a risk of facing communicable diseases. Android mobile had been used to detect the degradable, i.e. vegetables, and non-degradable, i.e. plastic cover objects and then send that retrieved information to the connected microcontroller unit through a Bluetooth module. After receiving that desired information, microcontroller unit operated the robotic arm for reaching the particular objects. Receiving '1' from the Bluetooth indicated the non-degradable object and receiving '0' signified the degradable objects. The

*Corresponding Author Email Address: skt047@gmail.com

robotic arm acted accordingly and took the separate objects for putting those into the separate boxes.

Hu et al. 0 developed a vision-based Selective Compliance Assembly Robot Arm (SCARA) system for obtaining spanners from the targeted location and putting these to desired location. The system was designed to be highly appropriate for the traditional factories. All the component materials are constructed from plastic and aluminum, apart from the motors. The SCARA had around 50 cm of ranges for working. It was equipped with 4 degree of freedom (DOF). The vision system process can be divided into three major sections, such as calibrating image, recognizing image and finally, localizing objects. Firstly, reforming the image distortion had taken place in image calibrations step. Secondly, the spanner located in its workplace had been captured as image and segmented by applying information regarding color in the step of image recognition. Finally, the information about the spanners was retrieved, for example, the center, end to end length, incline and length related tool number. Modbus-TCP communication interface was used to enable secure transmission of position and rotation command to motion controller.

Gecks et al. 0 built an industrial robot system, where a number of stationary cameras were assembled to oversee the workspace for safeguarding human-robot teamwork. Every robot transfer motion was scrutinized to avoid collision using obstacle detection through several CV approaches. The motion path of a robot was altered every time the possibility of a collision had been perceived. The algorithm, that had been proposed, assisted robots in executing secure pick-and-place operations by showing real time responsive activities.

Kato et al. 0 shared the idea of flexible robot manipulators which is suitable for construction with inexpensive setting. The flexible robotic arm had been developed to carry out pick and place tasks involving lightweight manufactured goods. The robotic arm was set in motion through a couple of DC motors along with a stepping motor. To control the twisting mechanism and to twist the flexible link, a wire was attached to the stepping motor. The wire was pulled to reduce the intended vibration of the flexible link's end tip.

Andhare et al. 0 transformed and mapped the 2D coordinates of an object by transforming pixel coordinate to real world coordinate. They integrated robotic arm controller on the basis of object location and orientation. They successfully picked and placed objects by placing under the vision sensor.

Li et al. 0 illustrated a new elliptical trajectory planning algorithm as the increasing speed of industrial pick and place robots requires optimization of the kinematic characteristics to operate high speed application efficiently. Their proposed algorithm was able to enhance the performance to operate the pick and place tasks. One elliptical trajectory defined with a precise secured height was created. In addition, one customized sine wave movement profile was commenced into that trajectory. The simulation results exhibit the efficacy and appropriateness of the process for implementing the industrial applications.

Lin et al. 0 assembled a robot vision system for detecting diverse target objects as well as their poses, which can be integrated in robot programming by demonstration, i.e. robot PbD in short. Lately, robot PbD has stepped into the trending topic scenario regarding robotics field. Although programming the robots is a prolonged procedure, needing deep technical knowledge, robot task programming can be streamlined by CV system. By analyzing human demonstration, this was implemented. They took the pick-and-place activities as robot PbD example. Several non-overlapped objects were positioned on a table and people picked one of those objects and moved to other place, one at a time. The robot could refine its next decision by acquiring initial information prior to learning from the human demonstration. For example, if the robot had detected the intended object and attuned its stance afterwards, then it was able to operate smoothly. Choosing the kind of gripper and/or the angle of grip beforehand helped the robot enhancing its operation. The developed robot vision system showed improvement concerning reciprocal trainability. The graphical user interface (GUI) helped in this regard. Common users, i.e. not experts, could easily choose the understandable features using the user friendly GUI. An uncomplicated scale-invariant pose assessment method was also projected. The system demonstrated itself as a feasible and effective one, sustained by the experimental results.

Lukač et al. 0 presented program code to control industrial robot. Version 2.2.2 of the renowned simulation software KUKA Sim Pro was used to run the robot cell simulation. The components, that were used, had been brought mostly from the incorporated library. However, some components were partially assembled from the scratch. The industrial robot, namely, KUKA KR6 R900 sixx, is considered to be one of the fastest robots in the current world.

Rahman et al. 0 developed a robotic sorter competent for identifying and sorting objects with different colors. It comprised of a robotic arm that picked up objects and placed those to a preprogrammed location after detecting colors. A Pixy cam supported by the CV software identified several colors. For robotic arm rotation few servomotors were used-09. The arms had the ability to move both horizontally as well as vertically concerning its base. Roshni et al. 0 proposed another technique for distinguishing objects from their surroundings by employing CV approaches and calculating their center of gravity.

Some researchers work with color and size detection individually, whereas very few researchers work with color and size detection together. They work with individual shape (triangular, rectangular, circular) detection only with different colors. However, in our work, we work with same shape (rectangular) with different height materials including color sorting techniques, which makes our work unique. This work can be very useful when there will be a need of sorting diverse products by its colors and just changes of heights.

The aforementioned works have some limitations. While most of these works have focused on the task of detecting and picking up objects, load calculation has been disregarded to some extent. Moreover, the force of motors should be measured for maximum efficacy. In this work, a CV based intelligent color and height sorting pick and place robot using Haar Cascade method is developed which can sort diverse products for assorted purpose. The maximum load of the robot manipulator arm is calculated that can be carried or supported by the arm. Also, the force of gripper motor and all other joint motors is computed in this work.

3. System Design

In order to assemble the system, some aspects were taken into consideration:

i. Servo motors are used due to its motion freedom and also, low power requirements and light weight make it suitable for designing in robotic arm.

ii. The power is supplied from a rechargeable nickel metal hydride (Ni-MH) battery.
iii. A continuous path controller, i.e. Arduino Nano was chosen and employed. Forward Kinematics is used to control the movement of robot in every direction and position from end effector to joint parameters. Force feedback is done with the help of kinematics. Error sensing feedback control is done by servo motors.

Table 1 shows the details of robotic arm.

Table 1 Details of Robotic Arm

Motor Axis	Part	Motion	Motor
A-Z	Base	Rotation	Servo
B-Y	Shoulder	Up-Down	Servo
C-X	Elbow	Forward-Backward	Servo
B-Y	Wrist	Up-Down	Servo
E-Y	Gripper	Up-Down	Servo
F-Linear	Gripper	Open/Close	DC

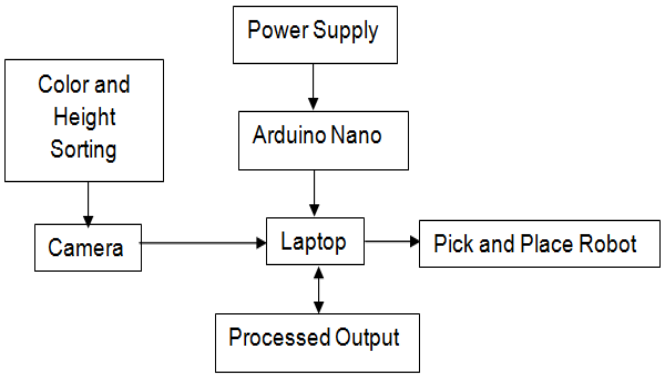

Fig. 1 Block Diagram

The prototype system has been developed using Haar Cascade method 0. For color detection, we use the function cv.cvtColor() and extract the color from the object. For height detection, Haar features have been used in CV approaches to categorize the pixel intensity by tracing inside a region. Haar features are symbolized as the rectangle regions in the image. We used edge detection technique for height detection, whereas the upper part is white, and lower part is black. For small object detection, two third of the object is white and one-third is white, whereas for black, it's just opposite. In this system, background is preferred as white for detecting the white parts without any contradictions. Object detection module trained the 300 different object pictures (30 pictures for each object) as positive images. As negative images, detection module is trained 180 pictures that should be outside of object like still picture, background and people's face. The classifiers comprise of couple of or three rectangle features for scanning features incessantly in the window. Since this scanning is a tedious and repetitive task, Cascade classifier is introduced to shed the overwork. It arranges a set of features with positive and negative images into an assorted level of classification structure 0. It defines an upper and lower threshold value for both the object sizes. One detection per object is introduced, which reduces overlapping detection, which can increase the performance of the system. The block diagram is depicted in Fig. 1. First of all, the camera is placed in standby position and the OpenCV window is opened afterwards. Then, the camera is activated in OpenCV and the objects are sorted as per color and height. The result is revealed in OpenCV. Finally, system is run to start the pick and place robotic movement.

Fig. 2 represents the arm of the robotic manipulator. All the diameters from link to link are shown here. Mechanical design of the pick and place robot is shown in Fig. 3, which includes all except the object.

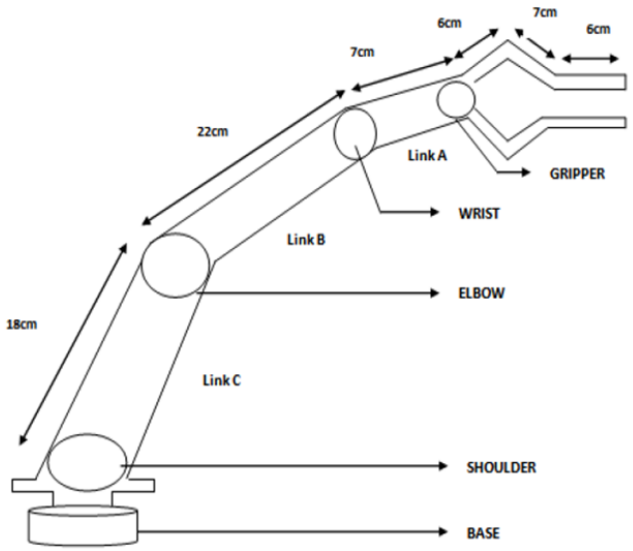

Fig. 2 Design of the Robotic Manipulator (arm)

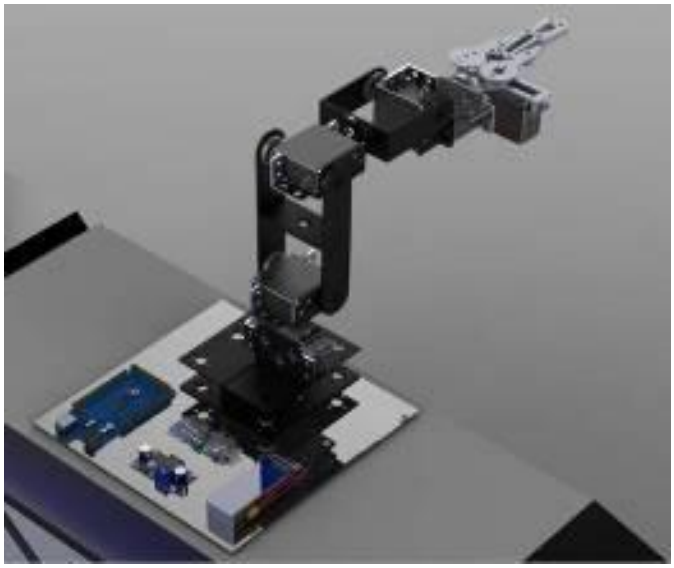

Fig. 3 Mechanical Design

Fig. 4 represents the flowchart of the pick and place robot. As the system starts, image processing using OpenCV with Haar Cascade Method is applied. Then, camera will sort out the products. If the product is yellow and large, the product will be placed by robot in 90˚ left side and if the product is small, the product will be placed in 45˚ left side. Moreover, if the color of product is black and large, then the robot will place the product in 90˚ right direction and if it is a small product, then the product will be placed in 45˚ right direction. All process is done with .net framework, Arduino Nano and OpenCV shows the resultant output in laptop.

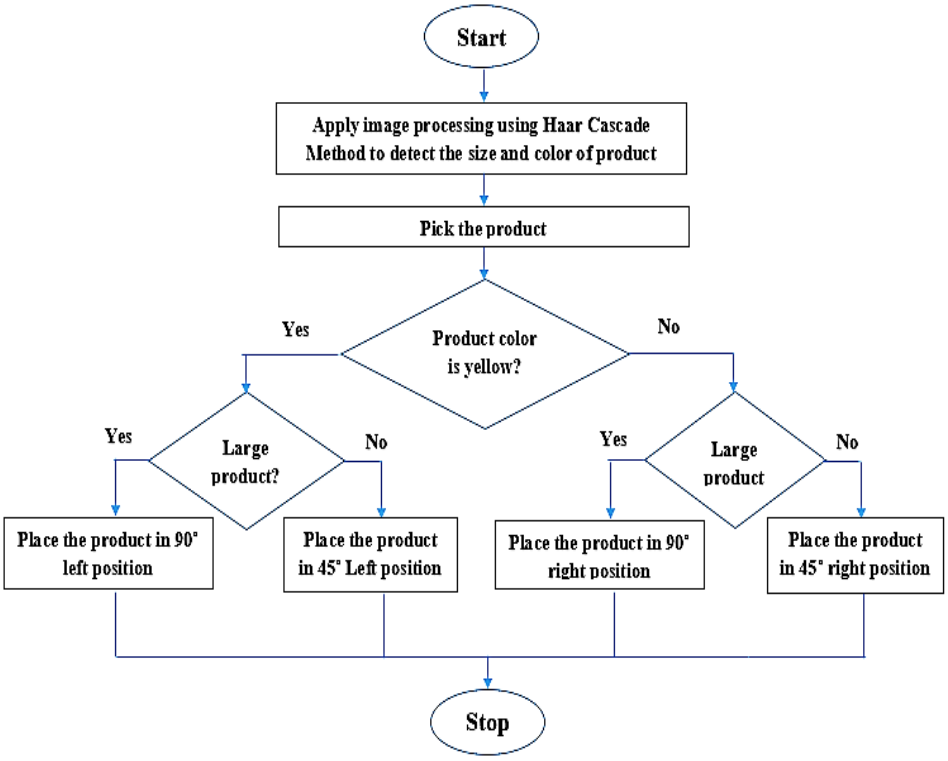

Fig. 4 Flowchart

4. Results Analysis

In this color and height sorting pick and place robot, Arduino Nano is connected with dc motor, servo motors and PC. Experimental setup is given in Fig. 5. The connection between Arduino to I/O with robot and camera feedback is done by the signal flow of block diagram and it's shown in Fig. 1.

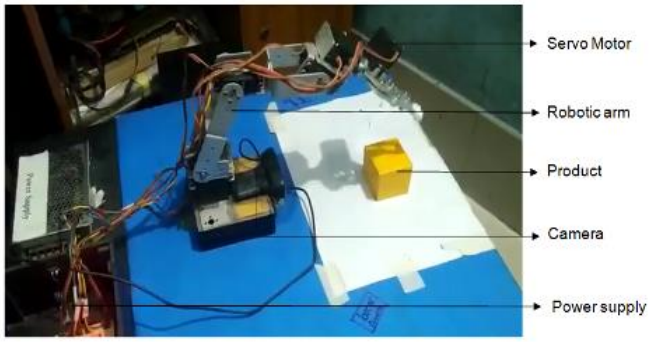

Fig. 5 Hardware Setup

Table 2 shows D-H parameters 0 of a 6 DOF Manipulator for this pick and place robot.

Table 2 D-H Parameters of a 6 DOF Manipulator

Joint $_i$	α_i	a_i	d_i	θ_i
1	0	a_1	d_1	θ_1
2	0	a_2	0	θ_2
3	-π/2	a_3	0	θ_3
4	-π/2	a_4	0	θ_4
5	0	0	0	θ_5
6	0	0	d_6	θ_6

$$ {}^{0}A_1 = \begin{bmatrix} c\theta_1 & -s\theta_1 & 0 & a_1c\theta_1 \\ s\theta_1 & c\theta_1 & 0 & a_1s\theta_1 \\ 0 & 0 & 1 & d_1 \\ 0 & 0 & 0 & 1 \end{bmatrix} \quad (1) $$

$$ {}^{1}A_2 = \begin{bmatrix} c\theta_2 & -s\theta_2 & 0 & a_2c\theta_2 \\ s\theta_2 & c\theta_2 & 0 & a_2s\theta_2 \\ 0 & 0 & 1 & 0 \\ 0 & 0 & 0 & 1 \end{bmatrix} \quad (2) $$

$$ {}^{2}A_3 = \begin{bmatrix} c\theta_3 & 0 & -s\theta_3 & a_3c\theta_3 \\ s\theta_3 & 0 & c\theta_3 & a_3s\theta_3 \\ 0 & -1 & 0 & 0 \\ 0 & 0 & 0 & 1 \end{bmatrix} \quad (3) $$

$$ {}^{3}A_4 = \begin{bmatrix} c\theta_4 & 0 & -s\theta_4 & a_4c\theta_4 \\ s\theta_4 & 0 & c\theta_4 & a_4s\theta_4 \\ 0 & -1 & 0 & 0 \\ 0 & 0 & 0 & 1 \end{bmatrix} \quad (4) $$

$$ {}^{4}A_5 = \begin{bmatrix} c\theta_5 & -s\theta_5 & 0 & 0 \\ s\theta_5 & c\theta_5 & 0 & 0 \\ 0 & 0 & 1 & 0 \\ 0 & 0 & 0 & 1 \end{bmatrix} \quad (5) $$

$$ {}^{5}A_6 = \begin{bmatrix} c\theta_6 & -s\theta_6 & 0 & 0 \\ s\theta_6 & c\theta_6 & 0 & 0 \\ 0 & 0 & 1 & d_6 \\ 0 & 0 & 0 & 1 \end{bmatrix} \quad (6) $$

Multiplying equations yields:

$$^{0}A_6 = {}^{0}A_1 \ {}^{*1}A_2 \ {}^{*2}A_3 \ {}^{*3}A_4 \ {}^{*4}A_5 \ {}^{*5}A_6 \quad (7)$$

$$^{0}A_6 = \begin{bmatrix} Ux & Vx & Wx & Qx \\ Uy & Vy & Wy & Qy \\ Uz & Vz & Wz & Qz \\ 0 & 0 & 0 & 1 \end{bmatrix} \quad (8)$$

$$Ux = C\theta_{123456} - C\theta_{3456}S\theta_{12} - C\theta_{1456}S\theta_{13} - C\theta_{2456}S\theta_{13} + C\theta_{126}\,S\theta_{35} - S\theta_{1235} + C\theta_{136}S\theta_{25} + C\theta_{236}S\theta_{15} - C\theta_{1234}\,S\theta_{56} + C\theta_{34}S\theta_{1256} + C\theta_{14}S\theta_{1356} + C\theta_{24}\,S\theta_{1356} + C\theta_{125}S\theta_{36} - S\theta_{1236} + C\theta_{135}\,S\theta_{26} + C\theta_{235}\,S\theta_{16} \quad (9)$$

$$Uy = C\theta_{23456}S\theta_1 + C\theta_{13456}S\theta_4 - S\theta_{123}C\theta_{456} + C\theta_{12456}S\theta_3 + C\theta_{26}S\theta_{135} + C\theta_{16}S\theta_{235} + S\theta_{125}C\theta_{36} - C\theta_{1236} - C\theta_{234}S\theta_{156} - C\theta_{134}S\theta_{256} - S\theta_{12356}C\theta_4 + C\theta_{124}S\theta_{356} + C\theta_{25}\,S\theta_{136} + C\theta_{15}\,S\theta_{236} + S\theta_{126}\,C\theta_{35} - C\theta_{1235} \quad (10)$$

$$Uz = -C\theta_{56}\,S\theta_4 - S\theta_{456} \quad (11)$$

$$Vx = -C\theta_{12345}\,S\theta_6 + C\theta_{345}S\theta_{126} + C\theta_{145}S\theta_{136} + C\theta_{245}S\theta_{136} - C\theta_{124}S\theta_{356} + S\theta_{12356} - C\theta_{13}S\theta_{256} - C\theta_{23}S\theta_{156} - C\theta_{12346}S\theta_5 + C\theta_{346}S\theta_{125} + C\theta_{146}S\theta_{135} + C\theta_{246}S\theta_{135} + C\theta_{1256}S\theta_3 - S\theta_{123} + C\theta_{1356}S\theta_2 + C\theta_{2356}S\theta_1 \quad (12)$$

$$Vy = -C\theta_{2345}\,S\theta_{16} - C\theta_{1345}\,S\theta_{26} + S\theta_{1236}\,C\theta_{45} - C\theta_{1245}\,S\theta_{36} - C\theta_2\,S\theta_{1356} - C\theta_1\,S\theta_{2356} - S\theta_{1256}\,C\theta_3 + C\theta_{123} - C\theta_{2346}S\theta_{15} - C\theta_{1346}S\theta_{25} - S\theta_{1235}C\theta_{46} + C\theta_{1246}S\theta_{35} + C\theta_{256}\,S\theta_{13} + C\theta_{156}\,S\theta_{23} + S\theta_{12}\,C\theta_{356} - C\theta_{12356} \quad (13)$$

$$Vz = C\theta_5 S\theta_{46} - S\theta_{456} \quad (14)$$

$$Wx = -C\theta_{123}\,S\theta_4 + C\theta_3 S\theta_{124} + C\theta_1\,S\theta_{134} + C\theta_2\,S\theta_{134} \quad (15)$$

$$Wy = -C\theta_{23}\,S\theta_{14} - C\theta_{13}\,S\theta_{24} + S\theta_{1234} - C\theta_{12}S\theta_{34} \quad (16)$$

$$Wz = -C\theta_4 \quad (17)$$

$$Qx = -d_6\,C\theta_{123}\,S\theta_4 + d_6C\theta_3S\theta_{124} + d_6C\theta_1S\theta_{134} + d_6C\theta_2S\theta_{134} + a_4C\theta_{1234} - a_4C\theta_{34}S\theta_{12} - C\theta_{14}S\theta_{13} - C\theta_{24}S\theta_{13} + a_3C\theta_{123} - a_3C\theta_3S\theta_{12} - a_3C\theta_1S\theta_{23} - a_3C\theta_2S\theta_{13} + a_2C\theta_{12} - a_2S\theta_{12} + a_1\,C\theta_1 \quad (18)$$

$$Qy = -d_6\,C\theta_{23}S\theta_{14} - d_6C\theta_{13}\,S\theta_{24} + d_6\,S\theta_{1234} - d_6C\theta_{12}\,S\theta_{34} + a_4\,C\theta_{234}S\theta_1 + a_4\,C\theta_{134}\,S\theta_2 - a_4\,C\theta_4\,S\theta_{123} + a_4C\theta_{124}S\theta_3 + a_3C\theta_{23}\,S\theta_1 + a_3C\theta_{13}\,S\theta_2 - a_3S\theta_{123} + a_3C\theta_{12}\,S\theta_3 + a_2C\theta_2\,S\theta_1 + a_2C\theta_1\,S\theta_2 + a_1S\theta_1 \quad (19)$$

$$Qz = -d_6C\theta_4 - a_4S\theta_4 + d_1 \quad (20)$$

When the black and large object is detected, it shows "Black object and large box detected" in OpenCV which is illustrated in Fig. 6. Furthermore, when yellow and large object is detected, then it shows "Yellow object and large box is detected" in OpenCV which is illustrated in Fig. 7. Furthermore, OpenCV shows "Black object and small box detected" when camera detects black and small object, which is shown in Fig. 8.

To perform this task with more objects in dataset for qualitative results, it uses yellow with small object, red with large and small objects, blue with large and small objects and, at last green with large and yellow objects. So, our dataset contains all of these objects and we can detect all the objects successfully.

With the help of confusion matrix, we get the precision and recall rates for our work, which shows that, our work is quite effective to work with.

Confusion matrix with precision and recall rates are shown below.

Confusion matrix =

[[96,1,0,3,0,0,0,0,0,0],
[1,98,0,0,0,0,1,0,0,0],
[0,0,100,0,0,0,0,0,0,0],
[1,0,0,95,3,1,0,0,0,0],
[0,0,3,0,95,0,0,0,0,2],
[0,2,0,0,1,97,0,0,0,0],
[0,0,0,0,0,0,100,0,0,0],
[0,2,1,0,0,1,0,94,2,0],
[1,0,0,0,0,1,0,0,97,1],
[0,0,0,0,0,0,0,0,0,100]])

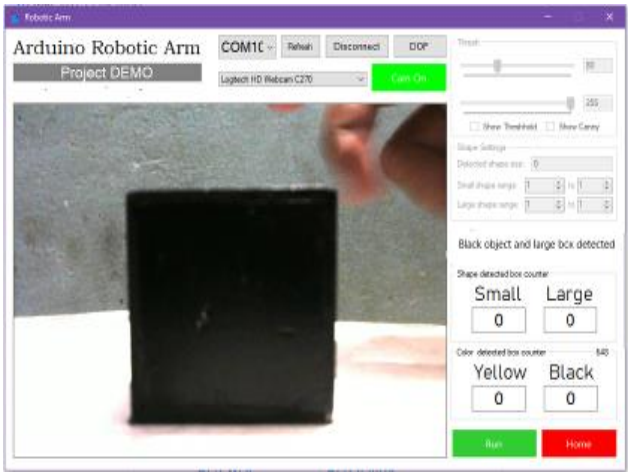

Fig. 6 OpenCV Detecting the Black and Large Object

Fig. 7 OpenCV Detecting the Yellow and Large Object

Precision and recall rates for the system is shown below.

Label	precision	recall
0	0.970	0.960
1	0.951	0.980
2	0.962	1.000
3	0.969	0.950
4	0.960	0.950
5	0.970	0.970
6	0.990	1.000
7	1.000	0.940
8	0.980	0.970
9	0.971	1.000

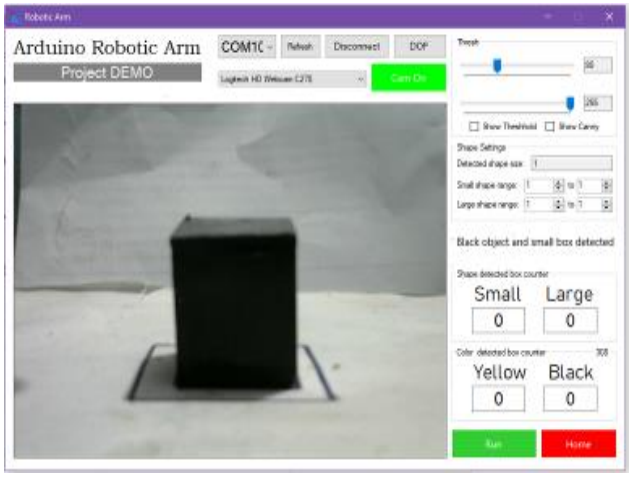

Fig. 8 OpenCV Detecting the Black and Small Object

This work is done with white background and level of illumination should be brightest as possible. When we did our qualitative task, for yellow object, two times it's failed to detect because of lower brightness.

DC servo motor has low power requirement and the light weight makes it suitable for this design. The torque is fully balanced by the inertia of the electric motors and the speed is significantly reduced by gear sets attached to the electric motors. In this aspect, several calculations were performed in order to attain the required servo mechanism for meeting the specification required for this work. Fig. 9 shows the torque calculation for each servo motor.

Numerous calculations were done in order to attain the required servo mechanism that will meet the specification on this work.

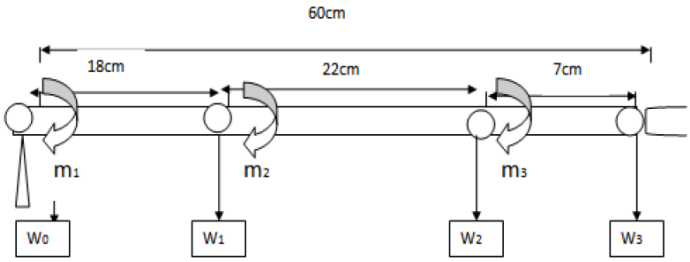

Fig. 9 Diagram Showing Torque Calculation on Each Servo

Assuming that the weight of the material is negligible since it light compares to the servo specification. W_0 =56g, W_1=56g, W_2=56g, W_3=36g, base weight=56+56+56+36=204g, (weights include gravitational force [f=mg]), base length=10 cm.

From Newton-Euler recursive formulation 0, we find that, for torque,

Outward iterations: i: 0 → 5

$$^{i+1}\omega_{i+1} = {}^{i+1}_{i}R\ {}^{i}\omega_i + \dot{\theta}_{i+1}\ {}^{i+1}\hat{Z}_{i+1} \quad (21)$$

$$^{i+1}\dot{\omega}_{i+1} = {}^{i+1}_{i}R\ {}^{i}\omega_i + {}^{i+1}_{i}R\ {}^{i}\omega_i \times \dot{\theta}_{i+1}\ {}^{i+1}\hat{Z}_{i+1} + \ddot{\theta}_{i+1}\ {}^{i+1}\hat{Z}_i \quad (22)$$

$$^{i+1}\dot{v}_{i+1} = {}^{i+1}_{i}R\ ({}^{i}\omega_i \times {}^{i}P_{i+1} + {}^{i}\omega_i \times ({}^{i}\omega_i \times {}^{i}P_{i+1}) + {}^{i}\dot{v}_I \quad (23)$$

$$^{i+1}\dot{v}c_{i+1} = {}^{i+1}\dot{\omega}_{i+1} \times {}^{i}Pc_{i+1} + {}^{i+1}\omega_{i+1} \times ({}^{i+1}\omega_{i+1} \times {}^{i}Pc_{i+1}) + {}^{i+1}\dot{v}_{i+1} \quad (24)$$

$$^{i+1}F_{i+1} = m_{i+1}\ {}^{I+1}\dot{v}c_{i+1} \quad (25)$$

$$^{i+1}N_{i+1} = {}^{ci+1}I_{i+1}\ {}^{i+1}\dot{\omega}_{i+1} + {}^{i+1}\omega_{i+1} \times {}^{ci+1}I_{i+1}\ {}^{i+1}\omega_{i+1} \quad (26)$$

Inline iterations: i: 6 →1

$$^{i}f_i = {}^{i}_{i+1}R\ {}^{i+1}f_{i+1} + {}^{i}F_i \quad (27)$$

$$^{i}n_i = {}^{i}N_i + {}^{i}_{i+1}R\ {}^{i+1}n_{i+1} + {}^{i}Pc_i \times {}^{i}F_i + {}^{i}P_{i+1} \times {}^{i}_{i+1}R\ {}^{i+1}f_{i+1} \quad (28)$$

$$\gamma_i = {}^{i}n_i^T\ {}^{i}\hat{Z}_i \quad (29)$$

Finally, for translational joint,

$$\varphi_i = f_i(R_{i-1}^{i})^T z \quad (30)$$

For angular joint,

$$\varphi_i = n_i(R_{i-1}^{i})^T z \quad (31)$$

After calculating all of this, for 6 DOF robotic arm, for torque, we find,

$$\begin{matrix} L & \dot{p}Ixx & -qrIyy & +qrIzz \\ M = & \dot{q}Ixx & +prIyy & -prIzz \\ N & \dot{r}Ixx & -pqIyy & +pqIzz \end{matrix} \quad (32)$$

And, for force,

$$\begin{matrix} Fx & u & +(qw - rv) \\ Fy = & v & +(ru - pw) \\ Fz & w & +(pv - qu) \end{matrix} \quad (33)$$

Where,
I, j, k = body center coordinate in x, y and z directions
u, v, w = linear velocities in x, y and z directions
p, q, r = angular velocity in x, y and z directions
Ixx, Iyy, Izz = Moment of inertia in x, y and z directions

Since moment of inertia of z-axis is zero, so torque,

$$\begin{matrix} L & \dot{p}Ixx & -qrIyy & 0 \\ M = & \dot{q}Ixx & +prIyy & 0 \\ N & \dot{r}Ixx & -pqIyy & 0 \end{matrix} \quad (34)$$

With the help of parallel axis theorem we find,

$$I_{xx} = I_{xx1} + M\,d_x^2 \quad (35)$$

$$I_{yy} = I_{yy1} + M\,d_y^2 \quad (36)$$

Because the axis of rotation is on the edge, so

$$I_{xx1} = M\,b^3/3 \quad (37)$$

$$I_{yy1} = M\,h^3/3 \quad (38)$$

After calculating, we find
I_{xx} = 0.00413 kg-cm^2
I_{yy} = 38 km-cm^2
For angular velocity,

$$^{6}\omega_6 = \begin{matrix} 0 \\ 0 \\ \dot{\theta}1 + \dot{\theta}2 + \dot{\theta}3 + \dot{\theta}4 + \dot{\theta}5 + \dot{\theta}6 \end{matrix} \quad (39)$$

So, angular velocity, p and q = 0.

$$r = \dot{\theta}1 + \dot{\theta}2 + \dot{\theta}3 + \dot{\theta}4 + \dot{\theta}5 + \dot{\theta}6 = 18.18\ rad/s \quad (40)$$

So, torque,

$$\begin{matrix} L & 0 & 0 & 0 \\ M = & 0 & 0 & 0 \\ N & 0.00413(\dot{\theta}1 + \dot{\theta}2 + \dot{\theta}3 + \dot{\theta}4 + \dot{\theta}5 + \dot{\theta}6) & 0 & 0 \end{matrix} \quad (41)$$

So, N_1 = 0.076818 kg-cm

Actual torque of the shoulder servo = 13 [kg-cm] (From datasheet)

Excess torque = Actual servo torque – Calculated torque

Therefore excess available torque at the shoulder = 13 – 0.076818 = 12.92 [kg-cm]

From the design analysis the maximum load the robotic manipulator can lift successfully is determine by the base servo. From the above analysis the excess torque of the base is 12.92 [kg-cm]. Hence, the calculated maximum load is 12.92 [kg]. The actual load will be less than the calculated value because the weight of the material used in constructing the arm was light and was not taken into consideration.

For linear velocity, w = 0. We also find p, q =0. After calculating, we get, u= 2 m/s, v ≈ 0.

So, force,

$$\begin{matrix} Fx \\ Fy \\ Fz \end{matrix} = \begin{matrix} u \\ 0 \\ 0 \end{matrix} \quad \begin{matrix} 0 \\ +18.18u \\ 0 \end{matrix} = \begin{matrix} 2 \\ 36.6 \\ 0 \end{matrix} \tag{42}$$

So, maximum force can be given as 2 N and 36.36 N for x and y direction respectively.

This system is quite effective and efficiency of the system is almost 99%.

5. Conclusion and Future Work

Since robots are used in flexible or even fixed automation systems, there are two reasons for selecting a robot to operate in a production line. The reasons include reducing labor costs and performing work that is tedious, unpleasant and hazardous for human beings. However, introducing too many robots for picking and placing is quite expensive and risky as well. Therefore, this work has introduced where only one robotic arm is used which is competent in picking and placing objects based on color and height. The whole process is regulated with Arduino Nano. The applications of this work are suited for industry, where product with different color and height can be sorted out.

The work can further be improved in the near future by introducing the conveyor belt, in which, the objects or products can come to a certain place and sorting robot can be used for picking the products. The conveyor belts can also be used for placing the objects or products according to their colors and sizes.

References

Dhayalini, K. and Mukesh, R., 2018, January. Deterioration & non-deterioration wastes separation using pick & place robot. In *2018 2nd International Conference on Inventive Systems and Control (ICISC)* (pp. 96-99). IEEE.

Hu, C.Y., Chen, C.R., Tseng, C.H., Yudha, A.P. and Kuo, C.H., 2016, March. Visual servoing spanner picking and placement with a SCARA manipulator. In *2016 IEEE International Conference on Industrial Technology (ICIT)* (pp. 1632-1637). IEEE.

Gecks, T. and Henrich, D., 2005, August. Human-robot cooperation: safe pick-and-place operations. In ROMAN 2005. *IEEE International Workshop on Robot and Human Interactive Communication*, 2005. (pp. 549-554). IEEE.

Kato, G., Onchi, D. and Abarca, M., 2013. Low cost flexible robot manipulator for pick and place tasks. In *2013 10th International Conference on Ubiquitous Robots and Ambient Intelligence (URAI)* (pp. 677-680). IEEE.

Andhare, P. and Rawat, S., 2016, August. Pick and place industrial robot controller with computer vision. In *2016 International Conference on Computing Communication Control and automation (ICCUBEA)* (pp. 1-4). IEEE.

Li, W., Xiao, Y., Bi, S. and Du, G., 2013, September. Automatic elliptical trajectory planning algorithm for pick and place operation. In *2013 International Conference on Advanced Mechatronic Systems* (pp. 36-39). IEEE.

Lin, H.I., Chen, Y.Y. and Chen, Y.Y., 2015, May. Robot vision to recognize both object and rotation for robot pick-and-place operation. In *2015 International Conference on Advanced Robotics and Intelligent Systems (ARIS)* (pp. 1-6). IEEE.

Lukač, D., 2018, May. Simulation of a pick-and-place cube robot by means of the simulation software KUKA Sim Pro. In *2018 41st International Convention on Information and Communication Technology, Electronics and Microelectronics (MIPRO)* (pp. 0846-0849). IEEE.

Rahman, M.J., Das, D.P., Islam, O. and Zaman, H.U., 2018, February. A Novel Design of a Robotic Object Sorter Based on Color Differences using Image Processing Techniques. In *2018 International Conference on Computer, Communication, Chemical, Material and Electronic Engineering (IC4ME2)* (pp. 1-4). IEEE.

Viola, P. and Jones, M., 2001, December. Rapid object detection using a boosted cascade of simple features. In *2001 IEEE computer society conference on computer vision and pattern recognition (CVPR)* (Vol. 1, pp. I-I). IEEE.

Roshni, N. and Kumar, T.S., 2017, March. Pick and place robot using the centre of gravity value of the moving object. In *2017 IEEE International Conference on Intelligent Techniques in Control, Optimization and Signal Processing (INCOS)* (pp. 1-5). IEEE.

Rahmad, C., Asmara, R.A., Putra, D.R.H., Dharma, I., Darmono, H. and Muhiqqin, I., 2020, January. Comparison of Viola-Jones Haar Cascade Classifier and Histogram of Oriented Gradients (HOG) for face detection. In *IOP Conference Series: Materials Science and Engineering* (Vol. 732, No. 1, p. 012038). IOP Publishing.

Craig, J.J., 2009. Introduction to robotics: mechanics and control, 3/E. *Pearson Education India*.

SciEn
Journal of Engineering Advancements Vol. 01(04) 2020, pp 123-129 https://doi.org/10.38032/jea.2020.04.003

Effect of Synthesis Conditions on the Molecular Weight and Activation Energy of Urea-Formaldehyde Prepolymer and Their Relationship

*Atqiya Anjum and G. M. Arifuzzaman Khan**

Department of Applied Chemistry and Chemical Engineering, Faculty of Engineering and Technology, Islamic University, Kushtia-7003, Bangladesh

Received: November 09, 2020, Revised: December 10, 2020, Accepted: December 10, 2020, Available Online: December 13, 2020

ABSTRACT

The aim of this study is to find out the viscosity change of urea-formaldehyde (UF) resin with the synthesis parameters namely formaldehyde/urea (F/U) mole ratios, pH and temperature. The viscosity of UF resins, related to molecular weight and activation energy is very important factor of their usability. Urea-formaldehyde (UF) prepolymer was synthesized through polycondensation reaction with F/U ratio 0.8, 1.0, 1.2, 1.4, 1.6. The synthesis was carried out by two steps: alkali catalysis at reaction pH 8.3, 90°C for 60 min and thereafter acid catalysis at pH 4.3, 83°C for 15 min. Viscosity of prepolymer was determined at acid catalysis step by simple glass viscometer. Weight average molecular weight (*Mw*) was calculated from the viscosity data of UF prepolymer using Mark-Houwink equation. Highest *Mw* (2020.9) of prepolymer was obtained at F/U molar ratio 1.0 and pH 4.3. In addition, it was found that pH 4.0 yielded greater *Mw* (2049) UF prepolymer among the four reactions which were performed at pH 4.0, 4.3, 4.7, and 5.0. The energy of activation (E_a) of UF prepolymer was also calculated from the measured viscosity at temperature 70, 75, 80 and 85°C. The highest values of E_a were also found at F/U molar ratio 1.0 and pH 4.0 & lowest values was obtained at F/U molar ratio 1.6 and pH 5.0. From the experimental data, it was shown that the values of E_a and *Mw* were varied comparably with the change of reaction parameters.

Keywords: Urea-formaldehyde Prepolymer; F/U Molar Ratio; pH; Viscosity; Molecular Weight; Activation Energy.

1. Introduction

Thermosetting polymers are used widely in various field like thermal and electrical insulation, utensils, building materials, engineering tools etc. due its hardness and good resistance to electric and heat [1]-[2]. However, their use become limited due to their inherent properties for instance low toughness, low flexibility, non-recyclable, difficult to coloration etc. [3]. To overcome the drawbacks and value addition, plenty of research have been carried out by the polymer scientists [4]. Some of those researches explore alternative use of thermosetting polymers where drawbacks are not considered. The use of formaldehyde based resin as adhesives of particle board, plywood has ushered in a new era [5]-[9]. These resins not only have adhesive properties but also have long lasting capacity because they contain some fraction of free formaldehyde. For this particular case, those compounds are unusable for making medical goods and food grade materials [10]. Among the formaldehyde based thermosetting resin, phenol formaldehyde resin is widely used in adhesive, wood and composite industries [11]. Nevertheless, phenol formaldehyde belongs phenolic resin is comparatively harmful to the environment [12]. Moreover, it is better to use urea formaldehyde because it is cheap in price, possess good quality, less foul-smelling and has a beautiful color [5], [13]-[14].

Urea formaldehyde resin is prepared by the polycondensation reaction of urea and formaldehyde (Scheme 1) [8]. The synthesis process of urea-formaldehyde may be divided into two stages, addition or alkaline methylolation and acidic condensation. At alkaline methylolation, dimer, trimer with low molecular weight methylol urea is formed by substitution reaction of urea and formaldehyde. Thereafter, with the change of reaction condition of acidic condensation relatively higher molecular compound might be obtained. In this stage polymerization is propagated by the formation of methylene (-CH_2-) and dimethylene ether (-CH_2-O-CH_2-) linkages with the reaction of methylol group and amino group [14]. Sun et al. studied the effect of catalysts on the UF resin preparation [17]. They found that in alkali catalyzed reaction, limited amount of UF prepolymer was formed and a large amount of free urea left. On the other hand acid catalyst enhanced the formation of methylene, ether linkages, and urons. Gonçalves et al. reported that degree of condensation is higher on the alkaline-acidic combined process than only strong acid catalyze stage [18].

The reaction parameter namely urea/formaldehyde (F/U) molar ratio, temperature, pH etc. are the major factor controlling the condensation reaction [19]-[22]. Dazmiri et al. stated that amount of free formaldehyde in resin increases at higher F/U ratio [21]. On the other hand, at low F/U ratio some unreacted urea remains in resin. In addition, high molecular weight UF resin is formed at strong acidic condition and high temperature [5]. The UF resin is converted into solid after curing with suitable crosslinking agent and curing condition. However, setting time of polymer resin should be longer. For quick solidification, unreacted urea and formaldehyde is remained in polymer and high molecular weight is seldom formed. One of big problem of thermosetting polymer is that, it could not melt or reshape if once it solidified. Therefore, it should keep in liquid state before use. It is mandatory to retain it in liquid form when use for adhesive purposes, because resin should be spread evenly on the solid

*Corresponding Author Email Address: arifuzzaman@acce.iu.ac.bd

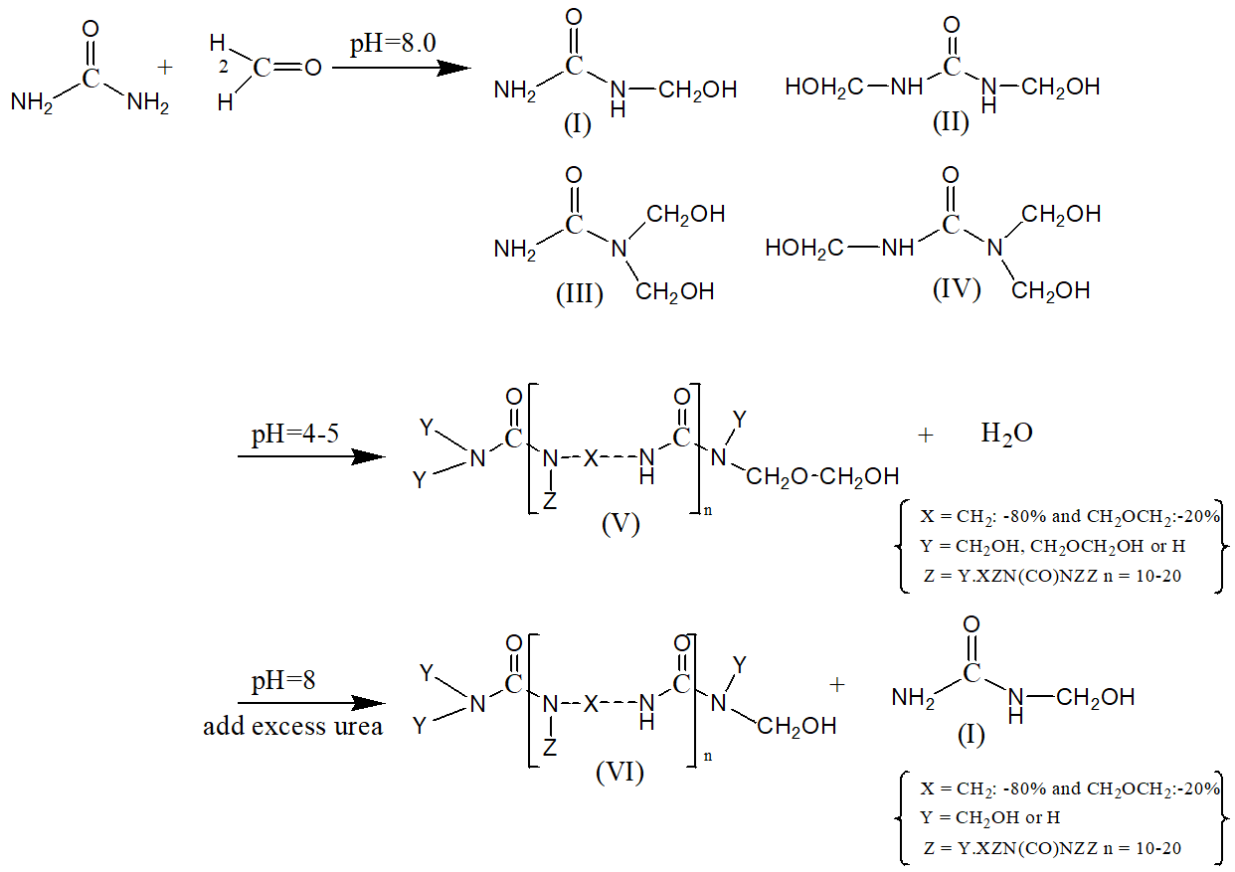

Scheme 1 Synthesis of UF resin from urea and formalin (I)-monomethylol urea,(II), (III)-dimethylol urea (IV)-trimethylol urea and (V), (VI)-uron derivatives.

surface. For blending with other materials purposes, it is also important to apply the resin in a liquid state. The use ability of liquid resin is depended on its viscosity [13], [23]-[24]. The low viscous resin can penetrate and spread easily on broad panel when use in adhesive purposes. The viscosity of a polymer adhesive is controlled by temperature, pH and concentration. Plenty of researches have been studied the effect of reaction parameters on the viscosity of UF resin [24]-[25]. They interpreted the experimental results differently. Since cross-linking reaction of uron derivatives takes place with condensation reaction, it is very difficult to get reproduce values. Different results can also be obtained due to the differences in the environment. That why, we have chosen the current topic to know the changes of viscous properties in our reaction setting.

The molecular weight of UF resin were measured by using gel permeable chromatography (GPC), NMR, viscometry etc. [13], [26]. Viscometry is very simple technique which able to provide important information of viscous polymer solution [27]. The viscosity of fluids is determined both by collision among particles and by the force fields which determines interactions among molecules. It has great analytical significant for the characterization of polymer molecules. As like viscosity, activation energy (E_a) is important property of viscous polymer solution which influence on solvent types, concentration of solution, etc. [28]. DSC is most common technique to measure the activation energy (E_a) of UF resin [29]. E_a can be calculated if viscosities of solution change with temperature. The viscosity of polymer solution is varied with temperature which has been investigated in previous studies [30]-[31]. The E_a could be calculated from viscosity-temperature data using Kissinger equation [32]. No published data has been found which determine the value of E_a of UF resin by viscosity measurement. In addition, no clear information is available in the literature which depicted the relation of E_a with synthesis parameter of UF resin (F/U molar ratio and pH). In the present research, attempt has been taken to find the value of *Mw* and E_a of UF prepolymers by viscosity measurement. A set of experiment has carried out to correlate the values of *Mw* and E_a.

2. Experimental

2.1 Materials

The technical grade urea granules (99%) and formalin (37%) were purchased from Merck, India. The other reagents used in this study were analytical grade.

2.2 Methods

2.2.1 Synthesis of UF prepolymer

UF prepolymer was prepared by conventional method with various F/U mole ratios of 0.8, 1.0, 1.2, 1.4, and 1.6 [20]. This method is divided into two parts: (1) alkali catalysis: 405 ml formalin was taken in open glass reactor (1000 ml Pyrex beaker) equipped with a thermometer and heater with stirrer. The urea was added in two steps and in each step 50% of it was used. The 50% of solid urea (predetermined) was dissolved in formalin under stirring at 40°C. The pH was adjusted to 7.8–8.0 by adding 0.01M sodium hydroxide solution. The reactor

was heated to 90°C and maintained for 60 min. The temperature was then cooled to 80°C. (2) Acid catalysis: at 83°C, the pH was adjusted to 4.3 by adding 0.05M acetic acid solution. The rest amount of urea was then added in solution and stirred continuously for 15 min at 83°C to complete dissolution of urea. White viscous suspension of UF resin prepolymer was obtained. The prepolymer was then kept at room temperature for slowing down the curing reaction. All the viscosities of the solution were quickly measured at same time by Ostwald viscometer. For comparative analysis, a set of prepolymer was prepared using F/U mole ratio 1.0 by maintaining pH 4.0, 4.3, 4.7 and 5.0 at acid catalysis step.

2.2.2 Molecular weight determination

For molecular weight determination, the solutions of resin sample (0.01, 0.02, 0.03, 0.04 and 0.05 ml/1 ml) were prepared using mixed solvent Ethanol/water (1:1) just before performing the experiment [24]. Then the viscometric flow times were measured for the samples. By using measured flow time of a solution, viscosity is calculated by Poiseuille's law at following equation [13]:

$$\eta = \frac{\pi r^4 pt}{8lv} \quad (1)$$

Where, η, kinematic viscosity, *v*, volume of solution, *r* & *l* are radius and length of the capillary tube of viscometer respectively, *t*, falling time through the capillary tube at pressure (*p*). The falling time is measured for the level of the liquid to pass between the two marks is proportional to the pressure imposed by gravity on the head of the liquid by a known volume.

By simplifying equation 1 the relative viscosity (η_r) and specific viscosity (η_{sp}) can be determined as:

$$\eta_r = \frac{\eta}{\eta_o} = \frac{t}{t_o} \quad (2)$$

$$\eta_{sp} = \frac{\eta - \eta_o}{\eta_o} = \frac{t - t_o}{t_o} \quad (3)$$

η_o is viscosity of the solvent, *t* is flow time of solution and t_o is flow time of solvent. The intrinsic viscosity [η] is a measure of molecular dimension and is defined as

$$[\eta] = {}_c \underset{\rightarrow 0}{Lt} \frac{\eta_{sp}}{C} = {}_c \underset{\rightarrow 0}{Lt} \frac{ln\,\eta_r}{C} \quad (4)$$

$\eta_{sp}/_C$, reduced viscosity of the solution; $ln\,\eta_r/_C$, inherent viscosity; and C, the concentration of solution in $\frac{g}{100ml}$. The following empirical equation might be work efficiently for dilute solution.

$$\eta_{sp}/_C = [\eta] + K_1[\eta]^2 C - -(Huggins) \quad (5)$$

$$ln\,\eta_r/_C = [\eta] + K_2[\eta]^2 C - -(Kraemer) \quad (6)$$

If a graph is made by plotting the observed reduced or inherent viscosities against the concentration, the intercept of the straight line at C = 0 gives the intrinsic viscosity.

From the measured intrinsic viscosity, the molecular weight was calculated using modified staudinger equation [31]:

$$[\eta] = KM^{\alpha} \quad (7)$$

From the intercept of the plot log [η] against log M, values of K and from the slope, value of 'α' were found. The values of 'K' and 'α' were found to be 0.74×10^{-3} and 1.05 respectively [33].

2.2.3 Activation energy measurement

Viscosity was measured by Ostwald viscometer at 70, 75, 80, 85 and 90^0C in a thermostatic water bath (for activation energy determination). The viscometer was fixed vertically into water bath where the highest level of the liquid in the viscometer was at least one centimeter below the water level in the bath. The prepared of prepolymer samples were quickly taken into the viscometer upto the mark. Since the viscosity of resin continuously changed with time, the viscometer containing experimental solution was allowed to stand only for about five minutes to attain the temperature of i.e. constant temperature bath before each measurement. Minimum 10 falling time was observed by stop watch for each experiment. After every measurement the viscometer was washed thoroughly and then checked by measuring the time of flow of distilled water. This energy is called the 'activation energy of viscous flow' (E_a). E_a is calculated using Eyring's equation [34] (equation 8 & 9).

$$\eta = Ae^{\frac{E_a}{RT}} \quad (8)$$

$$ln\,\eta = \frac{E_a}{RT} + lnA \quad (9)$$

The value of E_a is calculated from the slope of plot of lnη versus 1/T by using equation 9. The value of R is considered 8.314 J K^{-1} mol^{-1}.

3. Results and Discussion

The viscosities of UF prepolymer prepared at different F/U molar ratio 0.8, 1.0, 1.2, 1.4, 1.6 and pH 4.0, 4.3, 4.7, 5.0 are calculated from measured falling time at temperature 83°C. The falling time of solvent ethanol:water (1:1) was taken as reference sample. Every UF prepolymer sample taken for viscosity measurement is preserved at same condition.

The concentration of resin solution versus calculated reduce viscosity is plotted in Fig. 1. All the line presented in the figure of UF prepolymer with different F/U molar ratio shown the similar trend. The intrinsic viscosity is calculated from the intersection of those lines to Y axis. Microsoft excel software is used to get exact values. Weight average molecular weight (*Mw*) is obtained from intrinsic viscosity by Mark-Houwink equation and the values are given in Table 1. It has been noted that the intrinsic viscosity and *Mw* of the resins prepared at different F/U molar ratio under the same acid pH with the same condensation time and temperature are different. The highest *Mw* (2020.9) is found at F/U molar ratio 1.0 then decreases with the increase of F/U molar ratio. The lowest *Mw* is found 1735.7 at greater F/U molar ratio 1.6. At higher urea proportions (lower F/U), the condensation reaction is faster. This may be due at low F/U molar ratio more amine groups

available to react with formaldehyde [21]. It is also assumed that the gel time which directly related to viscosity is significantly affected by molar ratios. Moreover, at very low F/U molar ratio (0.8) urea is not disintegrated completely in formalin. M. Dunkey also reported some portion of resin was precipitated at lower F/U ratio (>0.9) during the acid condensation step, causing inhomogenities in the solutions [5]. No remarkable differences are shown in resin density. The R^2 values indicate better correlation between reduced viscosity and concentration of resin solution.

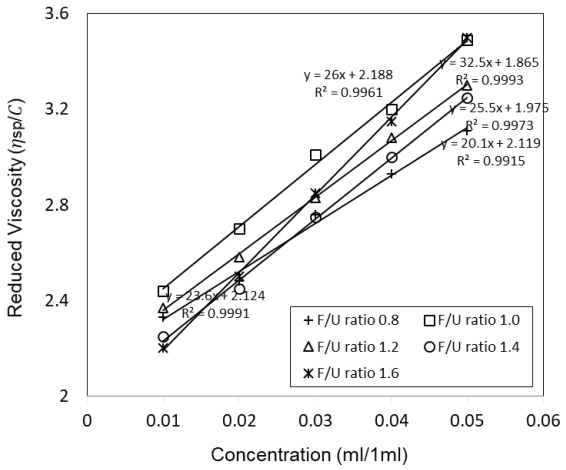

Fig. 1 Reduced viscosity vs concentration plot of UF prepolymers of different F/U molar ratio.

The intrinsic viscosities of UF prepolymer at pH 4.0, pH 4.3, pH 4.7 and pH 5.0 for F/U molar ratio 1.0 are obtained from Fig. 2 and the respective values of *Mw* are 2049, 2020, 1833, and 1726 respectively which shown in Table 1. The polymerization process of UF resin is propagated in the acid condensation step. The linear or branched molecules with medium and even higher *Mw* are formed with the reaction of methylols, urea and free formaldehyde. The numbers of stable methylene (-CH_2-) linkages are increased at lower pH and high temperature [5]. The highest *Mw* is found at pH 4.0 and became lowest at pH 5.0. The results indicate that molecular weight of UF resin is increasing with the decrease of reaction pH. The high percentage of uron derivatives might be formed under strong acidic conditions formulated in the past [34].

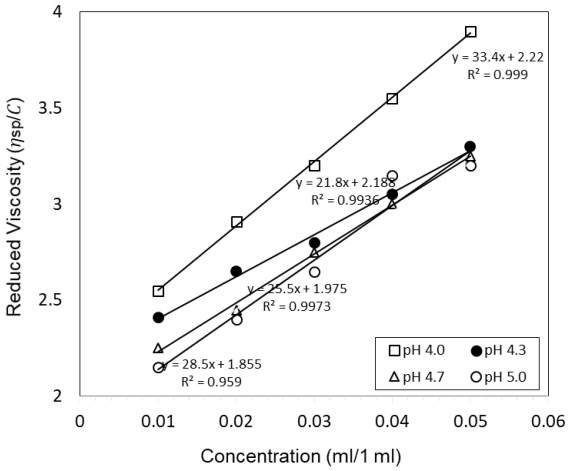

Fig. 2 Reduced viscosity vs concentration plot of UF prepolymers of different pH.

The change of viscosity with temperature variation can be explained the molecular movement in the solvent. It has been seen that molecular movement increases with the increase of temperature and hence decrease the viscosity. At high temperature the kinetic energy of the molecule increases and starts to move more rapidly and away from each other. Due to rapid movement of molecule at higher temperature, more bulk space is formed which diminishes interlayer movement restriction and therefore viscosity decreases. The increase of viscosity with the decrease of temperature is shown in Fig. 3. The plot shown, the viscosity of the prepolymer of different F/U molar ratio with temperatures gives similar trend. The resin contains higher formalin fraction exhibit lower viscosity values. In other word, concentrate solution have higher viscosities than dilute solution. Molecules of concentrate solution should have energy which overcomes the internal friction or resistance of fluid.

Table 1 Values of intrinsic viscosity, *Mw* and *Ea* at various reaction condition.

F/U ratio	pH	Density ($gm.cm^{-3}$)	Molecular weight *(Mw)*			Energy of activation (E_a)		
			[n]	R^2	*Mw*	δy/δx	R^2	E_a ($kj.\ mol^{-1}$)
0.8	4.3	1.56	2.119	0.9915	1960.1	124.17	0.9873	1.0323
1	4.3	1.52	2.188	0.9961	2020.9	131.88	0.9963	1.0965
1.2	4.3	1.49	2.124	0.9991	1964.5	124.45	0.9993	1.0347
1.4	4.3	1.47	1.975	0.9993	1833.1	120.88	0.9894	1.0050
1.6	4.3	1.44	1.865	0.9973	1735.7	118.17	0.9877	0.9825
1	4.0	1.51	2.220	0.9990	2049.0	144.87	0.9986	1.2044
1	4.3	1.52	2.188	0.9936	2020.9	131.8	0.9963	1.0958
1	4.7	1.51	1.975	0.9973	1833.1	117.55	0.9652	0.9773
1	5.0	1.49	1.855	0.9590	1726.8	114.88	0.9796	0.9551

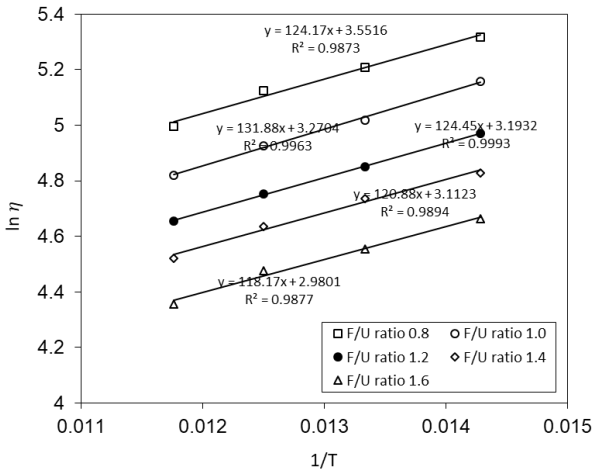

Fig. 3 Variation of viscosity of UF prepolymer with different F/U ratio at temperature 70, 75, 80 and 85°C.

According to Fig. 3, the steepness of all line graphs belongs to prepolymer resin of different F/U molar ratio looks similar. The resin prepared at F/U molar ratio 1.0 exhibit slightly steeper slope in the Eyring plot than other UF prepolymer. The calculated E_a for the different concentrations are given in Table 1. The E_a value of UF prepolymer prepared at F/U molar ratio 0.8, 1.0, 1.2, 1.4 and 1.6 is calculated and the values are1.0323, 1.0965, 1.0347, 1.0050 and 0.9825 kJ mol^{-1} respectively. It has been seen that the energy of activation is increased upto F/U molar ratio 1.0 and then decreased with the increase of formaldehyde content. The molecular mobility is decreased due to reduction of frictional resistance and hence decreases E_a. However, E_a of UF resin at F/U molar ratio 0.8 lower than resin found at F/U molar ratio 1.0. Probably at high proportion of urea is made precipitation at unreacted form during polycondensation reaction [5]. The previous studies also stated that the solid content of UF resin is greater at higher F/U molar proportion [25].

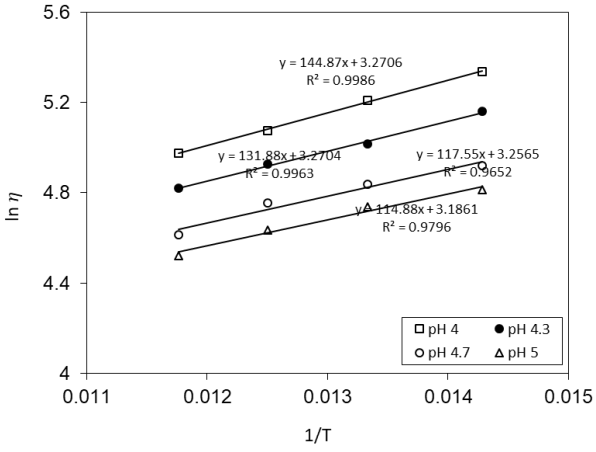

Fig. 4 Variation of viscosity of UF prepolymer with various pH at temperature 70, 75, 80 and 85°C.

Fig. 4 illustrated the change of viscosity of UF prepolymer prepared by different pH with temperature. It has been seen that the viscosity decreases with the increase of pH. In the experiment the higher molecular weight is found at pH 4.0. According to the studies of Tomita [35] known that lower pH favors the synthesis process of UF resin i.e. high molecular weight compound is formed at very strong acidic condition. Lee and Kim also declared that the mobility of the UF resin molecules and their reactive groups decreases when the molecular weight increases. In addition, molecules are crosslinked on the curing process which reduce the mobility significantly [36]. Therefore, the activation energy is found greater at lowest pH. The calculated values of *Ea* are 120.44×10^{-2}, 109.58×10^{-2}, 97.73×10^{-2} and 95.51×10^{-2} is found at pH 4.0, 4.3, 4.7 and 5.0 respectively. The R^2 values indicate better correlation between temperature and ln η.

Fig. 5 presented the relation of between molecular weight and activation energy of UF resin prepared by various F/U molar ratio and reaction pH. The similar trend of E_a and *Mw* curves is shown. The highest values of E_a and *Mw* are found at F/U molar ratio 1.0 and lowest values found at 1.6. Similarly, highest E_a and *Mw* are obtained at pH 4 and thereafter their values are decreased with the increase of pH.

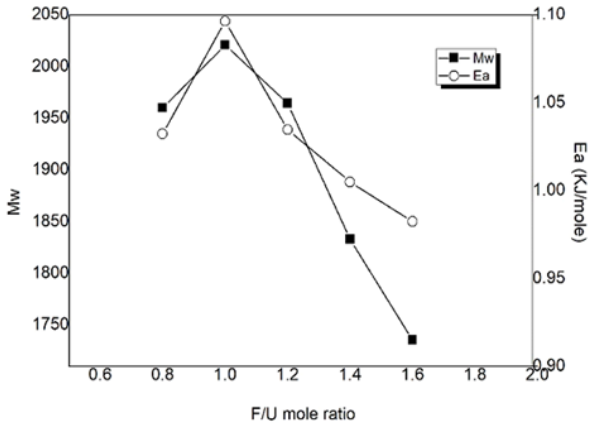

(a)

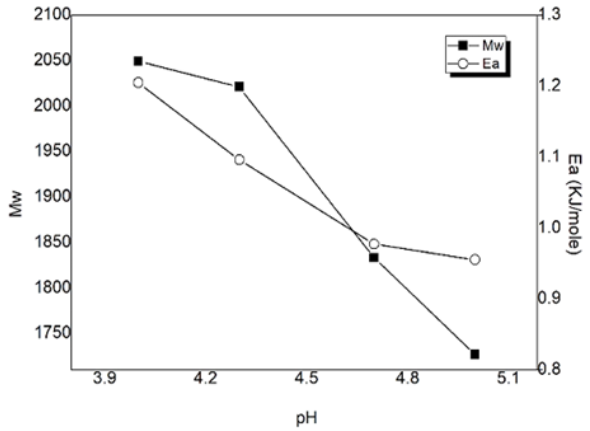

(b)

Fig. 5 Change of Mw and Ea of UF prepolymer prepared by various F/U ratio and pH

4. Conclusion

This paper describes the change of molecular weight (*Mw*) and activation energy (*Ea*) of urea-formaldehyde (UF) prepolymer prepared by F/U molar ratio 0.8, 1.0, 1.2, 1.4, 1.6 at pH 4.3. Another set of UF prepolymer made at pH 4.0, 4.7, 5.0 with F/U molar ratio 1.0. The value of *Mw* calculated from

intrinsic viscosity using Mark-Houwink (M-H) equation. The results showed that *Mw* of UF prepolymer varied remarkably with reaction parameters. The highest *Mw* was found at F/U molar ratio 1.0 and pH 4. The activation energy (E_a) of UF prepolymer samples calculated by Eyring's equation from intrinsic viscosity measured at temperature 70, 75, 80 and 85°C. The value of E_a changed with the variation of reaction parameter like *Mw*. Activation energy decreased at higher F/U mole ratio and pH value. The consistent of viscosity data of UF prepolymer samples given similar trend in *Mw* and E_a values change of with reaction parameter. Finally, it may suggest that the viscosity measurement is quite effective method for determination activation energy of UF resin.

References

[1] Moser, A. and Feuchter, M., 2016. Mechanical properties of composites used in high-voltage applications. *Polymers*, *8*(7), p.260.

[2] Post, W., Susa, A., Blaauw, R., Molenveld, K. and Knoop, R.J., 2020. A review on the potential and limitations of recyclable thermosets for structural applications. *Polymer Reviews*, *60*(2), pp.359-388.

[3] Jeong, D.H., Park, J.W., Jeon, Y.J. and Lee, J.H., 2019, October. Development of Thermoplastic Materials for the Application of Eco-friendly. In *2019 5th International Conference on Electric Power Equipment-Switching Technology (ICEPE-ST)* (pp. 476-479). IEEE.

[4] Tao, L., Sun, Z., Min, W., Ou, H., Qi, L. and Yu, M., 2020. Improving the toughness of thermosetting epoxy resins via blending triblock copolymers. *RSC Advances*, *10*(3), pp.1603-1612.

[5] Dunky, M., 1998. Urea–formaldehyde (UF) adhesive resins for wood. *International Journal of Adhesion and Adhesives*, *18*(2), pp.95-107.

[6] Khan, G.M.A., Abedin, S.M.A., Choudhury, M.J., Gafur, M.A. and Alam, M.S., 2014. Renewable okra bast fiber reinforced phenol formaldehyde resin composites: mechanical and thermal studies. *Res Rev: J Mater Sci*, *2*, pp.32-36.

[7] Khan, G.A., Haque, M.A. and Alam, M.S., 2014. Studies on okra bast fibre-reinforced phenol formaldehyde resin composites. In *Biomass and Bioenergy* (pp. 157-174). Springer, Cham.

[8] No, B.Y. and Kim, M.G., 2004. Syntheses and properties of low-level melamine-modified urea–melamine–formaldehyde resins. *Journal of Applied Polymer Science*, *93*(6), pp.2559-2569.

[9] Sreekala, M.S., Kumaran, M.G., Joseph, S., Jacob, M. and Thomas, S., 2000. Oil palm fibre reinforced phenol formaldehyde composites: influence of fibre surface modifications on the mechanical performance. *Applied Composite Materials*, *7*(5-6), pp.295-329.

[10] Kariuki, S.W., Wachira, J., Kawira, M. and Murithi, G., 2019. Formaldehyde Use and Alternative Biobased Binders for Particleboard Formulation: A Review. *Journal of Chemistry*, *2019*.

[11] Fink, J. K., 2013. Chapter 4 - Phenol/Formaldehyde Resins. In J. K. B. T.-R. P. F. and A. (Second E. Fink (Ed.), Plastics Design Library, pp. 155–177, William Andrew Publishing.

[12] Sarika, P.R., Nancarrow, P., Khansaheb, A. and Ibrahim, T., 2020. Bio-Based Alternatives to Phenol and Formaldehyde for the Production of Resins. Polymers, 12(10), p.2237.

[13] Jeong, B. and Park, B.D., 2019. Practical relationship between apparent viscosity and molecular weight of urea-formaldehyde resin adhesives. *Journal of Adhesion Science and Technology*, *33*(3), pp.209-216.

[14] Jeremejeff, J., 2012. Investigation of UF-resins-the Effect of the Formaldehyde/Urea Molar Ratio during Synthesis. *Master of Science Thesis*, pp.1–108.

[15] Que, Z., Furuno, T., Katoh, S. and Nishino, Y., 2007. Effects of urea–formaldehyde resin mole ratio on the properties of particleboard. *Building and Environment*, *42*(3), pp.1257-1263.

[16] Dunky, M., 2017. Adhesives in the wood industry. Handbook of Adhesive Technology, Third Edition, pp.511–574.

[17] Sun, Q.N., Hse, C.Y. and Shupe, T.F., 2014. Effect of different catalysts on urea–formaldehyde resin synthesis. *Journal of Applied Polymer Science*, *131*(16).

[18] Gonçalves, C., Pereira, J., Almeida, M., Paiva, N.T., Ferra, J.M., Martins, J.M., Magalhães, F.D., Barros-Timmons, A. and Carvalho, L.H., 2019. Impact of alkaline–acid and strongly acid process on the synthesis of urea–formaldehyde resins and derived composites: A comparison study. *European Journal of Wood and Wood Products*, *77*(6), pp.1177-1187.

[19] Akinterinwa, A., Ismaila, A., & Aliyu, B., 2020. Concise Chemistry of Urea Formaldehyde Resins and Formaldehyde Emission. *Insights in Chemistry and Biochemistry*, pp.1–6.

[20] Ferra, J.M., Mena, P.C., Martins, J., Mendes, A.M., Costa, M.R.N., Magalhães, F.D. and Carvalho, L.H., 2010. Optimization of the synthesis of urea-formaldehyde resins using response surface methodology. *Journal of Adhesion Science and Technology*, *24*(8-10), pp.1454-1471.

[21] Dazmiri, M.K., Kiamahalleh, M.V., Dorieh, A. and Pizzi, A., 2019. Effect of the initial F/U molar ratio in urea-formaldehyde resins synthesis and its influence on the performance of medium density fiberboard bonded with them. *International Journal of Adhesion and Adhesives*, *95*, p.102440.

[22] Nuryawan, A., Risnasari, I., Sucipto, T., Iswanto, A.H. and Dewi, R.R., 2017, July. Urea-formaldehyde resins: production, application, and testing. In *IOP Conference Series: Materials Science and Engineering* (Vol. 223, No. 1, p. 012053). IOP Publishing.

[23] Hepworth, D.G., Bruce, D.M., Vincent, J.F.V. and Jeronimidis, G., 2000. The manufacture and mechanical testing of thermosetting natural fibre composites. *Journal of materials science*, *35*(2), pp.293-298.

[24] Osemeahon, S.A., Barminas, J.T. and Aliyu, B.A., 2007. Effect of urea formaldehyde viscosity on some physical properties of a composite from reactive blending of urea formaldehyde with natural rubber. *International J Physical Sciences*, *2*(9), pp.242-248.

[25] Jeong, B. and Park, B.D., 2019. Effect of molecular weight of urea–formaldehyde resins on their cure kinetics, interphase, penetration into wood, and adhesion in bonding wood. *Wood Science and Technology*, *53*(3), pp.665-685.

[26] Liu, Y.Q., Tian, Y., Zhao, G.Z., Sun, Y.Y., Zhu, F.T. and Cao, Y., 2008. Synthesis of urea-formaldehyde resin by melt condensation polymerization. *Journal of Polymer Research*, *15*(6), p.501.

[27] Rohindra, D.R., Lata, R.A. and Coll, R.K., 2012. A simple experiment to determine the activation energy of the viscous flow of polymer solutions using a glass capillary viscometer. *European journal of physics*, *33*(5), p.1457.

[28] Chandler, H.D., 2013. Activation energy and entropy for viscosity of wormlike micelle solutions. *Journal of colloid and interface science*, *409*, pp.98-103.

[29] Chen, Y.Z. and Xiao, H., 2017. Characterization of pre-curing behavior of urea-formaldehyde resin affected by different temperatures. *E&ES*, *77*(1), p.012007.

[30] Budtova, T. and Navard, P., 2015. Viscosity-temperature dependence and activation energy of cellulose solutions. *Nordic Pulp and Paper Research Journal*, 30(1), pp.99–104.

[31] Rohindra, D.R., Lata, R.A. and Coll, R.K., 2012. A simple experiment to determine the activation energy of the viscous flow of polymer solutions using a glass capillary viscometer. *European journal of physics*, *33*(5), p.1457-1464.

[32] Nuryawan, A., Park, B.D. and Singh, A.P., 2014. Comparison of thermal curing behavior of liquid and solid urea–formaldehyde resins with different formaldehyde/urea mole ratios. *Journal of Thermal Analysis and Calorimetry*, *118*(1), pp.397-404.

[33] Edoga, M.O., 1997. *Stability Improvement of Urea-Formaldehyde Adhesives for Wood Products* (Doctoral dissertation, Ph. D Thesis submitted to Ahmadu Bello University, Zaria, Nigeria).

[34] Gedde, U.L.F., 1995. *Polymer physics*. Springer Science & Business Media.

[35] Hse, C.Y., Xia, Z.Y. and Tomita, B., 1994. Effects of reaction pH on properties and performance of urea-formaldehyde resins. *Holzforschung 48 (6):* 527-532.

[36] Lee, Y.K. and Kim, H.J., 2013. Relationship between curing activation energy and free formaldehyde content in urea-formaldehyde resins. *Journal of adhesion science and technology*, *27*(5-6), pp.598-609.

SciEn
Journal of Engineering Advancements Vol. 01(04) 2020, pp 130-138 https://doi.org/10.38032/jea.2020.04.004

Improvement of the Handover Performance and Channel Allocation Scheme using Fuzzy Logic, Artificial Neural Network and Neuro-Fuzzy System to Reduce Call Drop in Cellular Network

Md. Ariful Islam[1,], Md. Rakib Hasan[2] and Amena Begum[2]*

[1]Department of Robotics & Mechatronics Engineering, University of Dhaka, Dhaka, Bangladesh
[2]Department of Information & Communication Technology, Comilla University, Cumilla, Bangladesh

Received: November 27, 2020, Revised: December 16, 2020, Accepted: December 18, 2020, Available Online: December 19, 2020

ABSTRACT

Due to handover failure, call drop occurs frequently. When a large number of incoming and handoff calls arrive at the same time, the performance of the conventional handoff algorithms may fall down. Moreover, multiple factors such as signal quality and available channels of cellular network can't be evaluated in conventional algorithms. When mobile station (MS) moves, the connection of MS with nearby base station (BS) has to be switched from one to adjacent station. In this case, unnecessary handoffs will be occurred due to lack of proper decision of handoffs or lack of consideration about signal quality with available free channels. As a result call drop will occur frequently. For performing handoff efficiently, fuzzy logic based handoff decision algorithm, adaptive handoff threshold level using neural network and priority based dynamic channel allocation algorithm using neuro-fuzzy system has been proposed in this work. These algorithms will mainly focus on the proper decision of handoff based on evaluating signal strength, available free channels, spectrum efficiency, MS speed and distance from BS so that unnecessary and inefficient handoffs can't be performed. Simulation revealed that using neuro-fuzzy system, the channel capacity, SIR and Handoff management were improved better than the others in terms of spectrum utilization efficiency, MS speed and SIR. The efficacy of the methodology has been proved by imitating the proposed model using MATLAB software.

Keywords: Fuzzy Logic; Neural Network; Neuro-Fuzzy; Dynamic Channel Allocation; SIR; Handoff.

1. Introduction

Call drop is the sudden and undesirable termination of successfully established calls [1]. For customer's satisfaction, call drop curtailment is very important issue in wireless cellular communication system. It is the right of the taxpayer customers to have flexible and Reliable communication tie-up, better tele-health and Tele-medicine opportunity, emergency virtual meeting and Security management system etc. Bindia and Aggarwal published a paper on various handoff strategies using fuzzy logic [1]. They integrated heterogeneous wireless environment to trigger the network selection process to perform handoff satisfactorily. Nyambati and Oduol published a paper on handoff decision in order to analyze the impact of fuzzy based algorithm in a cellular network [2]. The impact of utilizing the fuzzy logic system for handover decision making considering the global system for cell phone communication (GSM) network has analyzed. Atayero and Luka [3] proposed adaptive neurofuzzy inference system for dynamic load balancing using the soft computing in 3GPP LTE. In this paper, they didn't take any consideration of the network parameters such as signal to interference ratio, available channel capacity or signal strength.

From the previous surveys, handover has contemplated as the main reason for call dropping. Due to wrong decision and improper threshold level, unsuccessful handoff occurs frequently which will lead to the effect of call drop [4]. With compared to these literature studies, this paper has tried to deal with network parameters by which handoff problem can be minimized to reduce call drop.

So this paper will propound possible solution based on Artificial Intelligence system to find out the right decision point with a view to ensuring successful handoff and Channel allocation based on measuring the value of network parameters. Artificial neural network, fuzzy logic and Neuro-fuzzy systems are the major AI tools [5] that have applied in this work.

2. Methodology

Three methods have provided below to find out the proper decision point and handoff threshold level for occurring successful handoff.

2.1 Two handoff level algorithm based on fuzzy logic

On the basis of two handoff algorithm, the request of handoff is commenced, when the signal toughness drops under the first handoff altitude. At this altitude, when the upcoming signal is brawny, the handoff will take place. The call will be handed off, when the second handoff altitude is outstretched. The received signal strength (RSS) itself includes interference and carrier signal [3]. The algorithm of two handoff level based on fuzzy logic is shown in Fig. 1.

The current received signal strength varying from -110dbm to -48dbm, signal to interference ratio varying from 12db to 24db and upcoming base station RSS are considered as the handoff decision matrices. These decision matrices are used as linguistic variables as shown in Table 1. Also handoff decision is considered as output of fuzzy inference system shown in Table 2.

*Corresponding Author Email Address: arif_eeedu@yahoo.com Published by: SciEn Publishing Group

Table 1 Fuzzy variable for three inputs of two handoff level algorithm

Serial Number	Fuzzy Variable and Span	Input Ranges		
		LOW	AVERAGE	HIGH
1.	Current RSS -110 dBm to -48 dBm	-110 dBm to -88 dBm	-92 dBm to -68 dBm	-72 dBm to -48 dBm
2.	New BS RSS -110 dBm to -48dBm	-110 dBm to -88 dBm	-92 dBm to -68 dBm	-72 dBm to -48 dBm
		Input Ranges		
		POOR	MEDIUM	BETTER
3.	SIR 14 dB to 24 dB	14 dB to 19 dB	17 dB to 21 dB	20 dB to 24 dB

Table 2 Fuzzy variable for output of two handoff level algorithm

Serial Number	Fuzzy Variable and Span	Output Ranges			
1.	Handoff Decision 0 to 1	NO	WAIT	BE-READY	YES

Table 3 Rule base for different inputs amalgamation

Rule Number	**Current RSS**	**SIR**	**New BS RSS**	**HOD**
1	LOW	POOR	LOW	YES
2	LOW	MEDIUM	LOW	BE-READY
3	LOW	BETTER	LOW	BE-READY
4	AVERAGE	POOR	LOW	YES
5	AVERAGE	MEDIUM	LOW	BE-READY
6	AVERAGE	BETTER	LOW	NO
7	HIGH	POOR	LOW	YES
8	HIGH	MEDIUM	LOW	BE-READY
9	HIGH	BETTER	LOW	NO
10	LOW	POOR	AVERAGE	YES
11	LOW	MEDIUM	AVERAGE	BE-READY
12	LOW	BETTER	AVERAGE	BE-READY
13	AVERAGE	POOR	AVERAGE	YES
14	AVERAGE	MEDIUM	AVERAGE	BE-READY
15	AVERAGE	BETTER	AVERAGE	AVERAGE
16	HIGH	POOR	AVERAGE	YES
17	HIGH	MEDIUM	AVERAGE	WAIT
18	HIGH	BETTER	AVERAGE	NO
19	LOW	POOR	HIGH	YES
20	LOW	MEDIUM	HIGH	BE-READY
21	LOW	BETTER	HIGH	WAIT
22	AVERAGE	POOR	HIGH	YES
23	AVERAGE	MEDIUM	HIGH	BE-READY
24	AVERAGE	BETTER	HIGH	NO
25	HIGH	POOR	HIGH	YES
26	HIGH	MEDIUM	HIGH	WAIT
27	HIGH	BETTER	HIGH	NO

Sugeno fuzzy inference system [5] will be used to process these matrices parameters. The output of the FIS means the membership value of handoff decision shown in Table 2. Based on the different amalgamation of the three inputs and one output parameters, the different twenty seven rules can be conceived as shown in Table 3.

The handoff decision parameter [6] depending on the three input parameters such as RSS of current base station, signal to interference ratio and RSS of new base station can be assessed as shown in Fig. 2.

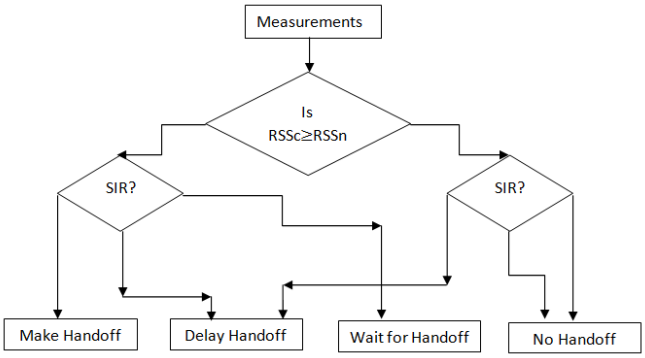

Fig. 1 Two handoff level algorithm based on fuzzy logic.

2.2 Artificial Neural network based Adaptive handoff threshold level algorithm

To manifold problems, artificial neural networks can be applied. The utility of three parameters [7] such as slope ratio, signal to interference ratio and the number of available free channels can be calculated using fuzzy logic system. The threshold value for handoff will be adopted to fortify successful handoff according to the value of such parameters.

Fig. 3 shows the training data sets considered as input data sets for learning. These inputs are applied to the fuzzy logic system and the FLS outputs can be computed. The ranges of slope ratio, signal to interference ratio are from 0 to 1, 14 db to 21 db and 0 to 12. The test data to validate the model is shown in Fig. 4. The FLS output data will serve as the target output shown in Fig. 5.

2.3 Neuro-fuzzy based Dynamic Channel Allocation Scheme

In this work, DCA [8] can be used to flourish a channel allocation policy. Neuro-adaptive learning mechanisms render a procedure for employing dynamic channel allocation stratagem to grasp information about a data set. For a given input or output data set, the toolbox function ANFIS contrives a fuzzy inference system (FIS). Back propagation algorithm can be used to tune the parameters of membership function [4]. By this process, the permission to learn from the modeling data will be obtained. Through the learning action, the related parameters can be changed.

In fuzzy control toolbox, a handy command called ANFIS exists. An optimization stratagem will be given by this command to find the parameters in the fuzzy system that will be the best to fit the data. In the first juncture, the crisp variables, spectrum utilization efficiency, speed of secondary user, distance from base station and in the fuzzification action, RSS will be transmuted into linguistic variables. The four input variables can be mapped into fuzzy altitude of fuzzy sets through fuzzification. A sigmoidal membership function has used as an activation function in this work. Center of gravity [5] method has used in defuzzification method. A typical neuro-fuzzy system is shown in Fig. 6. The rule evaluation for dynamic channel allocation scheme is shown in Fig. 7. Considering different combinations of four matrices, different outputs are generated to be trained in neuro-fuzzy system.

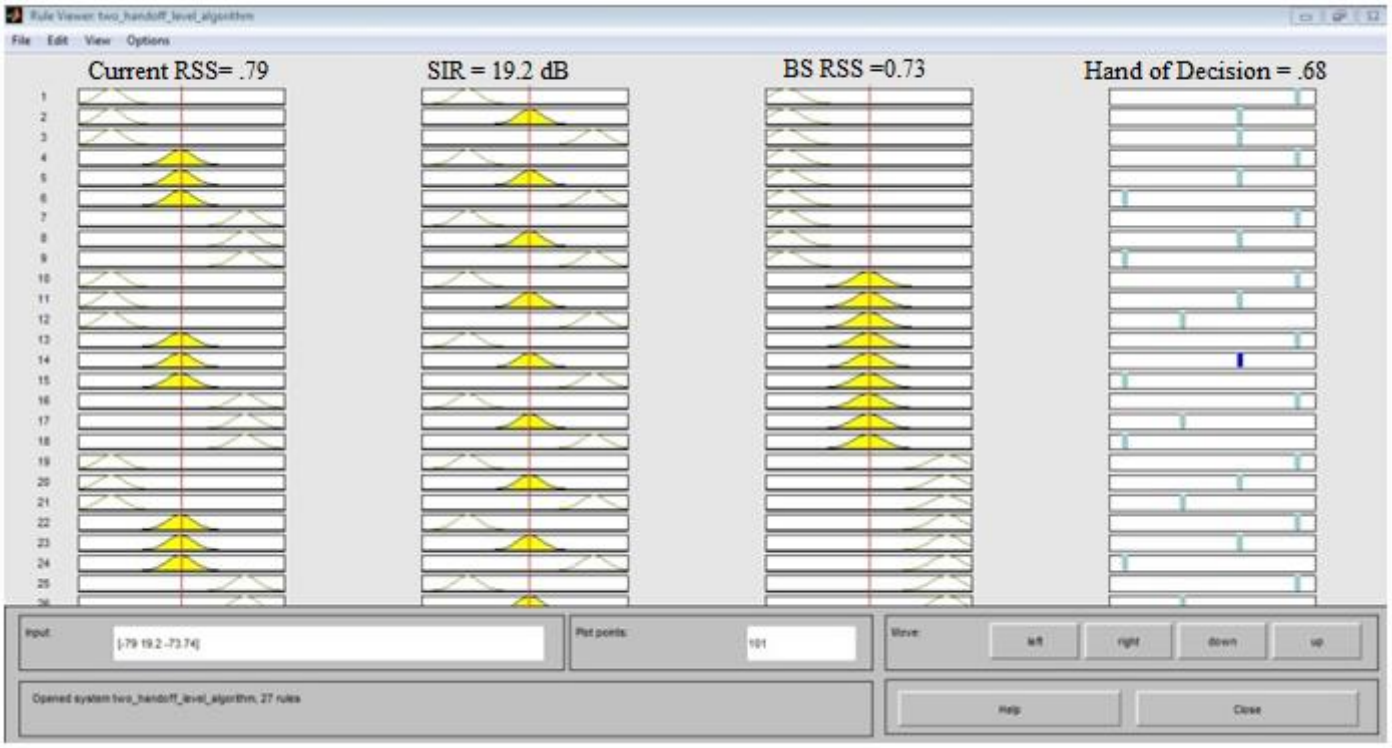

Fig. 2 Rule evaluation for determining handoff decision level

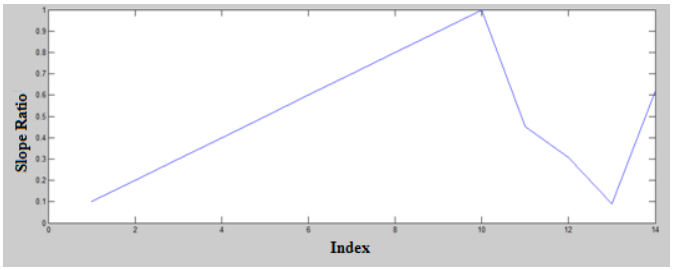

(a)

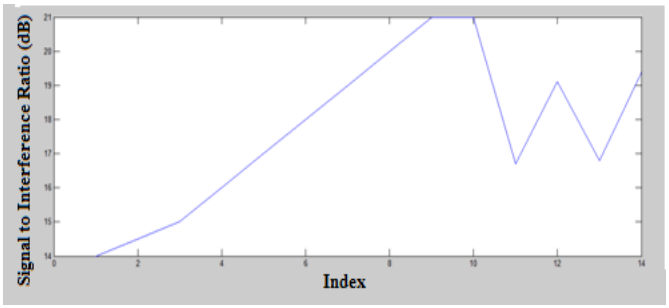

(b)

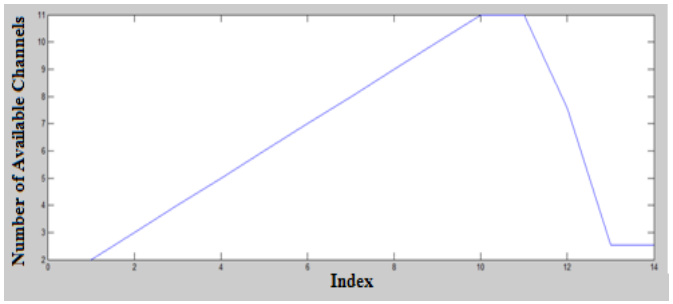

(c)

Fig. 3 Training data for Neural Networks

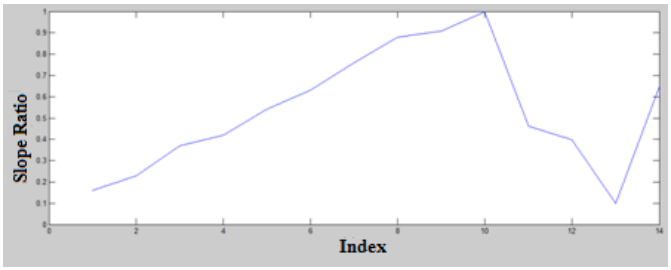

(a)

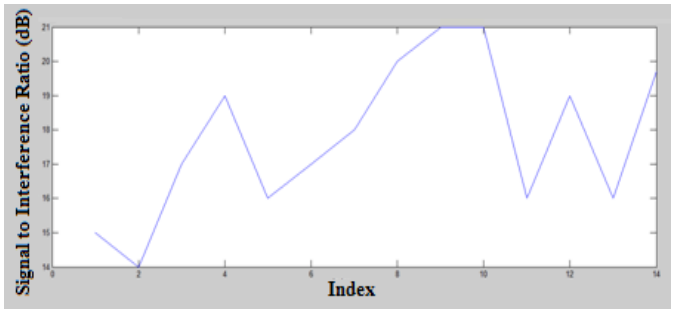

(b)

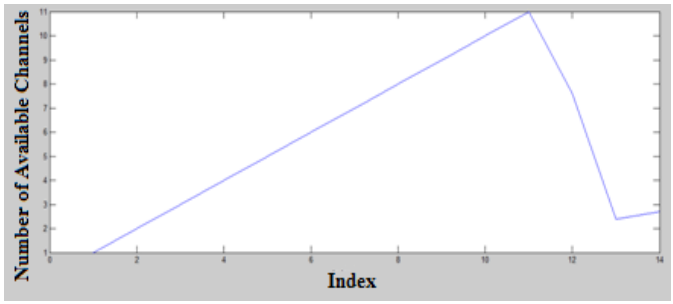

(c)

Fig. 4 Test data for neural network

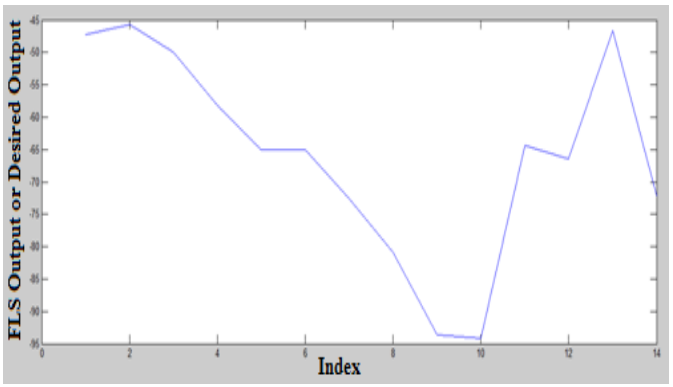

Fig. 5 FLS output or Desired Output

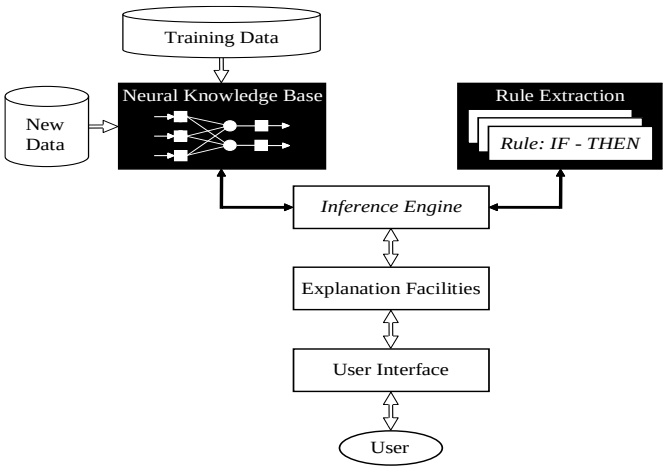

Fig. 6 Neuro-fuzzy system

Fig. 7 Rule evaluation for dynamic channel allocation

3. Results

3.1 Two handoff level algorithm based on fuzzy logic

The following alliance can be procured from the two handoff level algorithm based on fuzzy logic. As the current received signal strength decreases after a certain period, the handoff decision probability increases drastically shown in Fig. 8.

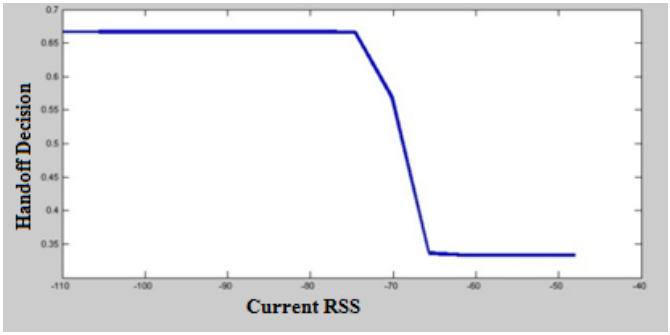

Fig. 8 Relationship between Current received signal strength and Handoff decision.

As the RSS of upcoming base station increases, the probability of switching from old BS to new BS increases shown in Fig. 9. Normally SIR drops as a function of distance. Besides due to interference, SIR can be decreased which is shown in Fig. 10. As the SIR decreases, the probability of handoff increases which switches the MSC from current BS to new BS.

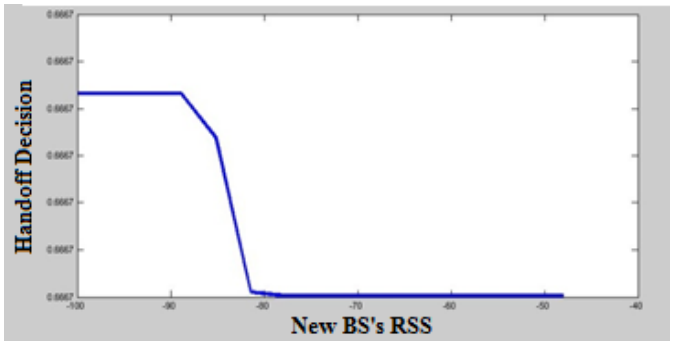

Fig. 9 Relationship between new BS received signal strength and Handoff decision.

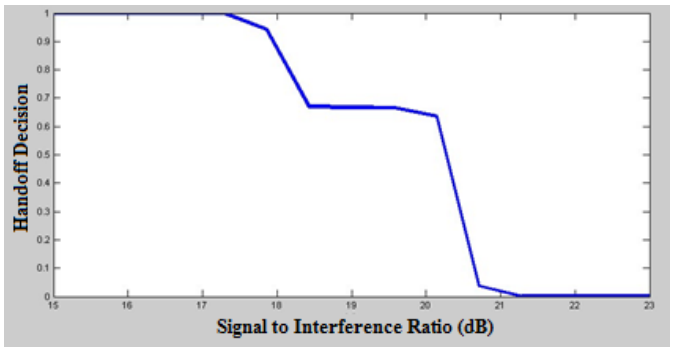

Fig. 10 Relationship between signal to interference ratio and Handoff decision.

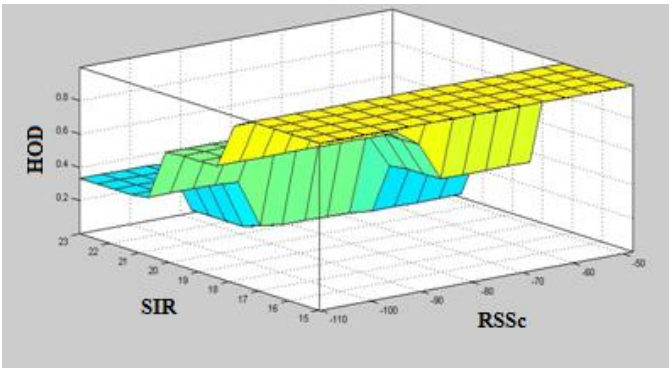

Fig. 11 Surface plot for current received signal strength and signal to interference ratio versus Handoff decision.

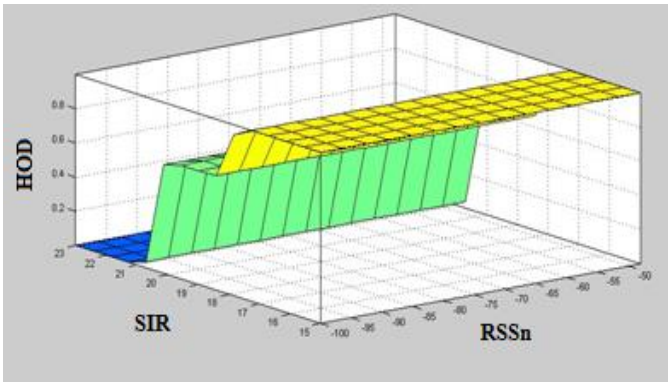

Fig. 12 Surface plot for new base station received signal strength and signal to interference ratio versus Handoff decision.

Fig. 11 represent the surface plot of handoff with respect to current RSS and SIR. As current RSS and SIR are decreasing, handoff is increasing. Fig. 12 represents the surface plot of handoff with respect to new RSS and SIR. As new RSS increases and SIR decreases, handoff increases gradually. Fig. 13 represents the surface plot of handoff with respect to new RSS and current RSS. The current RSS drops as a function of distance and after a distance the new BS RSS increases. When the new BS RSS is found greater than the old RSS, then the handoff process will be executed. When the fuzzy based two handoff level algorithm is used, the handoff decision can be properly taken and thus the channel performance and capacity is increased.

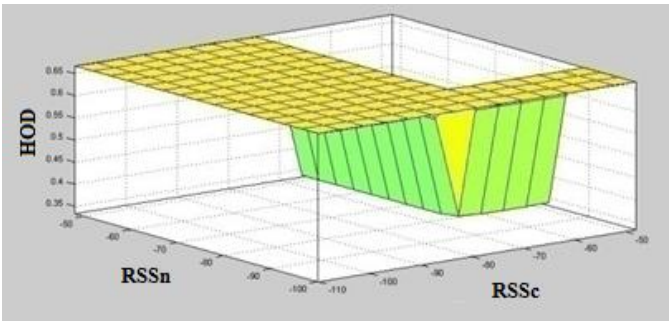

Fig. 13 Surface plot for current received signal strength and new base station received signal strength versus Handoff decision.

3.2 Artificial neural network based adaptive handoff threshold level algorithm

For different amalgamation of inputs data, the FLS output data is the desired output. Then the neural network is trained with these inputs and output. When the network is satisfactorily trained, any amalgamation of the test data will follow the desired output. The performance evaluation of actual and multi-layer protocol output is shown in Fig. 14. Blue line indicates the target or desired output, where the green line is the predicted output with 10 neurons, cyan line is the predicted output with 12 neurons, and red line is the predicted output with 15 neurons. As the number of neurons increase, the chance of getting authoritative desired output also increases with the cost of complexity. The red line is more close to the target output than the others.

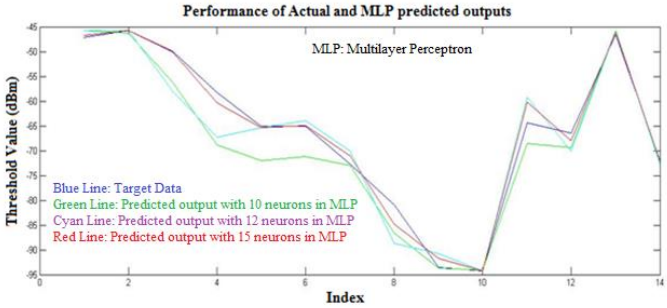

Fig. 14 Performance Evaluation of actual and MLP output.

Thus the fuzzy logic output is trained into the neural network so that the threshold level of handoff occurrence can adapt according to miscellaneous situations and gives the output close to the desired output. Thus the handoff process can be successfully accomplished. Hence the channel capacity is increased and call drop probability due to handoff is reduced. The relationship between different inputs can be discussed.

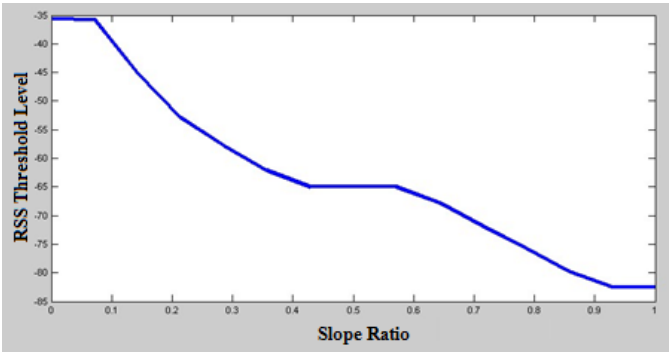

Fig. 15 Slope ratio Vs RSS threshold level

For different values of θ_1 and θ_2, the various values of slope ratio are obtained. When θ_2 is greater than θ_1, then handoff takes place. As θ_2 is decreased, the received signal strength is increased and also the slope ratio is increased which is shown in Fig. 15. As the slope ratio increases, the chance of handoff decreases which is shown in figure. So the threshold value should be set up in such a way that the no handoff can be performed unnecessarily.

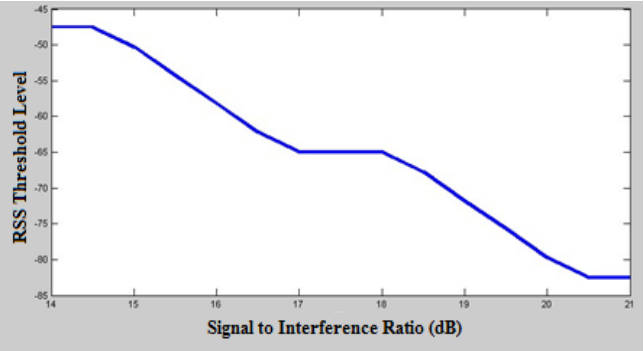

Fig. 16 SIR Vs RSS threshold level

As the signal to interference ratio is decreased, then the threshold level for handoff occurrence should be set to high value so that no call drop can be occurred. The tie-up between them is shown in Fig. 16.

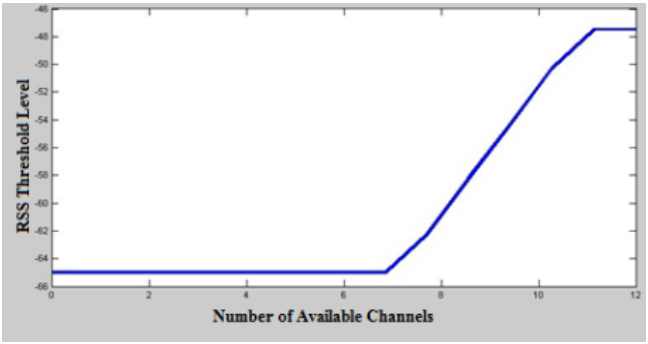

Fig. 17 Relationship between available free channels and RSS threshold level for handoff decision.

As the available free channels are decreased, then the threshold level for handoff occurrence must be set to possible lower value, so that the call can continue for the last moment without handoff as can as possible shown in Fig. 17.

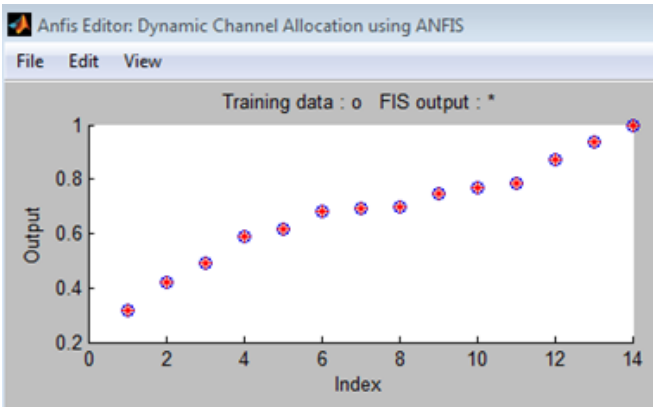

Fig. 18 Testing FIS against training data

3.3 Neuro-fuzzy based dynamic channel allocation scheme

To assemble the output of artificial neuro-fuzzy inference system that game the desired or wanted data, all the adaptable parameters have tuned. For this purpose, the learning action has been utilized. An amalgamation of learning algorithm has been adopted in such a way that the parameters of input-output membership functions can be adjusted to ameliorate the training efficiency.

The mean square error procedure has utilized to optimize the consequent parameters with keeping the antecedent parameters fixed. Then the back propagation algorithm has used to tune the surmise parameters, when the consequent parameters are updated.

When the training error result is acceptable, then the performance test of fuzzy inference system against either training, testing or checking data can be evaluated which is shown in Fig. 18 and

Fig. 19. Click test now and the following display will be seen.

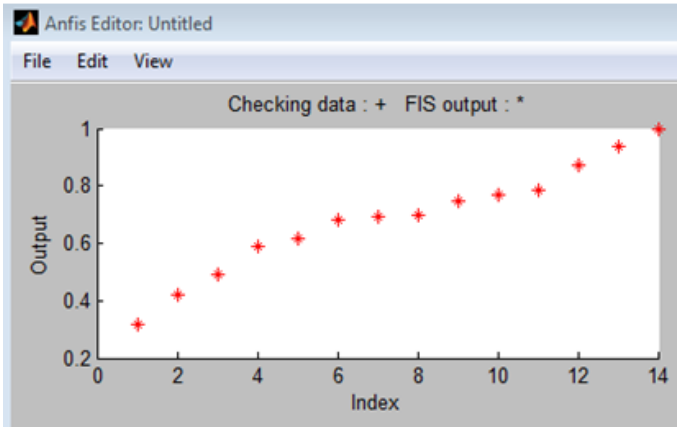

Fig. 19 Checking data

The training aids to select the quintessential rule to be fired. The relationship between the tuned parameters can be entrenched as follows:

Fig. 20 shows that as the spectrum efficiency increases, the allocation priority increases. Thus the channel can be allocated according to the user holding higher priority factor. Fig. 21 shows that when the secondary user speed is decreased, then the priority factor is increased. As the speed of secondary user increases, the ability to detect the primary user decreases. So allocation priority will be high with slow speed.

Fig. 22 shows that the closest between secondary user and primary user, the possibility of interference to primary user is greater. So allocation priority is high with far distance from base station.

Fig. 23 shows that with high received signal strength, the allocation priority is high. Thus the higher RSS value of secondary user can be allocated to new channel with high preference. Fig. 24 shows that the priority factor is higher with the higher value of spectrum efficiency and the distance. Depending on the higher priority factor, the channel can be allocated to the specific user holding high priority factor.

Fig. 25 shows that the priority factor is higher with the higher value of spectrum efficiency and the received signal strength. Depending on the higher priority factor, the channel can be assigned to the specific user. Fig. 26 shows that with smaller spectrum efficiency and faster speed, the priority factor is decreased. Unlike higher priority factor, the channel is not assigned to the specific secondary user normally.

Fig. 27 shows that with higher spectrum efficiency and slower speed, the priority factor is increased. With higher priority factor, the channel is assigned to the specific secondary user. The available channel allocation table is shown in Table 4.

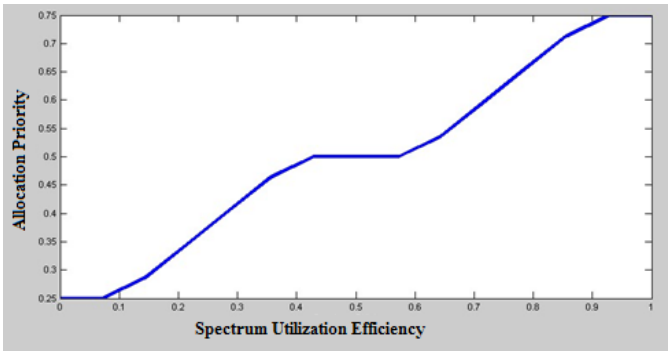

Fig. 20 Relationship between spectrum utilization efficiency and allocation priority

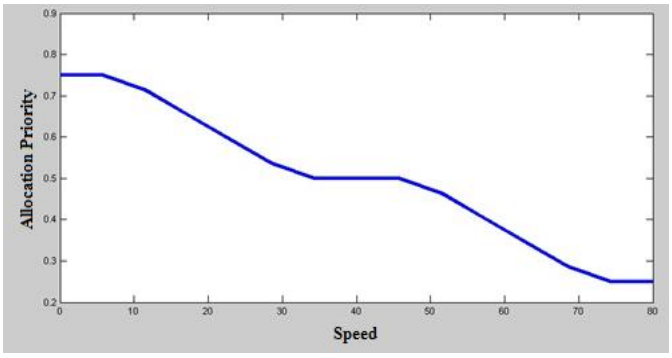

Fig. 21 Relationship between secondary user speed and allocation priority

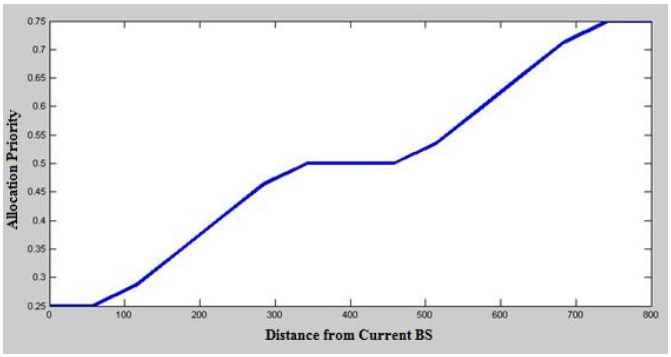

Fig. 22 Relationship between distance from BS and allocation priority

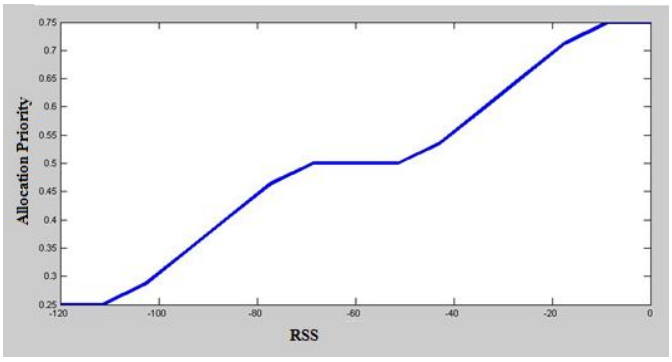

Fig. 23 Relationship between received signal strength and allocation priority

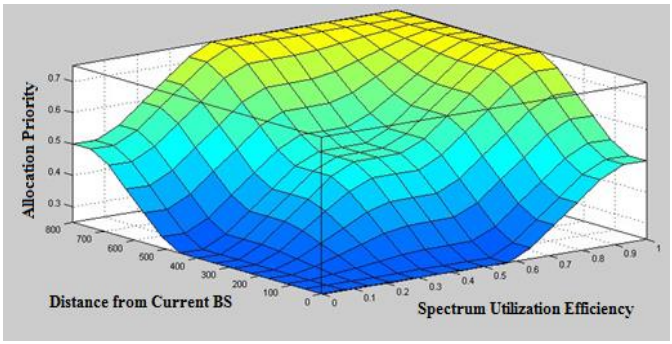

Fig. 24 Relationship between distance, spectrum efficiency and allocation priority

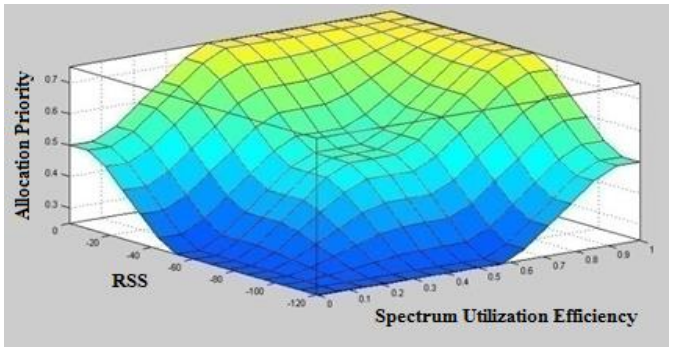

Fig. 25 Relationship between RSS, spectrum efficiency and allocation priority

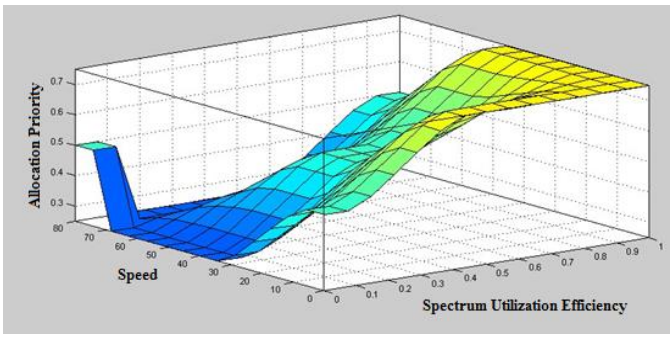

Fig. 26 Relationship between speed, spectrum efficiency and allocation priority

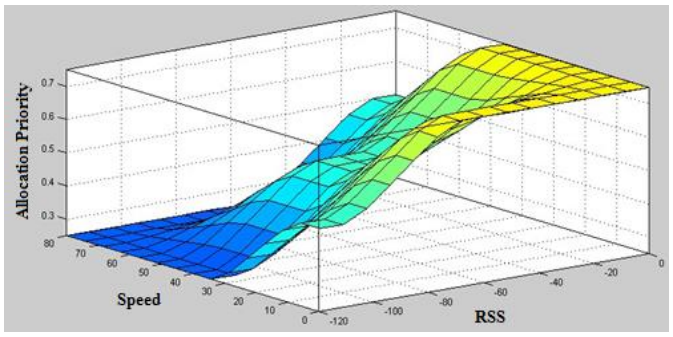

Fig. 27 Relationship between speed, RSS and allocation priority

Table 4 Channel allocation table

	Channel-1	Channel-2	Channel-3	Channel-4
SU 1	.382	0	0	….
SU 2	.769	0	.241	….
SU 3	.8558	0	.492	….
SU 4	.718	.608	0	….
….	….	….	…..	….

After calculation by fuzzy inference system, a priority factor of secondary user (SU) has generated and the channel will be allocated to the SU holding the highest priority factor. From, to use the channel, SUs contend with the priority factor generated by FIS. With the help of information existing in the channel allocation table, SU with higher priority factor will get the right to use the channel. There are four SUs shown in Table 4 and they compete for allocating channel 1, but due to high priority factor, channel 1 will be allocated to SU4 having the highest priority factor of 0.8558. The others may be concluded by the same procedure such as channel 2 will be allocated to SU2, channel 3 allocated to SU3.

3. Conclusion

In this research, handoff algorithm based on fuzzy logic and neural network have introduced that utilize the advantages of multi-criteria handoffs. With the help of well-known delicacy of handoff parameters, these handoff techniques have implemented to find out the proper decision. In two handoff level algorithm based on fuzzy logic technique, three network parameters have taken as linguistic variables of three degree of memberships such as LOW, AVERAGE and HIGH to generate output for handoff decision. Decision phase has classified into four levels such as NO, WAIT, BE-READY and YES based on the fuzzy rules inserted in the sugeno inference mechanism. In Artificial neural network based on adaptive handoff threshold level algorithm, three parameters such as slope ratio, available free channels and signal to interference ratio have taken into consideration to find the suitable point of handoffs decision. Different data sets of these parameters have used as linguistic variables and fuzzy rules have inserted to produce target outputs. Using this fuzzy model, different data sets have generated to be used as training data in neural network. Then any arbitrary level of these parameters will follow the target outputs to identify the decision point of handoffs. In dynamic channel allocation scheme using neuro-fuzzy model, four network parameters have considered such as distance from BS, MS speed, spectrum efficiency and received signal strength to determine priority factor for allocation of channels of the switching requested status of the mobile cellular network. This approach ameliorates channel capacity and signal quality in terms of quality of service and hence reduces call drop. The peril of call drops is very scathing and needs to be reconciled very soon. Other methods like Vertical handoff algorithm, BER reduction, RF optimization and Multiple Input Multiple Output antenna also evince to be worthwhile in achieving this target. In the future, the plan can be taken to flourish a systematic manner for priority based handoff mechanism using neural network.

References

[1] Bindia. Aggarwal, B. 2017. Various Handoff Strategies using Fuzzy Logic. *International Journal of Scientific Research and Management*, 5(03), pp 5199-5203.

[2] Nyambati, E.T. and Oduol, V.K., 2017. Analysis of The Impact of Fuzzy Logic Algorithm On Handover Decision in A Cellular Network. International Journal for Innovation Education and Research, 5(5), pp.46-62.

[3] Atayero, A.A. and Luka, M.K., 2012. Adaptive neuro-fuzzy inference system for dynamic load balancing in 3GPP LTE. *International Journal of Advanced Research in Artificial Intelligence*, 1(1), pp.11-16.

[4] Zeng, Q.A. and Agrawal, D.P., 2002. Handoff in wireless mobile networks. *Handbook of wireless networks and mobile computing*, 28, pp.1-25.

[5] Mir, G.M. and Shah, N.A., 2009. Decentralized Handoff for Microcellular Mobile Communication System using Fuzzy Logic. In *World Acadamy of Science, Engineering and Technology*, pp. 866-870.

[6] Garg, V., 2010. Wireless communications & networking. Elsevier.

[7] Wang, Y.H. and Liao, S.L., 2017, March. Applying a fuzzy-based dynamic channel allocation mechanism to cognitive radio networks. In 2017 *31st International Conference on Advanced Information Networking and Applications Workshops (WAINA)* (pp. 564-569). IEEE.

[8] P.Ramu. 2014. Optimized Handoff Scheme using Fuzzy Logic.Report, *Jaya Institute of Technology*, Chennai, India.

SciEn
Journal of Engineering Advancements Vol. 01(04) 2020, pp 139-143 https://doi.org/10.38032/jea.2020.04.005

Effect of Different Sewing Parameters on Lockstitch Seam Strength for Denim Fabric

Alimran Hossain[1,], Md. Rokonuzzaman[1], Md. Abu Bakar Siddiquee[1], Md. Abdullah Al Mamun[1], S. M. Farhana Iqbal[2] and Md. Azharul Islam[1]*

[1]Department of Textile Engineering, Mawlana Bhashani Science and Technology University, Tangail-1902, Bangladesh
[2]Department of Yarn Engineering, Bangladesh University of Textiles, Dhaka-1208, Bangladesh

Received: November 30, 2020, Revised: December 17, 2020, Accepted: December 18, 2020, Available Online: December 19, 2020

ABSTRACT

Seam strength plays a very important role in acquiring the desired quality seam which ultimately defines the quality of any clothing. The paper is aimed to study the strength of seam produced from denim fabric, how different sewing parameters like sewing thread type, type of seam, seam direction as well as the density of stitches influence the strength of seam, and it is observed that they have direct effect on lockstitch seam strength of denim fabric with various degree. For research denim fabric with 3/1 weaves structure and three different sewing threads namely 100% cotton spun with 14tex linear density, 100% polyester spun with 24tex and 60tex linear density were used. Seam class used for the research was superimposed seam prepared with two layers, SSa and three layers, SSb. The samples were made by stitching with lockstitch sewing machine both in warp and weft way. Three different stitch densities were used to sew the samples and they were-7, 9 and 11 stitches per inch. The strength of the produced seams was tested on a universal strength tester machine-the titan tensile strength tester. Test was performed according to ASTM D5034 test method. The outcome of the research shows that seam type, seam direction, thread types, and stitch density have direct effect on lockstitch seam strength of denim fabric with various degrees. Higher seam strength was obtained for the SSb type seam produced in warp direction with coarser sewing thread (60tex) and 11 stitches per inch (SPI). The influence of independent variables on the seam strength was assessed statistically using a multivariate variance analysis (ANOVA) with the help of SPSS software and it was found that they effect significantly. Regression analysis was done to develop the regression equation to predict lockstitch seam strength before production process.

Keywords: Denim Fabric, Seam Strength, Stitch Density, Seam Type, Stitch per Inch.

1. Introduction

Apparel manufacturing technology depends on the conversion of the fabric from two dimensional (2D) into three dimensional (3D) structures to fit human body [1]. Though there is a considerable improvement of techniques and technologies has been emerged in the apparel manufacturing, still the dominating group of methods for joining the garment elements is the sewn seams made by sewing threads [2].

The clothing industries are mainly concerned about the secondary characteristics of fabric that is the reactions of the fabric to an applied dynamic force and focus on the quality of seam at the time of fabrication and production of clothing [3],[4]. So good seams are important factors to determine clothing quality which is a big deal in today's competitive world market as quality can be seen as the synonym of excellence [5] and as a means to make differentiation of different products having perceived value [6].

On the other hand, quality of a seam can be viewed from its performance and appearance [7]. Seam performance that is, appearance, seam strength, elastic property, and durability depend on the seam type and stitch density of the seam, tension of the sewing thread and the seam efficiency of the fabric.

Seam durability can be measured through seam efficiency where seam strength is the driving factor [8]. As the standard of any garments is dependent on the quality of seam, the applied seams to make the garments have to fulfill the above mentioned criteria, among which seam strength and appearance of the seams have big importance [9], [10].

Another important matter is that the seam should have such stretchability so that the users can have free movement without breaking the seams.

In general, seam efficiency ranges between 85% and 90% but it can be optimized by optimizing seam strength considering different sewing parameters like type of seam, stitch types, stitch density, and type of sewing threads and selection of needle [12].

Rengasamy *et al.* [13] and Nayak *et al.* [14] showed the influence of types of sewing thread on the seam efficiency. Impact of linear density of sewing thread has been studied by different researchers [10],[15],[16] and it has been found that the linear density of sewing thread is one of the most influencing factors for the seam strength. Barbulov *et al.* [11] studied the impact of stitch density and of the type of sewing thread on seam strength. Akter and Khan (2015) [17] studied the influence of stitch type and sewing thread on seam strength and efficiency of the superimposed seam for cotton apparel. The effect of the different number of sewn layers was first studied by [1] Frydrych *et al.* (2016) along with other sewing parameters. Yassen (2017) [18] showed the effects of sewing thread count, sewing needle size, stitch density along with fabric characteristics on seam strength, and found that seam strength is significantly influenced by both sewing and fabric characteristics.

This research work is an attempt to investigate and show how different sewing parameters for example sewing thread, seam type, stitch density, sewn fabric layers affect seam quality in terms of seam strength as well as to develop a regression equation to predict the lockstitch seam strength for denim fabrics.

*Corresponding Author Email Address: alimrante003@gmail.com Published by: SciEn Publishing Group

2. Experimental Details

Denim fabric of 98% cotton and 2% spandex yarn, 3/1 twill was taken with the specifications given in Table 1. Sewing parameters and sewing threads properties were given in Table 2 and Table 3. A simplified flow chart of research methodology is given in Fig. 1.

Table 1 Fabric characteristics

Parameters	Unit	Value	Parameters	Unit	Value
Thickness	mm	0.52	Warp yarn count	tex	80
Surface density	g/m^2	182	Weft yarn count	tex	70
Warp breaking force	cN	1025	Warp yarn elongation at break	%	11
Weft breaking force	cN	890	Weft yarn elongation at break	%	8
Warp density (EPcm)	cm^{-1}	28	Warp yarn tenacity	cN/tex	12.81
Weft density (PPcm)	cm^{-1}	20	Weft yarn tenacity	cN/tex	12

Table 2 Selection of different sewing parameters

Sewing parameters	Expression/ Value	Elaboration
Seam class	SS	Superimposed seam *
Seam type	SSa	Superimposed seam with two layers*
	SSb	Superimposed seam with three layers*
Seam direction	Warp, Weft	Seams were prepared in warp and weft direction
Stitch density (SPI)	7, 9, 11	They are expressed as SD1, SD2 and SD3 respectively
Sewing thread	ST1, ST2, ST3	Represent sewing thread one, two and three respectively
Needle size (Metric)	100,100, 150	Corresponding sewing threads are ST1, ST2 and ST3 respectively

(* According to ASTM D 6193)

Table 3 Sewing threads properties

Parameters	Unit	ST1	ST2	ST3
Ply number	-	2	2	3
Composition	-	100% polyester Spun	100% Cotton Spun	100% polyester Spun
Linear density	tex	14	24	60
Ticket number		215	125	50
Breaking force	N	8.4	10.6	24
Elongation at break	%	17.87	7.37	46

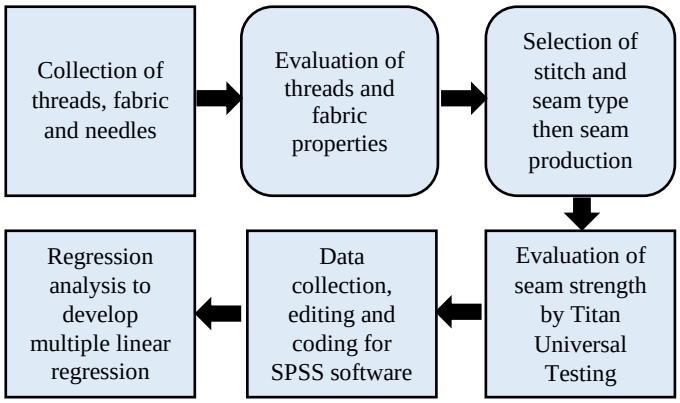

Fig. 1 Simplified research methodology

2.1 Sample Preparation

A superimposed seam class of SSa and SSb type with 25.4 mm seam allowance and according to ASTM D 6193, lockstitch class 301 were used for sewing the samples. Selection of needle size to sew the samples has been shown in the Table 2. Samples were stitched along the seam line both in warp and weft way of the fabric. The fabric was sewn with three different stitch densities to see the effect of stitch density on seam strength.

2.2 Seam strength evaluation

Grab test (ASTM D5034) as a test method was used to determine the seam strength. Samples with 350 mm length among which 150mm in one side of the seam line and 200mm on another side of the seam along with 100 mm in width which is parallel to the seam line were made as shown in Fig. 2. During the test, samples were subjected to 1% tension of the approximate breaking load. The value presented here is the average of five specimen tested consecutively.

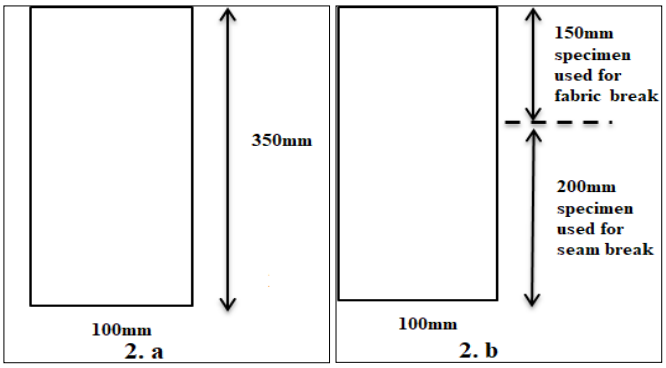

Fig. 2 Dimension of cut specimen from fabric (2.a) and Seamed specimen (2.b)

3. Results and Discussion

3.1 Effect of Seam Type on Seam Strength

Two different types of superimposed seams were made and they were SSa and SSb type seam that is they were different by their layers. Seam SSa has two layers of fabric whereas seam SSb has three layers of fabric. The graphical representation presented in Fig. 4(c) shows that there is noticeable difference in seam strength with the increase of layers of fabric in the seam and this can also be understood from the variance analysis presented in Table 4. It is also found that seam strength gets increased as the increase of fabric layers for all kind of sewing parameters that is seam direction, sewing thread and stitch density [see Fig. 3].

The fact is that, an increase in fabric layer increases contact points number between fabric yarns and sewing threads, as a result a tighter surface is obtained. Thus, the distribution of tensile forces will take place over a larger number of points and the resistance will be higher.

3.2 Effect of Seam Direction on Seam Strength

Though warp seam strength was higher than that of weft in most of the cases, in some cases, warp and weft seam strength were found equal [see Fig. 3]. From the Fig. 4(d), it is obvious that direction of seam has significant effect on strength of the seam of the sewn fabrics. The fact can be supposed that the lower seam strength of the fabric can result from the lesser number of intersection points between sewing thread and yarns of the fabric.

3.3 Effect of Sewing Thread on Seam Strength

It is an established truth that the higher the strength of sewing threads the higher the seam strength of the sewn fabrics. This is because, the strength of the sewing threads adds the strength to the seam sewn by the threads. This study also reveals the same result and supports the results of many other researchers [19],[20]. From the correlation analysis it is found that there is very strong correlation between sewing thread linear density and seam strength [see Table 4]. The effect of sewing threads on seam strength has been presented graphically in Fig. 4. a. The effect of sewing threads varying other sewing parameters has been represented in the Fig. 3 and it is found that seam strength always gets increased as the increase of sewing thread size for all kind of sewing parameters that is seam direction, fabric layers and stitch density. The fact is that the coarser sewing thread contains more number of fibres resulting in high seam strength.

3.4 Effect of Stitch Density on Seam Strength

The effect of stitch density on the strength of the lockstitch seam is found very prominent (see Fig. 4(b)) and it is found as the second most influential factor of seam strength; statistical analysis also reports the same issue (see Table 4). It has also been found that with the increase of stitch density the seam strength also increases and the effect is obvious for all kind of other sewing parameters like seam type, seam direction, sewing thread types (see Fig. 3). In fact, with the increase of stitch density the number of loops per unit length of the fabric increases; therefore, the higher force is required to deform such a seam.

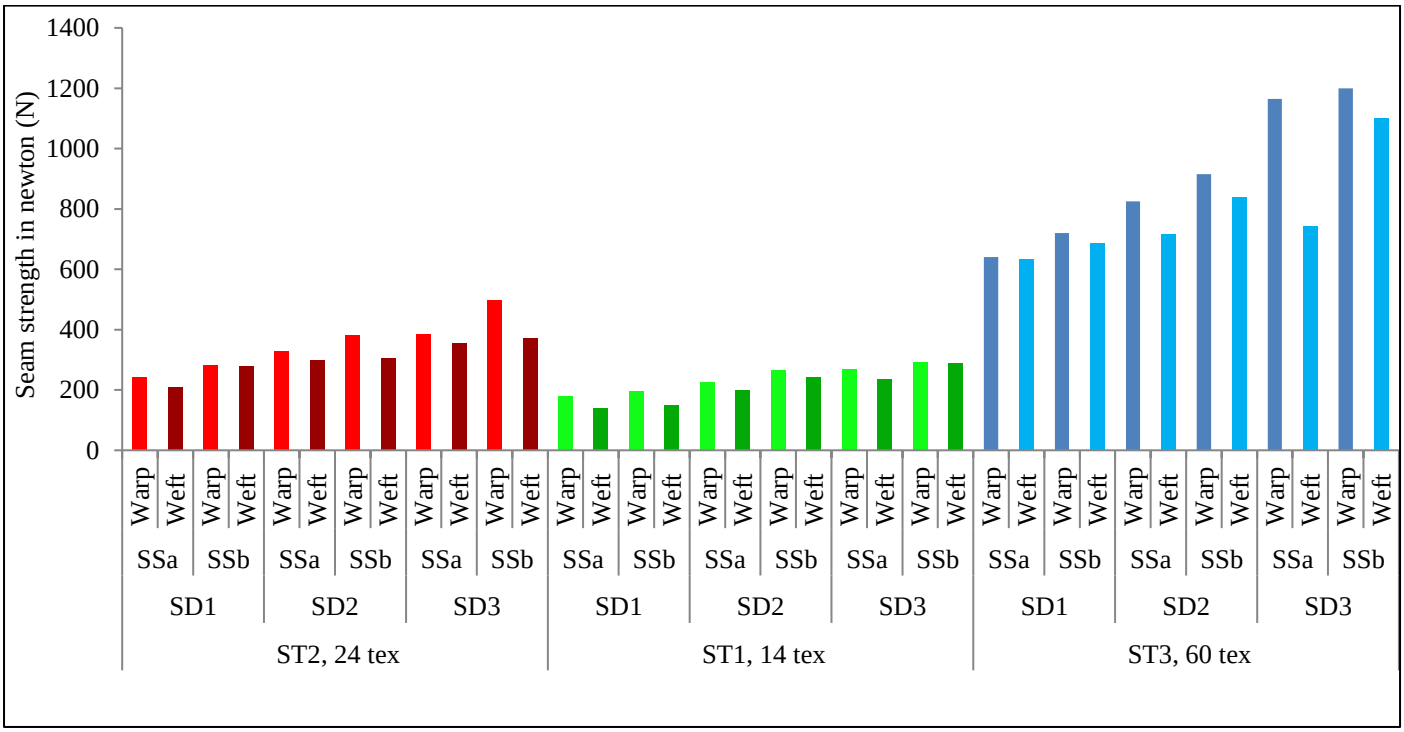

Fig. 3 Effect of seam type, seam direction, sewing thread, and stitch density on seam strength

Table 4 Correlation analysis of different parameters

Correlations					
Variables	Seam strength	Sewing Thread	Stitch Density	Seam type	Seam direction
Seam strength	1	0.851**	0.289	0.113	-0.113
Sewing Thread	0.851**	1	0	0	0
Stitch Density	0.289	0	1	0	0
Seam type	0.113	0	0	1	0
Seam direction	-0.113	0	0	0	1

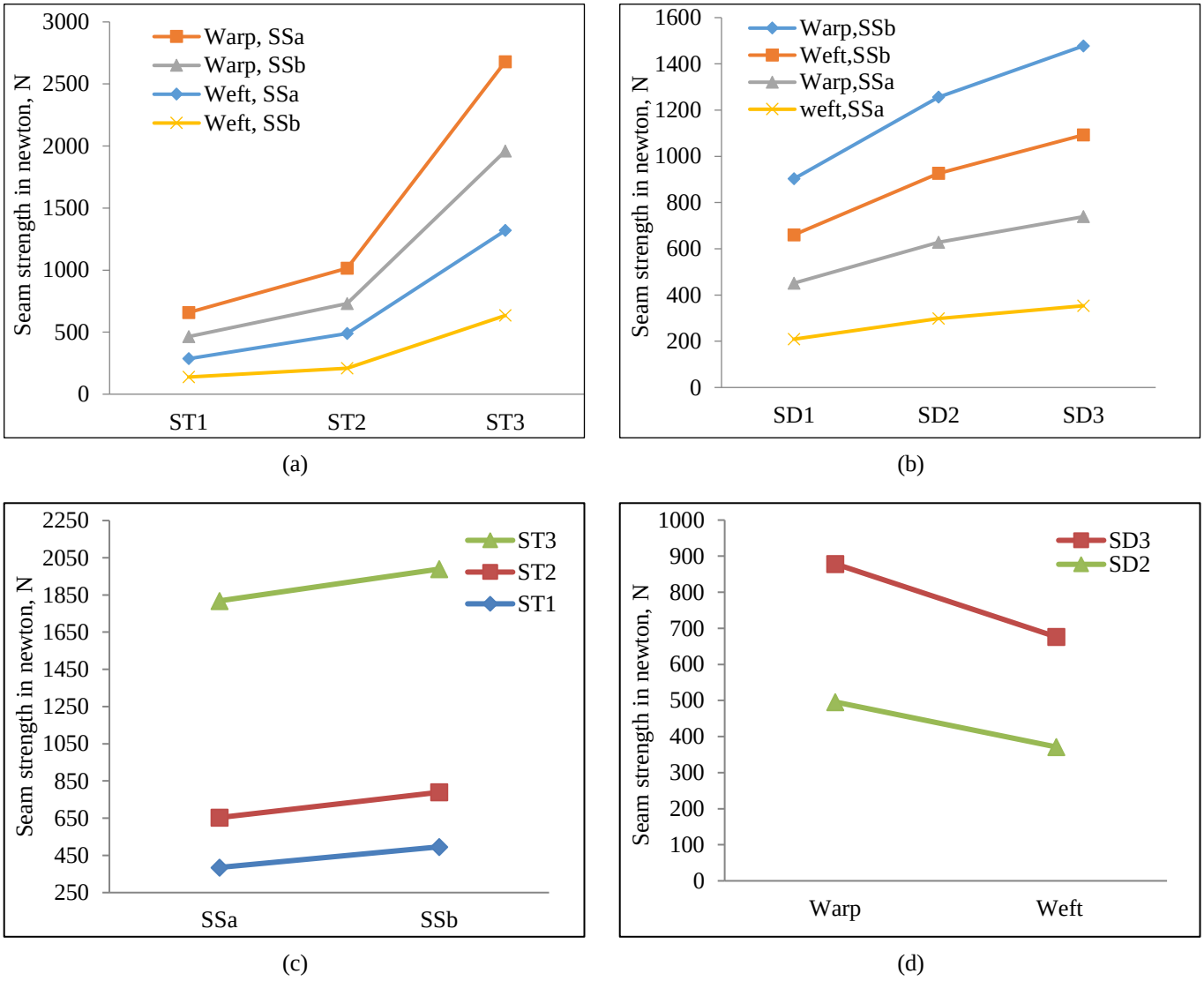

Fig. 4 Seam strength for various (a) seam type & (b) stich density and (c) seam type & (d) seam direction

3.5 Regression Analysis to Develop Regression Equation

The regression equation is given below:

$$\text{Seam strength} = -568.318 + 312.742 \times \text{Sewing Thread} + 53.029 \times \text{Stitch Density} + 68.011 \times \text{Seam type} - 67.996 \times \text{Seam direction} \quad (1)$$

Table 5 Regression model summary

R	R^2	Adjusted R^2	Std. Error	Sig.
.913[a]	.833	.812	131.9538486	.000

a Predictors: (Constant), Seam direction, Seam type, Stitch Density, Sewing Thread, Stitch Type

As in the Table 5, the R^2 value is 83.3% which indicates the prediction level of the model. The R^2 value also denotes that 83.3% of the changes in seam strength (dependent variables) can be explained by independent variables in the model. According to the results of ANOVA test presented in Table 6, it is found that the relation between dependent and independent variables was significant at 99% significance level as the significance value was found as $p < 0.01$**.** The regression equation (equation 1) given above was made with the coefficients obtained by the analysis in this study. The regression equation will help to predict seam strength when the other independent variables are known before the production process.

Table 6 Regression analysis, ANOVA[a]

Model	Sum of Squares	df	Mean Square	F	Sig.
Regression	2700578.351	4	675144.59	38.78	0[b]
Residual	539766.363	31	17411.82		
Total	3240344.714	35			

a. Dependent Variable: Seam strength
b. Predictors: (Constant), Seam direction, Seam type, Stitch Density, Sewing Thread

4. CONCLUSION

The outcome of the research shows that the studied sewing parameters affect the strength of lockstitch seam significantly. There is slight increase in seam strength as the layers of the fabric increased. Though seam strength is found higher with the coarser sewing threads and with the higher stitch densities, these two

factors should be selected in such a way so that the seam quality remains satisfactory because some samples were found with slipped seam at eleven stitches per inch; this may denote the unsuitability of eleven stitches per inch for the fabric. The effect of seam direction was more visible for the sewing thread three, ST3 (60 Tex). Prediction of seam quality before seam production is the most important issue for the manufacturers. And for this reason, regression model has been developed that will allow the producers to predict seam strength from given input parameters. The outcome of the work can be more generalized by including kind of fabrics as an independent variable and by producing seams with other stitches that are commonly used for denim fabrics.

REFERENCES

[1] Frydrych, I. and Greszta, A., 2016. Analysis of lockstitch seam strength and its efficiency. *International Journal of Clothing Science and Technology*, 28(4), pp.480-491.

[2] Abdul Ghani, S., 2011. Seam performance: Analysis and Modelling (Doctoral dissertation, University of Manchester).

[3] Tyler, D.J. ed., 2009. Carr and Latham's technology of clothing manufacture. *John Wiley & Sons*.

[4] B. K. Behera and S. Sharma, 1998. Low-stress behaviour and sewability of suiting and shirting fabrics, *Indian Journal of Fibre and Textile Research*, 23, pp. 233–241.

[5] Merkel, R.S., 1991. Textile product serviceability. *Macmillan*.

[6] Glock, R.E. and Kunz, G.I., 2005. Apparel manufacturing: Sewn product analysis (p. 345). Upper Saddle River, NJ: Pearson/Prentice Hall.

[7] Azam, M. S., Saleh, M. A., Nafiz, K., 2009, An introductory knowledge about garments manufacturing technology, Dhaka, Bangladesh: *Books Fair Publications*, Page No.155.

[8] Ukponmwan, J.O., Mukhopadhyay, A. and Chatterjee, K.N., 2000. Sewing threads. *Textile progress*, 30(3-4), pp.1-91.

[9] Bharani, M., Shiyamaladevi, P.S.S. and Mahendra Gowda, R.V., 2012. Characterization of seam strength and seam slippage on cotton fabric with woven structures and finish. *Research journal of engineering sciences*, 1(2), pp.41-50.

[10] Choudhary, A.K. and Goel, A., 2013. Effect of some fabric and sewing conditions on apparel seam characteristics. *Journal of Textiles*, 2013. pp. 1-7.

[11] Barbulov–Popov, D., Cirkovic, N. and Stepanović, J., 2012. The influence of stitch density and of the type of sewing thread on seam strength. *Tem Journal*, 1(2), pp.104-110.

[12] Solinger, J., 1980, Apparel Manufacturing Handbook, Newyork, USA: *Van Nostrand Reinhold Company*, pp. 168.

[13] Rengasamy, R.S., Kothari, V.K., Alagirusamy, R. and Modi, S., 2003. Studies on air-jet textured sewing threads. *Indian Journal of Fibre & Textile Research*, 28, pp. 281-287

[14] Nayak, R., Padhye, R., Dhamija, S. and Kumar, V., 2013. Sewability of air-jet textured sewing threads in denim. *Journal of Textile and Apparel Technology and Management* (JTATM), 8(1), pp.1-11.

[15] Zervent Ünal, B., 2012. The prediction of seam strength of denim fabrics with mathematical equations. *Journal of The Textile Institute*, 103(7), pp.744-751.

[16] Sarhan, T.M.A., 2013. Interaction between sewing thread size and stitch density and its effects on the seam quality of wool fabrics. *Journal of Applied Sciences Research*, 9(8), pp.4548-4557.

[17] Akter, M. and Khan, M.R., 2015. The effect of stitch types and sewing thread types on seam strength for cotton apparel. *International Journal of Scientific & Engineering Research*, 6(7), pp.198-205.

[18] Yassen, H.A., 2017. Study of the Relationship between sewing and fabric Parameters and Seam Strength. *International Design Journal*, 7(2), pp.125-129.

[19] Rajput, B., Kakde, M., Gulhane, S., Mohite, S. and Raichurkar, P.P., 2018. Effect of sewing parameters on seam strength and seam efficiency. *Trends in Textile Engineering and Fashion Technology*, 4 (1), pp.4-5.

[20] Regar, M.L., Sinha, S.K. and Choubisa, B., 2018. Eli-Twist sewing thread–an alternative to conventional thread. *Research Journal of Textile and Apparel*, 22 (2), pp.126-137.

SciEn
Journal of Engineering Advancements Vol. 01(04) 2020, pp 144-149 https://doi.org/10.38032/jea.2020.04.006

Mechanical Behaviors of Al-Based Metal Composites Fabricated by Stir Casting Technique

Mostafizur Rahman and Sadnan Mohosin Mondol*

Department of Mechanical Engineering, Chittagong University of Engineering & Technology, Chattogram-4349, Bangladesh

Received: December 02, 2020, Revised: December 17, 2020, Accepted: December 18, 2020, Available Online: December 20, 2020

ABSTRACT

Recently, the demands of composite materials used in various engineering applications are growing higher because of their outstanding mechanical and thermal properties. This study represents an experimental investigation to determine mechanical properties of Al-based composites materials using Cu and SiC as reinforcement. Al-30-wt%-Cu, Al-40-wt%-Cu, Al-30-wt%-SiC, and Al-40-wt%-SiC composite bars were fabricated using stir casting process to ensure uniform distribution of reinforced elements. The composite bars were prepared into required shape to conduct test for evaluating mechanical properties. Al-40-wt%-Cu shows improved properties such as, hardness, strength, and impact energy absorption than Al-30-wt%-Cu due to more presence of Cu content. Al-30-wt%-Cu and Al-40-wt%-Cu bars showed improved mechanical properties than both Al-30-wt%-SiC and Al-40-wt%-SiC. It is also seen that Al-30-wt%-Cu and Al-40-wt%-Cu showed high hardness, yield strength, and impact energy absorption compared to Al-30-wt%-SiC and Al-40-wt%-Cu respectively. On the other hand, Al-30-wt%-Cu is 3.5% lightweight than Al-30-wt%-SiC and Al-40-wt%-Cu is 2.11% lightweight than Al-40-wt%-SiC. Al-30-wt%-Cu and Al-40-wt%-Cu showed improved specific hardness, specific yield strength, and specific impact energy absorption compared to Al-30-wt%-SiC and Al-40-wt%-Cu respectively. In addition, Al-40-wt%-Cu showed better mechanical properties among the bars.

Keywords: Metal matrix composites; Reinforcement; Stir Casting; Hardness; Strength; Impact Energy.

1. Introduction

Modern arena is moving forward positively by remarkable changes, inventions, and innovations in materials development with the advancement of science and technology. Like, many great attempts and researches have been carried out in order to improve mechanical and thermal behaviors of materials [1]. Many studies were performed to accomplish the growing needs of light-weight materials with outstanding performance in automotive, aviation, naval, shipbuilding, sports goods, bio-medical equipment, prime movers, micro structure, and space industries. Composite metals have been attracted by the researchers and metallurgists to replace conventional materials for their improved mechanical and tribological behaviors such as, high strength to weight ratio, tensile and compressive behaviors, hardness, stiffness, durability, yield strength, density, low thermal expansion coefficient, counteraction to corrosion, thermal diffusivity, and good resistance to wear [2]. Composite materials consist of two or more than two macro, micro, and nano sized particles differing in physical formation and chemical composition in a suitably made mixtures to achieve required properties [3]. It is known to all that two or more materials are combined together to make composites given that all materials possessing different mechanical and chemical characteristics. It produces an individual material which differs from the properties of parent components when they are combined. In composites, reinforcement particle is usually the load carrying particle and matrix is the weaker phase.

Reinforcement gives high strength, stiffness and rigidity which helps to support externally applied load of any engineering structure. The organic or inorganic matrices or binders keep up the position and bearing of reinforcements accordingly [4]. In addition, the reinforced particles improve stiffness and strength of products which develops huge structural load carrying capacity. Composite materials are categorized into three such as, metal matrix composites (MMC), polymer matrix composites (PMC), and ceramic matrix composites (CMC) according to the chemical nature [5]. Recently, metal composites have drawn huge interests of the researchers and metallurgists because of their physical, mechanical, electrical, and tribological behaviors. In addition, automotive, automation, and aerospace industries are searching for advanced functional light materials to meet the requirements which is leading to speedy advancement of MMC's. Pure aluminium and its various alloys are used as matrix phase whereas, different non-metallic and metallic elements such as, Copper, silicon carbide, aluminium oxide, and sulphar dioxide are used as reinforcement in Aluminium metal composites (AMC) [6]. It is noted that the reinforcements are added with parent materials according to different composition to improve mechanical behaviors like hardness, impact energy absorption, stiffness, and strength of materials to meet requirements. Composite materials made from aluminium alloys with various reinforcements are widely used in many sophisticated engineering applications because of their outstanding properties as compared to others. [7]. AMC's are fabricated by varying proportion of reinforced particles and chemical composition of Aluminium and tested experimentally to get clear indication about changing of properties. For this consequences, Laplanche et al. [8] studied microstructures and mechanical behaviors of Al-based composite materials using Cu–Fe particles as reinforced at different composition and, Sohn et al. [9] experimented on Al–Cu based dendrite-ultrafine

*Corresponding Author Email Address: rmostafiz31@gmail.com

composites to analyze mechanically and micro-structurally. Kim et al. [10] fabricated a hierarchical multi-phase composites using Al-Ni based intermetallic compounds in the Al-Cu-Si-Ni alloy system also studied microstructural condition and mechanical behaviors. Viswanath et al. [11] investigated mechanical and creep behaviors of AZ91-SiCp composites fabricated by stir casting. Steinman et al. [12] studied experimentally and theoretically Al-based composite materials using its different grade alloys as reinforcements. AMC's are fabricated and produced in cost effectively and its applications are expanding rapidly due to cost effective manufacturing process. On the contrary, titanium shows better properties compared to other technological metals but it is rarely used in fabricating composites because of its high price and low tribological properties.

Huang et al. [13] suggested to use Al metal composites instead of Fe, Mg, Ni, and Cr because of their comparative mechanical and chemical properties. Al-Cu and Al-SiC was selected in this study considering the above reasons. Researchers and metallurgists suggest many fabrication techniques of composites using different matrix and reinforcement. Fabrication of metal composites are categorized into five such as, liquid-liquid phasing, liquid-solid phasing, solid-liquid phasing, deposition techniques, and suit processing according to type of mixture and processing temperature [14]. It is noted that stir casting is one of the simplest and most economical methods for fabrication of composite materials except some technical difficulties. Gopalakrishnan et al. [15] studied of making and wear analysis of composites using AA 6061 graded titanium carbide as reinforcement particulates by enhanced stir casting method. Raghuvaran et al. [16] investigated mechanical behaviors of Al7075-SiC composites prepared by using stir casting technique and Vairamuthu et al. [17] studied the effects of some processing parameters such as, pressure, temperature, stirring speed and rpm in synthesized copper composites fabricated by stir casting technique. Authors represented improved mechanical, thermal, and chemical properties of composites materials rather than conventional materials in two-step and three-step stir casting method. With the author's best knowledge and experience from this study, fabrication cost is reduced to about one-third for making of composites by stir casting method for high volume production compared with other conventional method. Stir casting technique was utilized to fabricate Al-Cu and Al-SiC composite bars varying weight percentage of reinforcements. This study aims to evaluate mechanical properties namely hardness, yield strength, tensile strength, microstructure, impact energy absorption of Al-Cu and Al-SiC composite bars so that this composites can be used in different emerging applications.

2. Stir Casting Technology

Recently, many promising techniques have been developed to fabricate metal composites using various particulate as reinforcement. This fabrication techniques are varied considerably depending on the type of reinforcement such as, powder metallurgy, spray decomposition, squeeze casting, liquid metal infiltration, and stir casting method etc. [18]. It is worthy to mention that stir casting process among the above mentioned techniques is used in fabricating metal composites due to its simple mechanism, flexibility, most economical route, high production rate, and low processing cost [19]. Usually, mother metals are heated above its melting point and particulate reinforcements are suffused into it by stirring which is a principal element of this process. It is noted that mixing strength, solidification rate, density difference, and wetting condition of given particles lead to proper distribution of particles in final mixture composites [20]. In addition, melting temperature, properties of the particulates added, mechanical stirrer's geometry, and placement of stirrer in the mixture determine the homogeneous distribution of particles in molten matrix. Due to technological advancement, double stir casting process can be termed as two-step mixing of final mixture, is being used in industry level to fabricate metal composites for using in different sectors [21]. In double stir casting process, the parent materials are heated above its melting temperature and kept them to cool down at temperature which is called liquidus and solidus point of semi-solid state. The preheated reinforced elements are added and mixed with parent materials at this point. After that, they are mixed thoroughly and the mixture is heated until a perfect liquid state is obtained. Surprisingly, the microstructures of composites are found to be more homogeneous in double stir casting process as compared with conventional stir casting. Double stir casting process has the capacity to break down gas layer remaining on particle's surface which can cause wetting condition between the particulates and molten metals that is the potential of this method. In addition, abrasive action of the particles due to their high melting viscosity is also responsible for breaking the gas layer at the time of mixing of particulates with parent materials in the semi-solid condition. Authors also designed and developed a triple-step stir casting process to fabricate and produce nano particles reinforced composites [21]. In this study, initially weighted Al bar was placed in the muffle furnace (Sante Furnace, STM-38-14-19) having a pot type crucible before completely melting. The furnace temperature was increased to around 700°C and kept at this condition about one and a half hour until Al bar melts completely. Afterward, copper powder were heated at around 820°C and almost, the same temperature was maintained until copper completely melts. 30-wt%-Cu powder which was used as reinforcement is preheated separately using muffle type furnace around 200°C about 30 minutes. The molten 30-wt%-Cu powder was poured into pure molten Al slowly. They were mixed thoroughly at 750°C until a perfect liquid state was obtained. Stirring operation was performed by a stirring rod for homogeneous distribution of 30-wt%-Cu particles into molten Al metal and continued about one minute. Temperature of Al-Cu mixture was maintained around 750°C for about 30 minutes after stirring. Dies were made of as desired shapes where Al-Cu composites were poured and kept aside before they are completely solidified. The production method of 40-wt%-Cu composites is same as 30-wt%-Cu composites. Similarly, SiC powder was taken as reinforcement and was heated in atmospheric pressure at 850°C for two hours. It was showered into the molten pure Al by fixed rate at around 800°C. SiC particles were heat treated so that they can form layer of silicon oxide on silicon carbide which fosters the placement of the SiC with Al. 30-wt%-SiC powder and 40-wt%-SiC which is used as reinforcement is preheated separately at atmospheric pressure around 200°C about 30 minutes and the 30-wt%-SiC, 40-wt%-SiC was poured into molten pure Al metal slowly. A total of five metal composites bar of each composition were produced for testing purpose in order to evaluate mechanical behaviors. Average value from five specimens of each composite bar was reported in case of density, hardness, yield strength, and impact energy absorption.

3. Experimental Procedure

3.1 Hardness Test

Brinell's hardness test was carried out by following ASTM A370 standard at room temperature. The specimens were machined from casted components having dimension of 40 mm × 40 mm× 5 mm. Hardness test was conducted in a standard Brinell hardness tester (HSM51, P. A. HILTON) with an equivalent constant load of 9.81 KN (1000kg). Ball diameter of the Brinell hardness testing machine was 10 mm.

3.2 Tensile Test

Tensile test was performed with ASTM A370 standard at room temperature. Samples of diameter 10 mm and length of 50 mm were tested in UTM (S12TO2, CNTROLS, Crosshead speed: 0.001-1000 mm/min) in order to perform tensile test. Crosshead speed ranging from about 10-30 mm/min was used in testing the fabricated composite bars. Five samples of each Al-30-wt%-Cu, Al-40-wt%-Cu, Al-30-wt%-SiC, and Al-40-wt%-SiC bars were tested to determine how much tensile strength is increased or decreased.

3.3 Density Test

50 mm×50 mm×10mm sized samples were weighted in a digital weight testing machine for measuring density.

3.4 Microstructure Test

The samples were polished properly using emery paper of grades starting from 280, 360, 500, and 1000 and followed by wafer polishing carried out by infixing silica gel with water. Finally, samples were undergone to etch using hydrochloric acid with distilled water by electrolytic methods. The microstructures of the specimens were analyzed by an optical microscope (Optu-Edu, A13.2602-B, and Magnification: 100 x 400 x 1000x).

3.5 Impact Test

Charpy impact test was conducted to determine amount of absorbed impact energy during deformation. Hence, this absorbed energy indicates the measure of toughness in the samples which acts as a tool to study temperature depended brittle-ductile transition. Composites bars were shaped into 55 mm×10 mm×7.5mm size to fit with Charpy impact test machine. Free fall angle α=67.5°, length of the hammer, R=0.345m, mass of the hammer, W=2.5 kg, impact angle, β=62° for all composites was measured in the Charpy impact testing machine (HSM41, Hi-Tech Education).

4. Results and Discussion

Fig. 1 shows variation of hardness for all composites bar after addition of reinforcement. Al-40-wt%-Cu shows about 4.34% greater hardness than Al-30-wt%-Cu whereas, Al-40-wt%-SiC gives 4.6% greater hardness than Al-30-wt%-SiC due to addition of Cu and SiC as reinforcements. It is noted that Al-30-wt%-Cu shows 16.6% more hardness than Al-30-wt%-SiC and Al-40-wt%-Cu shows 16.4% more than Al-40-wt%-SiC. Although Kumar et al. [22] studied silicon nitride, authors showed the increase of hardness with addition of reinforcement and percentage of increment was about 20%. This increment validates the theoretical background of composite materials. Kennedy et al. [23] mentioned hardness increases with density. However, it is contradictory in this study. It is shown from Fig. 2 that Al-30-wt%-SiC provides 3.5% greater density than Al-30-wt%-Cu. On the contrary, Al-40-wt%-SiC shows 2.11% greater density than Al-40-wt%-Cu. However, low density composite materials would be useful in application because of their lightweight. Hence, Al-Cu composites are giving better properties than Al-SiC in this study.

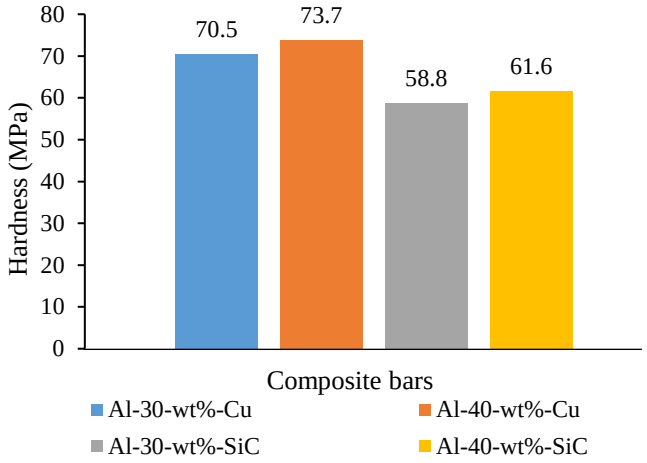

Fig. 1 Comparison of average hardness among the composite bars

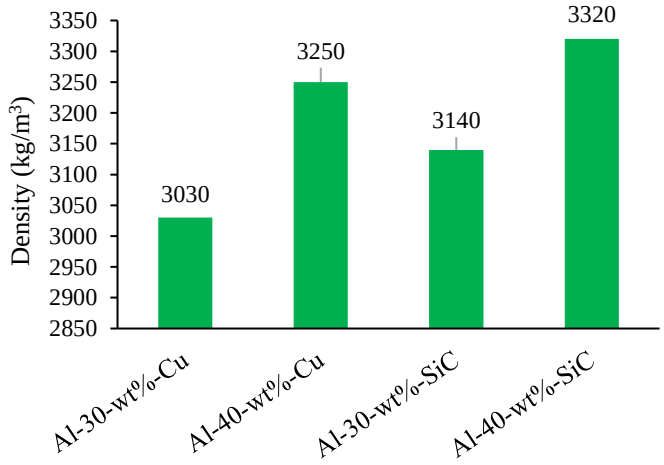

Fig. 2 Comparison of average density among the composite bars

In addition, specific hardness is another important property of composite metals. Specific hardness of all composite bars is shown in Fig. 3. Al-40-wt%-Cu shows highest specific hardness among the composite bars and it can be concluded that Al-40-wt%-Cu is the best composite among the fabricated bars in this study.

Tensile stress is gradually increased for all composites with strain for enhancement of higher reinforcement particles as shown in Fig. 4 and Fig. 5. In addition, increasing copper content with Al-30-wt%-Cu and SiC with Al-30-wt%-SiC composites results in the building of successive emollient between matrixes by the copper and silicon carbide particles [24]. Hence, it can be easily concluded that alloy creation, reinforcement, and good combination results in improving strength of metal composites. Raviraj et al. [25] reported that reinforcement enhances strengthening but the formability of the matrix reduces gradually; resulting in a lower level of strain.

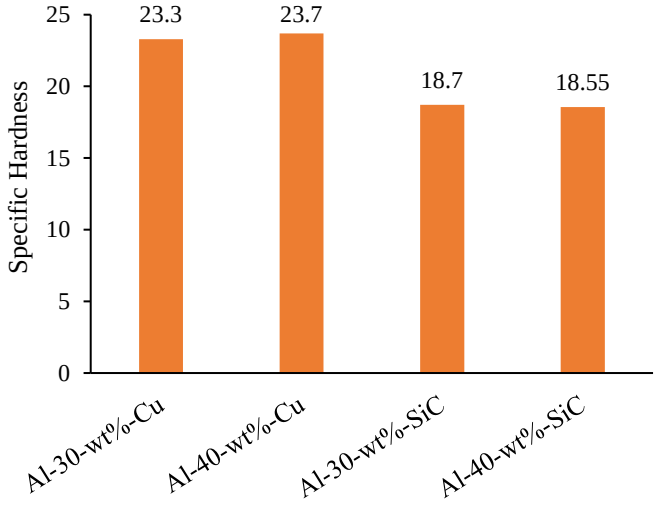

Fig. 3 Comparison of specific hardness among the composite bars

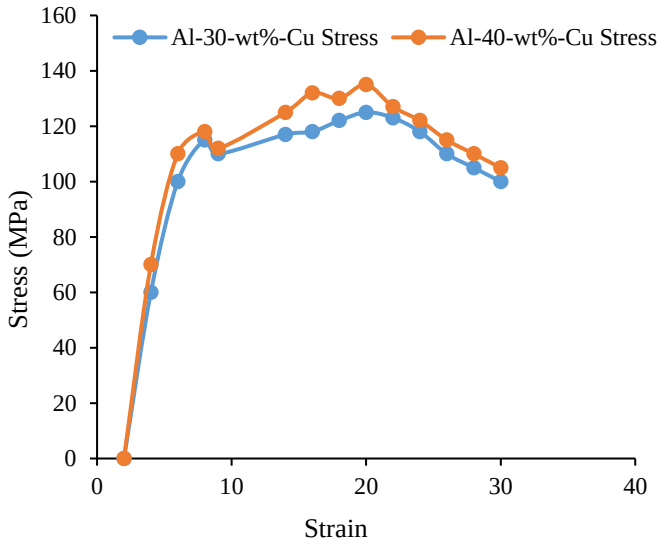

Fig. 4 Stress vs strain curve for Al-Cu composite bars

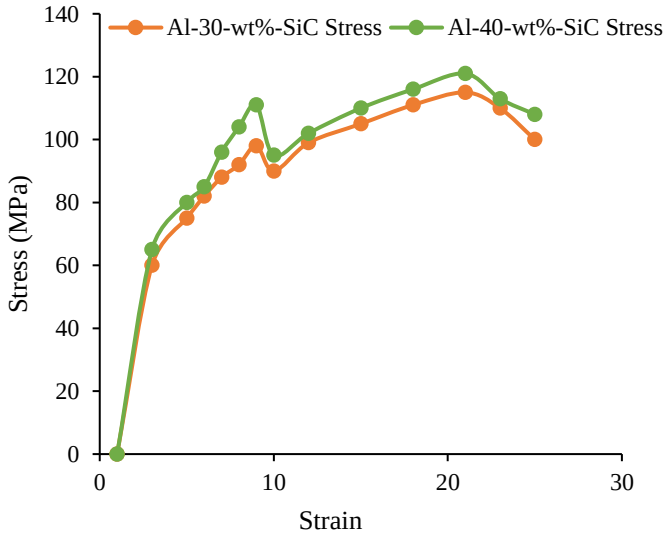

Fig. 5 Stress vs. strain curve for Al-SiC Composites bar.

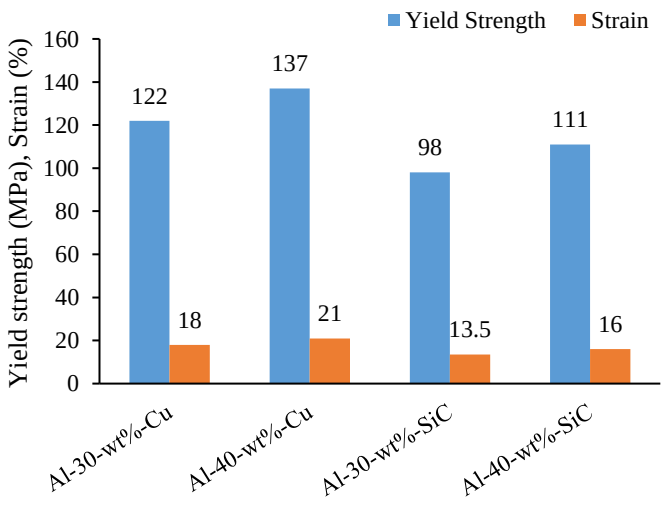

Fig. 6 Comparison of yield strength and strain between the composite bars.

Yield strength is an important mechanical property of materials that needs to be increased in composites with addition of reinforcement. It is shown in Fig. 6 that 11% yield strength has been increased in Al-40-wt%-Cu compared to Al-30-wt%-Cu whereas, 11.8% has been increased in Al-40-wt%-SiC than Al-30-wt%-SiC. Surprisingly, Al-30-wt%-Cu shows 19.7% greater yield strength than Al-30-wt%-SiC and Al-40-wt%-Cu provides 19% more yield strength than Al-40-wt%-SiC.

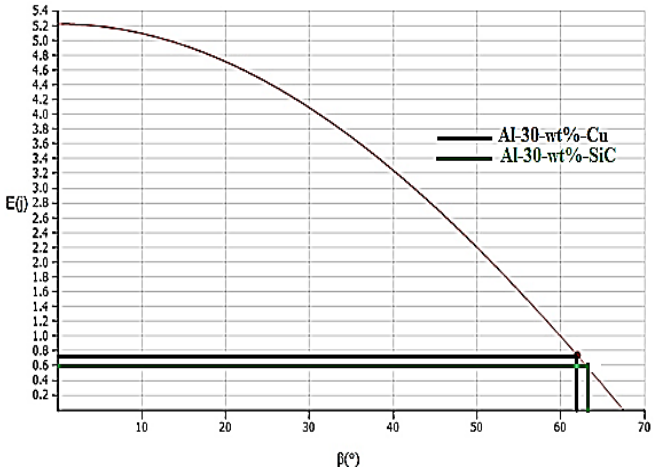

Fig. 7 Representation of impact energy absorption of Al-Cu and Al-SiC composite bars.

In addition, Al-40-wt%-Cu shows 4% improved specific yield strength than Al-30-wt%-Cu and Al-40-wt%-SiC shows 6.06% than Al-30-wt%-SiC. Al-40-wt%-Cu shows highest specific yield strength among the composite bars. Hence, increment of yield strength validates the theoretical explanations. Another important property of materials is absorption of energy in impact testing. Impact absorption energy was calculated from established mathematical formula. The impact hammer traveled 62^0 after impact and Al-30-wt%-Cu composite bar absorbed 0.73 J energy at the time of impact as shown by red line in Fig. 7 and respectively. On the other hand, it would have absorbed total 5.2 J energy if the impact hammer stopped at the time of impact. It is shown in Fig. 7 and Fig. 8 that Al-30-wt%-Cu absorbed energy, E=0.73 J, Al-30-wt%-SiC absorbed 0.6 J, Al-40-wt%-Cu absorbed 0.95 J, and Al-40-wt%-SiC absorbed 0.75 J.

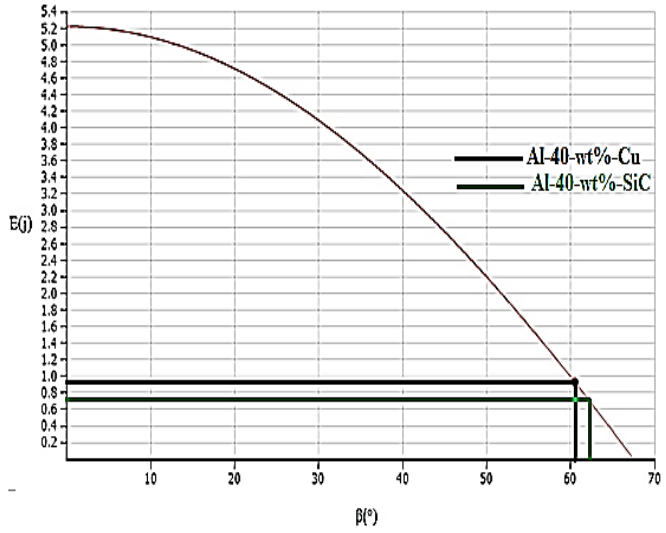

Fig. 8 Representation of impact energy absorption of Al-Cu and Al-SiC composite bars.

It is noted that Al-30-wt%-Cu absorbed about 17.8% greater energy than Al-30-wt%-SiC whereas, Al-40-wt%-Cu absorbed about 21% greater energy than Al-40-wt%-SiC. It is worthy to mention that better tensile strength, hardness properties of Al-Cu composite causes to greater energy absorption capability than Al-SiC composite. In addition, presence of enhanced copper and SiC content increases energy absorption capability in Al-Cu composites and Al-SiC composites.

Fig. 9 represents the microscopic views of the Al-Cu and Al-SiC composite bars fabricated in this study. This is somehow looking almost same microstructures of Al-30-wt%-Cu with Al-40-wt%-Cu and microstructures of Al-30-wt%-SiC with Al-40-wt%-SiC.

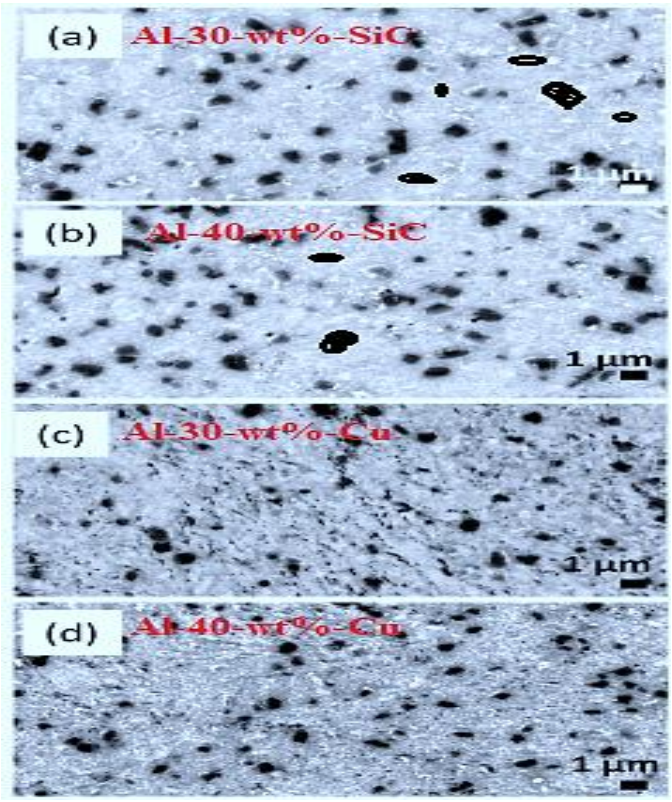

Fig. 9 Microscopic view of the composite bars

However, it is clearly indicating some differences between microstructures of Al-Cu and Al-SiC composite bars due to melting and mixing temperature difference and varied chemical compositions. Significant variation in properties of the Al-Cu and Al-SiC composite bars could be due to those differences of the microstructures. Microstructures reveal very fine grain size of 1 micrometer because of the homogeneous distribution of reinforcement in the parent metals.

5. Conclusion

This study represents an experimental investigation on mechanical behaviors of Al-Cu and Al-SiC composites bar fabricated by using stir casting process. Stir casting technology is cost economic and easy process for mass production of metal composites. Density of metal composites increases for higher concentration of reinforcement. In addition, tensile strength, yield strength, hardness, impact energy absorption simultaneously was increased in both Al-Cu and Al-SiC composites with increasing reinforcement element. Al-Cu composites represent better mechanical properties as compared to Al-SiC. Tensile strength, yield strength, hardness and impact energy absorption capability of Al-Cu composites are higher than Al-SiC composites. Al-40-wt%-Cu shows 1.7% improved specific hardness and 4% specific yield strength compared to Al-30-wt%-Cu whereas, Al-40-wt%-SiC shows 6.06% more specific yield strength and 0.8% specific hardness compared to Al-30-wt%-SiC. Overall, Al-40-wt%-Cu shows highest specific hardness, specific yield strength, and specific energy absorption among the fabricated composite bars.

Acknowledgements

Authors would like to express their gratefulness to Department of Mechanical Engineering, Chittagong University of Engineering &Technology (CUET), Bangladesh for providing financial support and experimental facility to do this research work.

Conflicts of Interest

The authors declares no conflicts of interest.

References

[1] Rezaei, M.R., Albooyeh, A., Shayestefar, M. and Shiraghaei, H., 2020. Microstructural and mechanical properties of a novel Al-based hybrid composite reinforced with metallic glass and ceramic particles. Materials Science and Engineering: A, p.139440.

[2] Das, D., Chakraborty, V., Chaubey, A.K. and Nayak, R.K., 2018. Investigation on properties of SiC reinforced Zn-Mg-Cu based Al metal matrix composites-a case study. Materials Today: Proceedings, 5(9), pp.19874-19882.

[3] Zhao, X., Gu, D., Ma, C., Xi, L. and Zhang, H., 2019. Microstructure characteristics and its formation mechanism of selective laser melting SiC reinforced Al-based composites. Vacuum, 160, pp.189-196.

[4] Sundaram, R.K., Sivashanmugam, N., Shameer, D., Deepak, R. and Saikrishnan, G., 2020. Experimental investigation of mechanical properties and drilling

characteristics on polymer matrix composite materials. Materials Today: Proceedings.

[5] Pascu, C.I., Gheorghe, Ș., Rotaru, A., Nicolicescu, C., Cioateră, N., Roșca, A.S., Sârbu, D. and Rotaru, P., 2020. Ti-based composite materials with enhanced thermal and mechanical properties. Ceramics International, 46(18), pp.29358-29372.

[6] Kumar, U.K.A.V., 2017. Method of stir casting of aluminum metal matrix composites: a review. Materials Today: Proceedings, 4(2), pp.1140-1146.

[7] Bharath, V., Nagaral, M., Auradi, V. and Kori, S.A., 2014. Preparation of 6061Al-Al2O3 MMC's by stir casting and evaluation of mechanical and wear properties. Procedia materials science, 6, pp.1658-1667.

[8] Laplanche, G., Joulain, A., Bonneville, J., Schaller, R. and El Kabir, T., 2010. Microstructures and mechanical properties of Al-base composite materials reinforced by Al–Cu–Fe particles. Journal of alloys and compounds, 493(1-2), pp.453-460.

[9] Sohn, S.W., Park, J.M., Kim, W.T. and Kim, D.H., 2012. Microalloying effect on the microstructure and mechanical properties in Al–Cu based dendrite-ultrafine composites. Journal of alloys and compounds, 541, pp.14-17. doi: 10.1016/j.jallcom.2012.06.127.

[10] Kim, J.T., Hong, S.H., Park, J.M., Eckert, J. and Kim, K.B., 2018. Microstructure and mechanical properties of hierarchical multi-phase composites based on Al-Ni-type intermetallic compounds in the Al-Ni-Cu-Si alloy system. Journal of Alloys and Compounds, 749, pp.205-210. doi: 10.1016/j.jallcom.2018.03.313.

[11] Viswanath, A., Dieringa, H., Kumar, K.A., Pillai, U.T.S. and Pai, B.C., 2015. Investigation on mechanical properties and creep behavior of stir cast AZ91-SiCp composites. Journal of Magnesium and alloys, 3(1), pp.16-22. doi: 10.1016/j.jma.2015.01.001.

[12] Steinman, A.E., Corthay, S., Firestein, K.L., Kvashnin, D.G., Kovalskii, A.M., Matveev, A.T., Sorokin, P.B., Golberg, D.V. and Shtansky, D.V., 2018. Al-based composites reinforced with AlB2, AlN and BN phases: experimental and theoretical studies. Materials & Design, 141, pp.88-98. doi: 10.1016/j.matdes.2017.12.022.

[13] Huang, G., Hou, W., Li, J. and Shen, Y., 2018. Development of surface composite based on Al-Cu system by friction stir processing: Evaluation of microstructure, formation mechanism and wear behavior. Surface and Coatings Technology, 344, pp.30-42.

[14] Santhanam, V., Dhanaraj, R., Chandrasekaran, M., Venkateshwaran, N. and Baskar, S., 2020. Experimental investigation on the mechanical properties of woven hybrid fiber reinforced epoxy composite. Materials Today: Proceedings. doi: 10.1016/j.matpr.2020.07.444.

[15] Gopalakrishnan, S. and Murugan, N., 2012. Production and wear characterisation of AA 6061 matrix titanium carbide particulate reinforced composite by enhanced stir casting method. Composites Part B: Engineering, 43(2), pp.302-308. doi: 10.1016/j.compositesb.2011.08.049.

[16] Raghuvaran, P., Baskaran, J., Aagash, C., Ganesh, A. and Krishna, S.G., 2020. Evaluation of mechanical properties of Al7075-SiC composites fabricated through stir casting technique. Materials Today: Proceedings. doi: 10.1016/j.matpr.2020.09.191.

[17] Vairamuthu, J., Stalin, B., Sivakumar, G.D., Fazil, B.M., Balaji, R. and Natarajan, V.A., 2020. The effect of process parameters for synthesized copper metal matrix using stir casting process. Materials Today: Proceedings. doi: 10.1016/j.matpr.2020.09.262.

[18] Satishkumar, P., Rakesh, A.I.J., Meenakshi, R. and Murthi, C.S., 2020. Characterization, mechanical and wear properties of Al6061/Sicp/fly ashp composites by stir casting technique. Materials Today: Proceedings. doi: 10.1016/j.matpr.2020.08.530.

[19] Kala, H., Mer, K.K.S. and Kumar, S., 2014. A review on mechanical and tribological behaviors of stir cast aluminum matrix composites. Procedia Materials Science, 6, pp.1951-1960.

[20] Alaneme, K.K. and Ajayi, O.J., 2017. Microstructure and mechanical behavior of stir-cast Zn–27Al based composites reinforced with rice husk ash, silicon carbide, and graphite. Journal of King Saud University-Engineering Sciences, 29(2), pp.172-177. doi: 10.1016/j.jksues.2015.06.004.

[21] Prabu, S.B., Karunamoorthy, L., Kathiresan, S. and Mohan, B., 2006. Influence of stirring speed and stirring time on distribution of particles in cast metal matrix composite. Journal of materials processing technology, 171(2), pp.268-273.

[22] Kumar, S.A., Vignesh, J.H. and Joshua, S.P., 2020. Investigating the effect of porosity on aluminium 7075 alloy reinforced with silicon nitride (Si3N4) metal matrix composites through STIR casting process. Materials Today: Proceedings. doi: 10.1016/j.matpr.2020.07.690.

[23] Kennedy, A.R., Karantzalis, A.E. and Wyatt, S.M., 1999. The microstructure and mechanical properties of TiC and TiB2-reinforced cast metal matrix composites. Journal of materials science, 34(5), pp.933-940. doi: 10.1023/A:1004519306186.

[24] Jing, S.U.N., WANG, X.Q., Yan, C.H.E.N., Fei, W.A.N.G. and WANG, H.W., 2020. Effect of Cu element on morphology of TiB2 particles in TiB2/Al− Cu composites. Transactions of Nonferrous Metals Society of China, 30(5), pp.1148-1156. doi: 10.1016/S1003-6326(20)65285-2.

[25] Raviraj, M.S., Sharanprabhu, C.M. and Mohankumar, G.C., 2014. Experimental analysis on processing and properties of Al-TiC metal matrix composites. Procedia Materials Science, 5, pp.2032-2038. doi: 10.1016/j.mspro.2014.07.536.

SciEn
Journal of Engineering Advancements Vol. 01(04) 2020, pp 150-169 https://doi.org/10.38032/jea.2020.04.007

An Extensive Literature Review and New Proposal on Optimal Capacitor Placement in Distribution Systems

S. M. Golam Mostafa[1], Jai Govind Singh[2] and H.M. Enamul Haque[2]*

[1]Department of Electrical and Electronics Engineering, International Islamic University, Chittagong, Bangladesh
[2]Department of Energy, Environment and Climate Change, Asian Institute of Technology, SERD, Khlong Luang, Thailand

Received: November 30, 2020, Revised: December 17, 2020, Accepted: December 18, 2020, Available Online: December 21, 2020

ABSTRACT

The main goal of power utilities is to supply reliable and quality power to the end-users and fulfill their total demands at all possible locations. Most of the loads are connected in the distribution systems are inductive. The excessive reactive power demand over the distribution network causes tremendous reactive power losses and changes the voltage profile, hence the system's reliability. Shunt Capacitor Bank (SCB) is widely used in the distribution system for reactive power support, voltage profile, and system performance improvement. But there are some challenges to employ SCB in the distribution network; among them, ensuring the most optimum location and size is a big challenge to get the maximum benefits. Some existing techniques showed better loss reduction but needed either larger SCBs sizes or cause improper node voltage. In this research study, the first section provides an extensive literature review of optimal SCBs placement and sizing. Later on, a new technique called Combinatorial Method has been developed for sizing and sitting of optimal Shunt Capacitors to reduce the distribution loss significantly. The developed method was tested for different case studies using Indian practical 22-bus and IEEE-69-bus network. The results were compared with DSA, Fuzzy GA, and TLBO method and found better distribution feeder loss minimization and voltage profile improvement.

Keywords: Distribution feeders; Shunt Capacitor Bank; Distribution Losses; SCBs Sizing and Sitting; Voltage Profile Improvement (VPI); Combinatorial Method.

Table of Contents

*Corresponding Author Email Address: mostafa_93eee@yahoo.com Published by: SciEn Publishing Group

1. Introduction

The concept of the electricity market, hence the restructuring and deregulation in existing utilities, had disintegrated the vertically integrated electrical power divisions. The power sectors had unbundled into three main parts: distribution, transmission, and generation sectors. Most power consumers are directly connected to the distribution side though some big customers feed by transmission lines. The reliability and security of distribution feeders are reduced because inductive loads cause greater feeder losses by lagging current. Consequently, any malfunctions or disconnection in any portion of the distribution side will cause a severe effect on reliable and secure power supply in consumer ends. So, it is a vital task of power utilities to reduce the feeder losses and maintain reliability and, hence, the power systems' security. Various FACTS devices and compensators are employed in distribution systems for these reasons [1].

To get the profits of feeder loss minimization, voltage profile enhancements, power factor (p.f.) improvements to a great extent at different scenarios, it is an inevitable task to power engineers to find the optimum placement of Shunt Capacitor Banks (SCBs) with suitable size. To reduce the distribution feeder losses, the SCBs are widely used near the Sub Station (SS). This capacitive compensation reduces the losses and improves the bus voltage and power factor up to the point of common coupling. To achieve a better benefit, it is wise to employ reactive compensating devices at the load center or near the loads. Nowadays, it is possible to connect SCBs at the primary distribution side through available pole-mounted devices and equipment [2]-[6].

In SCBs, the capacitors units are the main building blocks connected in series-parallel combinations in such a manner that keeps over and under voltage limits within 10% above or below from the nominal values [3]. The total reactive power (Q_{Cap}) supplied by the SCBs depends on the capacitive reactance (X_{Cap}) and the supplied voltage (Vs) that has been depicted by equation (1) [7]. The recent blackout reported in [8], [9] due to redundancy inadequate reactive power (Q_{Cap}) also draws more attention to manage reactive power (Q_{Cap}) in the system by employing SCBs locally. The researchers proposed a Shunt Capacitor Bank Series Group Shorting (CAPS) method in various low voltage conditions such as generator scheduling, direct load tripping, or in case of line restoration. In this method, the reactive power supplied by shorting various series groups of SCBs units, and these are approximately 20%-30% of the total capacitance of CAPS. The feasibility of CAPS incorporation on High Voltage (HV) and Extra High Voltage (EHV) has been studied in [10]. The optimal allocation of SCBs is the solution of feeder loss minimization, and voltage drop problems can be solved using voltage regulators' placement optimally [4].

$$Q_{Cap} = V_S^2 / X_{Cap} \quad (1)$$

The necessity of reactive power (Q_{Cap}) in distribution systems can be segregated for the following reasons.

1.1 Minimizing the Power Losses

There are two main problems usually found in distribution systems – voltage profile deterioration and higher power losses. Losses in distribution systems are classified as technical and non-technical losses [11], [12]. Technical losses are losses between the main sub-station to end users through various substation transformers, distribution transformers, primary and secondary lines, voltage regulators, surge arresters. The details of loss measurement have been described in the literature. According to the research conclusion of Energy Information Administration (EIA) and Electric Power Research Institute (EPRI) of America, the distribution losses vary between 33.7% - 64.9%. EPRI research shows the distribution losses in Fig. 1. Around 38% of total distribution losses occurred in primary and 54% distribution transformers, considering both copper and iron losses, whereas service and secondary loss found 9%. Fig. 1 depicts that many distribution transformers are the prime reason for higher distribution losses [13], [14].

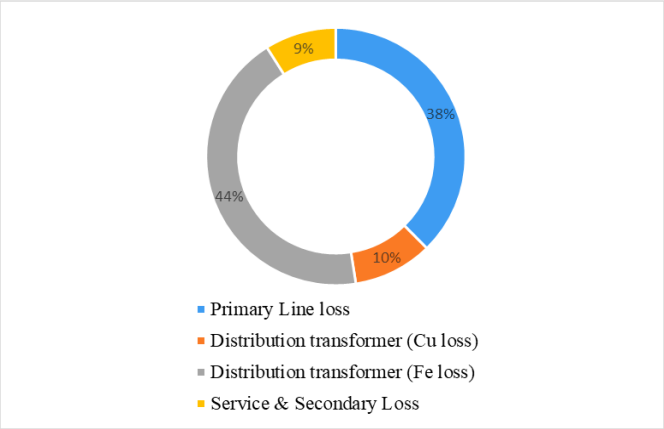

Fig. 1 Various distribution losses estimation, according to EPRI [14].

Hence, it became mandatory to minimize line losses in primary lines at a considerable amount. A different study shows that voltage limits and thermal limits are constrained by higher losses in distribution power systems where maximum loading is limited by mainly voltage limit rather than the thermal limit [15]. To avoid the penalty due to an inferior power factor (p.f.), the SCBs are used. To improve the p.f. three techniques are used, such as centralized compensation, group compensation, and individual compensation. Three different compensation techniques are available in the literature, including individual compensation, group compensation, and centralized compensation to improve the power factor. To get maximum advantages in p.f. correction all the methods, as mentioned earlier, can be used [16]. Synchronous condensers can also be used instead of static SCBs [19] because manufacturers want to produce equipment with improved power factor and higher efficiency [17].

1.2 The Impact of Reactive Power (QCap) in the Vertically Unbundled Electricity Market.

Due to the expansion of the electricity market, the unbundled electricity power system is now regulated by Regional Transmission Organizations (RTO) and Independent System Operator (ISO) to assure security, reliability, and quality of the electrical power services. The restructured power market parted as Generation Company (GenCOs), Distribution Company (Discos), and Transmission Company (TransCOs) [18]-[20]. The existing power systems became limited to transmit generated power from central generation to distribution systems due to aging because most of the power systems are more than 40 years old. Hence, these systems unable to cope up

with growing demands. Besides, transmission investment has reduced at an alarming rate for the last few decades. [21]. Transmission congestion can be relieved by employing FACTS devices, SCBs, Distributed Generations (DGs), voltage regulators, etc., rather than installing new transmission lines [22], [23]. But to supply extra kVAR, it is inevitable to sacrifice real power output. In the real scenario, the utilities prefer to generate more real power for profit maximization [24]. As in the real power market, reactive power is not easy to generate since it does not travel far. Consequently, reactive power has to generate locally [25].

Thus compensation of reactive power (Q_{Cap}) becomes vital because of deregulation in the power market and conversion of the Network from passive to active. SCBs will be the most cost-effective solution for reactive power compensation because of the lower initial investment, and there is no personnel and maintenance cost. The optimal allocation and sizing of SCBs became a very attractive topic among researchers since non-optimal sizing and sitting will cost real power losses in distribution feeder as capacitive MVAr and losses have deep bath curve relation [26].

1.3 Incorporation of DGs in Distribution System and Reactive Power Management by SCBs

We can call the Distributed Generation (DG) a small-scale generation. It is connected to the distribution level and is a real active power generating unit. Electricity production facilities are necessarily small with respect to central plants, according to IEEE. As a result, it facilitates the interconnection at any close point in the electric power system, as disperse resources. The DGs are considered an electric power generation source connected to the consumer site or the distribution network [27]. They can afford electricity at a cheap price by maintaining higher security and reliability and less environmental pollution than the old-style power generation. In addition, since DGs are not dependent on the main power grid, it can deliver power to a vast number of public services. For instance, educational institutions, airports, hospitals, military bases, police stations, natural gas distribution, transmission systems communication sectors, etc. Virginia Tech's Consortium on Energy Restructuring defines the distribution power network in two categories: the local and endpoint levels. The local generating power plants mostly consists of RE technologies that depend on site such as solar PV systems, WT-DG, geothermal power plant, hydro-thermal generating stations.

On the contrary, at the end-point level, the different customers can apply the same technology. For instance, the modular combustion engine can furnish as home back up and at the same time to other buildings. Hence, disperse generators contribute in a small amount to the main power grid. The main focus of DGs is -friendly to the environment, efficient, and economically viable. These distributed generation based power plants needed reactive power to maintain proper node voltage. Locally generated reactive power from SCBs will be the right choice in this regard.

1.4 Voltage Profile Improvement (VPI)

Generally, DGs are treated to supply active power [28]; voltage profile deterioration is a remarkable challenge to the utility due to high DGs penetration at heavy system loading. To maintain a voltage profile at an acceptable limit, certain reactive power always has to be maintained [29]. In the vertically unbundled electricity market, the responsibilities rested on ISO to keep voltage profile in preferable limits by GenCOs. The reactive power supply can be controlled in numerous ways, such as: changing the excitation, by changing tap changing transformers, or by removing reactors and adding capacitive type devices. Voltage control equipment must adhere to DGs because at light load DGs will cause voltage rise problems [30]. Due to environmental pollution and the Greenhouse effect, non-conventional energy resources based on power generation have become popular such as-wind and solar energy. Asynchronous induction generator in case wind power generation must need a local reactive power supply, but this problem can have addressed with Doubly Fed Induction Generator (DFIG). Various reactive power compensation technique has been described in [31] along with SCBs, over-excited synchronous motor, etc. STATCOMs. SVCs and other recent reactive power enhancement devices can be used at the generation level.

2. Optimum Shunt Capacitor Placement Techniques— A Review

Different researchers have proposed various formulas and techniques for optimum placement of SCBs considering numerous fitness functions such as power loss minimization, VPI, installation cost reduction, burden reduction on existing lines, maximization of system stability, etc. SCBs are placed in two different ways of fixed and variable (switched) combinations. The variable capacitors' size depends on the difference between existing reactive power demand and available fixed capacitive power. In contrast, fixed capacitors rely on average reactive power needed by the electric power systems. To control the variable SCBs, special control techniques are employed. SCBs (Q_{Cap}) are found in discrete sizes that are multiples of a minimum capacitor size Q_{min} that has been given in equation (2) [32], [33]. Both fixed and variable combinations of SCBs are used for continuous sizes. The absolute value of SCBs is achieved by employing a variable capacitor bank.

$$Q_{Cap} = n \times Q_{min} \tag{2}$$

The authors suggested various SCBs sitting problems in different research articles that have been discussed below. Moreover, multidimensional problems also have been addressed in some other research articles considering DGs, reconfiguration of the Network, and voltage regulators. The common algorithm of sitting and sizing of SCBs have demonstrated in Fig. 2.

2.1 Analytical Methods

A calculus-based analytical method was proposed at the early stage when suitable computational resources were not available, and computational procedures were reduced by considering approximation. These analytical methods were also had used SCBs sizing and sitting. The work has begun with placing single and multiple capacitors by Neagle in Non-uniform and uniform load conditions. He proposed SCBs to place at 1-(1/2) distance from the main substation (SS) [2]. Cook developed a more realistic algorithm considering the average Q load using fixed SCBs for uniformly distributed load conditions [34]. He proposed that the optimum location of a capacitor bank would be 2/3. The author also extended his work using variable

SCBs [35]. After that, several analytical methods were also proposed in various literature [36], [37]. Extended research of Cook [34] was done by Schmill [38] with equations for sitting and sizing of N number of capacitors with a uniformly distributed load on a uniform feeder. The optimal conditions of sitting and sizing for single or double SCBs on a feeder also considered discrete loads and Non-uniform resistance. In this literature, an iterative process had proposed to address the problem. Uniform and a concentrated end load on the distributed feeder was suggested by Chang et al. [39], [40]. Schmill had determined the optimum place of SCB based on the calculation of energy losses and peak power losses, whereas total savings determined the size.

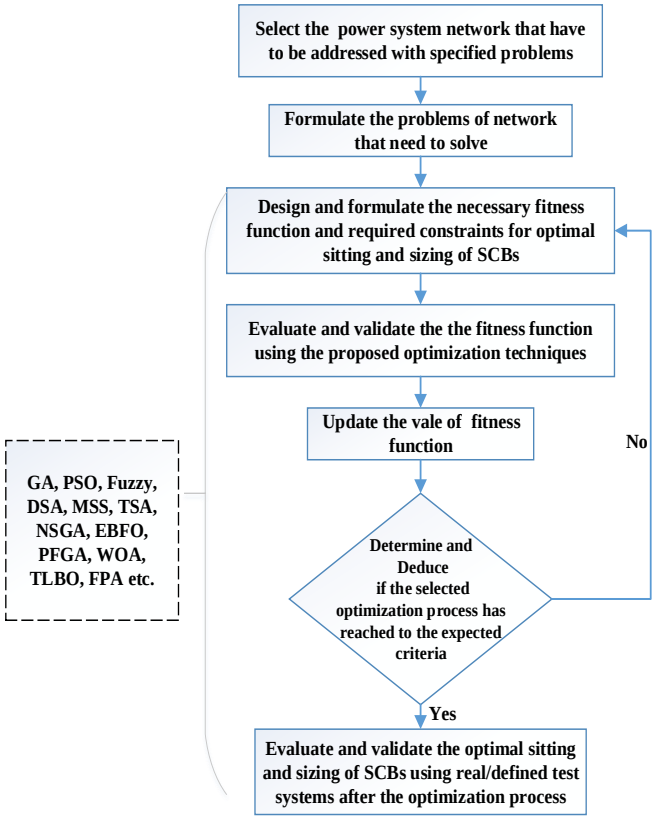

Fig. 2 General Algorithm for sitting and sizing of SCBs.

It is easy for the implementation of an analytical method, and its execution is faster. Since it takes simple presumption and considers one snapshot of the electric power system loading condition. Though Analytical methods are treated as the simplest method, many assumptions and scenarios have to make before finding optimal sizing and sitting of SCBs. The "2/3 rule" showed negative savings in various scenarios [41]. At the very beginning of the research, sitting and sizing of SCBs, sizes, and locations are considered as continuous variables. Consequently, the calculated results needed to be rounded to the closest real value that may give overvoltage problems or show loss savings in terms of the dollar lower than the calculated values. But recently proposed analytical methods much more convenient, accurate, and practical for distributed systems [37], [42]-[45]. Ardiaty proposed a new formula to measure the Reactive Contribution Index (RCI) of each node. His objective function was to achieve the most stable condition with feeder loss minimization [46]. In article [47], the authors proposed a probabilistic load flow analysis for radial distributions system (PLFRDS) considering stochastic load variations. M. Ihsan et al. developed the Exhaustive method for both real and reactive power reduction [48].

2.2 Numerical Programming Methods

In Numerical Programming methods, the mathematical models are formulated and solved arithmetically. It is an iterative process that can minimize or maximize the particular objective function of decision variables with some constraints. The application of Numerical Programming methods has been increased in power systems because of available larger memory chips and fast computation skills [49], [50]. In optimum sizing and sitting of SCBs problems, the researchers suggested various mathematical models and employed Numerical Programming methods to find optimum locations and sizes. The optimal location of SCBs was determined by Duran et al. using dynamic programming and accomplished Schmil work [38] for uniformly and randomly distributed load. The author used discrete capacitors and energy loss reduction, was the objective function [51]. Fawzi et al. extended Duran's work [51] and incorporated the extra kVA as a savings function [52]. The local variations method proposed by Ponnavsikko and Rao used the variable SCBs included the effects of variable load growth [53]. Lee developed an optimization technique that incorporates both fixed and variable SCBs to provide net monetary savings [50]. Baran and Wu used the mixed-integer programming approach for SCBs placement and sizing [54], [55]. The complete power flow model was used by Sharaf et al. used the full load flow model to find the optimum place of SCBs in a distribution feeder [56]. The author also said that the model developed in [57] is not suitable for optimal placement of SCBs since end-user bus voltage decreased as the system load increased quadratically. Overall energy savings were considered the objective function in the mixed-integer linear problem model proposed by Khodr for SCBs placement problems [58]. In [59], [60], the authors considered Monte Carlo Simulation to deal with stochastic load variations, and the objective function was minimizing was power losses. S. Soto applied the proposed MCS model in a practical sub-transmission system [59], and M.B. Jannat applied it in a 35kV real distribution system [60].

2.3 Heuristics Methods

Heuristics methods are called rules of thumb because they are based on suggestions or hints and were developed on experiences, senses, and judgments. These methods minimize the exhaustive search space and furnish almost real and quick decisions and give optimal results with full confidence [61], [62]. Hence, this method-based technique widely applies to optimum SCBs sitting and sizing [63]-[67]. In [63], the authors developed a heuristic method that identified the sensitive node and placed SCBs to reduce the feeder losses in a significant amount. Chis et al. had elaborated Abdel-Salam et al.'s work considering the cost of SCBs and minimization of energy and peak power loss [64]. The bus bar Sensitivity Index has considered fixing the optimal position and size of SCBs in [65]. Hamouda et al. had used the node voltage stability index to select the optimum location. The objectives function of this research were to maximize the net savings and capacitor investment due to the different size of SCBs [66].

Table 1 Summary of Analytical Methods.

Publi-shed	Ref.	SCB type	Design variables	Load profiles	Method	Objective function	Test systems
1956	[2]	Fixed	Location	Uniform and Non-uniform distributed load	1-1/2kVA/kVAr rule	Feeder loss reduction	Primary feeders
1959	[34]	Fixed	Location	Distributed load	2/3 rule	Feeder loss reduction	Primary feeders
1961	[35]	Fixed+Switched	Location	Uniform distributed load	Energy loss equation	Feeder loss reduction	Primary feeders
1965	[38]	Both	Location +Size	Uniform & random distributed	Iterative approach	Feeder active & reactive loss reduction	Distribution feeder
1969	[39]	Switched	Location +Size	Uniform load	Computer-based new Iterative approach	Optimization of total monetary savings	Primary feeders
1972	[40]	Switched	Location +Size	Concentrated and uniformly distributed load	Determining generalized loss equation	Economic savings	Distribution feeder
1978	[36]	Fixed	Location	Uniform distributed load	General loss equation	Yearly loss reduction	Distribution feeder
1981	[37]	Both	Location +Size	Uniform distributed load	Equal area criterion	Loss reduction	Distribution feeder
1985	[43]	Switched	Location +Size	Varying load condition	Step by step calculation	Peak power loss and energy loss reduction	Distribution feeder
1985	[42]	Switched	Location +Size	Uniform feeder with an end-load	General loss equation	Peak power loss and energy loss reduction	Distribution feeder
1997	[45]	Both	Location +Size	Time-varying load	Three-phases load flow	Minimizing the loss	Taiwan LY-37, BX33
1999	[44]	Switched	Location +Size	Time-varying load	Iterative approach	Significant loss savings	15-bus & 33-bus
2009	[156]	Fixed	Location +Size	Fixed load	BIBC & BCBV based new method	Minimizing power loss	12, 34, 69-bus
2016	[46]	Fixed	Location	Non-uniform load	Improved Modal Analysis with RCI	Achieve stable condition & Minimize power loss	IEEE 30-bus
2019	[47]	Fixed	Location +Size	Stochastic Load variation	PLFRDS method	Loss reduction & improve Voltage profile	30, 85-bus
2019	[48]	Fixed	Location +Size	Average load	Analytical expression & exhaustive method	P & Q Loss reduction & improve Voltage profile	IEEE 37-bus

Table 2 Summary of Numerical Programming Methods.

Publi-shed	Ref.	SCB type	Design variables	Load profiles	Method	Objective function	Test systems
1968	[51]	Switched	Location +Size	Discrete lumped loads	Dynamic programming	Minimize the power loss	Distribution feeder
1981	[37]	Both	Location +Size	Non-uniform load	Iterative technique	Net monetary savings	A certain point on feeder
1983	[52]	Switched	Location	Uniform & random distributed load	Dynamic programming	Minimize the power loss	Rural Distribution, Egypt
1983	[53]	Both	Location +Size	Load growth with varying load	Local variation method	Minimize the power loss	Indian Distribution feeder
1989	[54]	Both	Size	Time-varying load	non-linear programming	Power loss minimization & Voltage regulation	Distribution feeder
1989	[55]	Switched	Location +Size	Uniform concentrated end load	Mixed-integer program	Peak power loss and energy loss reduction	TS1, TS2 Distribution feeder
1996	[56]	Switched	Location +Size	Distributed load	FLFM, EGSLM model	Cost minimization	18-bus system
2008	[58]	Switched	Location +Size	Single load level	mixed-integer linear problem	Minimize the power loss	15-bus, 33bus test
2016	[59]	Fixed	Location	Stochastic Load	MCS	Power loss minimization	Real sub-transmission system
2016	[60]	Fixed	Location	Random Load	MCS	Active energy loss minimization	35kV real distribution network

To fix the optimum place of SCBs, the weakest line has taken as candidate bus, and the optimum size was selected by using PSO that gave minimum feeder losses. Raju et al. proposed the DSA algorithm that assures net savings maximization and voltage profile improvement. The optimal size and location of fixed and variable SCBs were determined in the radial feeder by applying the DSA algorithm [67]. To determine location and size, both fixed and variable SCBs have been used in articles [68]-[71]. Accelerated PSO has been used to reduce net benefits, and Cuckoo Search Algorithm (CSA) has been used to minify system operating & improve voltage profiles at different load levels [67], [68]. SSO algorithm used for Cost minimization due to energy loss & reactive power compensation [70] and Modified Gbest-guided Artificial Bee Colony (MGABC) algorithm has applied for minimization of power loss, total annual expense and voltage deviation [70] in 34 & 118-bus distribution systems. Researchers also proposed numerous SCBs algorithms and methods such as the HCODECQ method [72], BFOA method [73], Crow Search Algorithm (CSA) [74], HSA-PABC algorithm [75]. A. Mujezinović et al. developed a Load flow calculation algorithm and integer genetic algorithm on a 10 kV distribution network in Bosnia & Herzegovina that reduce power losses and improve bus voltages [76].

Table 3 Summary of Heuristics Methods.

Publ-ished	Ref.	SCB type	Design variables	Load profiles	Method	Objective function	Test systems
1994	[63]	Fixed	Size	Variable load	New loss reduction technique	Minimize reactive loss	45-bus
1997	[64]	Fixed	Location +Size	Average load	Sensitive node searching	Minimize the power loss	34-bus
2008	[65]	Fixed	Location	Different load conditions	HCA algorithm	Net annual savings	70, 476-bus
2012	[26]	Both	Location +Size	Different load conditions	RVSI V Indexing method	Minimize the power loss	12,33,69-bus
2012	[67]	Both	Location +Size	Average load	Direct Search Algorithm	Net savings and improve voltage profiles	22,69,85-bus
2013	[66]	Both	Location +Size	Average load	Heuristic search method	Net savings and improve voltage profiles	10,22,69-bus
2014	[68]	Both	Location +Size	Different load conditions	Accelerated PSO	Maximize net benefits	34 & 118-bus
2014	[69]	Both	Location +Size	Different loading levels	Cuckoo Search Algorithm	Minify system operating & improve voltage profiles	69 & 118-bus
2015	[70]	Fixed	Location	Average load	HCODECQ method	Power loss minimization	33, 66 ,132-bus
2015	[73]	Switched	Location +Size	Different loading levels	BFOA method	Minimize the power loss	34 & 85-bus
2016	[74]	Fixed	Location	Different load conditions	Crow Search Algorithm	Minimize power losses and improve voltage profiles	9 & 33-bus
2016	[70]	Both	Location +Size	Average load	Shark Smell Optimization (SSO) algorithm	Cost minimization due to energy loss & reactive power compensation	34 & 118-bus
2018	[71]	Both	Location +Size	Various load levels	MGABC algorithm	minimization of power loss, total annual expense, and voltage deviation	34, 118-bus
2018	[75]	Switched	Location +Size	Voltage-dependent load models	HSA-PABC algorithm	Power loss reduction, voltage stability improvement, and net annual savings	69, 118-bus
2019	[76]	Fixed	Location +Size	Average load	Load flow calculation algorithm & integer genetic algorithm	Minimize power losses and improve voltage profiles	10 kV dist. real Network in Bosnia

2.4 Artificial Intelligent Methods

Exhaustive search is the simplest search algorithm in the optimization technique since it searches all probable solutions from a set of predefined values. But this method is considered an inefficient technique because it needed higher computational time and space. Kokash proposed a new special class of heuristic techniques based on nature, intelligence, and greedy known as the Artificial Intelligent (AI) method [77]. This AI method has been employed to find the optimal place and size of SCBs on distribution systems. Many researchers use AI methods as one of the most potent methods to solve power system problems, but it is needed higher computation time and memory space [78]. Different researcher has been proposed various algorithm such as: GA [79]-[84], Fuzzy [85], [86], Fuzzy-GA [87]-[88], Particle Swarm Optimization (PSO) [89]-[90], Immune Algorithm (IA) [91], Plant Growth Simulation Algorithm (PGSA) [92], Tabu Search (TS) [93], Memetic-Algorithm Approach [94], TLBO algorithm [95], Ant Colony [96], Graph Search Algorithm (GSA) [97]-[98], Artificial Bee Colony (ABC) [99], and Hybrid Algorithm [100]-[102]. The authors proposed CSA Optimization [68], a new algorithm of Inclusion and interchange of variables [103], Flower Pollination Algorithm [104] in the various distribution network to minify total cost. Moreover, to improve net savings and bus voltage, the researcher suggested different methods to connect fixed and switched SCBs that given as Fuzzy-Real Coded GA algorithm [105], BA and CS method [106], Loss sensitivity approach [107], GAs and SA analysis [108], PSO and Improved BSFS [109], WOA Algorithm [110].

Table 4 Summary of Artificial intelligent Methods.

Publi-shed	Ref.	SCB type	Design variables	Load profiles	Method	Objective function	Test systems
1990	[113]	Fixed	Size	Linear and time-invariant load	Numerical algorithm	Reduction of total power loss & THD	Radial Dist. Feeder
1993	[83]	Fixed	Location	Differential load pattern	GA method	Minimize the power loss	69-bus
1994	[79]	Both	Location +Size	Average load	GA method	Minimize the power loss	9,30-bus
1995	[114]	Both	Size	Different load levels	MSS method	Cost and substation Harmonic reduction	23 kV distributor
1999	[102]	Fixed	Location +Size	Various load levels	Basic search technique	Minimize system cost	Distribution feeder
2000	[82]	Fixed	Location	Differential load pattern	GA & Fast energy loss reduction technique	Overall power and energy loss minimization	Single feeder fed by 24 kV, 15MVA
2000	[85]	Fixed	Size	Average load	Approximate reasoning with FES	Net energy savings	34-bus
2000	[91]	Fixed	Location	Different load levels	IA based optimization	Minimize power loss	69-bus
2000	[97]	Both	Location +Size	Average load	Graph search algorithm	Overall savings	Practical feeder
2001	[100]	Fixed	Location +Size	Different load levels	Hybrid method	Cost savings	9,65,135-bus
2001	[132]	Switched	Location	Different load levels	Simulated annealing technique	Minimize power loss and improve voltage profiles	IEEE 3-feeder system
2002	[80]	Both	Size	Varying load	GA method	Minimize reactive loss	69-bus
2002	[117]	Both	Location +Size	Linear and nonlinear loads	HARMFLOW algorithm and MSS method	Minimize system losses and capacitor cost	18-Bus IEEE Distorted System
2004	[111]	Fixed	Location	Different load levels	NSGA method	Power loss reduction, p.f. correction	Distribution feeder
2004	[115]	Switched	Location +Size	Different load levels	PSO algorithm	Minimize capacitor cost, energy & power loss	IEEE 9-bus
2004	[116]	Fixed	Location	Average load	New GA approach	Minimize energy, power loss, and capacitor cost	6 & 18-Bus IEEE Distorted System
2004	[118]	Both	Location +Size	Different load levels	MSS-LV optimization	Minimize capacitor cost, energy & power loss	IEEE 18-bus distorted System
2004	[119]	Fixed	Location +Size	Linear and nonlinear loads	Fuzzy based approach	Minimize system losses and capacitor cost	18-Bus IEEE Distorted System
2005	[93]	Fixed	Location	Different load levels	Tabu Search approach	Minimize power loss and capacitor cost	94-bus practical system

Publi-shed	Ref.	SCB type	Design variables	Load profiles	Method	Objective function	Test systems
2005	[94]	Fixed	Location +Size	Average load	Evolutionary algorithms	Annual cost savings	9,69-bus
2007	[81]	Both	Location +Size	Uncertain and time varying loads	GA method with new coding	Minimize power loss and improve voltage profiles	37,69-bus, a real Iranian network
2007	[87]	Both	Location +Size	Different load levels	Fuzzy-GA method	Net savings and improve voltage profiles	69-bus
2009	[86]	Fixed	Location +Size	Different loading conditions	A fuzzy based new method	Minimize power loss and improve voltage profiles	10,23,34-bus
2011	[101]	Switched	Size	Average load	Fuzzy-DE, Fuzzy-MAPSO methods	Minimize power loss and improve voltage profiles	15,34-bus
2012	[89]	Both	Location +Size	Different load levels	PSO static and dynamic sensitivity	Minimize capacitor cost function & energy loss	70 & 135-bus
2012	[92]	Both	Location +Size	Different load levels	Plant Growth-Based Optimization	Emission decrement & power loss improvement	69,123 & 17-bus Taipower company
2013	[96]	Fixed	Location +Size	Load growth model	Multi period dynamic model	Minimizing the total	69-bus
2014	[95]	Both	Location +Size	Different load levels	TLBO approach	Minimize power loss and energy cost	22,69, 85 & 141-bus
2014	[68]	Both	Location +Size	Different loading conditions	CSA Optimization	Minify operating cost	69 & 118-bus
2014	[69]	Both	Location +Size	Different load levels	Fuzzy-Real Coded GA	enhance voltage stability & Net savings	33-bus
2015	[84]	Fixed	Location +Size	Average load	GA	Improve voltage profiles & Minimize power loss	34-bus
2015	[106]	Both	Location +Size	Different load levels	BA and CS method	Minimize power loss & maximize network savings	34, 85-bus
2015	[107]	Switched	Location +Size	Time varying ZIP loads	Loss sensitivity approach	Minimize power loss and improve voltage profiles	38-bus UK distribution System
2015	[90]	Fixed	Location	Different load levels	PSO method	Reduce peak power loss and improve node voltage	69-bus
2015	[98]	Fixed	Location +Size	Average load	GSA method	Minimize kW loss and maximize net savings	33, 69, 85, 141-bus
2016	[108]	Fixed	Location	Average load	GAs and SA analysis	Minimize power loss and improve voltage profiles	34, 70-bus
2016	[109]	Switched	Location	Different load levels	PSO and Improved BSFS	Maximize the net annual returns	A real unbalanced MV network
2016	[88]	Both	Location +Size	Various load levels	Fuzzy GA Method	Improve the substation power factor	51, 69-bus
2016	[121]	Switched	Location +Size	Future load and contingency	EBFO Method	Thermal re-rating of critical cables	Real-world 110 kV sub-trans. net.
2016	[122]	Fixed	Location +Size	Different load models	PFGA algorithm	Cost reduction & power quality improvement	18, 69, 141-bus
2017	[120]	Both	Location +Size	Different load levels	MSPSO algorithm	Maximize net savings, THD of voltage	18, 69-bus
2017	[110]	Fixed	Location +Size	Average load	WOA Algorithm	Operating cost and power loss minimization	34, 85-bus
2017	[103]	Both	Location +Size	Different load states	Algorithm of Inclusion and interchange of variables	Minimize the annual total cost	69-bus
2017	[112]	Fixed	Location +Size	Average load	NSGA II	power loss and the THD minimization	9, 85-bus
2018	[104]	Fixed	Location +Size	Average load	Flower Pollination Algorithm (FPA)	Minimize the total power loss and cost of capacitor installation	33, 34 ,69, 85-bus

A multi-criteria SCBs placement problem had proposed using the Non-dominated Sorting Genetic Algorithm (NSGA) in [111]. It is needed to optimize the number of objectives simultaneously in NSGA. Moreover, in NSGA, any objective can be optimized without deterioration of other objective functions. So, Pareto-Optimal solutions are considered to fulfill the objective function [10]. Baghzouz and Wu had developed a method to optimize the size of SCBs in radial distribution feeder considering r.m.s. voltage and their corresponding total harmonic distortion. NSGS-II was introduced in [112] to reduce power losses and ensure the THD maintains power quality. The authors found that the optimal sizing of SCBs will cause unexpected distortion in voltage profiles when harmonic distortion is neglected [113]-[114]. The researcher used the PSO algorithm for finding the optimum size, location, and type considering non-linear loads in [115]. Yu et al. applied the GA algorithm to address the SCBs placement and sizing problem by incorporating the impact of voltage and current harmonics [116]. The researcher had demanded that the applied method minimized THD and confirm higher annual benefits in contrast with [117]-[119]. MSPSO algorithm was applied in [120] where the fitness function was a net yearly benefit, maximum THD of voltage, maximum voltage deviation, and a resonance constraint. A.M. Othman developed the EBFO technique that incorporates optimal SCBs sizing and sitting with thermal cable evaluation on a practical 110kV sub-transmission line [121]. PFGA algorithm has provided Cost reduction & power quality improvement in radial distribution systems [122].

2.5 Multi-dimensional Problems

In some research articles, authors considered other power system problems with SCBs such as- Placement of Distributed Generations (DGs) [123]-[131], reconfiguration of the Network [132]-[140], load tap changer [141], placement of voltage regulators [142]-[148], etc. Voltage regulator and SCBs placement performed simultaneously to control voltage and var [142]-[144]. Hung et al. proposed a multidimensional algorithm that associated SCBs, DGs, and network reconfiguration in a single objective function to reduce distribution feeder losses significantly [149]. Adel et al. proposed a Water Cycle Algorithm (WCA) to size and sit of SCBs and DGs that reduce power losses, voltage deviation, electrical energy cost, and total emissions [150]. WCA was also incorporated in the article [151], where the authors suggested two load power factor models to minify feeder losses and voltage profile enhancement. GA interfaced with COM model has developed for optimal phase reconfiguration and SCBs placement [152]. In [153], a Hybrid WIPSO-GSA algorithm has been proposed in distribution systems considering feeder failure rate. Feeders reconfiguration and SCBs placement done by Mixed-integer second-order cone programming model [154]. The authors proposed a methodology for the sustainable operation of distribution systems along with sitting and sizing of SCBs and dispatchable DGs. Sensitivity analysis based on voltage stability index has been employed to minimize feeder current, power loss, and improve voltage profiles [155].

Table 5 Summary of Multi-dimensional problems.

Publi-shed	Ref.	SCB type	Design variables	Load profiles	Method	Objective function	Test systems
1985	[142]	Both	Location +Size	Variable load conditions	Analytical Method	Minimize the peak power and energy losses	23 kV Carolina Power & Light Co. sys.
1995	[137]	Switched	Location	Variable loads	Dynamic Programming Techniques	Power loss minimization & network reconfiguration	20kV, 63-node dist. Feeder
1996	[145]	Switched	Location	Different load conditions	A Neural Network (NN)	Minimize I^2R losses and maintain all bus voltages	30-bus
2002	[135]	Fixed	Location	Average load	MNV & GA algorithm	Power loss reduction	69-bus
2006	[146]	Fixed	Location +Size	Non-linear and Unbalanced Loads	Genetic Algorithm	Minimize power loss and harmonic distortion	34-bus
2008	[136]	Switched	Location	Average load	Ant Colony Search Algorithm (ACSA).	Minimize power loss	3-feeder dist. System
2009	[125]	Fixed	Location +Size	Linear and nonlinear load models	Genetic Algorithms (GA)	Power and energy Losses minimization	11 kV, 30-node feeder
2010	[138]	Fixed	Location	Different load levels	Mixed-integer non-linear programming	Minimize the energy loss	16, 33 & 83-bus
2011	[134]	Fixed	Location	Average load	Harmony Search (HA)	Minimization of losses cost and reliability cost	83-bus
2012	[124]	Switched	Location	Different load levels	SAIDI, SAIFI	Minimize capacitor investment & energy cost	Tabriz power electric dist., Iran
2012	[147]	Both	Location	Different load levels	GA and OPF	Multi objectives	70-bus
2013	[123]	Fixed	Location +Size	Different load levels	Memetic algorithm	Minimize power loss and improve voltage profiles	34-bus
2013	[148]	Fixed	Location +Size	Different load levels	Mixed-integer LP	Minimize power loss and improve voltage profiles	136 & 69-bus

Publi-shed	Ref.	SCB type	Design variables	Load profiles	Method	Objective function	Test systems
2013	[141]	Both	Location +Size	Different load levels	Modified Discrete PSO	Minimize capacitor investment & energy cost	33, 37-bus
2014	[126]	Switched	Location +Size	Different load levels	ICA/GA hybrid method	Multi objectives	33 & 69-bus
2014	[127]	Fixed	Size	Linear and non-linear loads	Genetic algorithm	Minimize THD, power loss & improve voltage profiles	33-bus
2015	[128]	Fixed	Location +Size	Uncertain load variations	MOPSO method	Minimize power loss and improve bus voltage	33, 94-bus
2016	[129]	Switched	Location +Size	Average load	IMDE algorithm	Minimize power loss	33, 69-bus
2017	[139]	Both	Location +Size	Discrete load levels	HS-PABC algorithm	Minimize power loss and improve bus voltage	69, 118-bus
2017	[130]	Fixed	Location +Size	Two Different load level	IVM & PLI algorithm	Minimize power loss	33, 85-bus
2017	[131]	Switched	Location +Size	Variable load levels	MOEA/D algorithm	Minimizing system real and reactive power losses.	33, 69,83, 119-bus
2018	[150]	Switched	Location +Size	Average load	Water Cycle Algorithm	Minimizing power losses, voltage deviation, electrical energy cost, total emissions	33, 69-bus & real Egyptian system
2018	[140]	Fixed	Location +Size	Average load	Multi-Objective Optimization Problem	Minimized losses & reduced voltage unbalancing	IEEE-37 and 123-node
2019	[151]	Fixed	Location +Size	Two load power factor	Water Cycle Algorithm (WCA)	Minimize power loss and improve bus voltage	33-bus
2019	[152]	Fixed	Location +Size	Average load	GA interfaced with COM model	Minimize power loss and improve voltage profiles	IEEE-13,37-bus
2019	[153]	Switched	Location +Size	Average load	Hybrid WIPSO-GSA algorithm	Maximization of total cost benefit	33-bus & Indian 85-bus
2019	[154]	Both	Location	Voltage-dependent load	The mixed-integer second-order cone programming model	Minimize power loss and improve voltage profiles	69,2313-node dist. Sys.
2019	[155]	Fixed	Location +Size	Different load condition	Sensitivity analysis based on voltage stability index	Minimize feeder current, power loss and improve voltage profiles	33-bus dist. System

2.6 Evaluation of the Methods

It is easy for the implementation of the analytical method, and its execution is faster. Since it takes a simple presumption and considers one snapshot of an electric power system loading condition, their results are suggestive. The strength of the Exhaustive Search (ES) method is -it is assured to the finding of global optimum, but it does not itself a simulation technique and appropriate for the large electric system.

Hence, in a dynamic programming method, this ES method is not suitable. All Heuristic methods are robust. It can furnish very accurate solutions for optimal SCBs placement for large and complex systems. They needed huge computations.

Nevertheless, this drawback is not essential that much critical in the applications of SCBs placement. The most frequently applied methods are AI methods for SCBs placement because it finds optimum solutions very fast. Most of the current researches is running based on AI methods and employed in Multi-dimensional problem solutions for their accuracy and fast convergence characteristics.

3. Combinatorial Method

The Combinatorial Method (CM) is for radial distribution system with source (substation) bus as slack bus and all other load buses taken as PQ buses. The algorithm proposed is described in the following steps shown in Fig. 3 for deciding the optimal sizes of the capacitors in terms of standard sizes available in the market and their locations (only load buses):

(i). Input Data and Initialization: The distribution system data is initialized in this step

(ii). Base Case Results: The “Forward/Backward Sweep” method of the Deterministic Load Flow (DLF) is carried out for the base case study to store the base case results, which will be used to compare the results with (1).

(iii). Generation of Combinations: All possible combinations of different commercially available capacitors are generated. Similarly, all possible combinations of the node are created.

(iv). Capacitor Placement: Each capacitor of the first combination is kept at corresponding load buses of the first combination of node and run the DLF to get the feeder loss. Similarly, DLF is performed to get the loss by placing capacitors

from the first combination to the second, third until the last combination of nodes, and getting the losses. After finishing, the second combination of the capacitor is placed to all combinations corresponding to the same previous procedures to get the losses. This procedure is repeated for all capacitors combination.

(v). The program is terminated when DLF is performed at all node combinations by each capacitor of all capacitor combinations. Finally, the minimum feeder loss and a corresponding combination of the capacitor and node are determined.

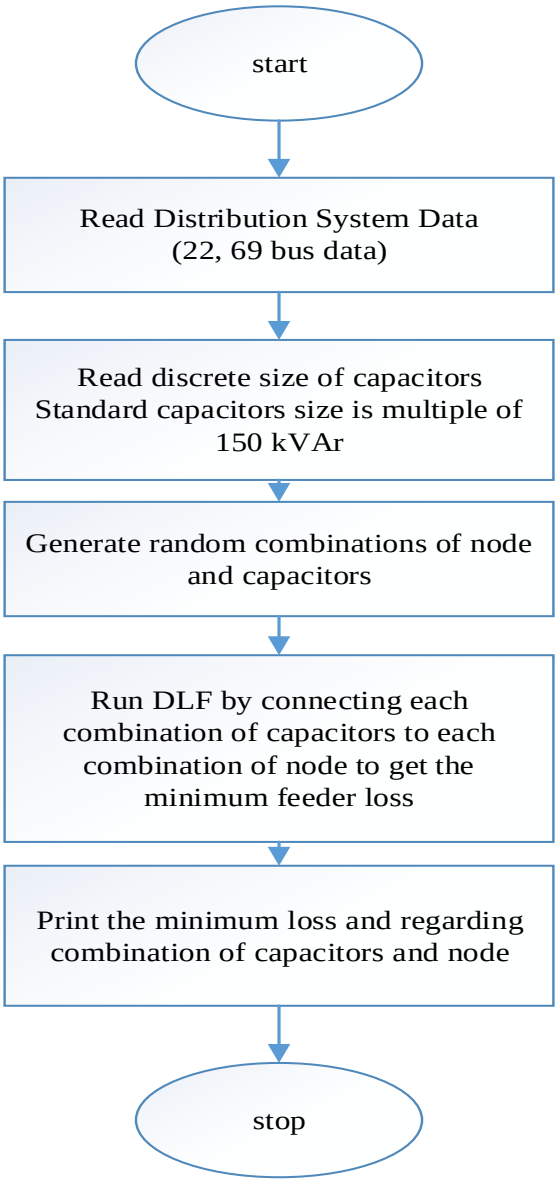

Fig. 3 Algorithm of the combinatorial method based capacitor placement.

Since every capacitor combination is checked with all node combinations, the program needs huge computational time. Still, it has given more accurate results comparatively with another capacitor placement algorithm. In this study, two standard test systems are considered for analysis and demonstrating the above algorithm with practical Indian 22-bus and IEEE 69-bus system.

Standard capacitor sizes available in the literature (in kVAr): 150, 300, 450, 600, 750, 900, 1050, 1200, 1350, 1500, 1650, 1800, 1950, 2100, 2250, 2400, 2550, 2700, 2850, 3000, 3150, 3300, 3450, 3600, 3750, 3900, 4050.

3.1 22-bus Radial Practical Test System

The data for the 22-bus agricultural test system is given in [67]. This 22-bus system belongs to a small part of India's Eastern Power Distribution system with 11 kV base voltage. It has a 662.311 kW real power load and 667.40 kVAr reactive power load comprised of 21 branches and 22-buses in Fig. 4. This practical test system is rated with voltage 11 kV, Vmax =1.1 pu, and Vmin = 0.9 pu, along with a base 10 MVA complex power rating.

The optimal locations are found at node-9, 13, 17, and node-20 with 150 kVAr in every node for the nominal load (100%) after completing the simulation using the proposed combinatorial method. The minimum loss is 9.30 kW, and the lowest voltage is 0.9817 pu at node-22, but for the light load (50%) condition, the loss became 2.39 kW that have 0.9904 pu voltage at node-22 while optimal location found node-9 and node-17 with 150 kVAr each. Besides, for peak load (160%) condition, feeder loss is 24.41 kW, and lowest voltage at node is 22 with 0.9700 pu using a total of 900 kVAr capacitor bank in four optimal locations (Table 7).

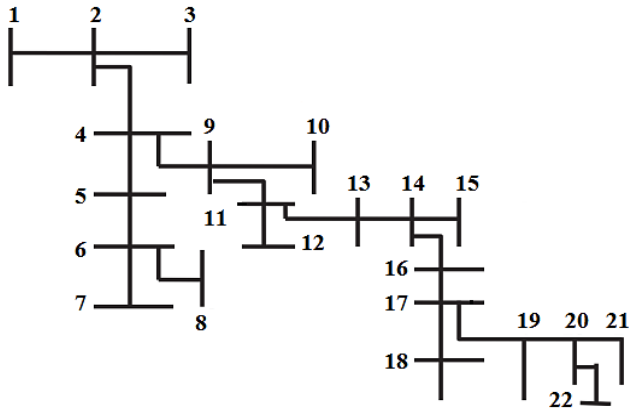

Fig. 4 22-bus agricultural practical Indian agricultural test system.

The simulated results are compared with DSA [67], [95]. The optimal locations and sizes have appended in Table 7, including feeder loss and lowest voltage level considering three different loading conditions such as nominal load (100%), light load (50%), and peak load (160%). One year or 8760 hours have been divided into 5260 hours for nominal load, 2000 hours for a light load, and 1500 hours for peak load.

Table 6 Load level and load duration time.

Load level	0.5 (light)	1.0 (normal)	1.6 (peak)
Duration (hr)	2000	5260	1500

The real power loss in the whole feeder is 17.7 kW, 4.30 kW, and 46.08 kW for nominal, light, and peak load, respectively, by the analytical method without using any capacitor compensation. It is found that simulations carried out using Combinatorial Method provide a better total cost, cost of energy loss, and cost of capacitor installation than that obtained from the Direct Search Algorithm (DSA) found in the literature. Also, it is seen that there is more minimization in power loss in nominal (100%) and peak (160%) load conditions with respect to DSA and TLBO, but voltage level reduced a little bit in every load condition.

Table 7 Real power loss and voltage profile with different load scenarios in 22-bus.

22-bus system	DSA [67]		TLBO [95]		Combinatorial Method (CM)	
1. Nominal load (100%) Optimal Placement	Location	Size (kVAr)	Location	Size (kVAr)	Location	Size (kVAr)
	4	150	9	150	9	150
	13	300	14	150	13	150
	16	150	17	150	17	150
	17	150	20	150	20	150
Minimum voltage node	22		22		22	
Minimum voltage (pu)	0.9824		0.9822		0.9817	
Power Loss (kW)	9.66		9.31		9.30	
2. Light load (50%) Optimal Placement	4	0	9	150	9	150
	13	150	14	0	13	0
	16	150	17	150	17	150
	17	0	20	0	20	0
Minimum voltage node	22		22		22	
Minimum voltage (pu)	0.9909		0.9903		0.9904	
Power Loss (kW)	2.39		2.39		2.39	
3. Peak load (160%) Optimal Placement	4	150	9	150	9	150
	13	450	14	300	13	300
	16	300	17	150	17	150
	17	150	20	300	20	300
Minimum voltage node	22		22		22	
Minimum voltage (pu)	0.9701		0.9712		0.9700	
Power Loss (kW)	24.89		24.43		24.41	
Ratings of the installed capacitor (maximum one) kVAr)	150, 450, 300, 150 (Total=1050)		150, 300, 150, 300 (Total=900)		150, 300, 150, 300 (Total=900)	
Capacitor cost ($)	1050*3=3,150		900*3=2,700		900*3=2,700	
The energy lost cost ($)	5575.59		5421.53		5421.53	
Total cost with capacitor ($)	8,725.59		8,121.53		8,121.53	

Comparison of voltage profiles has demonstrated in Fig. 5 for different loading conditions. It is seen that the voltage level has improved due to the employment of SCBs except for peak load conditions. It is because extra loads cause more voltage deviation than nominal load, and without reactive compensation, the scenario will be worse. Comparison of percentage improvement of voltage profile and total feeder loss minimization for DSA, TLBO, and CM methods have shown in Fig. 6. There are remarkable improvements in power loss reduction after SCBs connection where CM gives 47.42% loss reduction than without SCBs compensation. This figure is much better than DSA (45.39%) and TLBO (47.37%) at nominal load. A similar loss reduction pattern has been maintained for light load and peak load conditions. Voltage profiles also improved, but in peak load, the condition the amount is appreciable than nominal and load. CM shows more voltage level enhancement than DSA and TLBO in the 22-bus distribution system.

Per unit cost of energy has taken $0.06/ kWh, and the cost of capacitor bank has been considered $3.0/ kVAr [67] in cost calculations. Without installing the capacitor bank, the total cost of energy loss in different load conditions is $10,249.32/year. After using capacitors, it became $8,121.53/year that saved $2,127.79 annually, and this amount is better than the DSA ($8,725.59/year) techniques (Table 7).

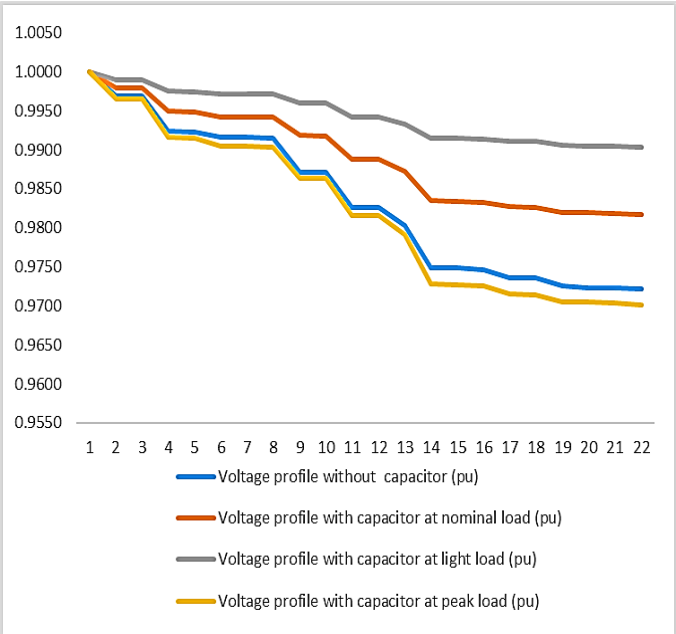

Fig. 5 The contrast of voltage profile employing SCBs at different loading conditions.

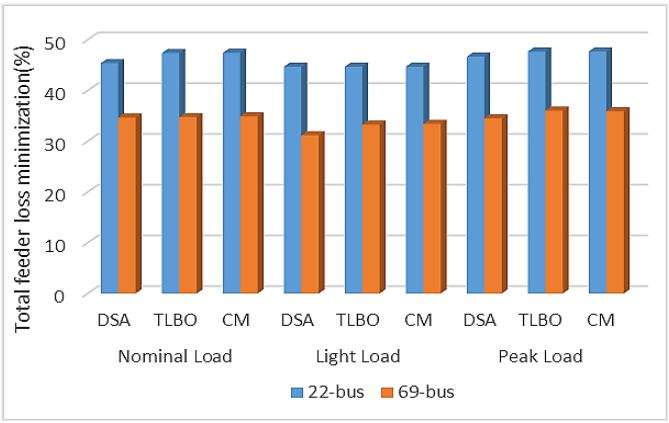

(a)

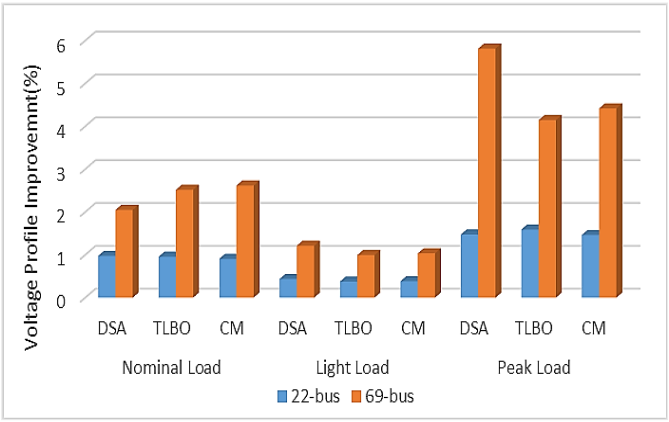

(b)

Fig. 6 The contrast of 3-different methods of SCBs sitting: (a) Percentage of line loss reduction, (b) Percentage of VPI.

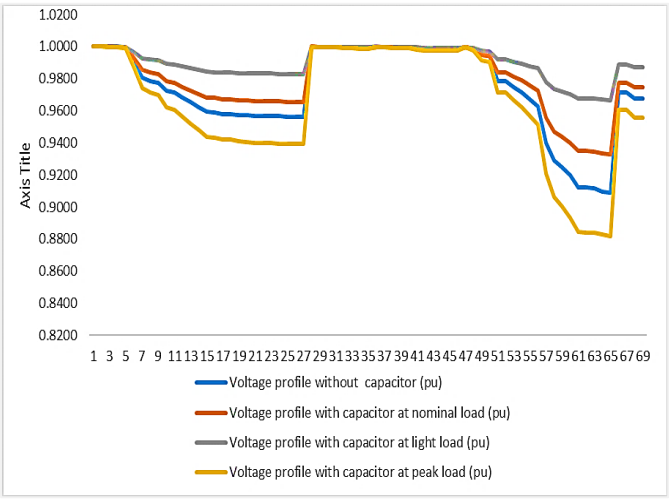

Fig. 7 The contrast of voltage profile employing SCBs at different loading conditions.

3.2 69-bus Radial Practical Test Systems

The complete system data has been taken from D. Das et al., 2008. This 69-bus radial test system comprises 69 nodes and 68 branches with base MVA 10 MVAr and 12.7 kV base voltage and a total of 1.896 MW real power load and 1.347 MVAr reactive power loads. The maximum voltage rating is Vmax =1.1 pu, and the minimum voltage rating is Vmin = 0.9 pu. This radial test system's real power loss is 225 kW [87] without employing any reactive power compensation. Simulation using the backward-forward sweep method obtained the same results.

Different groupings of 150 kVAr, 300 kVAr, 450 kVAr, 750 kVAr, and 1050 kVAr commercially available static capacitors have been used to generate combinations using three optimal places to get the lowest real power loss and voltage profile. Node-61, 64, 18 with 1050 kVAr, 300 kVAr, and 300 kVAr rating gives the minimum 146.50 kW loss that maintains 0.9330 pu voltage level that is a better result than Fuzzy GA [87] and DSA [67].

The simulated output using the combinatorial method and backward-forward power flow is assessed with DSA and Fuzzy GA. The minimum loss locations and sizes are given in Table 8, considering three different loadings. The real power loss 146.50 kW for the nominal load (100%), 34.36 kW for the light load (50%), and 417.60 kW for peak load (160%) with no additional reactive power supply. It is observed that simulation performing with combinatorial method furnished relatively than Fuzzy GA and DSA. Besides, it is found that there is more minimization in power loss in nominal and light load conditions rather than GA and DSA techniques. Meanwhile, the voltage profile is slightly decreased in light and peak load but shows an improved level than in nominal load condition (0.9330 p.u.) than DSA. Without installing the capacitor bank, the total cost of feeder energy loss in various loading conditions is $135,936.00/year (Table 8). After using capacitors, it became $87,999.3/year that saved $41,636.70 annually, and this amount is better than the Fuzzy GA and DSA techniques.

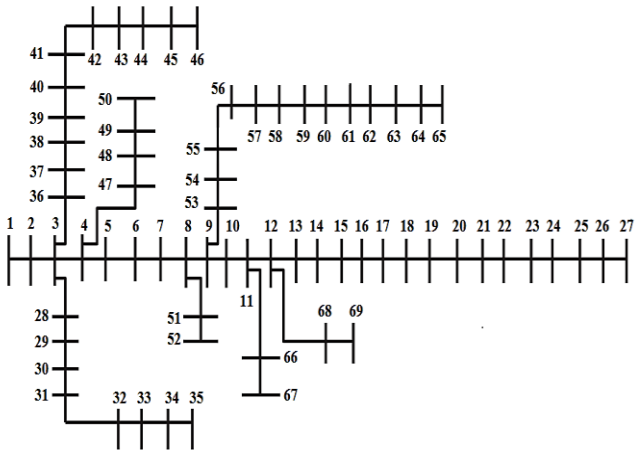

Fig. 8 69-bus radial distribution test system.

Like a 22-bus distribution system, voltage improves significantly in the 69-bus test system after employing SCBs except for peak load, where nominal load provides better VPI (Fig. 7). Moreover, Fig. 6 (a) shows the percentage of feeder loss minimization for 69-bus distribution feeder. CM provides a better loss of minimization than DSA and TLBO. For nominal load and light, load CM provides 34.89% and 33.41% loss reduction, where DSA and TLBO provide 34.65%, 34.74%, and 31.16%, 33.27%, respectively. But for peak load condition, TLBO shows better loss reduction (36.04%) than CM (35.89%). The percentage VPI for the 69-bus system is much better than the 22-bus radial system. It is seen from Fig. 6 that for nominal load level CM gives better bus voltage improvement compare to DSA and TLBO were 2.62%, 2.52%, 2.05% VPI for CM, DSA, and TLBO.

Table 8 Real power loss and voltage profile with different load scenarios in 69-bus.

69-bus system	Fuzzy GA [87]		DSA [67]		TLBO [95]		Combinatorial Method (CM)	
1. Nominal load (100%) Optimal Placement	Location	Size (kVAr)	Location	Size (kVAr)	Location	Size (kVAr)	Location	Size (kVAr)
	59	100	15	450	22	300	61	1050
	61	700	60	450	61	1050	64	300
	64	800	61	900	62	300	18	300
Minimum voltage node	65		65		65		65	
Minimum voltage (pu)	0.93693		0.9318		0.9321		0.9330	
Power Loss (kW)	156.52		147.00		146.80		146.50	
2. Light load (50%) Optimal Placement	59	0.00	15	300	22	150	61	450
	61	0.00	60	300	61	450	64	150
	64	300	61	450	62	150	18	150
Minimum voltage node	65		65		65		65	
Minimum voltage (pu)	0.9622		0.9683		0.9662		0.9666	
Power Loss (kW)	40.48		35.52		34.43		34.36	
3. Peak load (160%) Optimal Placement	59	1100	15	900	22	300	61	1050
	61	800	60	900	61	1050	64	750
	64	1200	61	1800	62	750	18	300
Minimum voltage node	65		65		65		65	
Minimum voltage (pu)	0.90014		0.8936		0.8795		0.8818	
Power Loss (kW)	460.45		427.30		417.28		417.60	
Ratings of the installed capacitor (maximum one) kVAr)	1100, 800, 1200, (Total=3100)		900, 900, 1800 (Total=3600)		1050, 750, 300 (Total=2100)		1050, 750, 300 (Total=2100)	
Capacitor cost ($)	3100*3=9,300		3600*3=10,800		3150*3=6,300		3150*3=6,300	
The energy lost cost ($)	95727.00		89,112.60		87,999.30		87,999.30	
Total cost with capacitor ($)	105,027.00		99,912.60		94,299.30		94,299.30	

4. Conclusion

In this paper, the second section has presented an in-depth comparative review of SCBs placement and sizing that included types, design variables, load profiles, methods, and test distribution systems sequentially through classification and analyzation of present and future trends. There are four types of SCBs problems that have been reviewed; however, Analytical methods and Numerical methods have provided the most robust solution, but these methods needed higher computational time. Contrary, AI methods seek the optimum solution that depends on the searching ability of the algorithm hence save computational time. The most frequently applied methods are the AI method for SCBs placement in recent research due to its computational characteristics.

A new approach called Combinatorial Method has developed for optimal placement and sizing of SCBs in distribution systems in the third section. The locations and sizes have been determined by generating random combinations and running deterministic load flow each time. The results obtained from the proposed technique have been compared with DSA and FGA, and TLBO algorithm. The research study has been carried out on modified Indian practical 22-bus and IEEE 69-bus system. The results showed that around forty-seven percent loss minimized in the 22-bus system, and almost thirty-five percent loss was reduced in 69-bus radial distribution systems. Besides, reactive compensation still maintains a satisfactory voltage level at all buses and SCB connection points. The proposed algorithm saved more in terms of money annually than the DSA and Fuzzy GA and TLBO method by optimal sizing and sitting of SCBs. Though the proposed CM method is time-consuming, this method would help the researcher achieve better results for planning purposes. Due to feeder loss minimization and voltage profile improvement in distribution feeders, both utilities and individual owners will be encouraged to accommodate more DGs.

4.1 Future Study

Though many works are already done for optimal sitting and sizing of SCBs, further research is necessary to enhance the performance and capability of SCBs to solve more complex

problems introduced by renewable energy integration on the existing grid. Wind velocity and solar radiations are not the only uncertain parameters, but there are other Distributed Energy Resources (DERs) and metrics that are stochastic such as: market price, future capital cost, fuel price, future fuel supply system, future load growth, and power of plug-in Electric Vehicles (EVs). Moreover, Network reconfiguration, optimal sitting, and sizing of DGs, Protective device placement, optimal allocation of Energy Storage System (ESS), substation, and line expansion also need to investigate simultaneously with optimal SCBs sitting and sizing. However, in the optimal SCBs placement problem, ancillary services should be considered. Because to maintain reliable grid operation, optimal SCBs placement can provide ancillary services by supplying necessary reactive power to the grid when needed. Finally, more robust and fast programming methods are required that give more accurate measures with minimum memory requirement.

Acknowledgments

The first author would like to thanks ADB-JSP for providing the scholarship to pursue his master's degree and carry out this work at the Asian Institute of Technology, Thailand.

References

[1] Arulraj, R. and Kumarappan, N., 2019. Optimal economic-driven planning of multiple DG and capacitor in distribution network considering different compensation coefficients in feeder's failure rate evaluation. *Engineering Science and Technology, an International Journal*, *22*(1), pp.67-77.

[2] Neagle, N.M. and Samson, D.R., 1956. Loss reduction from capacitors installed on primary feeders [includes discussion]. *Transactions of the American Institute of Electrical Engineers. Part III: Power Apparatus and Systems*, *75*(3), pp.950-959.

[3] Kasztenny, B., Schaefer, J. and Clark, E., 2007, March. Fundamentals of adaptive protection of large capacitor banks. In *2007 Power Systems Conference: Advanced Metering, Protection, Control, Communication, and Distributed Resources* (pp. 154-186). IEEE.

[4] Segura, S., Romero, R. and Rider, M.J., 2010. Efficient heuristic algorithm used for optimal capacitor placement in distribution systems. *International journal of electrical power & energy systems*, *32*(1), pp.71-78.

[5] Lidula, N.W.A. and Rajapakse, A.D., 2011. Microgrids research: A review of experimental microgrids and test systems. *Renewable and Sustainable Energy Reviews*, *15*(1), pp.186-202.

[6] Eltawil, M.A. and Zhao, Z., 2010. Grid-connected photovoltaic power systems: Technical and potential problems—A review. *Renewable and sustainable energy reviews*, *14*(1), pp.112-129.

[7] Taylor, C.W., 2003. Shunt Compensation for Voltage Stability. *IFAC Proceedings Volumes*, *36*(20), pp.43-48.

[8] Andersson, G., Donalek, P., Farmer, R., Hatziargyriou, N., Kamwa, I., Kundur, P., Martins, N., Paserba, J., Pourbeik, P., Sanchez-Gasca, J. and Schulz, R., 2005. Causes of the 2003 major grid blackouts in North America and Europe, and recommended means to improve system dynamic performance. *IEEE transactions on Power Systems*, *20*(4), pp.1922-1928.

[9] Pereira, L., 2004. Cascade to black [system blackouts]. *IEEE Power and Energy Magazine*, *2*(3), pp.54-57.

[10] Bruns, D.P., Newcomb, G.R., Miske, S.A., Taylor, C.W., Lee, G.E. and Edris, A., 2001. Shunt capacitor bank series group shorting (CAPS) design and application. *IEEE Transactions on Power Delivery*, *16*(1), pp.24-32.

[11] Dortolina, C.A. and Nadira, R., 2005. The loss that is unknown is no loss at all: A top-down/bottom-up approach for estimating distribution losses. *IEEE Transactions on Power Systems*, *20*(2), pp.1119-1125.

[12] Targosz, R., Belmans, R., Declercq, J., De Keulenaer, H., Furuya, K., Karmarkar, M., Martinez, M., McDermott, M. and Pinkiewicz, I., 2005. The potential for global energy savings from high efficiency distribution transformers. *Leonardo Energy Transformer–European Copper Institute*.

[13] EPRI. Assessment of transmission and distribution losses in New York.

[14] EIA, 2011. Annual Energy Outlook 2011. Available from ⟨http://www.eia.gov/forecasts/archive/aeo11/⟩ Last Accessed on: 20-Dec-20202. Information Administration, Washington, DC. 2011.

[15] Prada, R.B. and Souza, L.J., 1998. Voltage stability and thermal limit: constraints on the maximum loading of electrical energy distribution feeders. *IEE Proceedings-Generation, Transmission and Distribution*, *145*(5), pp.573-577.

[16] ENERGI. Guidelines to install, operate and maintain ht capacitors & its associated equipment ⟨http://www.energegroup.com/CapacitorManual.pdf⟩.

[17] Aman, M.M., Jasmon, G.B., Mokhlis, H. and Bakar, A.H.A., 2013. Analysis of the performance of domestic lighting lamps. *Energy policy*, *52*, pp.482-500.

[18] Milligan M, Ela E, Hein J, Schneider T, Brinkman G, Denholm P., 2012. Exploration of high-penetration renewable electricity futures. Vol. 4 of renewable electricity futures study. NREL/TP-6A20-52409-4. Golden, CO: National Renewable Energy Laboratory.

[19] EURELECTRIC. Power outages in 2003-global regulatory Network.

[20] Mostafa, S.M.G., Singh, J.G., Masrur, H. and Ullah, M.S., 2016, October. A prospective model of Bangladesh electricity market. In *2016 International Conference on Innovations in Science, Engineering and Technology (ICISET)* (pp. 1-5). IEEE.

[21] Root, C.E., 2006. The future beckons [electric power industry]. *IEEE Power and Energy Magazine*, *4*(1), pp.24-31.

[22] Singh, H., Hao, S. and Papalexopoulos, A., 1998. Transmission congestion management in competitive electricity markets. *IEEE Transactions on power systems*, *13*(2), pp.672-680.

[23] Hemmati, R., Hooshmand, R.A. and Khodabakhshian, A., 2013. State-of-the-art of transmission expansion planning: Comprehensive review. *Renewable and Sustainable Energy Reviews*, *23*, pp.312-319.

[24] Baldick, R., 2004. Reactive issues- reactive power in restructured markets. *IEEE Power & Energy Magazine*, *2*(6), pp.14-17.

[25] Hogan, W.W., 1996. Markets in real electric networks require reactive prices. In *Electricity transmission pricing and technology* (pp. 143-182). Springer, Dordrecht.

[26] Aman, M.M., Jasmon, G.B., Bakar, A.H.A. and Mokhlis, H., 2012. Optimum capacitor placement and sizing for distribution system based on an improved voltage stability index. *International Review of Electrical Engineering*, *7*(3), pp.4622-4630.

[27] Gonzalez-Longatt, F. and Fortoul, C., 2005, March. Review of the distributed generation concept: Attempt of unification. In *International Conference on Renewable Energies and Power Quality (ICREPQ 05), España* (pp. 16-18).

[28] Ackermann, T., Andersson, G. and Söder, L., 2001. Distributed generation: a definition. *Electric power systems research*, *57*(3), pp.195-204.

[29] Mahmud, M.A., Hossain, M.J., Pota, H.R. and Nasiruzzaman, A.B.M., 2011, November. Voltage control of distribution networks with distributed generation using reactive power compensation. In *IECON 2011-37th Annual Conference of the IEEE Industrial Electronics Society*, pp. 985-990.

[30] Liew, S.N. and Strbac, G., 2002. Maximising penetration of wind generation in existing distribution networks. *IEE Proceedings-Generation, Transmission and Distribution*, *149*(3), pp.256-262.

[31] Turitsyn, K., Sulc, P., Backhaus, S. and Chertkov, M., 2011. Options for control of reactive power by distributed photovoltaic generators. *Proceedings of the IEEE*, *99*(6), pp.1063-1073.

[32] Rao, R.S., Narasimham, S.V.L. and Ramalingaraju, M., 2011. Optimal capacitor placement in a radial distribution system using plant growth simulation algorithm. *International journal of electrical power & energy systems*, *33*(5), pp.1133-1139.

[33] Mekhamer, S.F., Soliman, S.A., Moustafa, M.A. and El-Hawary, M.E., 2002. Load flow solution of radial distribution feeders: a new contribution. *International journal of electrical power & energy systems*, *24*(9), pp.701-707.

[34] Cook, R.F., 1959. Analysis of capacitor application as affected by load cycle. *Transactions of the American Institute of Electrical Engineers. Part III: Power Apparatus and Systems*, *78*(3), pp.950-956.

[35] Cook, R.F., 1961. Optimizing the application of shunt capacitors for reactive-volt-ampere control and loss reduction. *Transactions of the American Institute of Electrical Engineers. Part III: Power Apparatus and Systems*, *80*(3), pp.430-441.

[36] Bae, Y.G., 1978. Analytical method of capacitor allocation on distribution primary feeders. *IEEE Transactions on Power Apparatus and Systems*, (4), pp.1232-1238.

[37] Grainger, J.J. and Lee, S.H., 1981. Optimum size and location of shunt capacitors for reduction of losses on distribution feeders. *IEEE Transactions on Power Apparatus and Systems*, (3), pp.1105-1118.

[38] Schmill, J.V., 1965. Optimum size and location of shunt capacitors on distribution feeders. *IEEE Transactions on Power Apparatus and Systems*, *84*(9), pp.825-832.

[39] Chang, N.E., 1969. Locating shunt capacitors on primary feeder for voltage control and loss reduction. *IEEE Transactions on Power Apparatus and Systems*, (10), pp.1574-1577.

[40] Chang, N.E., 1972. Generalized equations on loss reduction with shunt capacitor. *IEEE Transactions on Power Apparatus and Systems*, (5), pp.2189-2195.

[41] Lee, S.H. and Grainger, J.J., 1981. Optimum placement of fixed and switched capacitors on primary distribution feeders. *IEEE Transactions on Power Apparatus and Systems*, (1), pp.345-352.

[42] Salama, M.M.A., Chikhani, A.Y. and Hackam, R., 1985. Control of reactive power in distribution systems with an end-load and fixed load condition. *IEEE transactions on power apparatus and systems*, (10), pp.2779-2788.

[43] Salama, M.M.A., Mansour, E.A.A., Chikhani, A.Y. and Hackam, R., 1985. Control of reactive power in distribution systems with an end-load and varying load condition. *IEEE transactions on power apparatus and systems*, (4), pp.941-947.

[44] Haque, M.H., 1999. Capacitor placement in radial distribution systems for loss reduction. *IEE Proceedings-Generation, Transmission and Distribution*, *146*(5), pp.501-505.

[45] Cho, M.Y. and Chen, Y.W., 1997. Fixed/switched type shunt capacitor planning of distribution systems by considering customer load patterns and simplified feeder model. *IEE Proceedings-Generation, Transmission and Distribution*, *144*(6), pp.533-540.

[46] Arief, A. and Nappu, M.B., 2016. An analytical method for optimal capacitors placement from the inversed reduced jacobian matrix. *Energy Procedia*, *100*(100), pp.307-310.

[47] Kamel, S., Hamdy, W., Abd-elgwad, S., Selim, A. and Jurado, F., 2019, March. Development of Probabilistic Power Flow Algorithm for Radial Distribution Systems with Capacitors Using Analytical Approach. In *IEEE 10th International Renewable Energy Congress (IREC 2019), Sousse-Tunisia*.

[48] Ihsan, M., Shahzad, M. and Ullah, N., 2019, January. Analytical Method for Optimal Reactive Power Support in Power Network. In *2019 2nd International Conference on Computing, Mathematics and Engineering Technologies (iCoMET)* (pp. 1-6). IEEE.

[49] Crow, M.L., 2003. *Computational methods for electric power systems*. Crc Press.

[50] Saadat, H., 1999. *Power system analysis* (Vol. 2). McGraw-Hill.

[51] Dura, H., 1968. Optimum number, location, and size of shunt capacitors in radial distribution feeders a dynamic programming approach. *IEEE Transactions on Power Apparatus and Systems*, (9), pp.1769-1774.

[52] Fawzi, T.H., El-Sobki, S.M. and Abdel-halim, M.A., 1983. New approach for the application of shunt capacitors to the primary distribution feeders. *IEEE Transactions on Power Apparatus and Systems*, (1), pp.10-13.

[53] Ponnavsikko, M. and Rao, K.P., 1983. Optimal choice of fixed and switched shunt capacitors on radial distributors by the method of local variations. *IEEE transactions on power apparatus and systems*, (6), pp.1607-1615.

[54] Baran, M. and Wu, F.F., 1989. Optimal sizing of capacitors placed on a radial distribution system. *IEEE Transactions on power Delivery*, *4*(1), pp.735-743.

[55] Baran, M.E. and Wu, F.F., 1989. Optimal capacitor placement on radial distribution systems. *IEEE Transactions on power Delivery*, *4*(1), pp.725-734.

[56] Sharaf, A.M. and Ibrahim, S.T., 1996. Optimal capacitor placement in distribution networks. *Electric power systems research*, *37*(3), pp.181-187.

[57] Jasmon, G.B. and Lee, L.H.C.C., 1991. Distribution network reduction for voltage stability analysis and loadflow calculations. *International Journal of Electrical Power & Energy Systems*, *13*(1), pp.9-13.

[58] Khodr, H.M., Olsina, F.G., De Oliveira-De Jesus, P.M. and Yusta, J.M., 2008. Maximum savings approach for location and sizing of capacitors in distribution systems. *Electric Power Systems Research*, *78*(7), pp.1192-1203.

[59] Soto, S. and Hinojosa, V., 2016. Stochastic optimal allocation of reactive power banks for system loss minimization. *IEEE Latin America Transactions*, *14*(4), pp.1980-1987.

[60] Jannat, M.B. and Savić, A.S., 2016. Optimal capacitor placement in distribution networks regarding uncertainty in active power load and distributed generation units production. *IET Generation, Transmission & Distribution*, *10*(12), pp.3060-3067.

[61] Minsky, M.L., 1958, November. Some methods of artificial intelligence and heuristic programming. In *Proc. Symposium on the Mechanization of Thought Processes, Teddington*.

[62] Ng, H.N., Salama, M.M.A. and Chikhani, A.Y., 2000. Classification of capacitor allocation techniques. *IEEE Transactions on power delivery*, *15*(1), pp.387-392.

[63] Abdel-Salam, T.S., Chikhani, A.Y. and Hackam, R., 1994. A new technique for loss reduction using compensating capacitors applied to distribution systems with varying load condition. *IEEE Transactions on Power Delivery*, *9*(2), pp.819-827.

[64] Chis, M., Salama, M.M.A. and Jayaram, S., 1997. Capacitor placement in distribution systems using heuristic search strategies. *IEE Proceedings-Generation, Transmission and Distribution*, *144*(3), pp.225-230.

[65] da Silva, I.C., Carneiro, S., de Oliveira, E.J., de Souza Costa, J., Pereira, J.L.R. and Garcia, P.A.N., 2008. A heuristic constructive algorithm for capacitor placement on distribution systems. *IEEE Transactions on Power Systems*, *23*(4), pp.1619-1626.

[66] Hamouda, A. and Sayah, S., 2013. Optimal capacitors sizing in distribution feeders using heuristic search based node stability-indices. *International Journal of Electrical Power & Energy Systems*, *46*, pp.56-64.

[67] Raju, M.R., Murthy, K.R. and Ravindra, K., 2012. Direct search algorithm for capacitive compensation in radial distribution systems. *International Journal of Electrical Power & Energy Systems*, *42*(1), pp.24-30.

[68] El-Fergany, A.A. and Abdelaziz, A.Y., 2014. Capacitor allocations in radial distribution networks using cuckoo search algorithm. *IET Generation, Transmission & Distribution*, *8*(2), pp.223-232.

[69] El-Fergany, A.A. and Abdelaziz, A.Y., 2014. Efficient heuristic-based approach for multi-objective capacitor allocation in radial distribution networks. *IET Generation, Transmission & Distribution*, *8*(1), pp.70-80.

[70] Gnanasekaran, N., Chandramohan, S., Kumar, P.S. and Imran, A.M., 2016. Optimal placement of capacitors in radial distribution system using shark smell optimization algorithm. *Ain Shams Engineering Journal*, *7*(2), pp.907-916.

[71] Dixit, M., Kundu, P. and Jariwala, H.R., 2018. Optimal integration of shunt capacitor banks in distribution networks for assessment of techno-economic asset. *Computers & Electrical Engineering*, *71*, pp.331-345.

[72] Chiou, J.P. and Chang, C.F., 2015. Development of a novel algorithm for optimal capacitor placement in distribution systems. *International Journal of Electrical Power & Energy Systems*, *73*, pp.684-690.

[73] Devabalaji, K.R., Ravi, K. and Kothari, D.P., 2015. Optimal location and sizing of capacitor placement in radial distribution system using bacterial foraging optimization algorithm. *International Journal of Electrical Power & Energy Systems*, *71*, pp.383-390.

[74] Askarzadeh, A., 2016. Capacitor placement in distribution systems for power loss reduction and voltage improvement: a new methodology. *IET Generation, Transmission & Distribution*, *10*(14), pp.3631-3638.

[75] Muthukumar, K. and Jayalalitha, S., 2018. Multiobjective hybrid evolutionary approach for optimal planning of shunt capacitors in radial distribution systems with load models. *Ain Shams Engineering Journal*, *9*(4), pp.1975-1988.

[76] Mujezinović, A., Turković, N., Dautbašić, N., Dedović, M.M. and Turković, I., 2019, March. Use of Integer Genetic Algorithm for Optimal Allocation and Sizing of the Shunt Capacitor Banks in the Radial Distribution Networks. In *2019 18th International Symposium INFOTEH-JAHORINA (INFOTEH)* (pp. 1-6). IEEE.

[77] Kokash, N., 2005. An introduction to heuristic algorithms. Department of Informatics and Telecommunications. *University of Trento*.

[78] Aman, M.M., Jasmon, G.B., Bakar, A.H.A., Mokhlis, H. and Karimi, M., 2014. Optimum shunt capacitor placement in distribution system—A review and comparative study. *Renewable and Sustainable Energy Reviews*, *30*, pp.429-439.

[79] Sundhararajan, S. and Pahwa, A., 1994. Optimal selection of capacitors for radial distribution systems using a genetic algorithm. *IEEE transactions on Power Systems*, *9*(3), pp.1499-1507.

[80] Das, D., 2002. Reactive power compensation for radial distribution networks using genetic algorithm. *International journal of electrical power & energy systems*, *24*(7), pp.573-581.

[81] Haghifam, M.R. and Malik, O.P., 2007. Genetic algorithm-based approach for fixed and switchable

capacitors placement in distribution systems with uncertainty and time varying loads. *IET generation, transmission & distribution*, *1*(2), pp.244-252.

[82] Levitin, G., Kalyuzhny, A., Shenkman, A. and Chertkov, M., 2000. Optimal capacitor allocation in distribution systems using a genetic algorithm and a fast energy loss computation technique. *IEEE Transactions on Power Delivery*, *15*(2), pp.623-628.

[83] Boone, G. and Chiang, H.D., 1993. Optimal capacitor placement in distribution systems by genetic algorithm. *International Journal of Electrical Power & Energy Systems*, *15*(3), pp.155-161.

[84] Pazouki, S., Mohsenzadeh, A., Haghifam, M.R. and Ardalan, S., 2015. Simultaneous allocation of charging stations and capacitors in distribution networks improving voltage and power loss. *Canadian Journal of Electrical and Computer Engineering*, *38*(2), pp.100-105.

[85] Ng, H.N., Salama, M.M.A. and Chikhani, A.Y., 2000. Capacitor allocation by approximate reasoning: fuzzy capacitor placement. *IEEE transactions on power delivery*, *15*(1), pp.393-398.

[86] Bhattacharya, S.K. and Goswami, S.K., 2009. A new fuzzy based solution of the capacitor placement problem in radial distribution system. *Expert systems with applications*, *36*(3), pp.4207-4212.

[87] Das, D., 2008. Optimal placement of capacitors in radial distribution system using a Fuzzy-GA method. *International Journal of Electrical Power & Energy Systems*, *30*(6-7), pp.361-367.

[88] Gampa, S.R. and Das, D., 2016. Optimum placement of shunt capacitors in a radial distribution system for substation power factor improvement using fuzzy GA method. *International Journal of Electrical Power & Energy Systems*, *77*, pp.314-326.

[89] Singh, S.P. and Rao, A.R., 2012. Optimal allocation of capacitors in distribution systems using particle swarm optimization. *International Journal of Electrical Power & Energy Systems*, *43*(1), pp.1267-1275.

[90] Kanwar, N., Gupta, N., Swarnkar, A., Niazi, K.R. and Bansal, R.C., 2015. New sensitivity based approach for optimal allocation of shunt capacitors in distribution networks using PSO. *Energy Procedia*, *75*, pp.1153-1158.

[91] Huang, S.J., 2000. An immune-based optimization method to capacitor placement in a radial distribution system. *IEEE Transactions on Power Delivery*, *15*(2), pp.744-749.

[92] Huang, S.J. and Liu, X.Z., 2012. A plant growth-based optimization approach applied to capacitor placement in power systems. *IEEE Transactions on Power Systems*, *27*(4), pp.2138-2145.

[93] Pires, D.F., Martins, A.G. and Antunes, C.H., 2005. A multiobjective model for VAR planning in radial distribution networks based on tabu search. *IEEE Transactions On Power Systems*, *20*(2), pp.1089-1094.

[94] Mendes, A., Franca, P.M., Lyra, C., Pissarra, C. and Cavellucci, C., 2005. Capacitor placement in large-sized radial distribution networks. *IEE Proceedings-Generation, Transmission and Distribution*, *152*(4), pp.496-502.

[95] Sultana, S. and Roy, P.K., 2014. Optimal capacitor placement in radial distribution systems using teaching learning based optimization. *International Journal of Electrical Power & Energy Systems*, *54*, pp.387-398.

[96] Kaur, D. and Sharma, J., 2013. Multiperiod shunt capacitor allocation in radial distribution systems. *International Journal of Electrical Power & Energy Systems*, *52*, pp.247-253.

[97] Carlisle, J.C. and El-Keib, A.A., 2000. A graph search algorithm for optimal placement of fixed and switched capacitors on radial distribution systems. *IEEE Transactions on Power Delivery*, *15*(1), pp.423-428.

[98] Shuaib, Y.M., Kalavathi, M.S. and Rajan, C.C.A., 2015. Optimal capacitor placement in radial distribution system using gravitational search algorithm. *International Journal of Electrical Power & Energy Systems*, *64*, pp.384-397.

[99] Abu-Mouti, F.S. and El-Hawary, M.E., 2011. Optimal distributed generation allocation and sizing in distribution systems via artificial bee colony algorithm. *IEEE transactions on power delivery*, *26*(4), pp.2090-2101.

[100] Gallego, R.A., Monticelli, A.J. and Romero, R., 2001. Optimal capacitor placement in radial distribution networks. *IEEE Transactions on Power Systems*, *16*(4), pp.630-637.

[101] Kannan, S.M., Renuga, P., Kalyani, S. and Muthukumaran, E., 2011. Optimal capacitor placement and sizing using Fuzzy-DE and Fuzzy-MAPSO methods. *Applied Soft Computing*, *11*(8), pp.4997-5005.

[102] Goswami, S.K., Ghose, T. and Basu, S.K., 1999. An approximate method for capacitor placement in distribution system using heuristics and greedy search technique. *Electric Power Systems Research*, *51*(3), pp.143-151.

[103] Abril, I.P., 2017. Algorithm of inclusion and interchange of variables for capacitors placement. *Electric Power Systems Research*, *148*, pp.117-126.

[104] Tamilselvan, V., Jayabarathi, T., Raghunathan, T. and Yang, X.S., 2018. Optimal capacitor placement in radial distribution systems using flower pollination algorithm. *Alexandria engineering journal*, *57*(4), pp.2775-2786.

[105] Abul'Wafa, A.R., 2014. Optimal capacitor placement for enhancing voltage stability in distribution systems using analytical algorithm and Fuzzy-Real Coded GA. *International Journal of Electrical Power & Energy Systems*, *55*, pp.246-252.

[106] Injeti, S.K., Thunuguntla, V.K. and Shareef, M., 2015. Optimal allocation of capacitor banks in radial distribution systems for minimization of real power loss and maximization of network savings using bio-inspired optimization algorithms. *International Journal of Electrical Power & Energy Systems*, *69*, pp.441-455.

[107] Murty, V.V.S.N. and Kumar, A., 2015. Capacitor allocation in radial distribution system with time varying ZIP load model and energy savings. *Procedia Computer Science*, *70*, pp.377-383.

[108] da Rosa, W.M., Rossoni, P., Teixeira, J.C., Belati, E.A. and Asano, P.T.L., 2016. Optimal allocation of

capacitor banks using genetic algorithm and sensitivity analysis. *IEEE Latin America Transactions*, *14*(8), pp.3702-3707.

[109] Askarzadeh, A., 2016. Capacitor placement in distribution systems for power loss reduction and voltage improvement: a new methodology. *IET Generation, Transmission & Distribution*, *10*(14), pp.3631-3638.

[110] Prakash, D.B. and Lakshminarayana, C., 2017. Optimal siting of capacitors in radial distribution network using whale optimization algorithm. *Alexandria Engineering Journal*, *56*(4), pp.499-509.

[111] Milosevic, B. and Begovic, M., 2004. Capacitor placement for conservative voltage reduction on distribution feeders. *IEEE transactions on power delivery*, *19*(3), pp.1360-1367.

[112] Javadi, M.S., Nezhad, A.E., Siano, P., Shafie-khah, M. and Catalão, J.P., 2017. Shunt capacitor placement in radial distribution networks considering switching transients decision making approach. *International Journal of Electrical Power & Energy Systems*, *92*, pp.167-180.

[113] Baghzouz, Y. and Ertem, S., 1990. Shunt capacitor sizing for radial distribution feeders with distorted substation voltages. *IEEE Transactions on Power Delivery*, *5*(2), pp.650-657.

[114] Wu, Z.Q. and Lo, K.L., 1995. Optimal choice of fixed and switched capacitors in radial distributors with distorted substation voltage. *IEE Proceedings-Generation, Transmission and Distribution*, *142*(1), pp.24-28.

[115] Yu, X.M., Xiong, X.Y. and Wu, Y.W., 2004. A PSO-based approach to optimal capacitor placement with harmonic distortion consideration. *Electric Power Systems Research*, *71*(1), pp.27-33.

[116] Masoum, M.A., Ladjevardi, M., Jafarian, A. and Fuchs, E.F., 2004. Optimal placement, replacement and sizing of capacitor banks in distorted distribution networks by genetic algorithms. *IEEE transactions on power delivery*, *19*(4), pp.1794-1801.

[117] Masoum, M.A.S., Ladjevardi, M., Fuchs, E.F. and Grady, E.M., 2002, July. Optimal placement and sizing of fixed and switched capacitor banks under nonsinusoidal operating conditions. In *IEEE Power Engineering Society Summer Meeting*, (Vol. 2, pp. 807-813). IEEE.

[118] Masoum, M.A.S., Ladjevardi, M., Fuchs, E.F. and Grady, W.M., 2004. Application of local variations and maximum sensitivities selection for optimal placement of shunt capacitor banks under nonsinusoidal operating conditions. *International Journal of Electrical Power & Energy Systems*, *26*(10), pp.761-769.

[119] Masoum, M.A., Jafarian, A., Ladjevardi, M., Fuchs, E.F. and Grady, W.M., 2004. Fuzzy approach for optimal placement and sizing of capacitor banks in the presence of harmonics. *IEEE Transactions on Power Delivery*, *19*(2), pp.822-829.

[120] Ayoubi, M., Hooshmand, R.A. and Esfahani, M.T., 2017. Optimal capacitor placement in distorted distribution systems considering resonance constraint using multi-swarm particle swarm optimisation algorithm. *IET Generation, Transmission & Distribution*, *11*(13), pp.3210-3221.

[121] Othman, A.M., 2016. Optimal capacitor placement by Enhanced Bacterial Foraging Optimization (EBFO) with accurate thermal re-rating of critical cables. *Electric Power Systems Research*, *140*, pp.671-680.

[122] Vuletić, J. and Todorovski, M., 2016. Optimal capacitor placement in distorted distribution networks with different load models using Penalty Free Genetic Algorithm. *International Journal of Electrical Power & Energy Systems*, *78*, pp.174-182.

[123] Sajjadi, S.M., Haghifam, M.R. and Salehi, J., 2013. Simultaneous placement of distributed generation and capacitors in distribution networks considering voltage stability index. *International Journal of Electrical Power & Energy Systems*, *46*, pp.366-375.

[124] Mahaei, S.M., Sami, T., Shilebaf, A. and Jafarzadeh, J., 2012, May. Simultaneous placement of distributed generations and capacitors with multi-objective function. In *2012 Proceedings of 17th Conference on Electrical Power Distribution* (pp. 1-9). IEEE.

[125] Mady, I.B., 2009. Optimal sizing of capacitor banks and distributed generation in distorted distribution networks by genetic algorithms. *IEEE/ICEED*, pp.1-4.

[126] Moradi, M.H., Zeinalzadeh, A., Mohammadi, Y. and Abedini, M., 2014. An efficient hybrid method for solving the optimal sitting and sizing problem of DG and shunt capacitor banks simultaneously based on imperialist competitive algorithm and genetic algorithm. *International Journal of Electrical Power & Energy Systems*, *54*, pp.101-111.

[127] Biswas, S., Goswami, S.K. and Chatterjee, A., 2014. Optimal distributed generation placement in shunt capacitor compensated distribution systems considering voltage sag and harmonics distortions. *IET Generation, Transmission & Distribution*, *8*(5), pp.783-797.

[128] Zeinalzadeh, A., Mohammadi, Y. and Moradi, M.H., 2015. Optimal multi objective placement and sizing of multiple DGs and shunt capacitor banks simultaneously considering load uncertainty via MOPSO approach. *International Journal of Electrical Power & Energy Systems*, *67*, pp.336-349.

[129] Khodabakhshian, A. and Andishgar, M.H., 2016. Simultaneous placement and sizing of DGs and shunt capacitors in distribution systems by using IMDE algorithm. *International Journal of Electrical Power & Energy Systems*, *82*, pp.599-607.

[130] Dixit, M., Kundu, P. and Jariwala, H.R., 2017. Incorporation of distributed generation and shunt capacitor in radial distribution system for techno-economic benefits. *Engineering Science and Technology, an International Journal*, *20*(2), pp.482-493.

[131] Biswas, P.P., Mallipeddi, R., Suganthan, P.N. and Amaratunga, G.A., 2017. A multiobjective approach for optimal placement and sizing of distributed generators and capacitors in distribution network. *Applied Soft Computing*, *60*, pp.268-280.

[132] Su, C.T. and Lee, C.S., 2001. Feeder reconfiguration and capacitor setting for loss reduction of distribution

systems. *Electric power systems research*, *58*(2), pp.97-102.

[133] Jiang, D. and Baldick, R., 1996. Optimal electric distribution system switch reconfiguration and capacitor control. *IEEE transactions on Power Systems*, *11*(2), pp.890-897.

[134] Rezaei, P., Vakilian, M. and Hajipour, E., 2011, September. Reconfiguration and capacitor placement in radial distribution systems for loss reduction and reliability enhancement. In *2011 16th International Conference on Intelligent System Applications to Power Systems* (pp. 1-6). IEEE.

[135] Rong, Z., Xiyuan, P., Jinliang, H. and Xinfu, S., 2002, October. Reconfiguration and capacitor placement for loss reduction of distribution system. In *2002 IEEE Region 10 Conference on Computers, Communications, Control and Power Engineering. TENCOM'02. Proceedings.* (Vol. 3, pp. 1945-1949). IEEE.

[136] Chang, C.F., 2008. Reconfiguration and capacitor placement for loss reduction of distribution systems by ant colony search algorithm. *IEEE Transactions on Power Systems*, *23*(4), pp.1747-1755.

[137] Peponis, G.J., Papadopoulos, M.P. and Hatziargyriou, N.D., 1995. Distribution network reconfiguration to minimize resistive line losses. *IEEE Transactions on Power Delivery*, *10*(3), pp.1338-1342.

[138] de Oliveira, L.W., Carneiro Jr, S., De Oliveira, E.J., Pereira, J.L.R., Silva Jr, I.C. and Costa, J.S., 2010. Optimal reconfiguration and capacitor allocation in radial distribution systems for energy losses minimization. *International Journal of Electrical Power & Energy Systems*, *32*(8), pp.840-848.

[139] Muthukumar, K. and Jayalalitha, S., 2017. Integrated approach of network reconfiguration with distributed generation and shunt capacitors placement for power loss minimization in radial distribution networks. *Applied Soft Computing*, *52*, pp.1262-1284.

[140] Mehmood, K.K., Kim, C.H., Khan, S.U. and Haider, Z.M., 2018. Unified Planning of Wind Generators and Switched Capacitor Banks: A Multiagent Clustering-Based Distributed Approach. *IEEE Transactions on Power Systems*, *33*(6), pp.6978-6988.

[141] Ziari, I., Ledwich, G. and Ghosh, A., 2013. A new technique for optimal allocation and sizing of capacitors and setting of LTC. *International Journal of Electrical Power & Energy Systems*, *46*, pp.250-257.

[142] Grainger, J.J. and Civanlar, S., 1985. Volt/var control on distribution systems with lateral branches using shunt capacitors and voltage regulators part I: The overall problem. *IEEE Transactions on Power Apparatus and Systems*, (11), pp.3278-3283.

[143] Civanlar, S. and Grainger, J.J., 1985. Volt/Var control on distribution systems with lateral branches using shunt capacitors and voltage regulators Part II: The solution method. *IEEE transactions on power apparatus and systems*, (11), pp.3284-3290.

[144] Civanlar, S. and Grainger, J.J., 1985. Volt/Var control on distribution systems with lateral branches using shunt capacitors and voltage regulators Part III: The numerical results. *IEEE transactions on power apparatus and systems*, (11), pp.3291-3297.

[145] Gu, Z. and Rizy, D.T., 1996. Neural networks for combined control of capacitor banks and voltage regulators in distribution systems. *IEEE transactions on power delivery*, *11*(4), pp.1921-1928.

[146] Carpinelli, G., Noce, C., Proto, D. and Varilone, P., 2006. Voltage regulators and capacitor placement in three-phase distribution systems with non-linear and unbalanced loads. *International journal of Emerging electric power systems*, *7*(4).

[147] Szuvovivski, I., Fernandes, T.S.P. and Aoki, A.R., 2012. Simultaneous allocation of capacitors and voltage regulators at distribution networks using genetic algorithms and optimal power flow. *International Journal of Electrical Power & Energy Systems*, *40*(1), pp.62-69.

[148] Franco, J.F., Rider, M.J., Lavorato, M. and Romero, R., 2013. A mixed-integer LP model for the optimal allocation of voltage regulators and capacitors in radial distribution systems. *International Journal of Electrical Power & Energy Systems*, *48*, pp.123-130.

[149] Hung, D.Q., Mithulananthan, N. and Bansal, R.C., 2015. A combined practical approach for distribution system loss reduction. *International Journal of Ambient Energy*, *36*(3), pp.123-131.

[150] Abou El-Ela, A.A., El-Sehiemy, R.A. and Abbas, A.S., 2018. Optimal placement and sizing of distributed generation and capacitor banks in distribution systems using water cycle algorithm. *IEEE Systems Journal*, *12*(4), pp.3629-3636.

[151] Saleh, A.A., Mohamed, A.A.A., Hemeida, A.M. and Ibrahim, A.A., 2019, February. Multi-Objective Whale Optimization Algorithm for Optimal Allocation of Distributed Generation and Capacitor Bank. In *2019 International Conference on Innovative Trends in Computer Engineering (ITCE)* (pp. 459-465). IEEE.

[152] Laconico, K.C.C. and Aguirre, R.A., 2019, March. Optimal Load Balancing and Capacitor Sizing and Siting of an Unbalanced Radial Distribution Network. In *2019 IEEE PES GTD Grand International Conference and Exposition Asia (GTD Asia)* (pp. 939-944). IEEE.

[153] Arulraj, R. and Kumarappan, N., 2019. Optimal economic-driven planning of multiple DG and capacitor in distribution network considering different compensation coefficients in feeder's failure rate evaluation. *Engineering Science and Technology, an International Journal*, *22*(1), pp.67-77.

[154] Home-Ortiz, J.M., Vargas, R., Macedo, L.H. and Romero, R., 2019. Joint reconfiguration of feeders and allocation of capacitor banks in radial distribution systems considering voltage-dependent models. *International Journal of Electrical Power & Energy Systems*, *107*, pp.298-310.

[155] Das, S., Das, D. and Patra, A., 2019. Operation of distribution network with optimal placement and sizing of dispatchable DGs and shunt capacitors. *Renewable and Sustainable Energy Reviews*, *113*, p.109219.

[156] Gözel, T. and Hocaoglu, M.H., 2009. An analytical method for the sizing and siting of distributed generators in radial systems. *Electric power systems research*, *79*(6), pp.912-918.

SciEn
Journal of Engineering Advancements Vol. 01(04) 2020, pp 170-182 https://doi.org/10.38032/jea.2020.04.008

Security Threats and Research Challenges of IoT-A Review

AKM Bahalul Haque and Sonia Tasmin*

Department of Electrical and Computer Engineering, North South University, Dhaka, Bangladesh

Received: November 23, 2020, Revised: December 18, 2020, Accepted: December 18, 2020, Available Online: December 22, 2020

ABSTRACT

Internet of things (IoT) is the epitome of sustainable development. It has facilitated the development of smart systems, industrialization, and the state-of-the-art quality of life. IoT architecture is one of the essential baselines of understanding the widespread adoption. Security issues are very crucial for any technical infrastructure. Since IoT comprises heterogeneous devices, its security issues are diverse too. Various security attacks can be responsible for compromising confidentiality, integrity, and availability. In this paper, at first, the IoT architecture is described briefly. After that, the components of IoT are explained with perspective to various IoT based applications and services. Finally, various security issues, including recommended solutions, are elaborately described and the potential research challenges and future research directions.

Keywords: IoT, Security, Privacy, Attacks, Vulnerability, Threats, Challenges.

1. Introduction

The Internet of Things (IoT) has gained popularity in recent times. It is an interconnected network of devices like sensors, actuators, electronics, and software. A network or correlation among those gadgets helps to collect and share data between them. Each and everything can be defined uniquely utilizing an embedded computing device but can communicate within the current Internet infrastructure. IoT makes it possible to monitor and sense using the network infrastructure [1] to create opportunities for more effective physical incorporation into computer-driven networks. Besides, to minimize human interference, increase performance, precision, and economic benefit [2],[3] the IoT devices play a vital role. Internet of Things facilitates smart human living, sustainability, and a greener lifestyle. Moreover, IoT devices used in the industrial environment increase efficient product management through proper monitoring and risk management [4],[5].

IoT comprises sensors and actuators. It is an example of a broader class of cyber-physical networks involving intelligent grids, smart buildings, VPP (Virtual Power Plants), smart transport, and smart cities. It has a significant impact on the medical sector also. Among the applications, a wide range of equipment such as cardiovascular implants, biochip transponders for farm animals, cameras for broadcasting wild animal live feed in coastal waters, vehicles with embedded captors, environmental DNA analysis, food, surveillance for pathogens [6], or on-site operations supports firefighters in search and rescue operations [7]. IoT has spread its domain in every sector of socio-economic sectors. Legal scholars propose "thing" as a combination of hardware, software, information.

Similar to every other technology IoT has several issues regarding security and privacy. Since the IoT network is a combination of devices, communication technologies, and various protocols, security issues regarding availability, data integrity, data confidentiality, and authentication exist [8]. These issues hamper operational inefficiency, robustness, and throughput. For a sustainable and robust IoT network, security and privacy issues need to be adequately addressed. The reasons mentioned above can be a very impactful motivation for a comprehensive study regarding leveraging various issues.

Being IoT an impactful technology of recent times, it needs to be studied vigorously. Several pieces of research are going on for improving IoT and removing the security threats. Moreover, IoT has a tremendous impact on the industry and recent smart city improvement. Considering all the factors, it is indispensable to study IoT and perform critical research analysis, including contemporary literature. The analysis can be used to outline a sophisticated piece of literature that can help those trying to initialize their career in IoT and existing researchers looking for research gaps and current research challenges.

The rest of the paper is organized as follows-

Section 2 comprises an architectural analysis of IoT that includes various IoT layers. Section 3 consists of various IoT components that make the IoT system. An extensive analysis of security and privacy issues, including their state of the art recommended solution, is outlined in Section 4 and 5. In addition to the recommended solutions, Section 5 also comprises a recent literature analysis about IoT privacy and security issues. Section 6 outlines the future research directions that can be helpful for researchers and scientists. Finally, the paper concludes with a conclusion in Section 7.

2. IoT Architectures

Software integrated hardware devices process raw data and turn it into a usable format. Furthermore, the data is transmitted, stored, recovered, and analyzed with advanced IoT-integrated computer devices. Only a dependable IoT architecture layer can ensure a steady, durable, and swift connection between information and communication technology. Researchers have proposed several different architectures for the IoT environment. However, the three-layer structure is the most popular type among researchers and publications [9].

2.1 The Three-Layer Architecture

One of the primary and significant IoT architectures is the three-layer architecture. It is one of the most functional,

*Corresponding Author Email Address: bahalul.haque@northsouth.edu

convenient, and easy to use architectures. The three-layers of this architecture are,

1. Application layer
2. Network layer
3. Edge/Perception layer

2.1.1 Application Layer

This layer defines all applications; no absolute norm is given. Its crucial function is to provide the customer with a particular service depending on the type of application. It can be seen in a variety of areas of IoT, such as applications for smart communities and homes, healthcare [10],[11], smart grids [12],[13], and automated vehicles [14],[15]. This layer may also work as a connectivity protocol, middleware [16], and cloud storage to enable server support. Therefore, security issues will vary depending on the context and industry of the application. In this specific architecture, various components are specified and focus on the IoT environment. We will need special binary programs or a special API (Application Programming Interface) on server-sides and client-sides [17]. The security architectures in most applications rely on the security of the DTLS CoAP protocol.

2.1.2 Network Layer

Its feature is to handle the transmitting and retrieving of information, with internet connectivity of different devices, among other layers. Besides, the network layer allows access to the edge/perception layer across various protocols and standards such as GPS, IEEE 802.X, and Near Field Communications (NFC). Internet protocols, cloud back-end networks, and smart devices support this layer [18]. Besides, the network layer can be managed based on the implemented environment with distinct aspects. However, Key Encryption Management and Systems, Intelligence Intrusion Detection Systems, and BlockChain technology [19],[20] constitute the most common network-level security framework in IoT architectures.

2.1.3 Perception or Edge Layer

The characteristics of the perception layer would be sensing abilities. IoT devices may communicate with customers or their working domains (sensors, smart meters, or IoT gateway edge-level servers). Those also collect environmental information with the help of smart objects. This layer undergoes multiple attacks due to the physical visibility of the edge layer in the IoT architecture. Safe channeling, an endpoint anti-malware solution, a multi-factor authentication system, and applications based on machine learning for cloud-based exception detection are the essential security components used in this layer [21][22].

A wide range of IoT systems deficiencies has led to IoT devices' transformative use with computational capabilities in different application areas. In various disciplines, these limitations can create critical mistakes and data loss. In recent years, the protection of IoT ecosystems has also been identified as one of the trending issues that attracted the research society's attention [23].

3. **IoT Components**

Understanding the building blocks of IoT allows you to gain a deeper perspective of IoT's actual purpose and usefulness. We address six key elements required to carry out the functionalities of the IoT in the following parts.

3.1 Identification

For the IoT to align and rename facilities with their request, recognition is key. Many recognition mechanisms, such as ubiquitous codes (uCode) and electronic product codes (EPC) [24], are obtainable for the IoT. Furthermore, distinguishing between IoT objects and their addresses is essential. Object ID points to the object's name, for example, "T1" as a given temperature sensor. The address of the object corresponds to the address of the communication network. Besides, IPv6 and IPv4 provide the addressing methods of IoT objects. 6LoWPAN [25],[26] offers a compression mechanism for IPv6 headers, making IPv6 suitable for wireless networks with low capacity. It is imperative to differentiate between object identity and address because identification approaches are not globally unique, so addressing objects helps recognize those individually. Network objects within the range may also use public IPs instead of private ones. Identification techniques can be used for each object in the scheme to provide a particular identification.

3.2 Sensing

IoT sensing is a collection of data from linked items inside the network and a return to the data store, archive, or cloud. The collected data is analyzed for crucial decision-making purposes. The sensors used by IoT systems are wearable, smart actuators. Companies such as SmartStuff, Revolve, and Wemo, for instance, have smart hubs and mobile applications for thousands of smart devices and equipment to be monitored and controlled inside buildings via smartphones [27],[28]. In most IoT products (e.g., BeagleBone Black, Raspberry PI, Arduino Yun, etc.) A single-board computer (SBC) is embedded with sensors and incorporated protection features and IP/TCP. These systems typically bind to the central management portal to deliver relevant data to customers.

3.3 Communication

Heterogeneous objects are linked by IoT connectivity technologies to provide unique smart services. Usually, in the case of missing and noisy connections, low-power IoT nodes will operate. LTE-Advanced, Bluetooth, Z-wave, WiFi, and IEEE 802.15.4. provide networking protocols used by IoT. Some basic networking systems, such as Ultra-Wide Bandwidth (UWB), Near Field Communication (NFC), and RFID, are still used.

3.3.1 Communication Technologies

RFID (tags and readers) is the first technology used to incorporate the M2M principle. The RFID tag is a fundamental chip or tag that provides object identification. Furthermore, an RFID card reader sends a query signal or message to the tag, and the tag that is sent to the database gives a mirrored signal. The database is based on reflector signals (10 cm to 200 m) [29]. The items are connected to the processing center.

The RFID transponders may be active, passive, semi-active, or semi-passive.

A battery drives active tags; here, passive tags are not needed. The control of the board is used when required for semi-passive / active labels.

The NFC Protocol supports up to 424 kbps of data with a high-frequency band of 13.56 MHz. When contact between active readers and passive tags or two active readers is established, the width can be 10 cm [30].

The UWB communication mechanism has been developed for low-level, low-energy, and high-bandwidth communications, which have recently improved their sensor connectivity capacities [31]. WLAN / WiFi, which uses radio waves for data sharing in a range of 100 m, is another networking technology [32]. In specific ad hoc environments, WiFi helps intelligent devices to link and share data without a modem. In short distances, Bluetooth is a networking system that uses short wave radio to relay data between devices to minimize energy consumption [33]. The Bluetooth-SIG (Bluetooth Special Interest Group) recently developed Bluetooth 4.1 that supports low-energy Bluetooth and high speed and IP networks [34].

3.3.2 Communication Protocols

For low-performance wireless communications aimed at extensible and safe networking, the IEEE802.15.4 specification defines all media and physical communication access [35]. The standard wireless connection between a GSM / UMTS network technology is originally LTE (Long-Term Evolution), based on high-speed data transfer from mobile phones [36]. It will protect high-speed devices and have multi-channel and transmitting services. LTE-A is an improved LTE version [37], with up to 100 MHz bandwidth, up and downlink space multiplexing, expanded coverage, increased latency, and decreased latency.

3.4 Computation

"The brain" and IoT's computing capabilities are control devices (*e.g.*, FPGAs, microprocessors, microcontrollers, SOCs) and application software. Several hardware platforms have been developed to run IoT based applications. Besides, many application platforms are being used to have IoT capabilities. Operating systems (OS) are critical among such systems because they operate over the entire activation period. There are plenty of RTOS (Real-Time Operating Systems) that are excellent targets for RTOS-based IoT systems growth. To begin with, the Contiki RTOS was used extensively in IoT situations. Researchers and developers were aided by a simulator called Cooja (by Contiki) to simulate IoT and WSNs (Wireless Sensor Networks) [38].

Lightweight OS, Riot OS [39],[40], LiteOS, and TinyOS are also available for IoT environments. Many Google auto industry leaders founded the Open Auto Alliance (OAA). Furthermore, to step up the deployment of the IoV (Internet of Vehicles) model [41], they are aiming to make modifications to the Android version. Per the operating system has different characteristics. Another important computational aspect of IoT is Cloud Systems. These devices have the potential to move their data to the cloud with intelligent objects. This large amount of data can be analyzed in real-time to benefit the end-user. The host of IoT assistance is equipped with various free and commercial cloud systems and structures [42].

3.5 Services

Among all the IoT based services, identification programs are the most rudimentary and essential providers. Object detection is indispensable for an algorithm that brings real-life objects into the virtual world. Collaborative systems run in the Information Aggregation Systems background and use the collected information to evaluate and respond accordingly. Ubiquitous networks are therefore intended at all times and everywhere to provide Collaborative Aware Facilities. Both IoT implementations aim essentially to achieve a standard with universal services. Recent applications provide collaborative-aware services, information aggregation, and identity. Intelligent healthcare and smart grids come into the data collection group. Moreover, collective consciousness is closer to industrial automation, smart buildings, and smart transportation systems (ITS).

4. IoT Security and Privacy Issues

The IoT model involves addressing security flaws on various levels, including multiple applications and devices, from microchips to massive high-level computers. As mentioned below, we categorize the security risks surrounding the IoT deployment architecture,

- Low-level
- Intermediate-level and
- High-level

4.1 Low-level Security Concerns

As detailed below, the first protection level is concerned with safety problems in the data connection and physical layers of hardware and communication.

4.1.1 Sybil Low-level Threats and Spoofing

Sybil attacks are triggered by fraudulent Sybil nodes using false documents. A Sybil node will utilize arbitrarily fabricated MAC values to mask network resources as a separate unit on the physical level. Connection to infrastructure can then be declined to valid nodes [43].

4.1.2 Jamming Attacks

The jamming threats on wireless networks were directed at the weakening of the network through propagation without a clear radio waves specification. Radio disruption has a significant effect on network activities, resulting in failure or erratic actions by transmitting and receiving data by legitimate nodes [44],[45].

4.1.3 Attack of Sleep Privation

The energy-restricted IoT devices are vulnerable to attacks that lead to the sensor nodes remaining awake and "sleep loss". It contributes to battery failure as several activities in the 6LoWPAN setting are set to be carried out [46].

4.1.4 Insecure Start-up

A stable framework for IoT setup and configuration in the physical layer assures all devices' correct operation without infringing on privacy or network service interruption. The communication between the edge layer and the network layer must be protected against unauthorized access [47],[48].

4.1.5 Physical Interface Unreliable

Various physical conditions are associated with significant risks to the proper operation of IoT systems. Weak physical protection, software access through testing/debugging tools, and physical interfaces may impact network nodes [49].

4.2 Intermediate-level Security Concerns

Security problems at the intermediate level are directly associated with the routing, session management, and connectivity of the transport layers and IoT network, as mentioned below.

4.2.1 Sybil Attack

Sybil nodes can be added to degrade network efficiency and even violate data privacy, comparable to Sybil attacks on low-level layers. Sybil nodes can spam, disseminate malware, or trigger phishing attachments by interacting with a network's false identity. The network management system should authenticate all types of devices and users before logging in. Any network protection backdoor or wide security loopholes will expose the network to many vulnerabilities. The network is not safe. For example, the excess cost of Datagram Transport Level Security (DTLS) has to be reduced because of limited resources. The cryptographic methods to protect data transfer in IoT must consider the usefulness and lack of other tools [50],[51].

Message authentication protocols are very crucial for a successful and secure data transfer. As mentioned earlier, devices need to be authenticated with valid credentials. During data transfer, the route discovery process takes various phases, including address adjustment and router finding. The use of adjacent discovery packaging could have severe repercussions and denial of service without sufficient authentication [52].

4.2.2 Assault of RPL

The Lossy and Low-power Networks (RPL) IPv6 Routing Protocol is vulnerable to multiple attacks caused by the infected nodes. The attack will lead to resource depletion and deterioration [53]. Since a receiver node needs a buffer space to reassemble incoming packets, an attacker can be abused to deliver incomplete packets. This attack leads to denial of service because the space filled by the unfinished packets the attacker sends out is discarded for other fragment packets [54].

4.2.3 Fragmentation Repeat or Replication Assaults

Technologies adhering to the IEEE 802.15.4 specification, represented by limited frame dimensions, enable the convergence of IPv6 systems. The restoration of the 6LoWPAN layer of packet fragment fields could deplete capital, overflow buffer, and reboot the computers. The duplicate fragments sent via malicious nodes impact the reassembly and hamper other valid packets [55].

4.2.4 Sinkhole and a Wormhole Attack

The sinkhole attacks respond to routing requests by the attacker node, which allows the packet to travel the attacker node and then conduct a malicious operation on the network. The network attacks can further impair 6LoWPAN functions by wormhole attacks that build a tunnel between two nodes, causing bundles returning at a node to enter other nodes automatically. These attacks have significant effects, including denial of service, breach of privacy, and eavesdropping [56],[57],[58].

4.2.5 End-to-end Transportation Safety

The purpose of the transport-level end-to-end encryption is to provide a safe framework for efficiently retrieving the information from the sender node. Comprehensive authentication mechanisms are necessary to ensure the secure transmission of the message in encrypted form while ensuring minimal overheads.

Session hijacking with forged messages on the transport layer will result in denial-of-service. To begin the session between two nodes, the target node will be imitated by an invading node. The nodes will also need re-transmission by modifying the sequence numbers.

Different attacks that may breach location and identity protection can be seen on IoT's delay-tolerant networking (DTL) or cloud-based system. Likewise, an IoT deployment-based malicious cloud service provider may access sensitive information transmitted to the appropriate destination [59],[60],[61].

4.3 High-level Security Concerns

High-level security problems concern mainly the IoT applications, as mentioned below.

4.3.1 Unsafe Interfaces

The interfaces used by the internet, device, and cloud to access IoT resources are vulnerable to multiple attacks that seriously impact data privacy [49].

4.3.2 Security of Middleware

IoT middleware designed to make IoT paradigm interactions between heterogeneous organizations must be sufficiently secure to provide services. To ensure safe connectivity, various interfaces and environments use middleware [62],[63].

4.3.3 CoAP Security Issues

The high-level layer of the application layer is susceptible to attacks as well. A web transfer protocol for restricted computers, the Constrained Application Protocol (CoAP) uses DTLS connectors with different protection modes to ensure complete stability. To protect correspondence, the CoAP messages adopt a particular RFC-7252 format. Similarly, authentication and key management (AKM) are needed for the multicast support in CoAP [64],[65],[66].

4.3.4 Uncertain Software/firmware

Different IoT vulnerabilities include those triggered by insecure firmware/software. The code must be checked carefully for languages like JSON, XML, SQLi, and XSS. Similarly, firmwares must be updated securely and safely.

5. Recommended Solutions

IoT security threats target multiple elements that occur at all levels, such as firmware, network resources, physical equipment, software, applications, and interfaces. Users interact with the components via interfaces in IoT systems. Furthermore, their security mechanisms may even be dismantled. The protection threats countermeasures fix this communication's vulnerabilities in various layers to ensure a certain safety level. These countermeasures are further complicated by numerous protocols enabling component deployment. This section offers a summary of the critical safety strategies.

5.1 Low-level Pprivacy and Security Solutions

Some of the categorized security solutions are depicted as follows-

5.1.1 Anti-jamming Mechanism

The jamming attacks refer to interference that leads to communication conflicts or overflows for networks of wireless sensors. Young et al. are suggesting an approach to detect jamming attacks. The detection of attacks is possible by measuring the connection speed used for the set of vibration

signals. These numbers are then evaluated to an adjusted optimum range for detection accuracy. By computing a successful packet delivery ratio, Xu et al. proposed to prevent jamming attacks by doing accuracy tests on signal intensity and the nodes' locations, the proposed algorithms work. Noubir et al. are considering another anti-jamming method using error-correcting codes and cryptographic functions. The system operates by splitting packets into blocks and interlines the encrypted packet bits. Likewise, spatial retreat and streaming techniques are recommended for coping with jam-attacks. Channel surfing allows legal channel frequency shift to contact devices. The space retreats, by comparison, allow specific devices to adjust their position at a certain distance when traveling to the target spot [67],[68],[69].

5.1.2 Safe Physical Layer Communication

Pecorella *et al.* suggest a system designed to ensure safe physical layer communication for the initialization of IoT. For the transmitted and receiving nodes, a low transfer speed is set to provide a missing eavesdropper. Other approaches to the implementation of artificial noise in signals are also used [70],[71],[72].

5.1.3 Detect Sybil Attack and Spoofing Threats

As a separate computer, a malicious Sybil node will use bogus MAC properties to masquerade as a different machine. That would lead to the loss of energy and the denial of connectivity to legitimate network equipment. Their strategy is used to evaluate the sender location by using tracker nodes during the message communication. Another message corresponds with the same sender location, but another user's identity is inferred as a Sybil attack. For detecting spoofing threats, other techniques by Li et al. and Chen et al. utilize signal intensity calculations for MAC addresses. Another Xiao et al. method involves channel prediction for detecting attacks from Sybil. The methodology uses multiple channel estimation identities and additional criteria to identify Sybil nodes [73],[74],[75].

5.1.4 Inappropriate Physical Protection

Devices with inappropriate physical protection are distinguished by external interfaces that offer access to firmware or applications and vulnerable utility tools for checking and debugging. Recommendations are issued by the Open Network Application Security Project (OWASP) to enhance IoT devices' physical security. Redundant hardware interfaces are essential to avoid. Debugging and testing methods must be removed. Hardware-based systems (e.g., Trusted Platform Modules) increases physical stability.

5.1.5 Sleep Deprivation Attacks

A system is developed to counteract wireless sensor sleep deprivation attacks. A cluster-based approach integrates the proposed structure, where each cluster is separated into many sectors. By eliminating long-distance communication, the consumption of electricity is minimized. With a five-layer architecture of the wireless sensors, the system performs intrusion detection. In the WSN model's upper layers, a cluster coordinator requires an expanded security mechanism and sink nodes and leader nodes. Similarly, in the lower levels of the WSN architecture, the follow-up nodes are fitted with basic intrusion detection systems [76].

5.2 Intermediate-level Privacy Solutions

Riaz et al. propose a safety system with device modules for secure data encryption, neighborhood discovery, authentication, and key generation. The elliptical curve encryption (ECC) is used for protected neighbor discovery. The ECC public key signatures are used in this process. Depending on the implementation specifications, both symmetric and asymmetric key management schemes are planned to be implemented. Data transfer across nodes happens in an encrypted manner to ensure confidentiality and integrity [77],[78].

For authenticating version numbers and ranks, the Authentication System called VeRA uses the Hash [79], MAC [80], and Digital Signature [81] Features. A rank and version number based authentication security service is proposed to mitigate adverse invasion while mapping through the IPv6 LLN (Low-Power and Lossy Network) routing protocol by Dvir *et al.* A lower parent node rank than the RPL norm requires the baby. No DAO messages are sent by the infected node, resulting in traffic delays by malicious nodes during transmission. A node's rank value can be reduced to find the root for eavesdropping [82],[83].

Zhou *et al.* [84] are aided in maintaining identification and privacy in a cloud-based IoT via a secure packet forwarding authentication method. The proposed architecture proposes an IoT network configuration from a central location for a hostile cloud service provider to protect an IoT network. Similarly, in the SMARTIE project, a forum for protecting data exchanged between IoT devices is suggested. Henze et al. are proposing a distributed platform for safe communication between IoT networks. Log message authentication is then used to denote hostile activity, which prevents cloud-based IoT from messages being changed, withheld, added, and reordered. To check across various gateways, it records control messages at several locations [85].

The RERUM project [86] suggests a system for Smart City IoT apps to ensure safety and stability. For IoT-based scenarios such as the smart healthcare sector and smart city, the project aims at validating trust and security. Similarly, for IoT environments, including smart communities, smart shopping, smart hospitals, and smart houses, the BUTLER project [87] advocates context-aware information systems. In the ARMOUR project [88], another mechanism for playing with security standards is introduced in an IoT base. The ARMOUR experiment determines defense design, creates testbeds, conducts tests, and produces qualification marks. As well as layer-specific safety specifications, the tests can be used to guarantee secure end-to-end communication. Lightweight cryptographic protocols were used in the project to enhance data security and integrity. Authentication-based techniques and Data integrity are being applied to build trustworthy applications.

5.3 High-level Privacy/security Solutions

Granjal *et al.* [89] proposed another solution to protecting messages for apps that connect via the web using different CoAP protection options. Brachmann *et al.* [90] suggest a solution that combines TLS and DTLS to stable CoAP-based Lossy and Low-power Network linked to the internet. Similarly, for IP networks, a security paradigm of 6LBR is proposed to filter messages and provide end-to-end security [91]. The SecurityEncap alternative uses the security options configuration and primarily performs the data transfer necessary for authentication and replay

protection. TLS and DTLS routing is proposed to allow end-to-end protection that prevents LLNs from web-based threats.

A power-efficient security policy with a public-key authentication is suggested by Sethi *et al.* [92] for IoT-based CoAP. The proposed safety framework implemented by a test utilizes the Mirror Proxy (MP) and service directory that the server provides for sleep requests and a server (or endpoint) resource list. Project OWASP [93] lays out guidelines for IoT protection countermeasures. Protection protocols include configurations that check the interface against well-known bugs of the development tool (XSS and SQLi), use HTTPS and firewalls to deal with unsafe high-level interfaces, and discourage bad passwords.

Conzon et al. proposed the VIRTUS middleware that is used to protect distributed apps operating in an IoT system. The middleware uses a case-based connection method by integrating TLS and SASL for data integrity, XML stream encryption, and validation [94]. The authentication method guarantees resource protection and data sharing for registered users only. Integrated with network servers, the VIRTUS middleware helps in stable and flexible IoT applications being deployed. A semantic system called Otsopack [63] serves as a middleware to allow heterogeneous applications to communicate safely. Ferreira et al. are suggesting another protection architecture for IoT middleware. Liu *et al.* [63] propose a middleware server that promotes filtration of data during the connection between heterogeneous IoT systems. The standard features of authorization, authentication, and accounting are introduced via a critical hierarchy of app, root, and service keys. The proposed middleware enables an essential method for profiling, addressing, and naming through heterogeneous environments [95],[96].

5.4 Recent Critical Literature Contribution and Analysis

There has been a large number of studies during recent years. Some of the notable pieces of literature and their contributions are mentioned in a tabular format in Table 1 below-

Table 1 Recent Literature Contributions Related IoT Security and Privacy

References	**Year**	**Contribution**
Dorri *et al.* [97]	2017	Assessing the requirements of IoT based smart city; Blockchain integration for security and privacy
Fremantle *et al.* [98]	2017	IoT and Blockchain integrated framework for IoT security threats
Oracevic *et al.* [99]	2017	Analysis of security issues and state of the art recommended solutions
Oh *et al.* [100]	2017	Comprehensive security analysis based on IoT elements; Proposed security requirements.
Ahemd *et al.* [101]	2017	Analysis of threats and countermeasures of various IoT layers; Assessing security providing technologies for addressing the risks.
Ouaddah *et al.* [102]	2017	Proposed blockchain and smart contract-based framework for IoT security
Salman *et al.* [103]	2017	Security and privacy issues analysis; Proposed a software model for securing IoT
Miraz *et al.* [104]	2018	Assessing blockchain-enabled cryptographic security mechanism for IoT Security; Depicting recent challenges faced while providing IoT security
Román-Castro *et al.* [105]	2018	Evaluating stateof the art security and privacy scenario and analyzing their prospects;
Vorakulpipat [106]	2018	In dept analysis and performance analysis of IoT architecture, applications, and various vulnerabilities and countermeasures
Roy *et al.* [107]	2018	In-depth analysis of blockchain and IoT architectures and their integration issues; Feasibility and possible integration analysis of blockchain for leveraging IoT security issues.

References	Year	Contribution
Xiao *et al.* [108]	2018	Feasibility assessment of implementing artificial intelligence against IoT security attack; Various attack detection and secure authentication management using artificial intelligence.
Stergiou *et al.* [109]	2018	Integrating cloud computing and IoT ; Proposed architecture for preventing security threats; Efficiency and robustness analysis.
Sollins *et al.* [110]	2019	Big data related security and privacy attribute analysis; Big data and IoT relationship assessment and propose design aspects addressing the security issues
Chaabouni *et al.* [111]	2019	Intrusion detection analysis of IoT networks for improving cyber defense; Previous machine learning-based system development analysis during the recent past and addressing the future research challenges for IoT.
Nizzi *et al.* [112]	2019	Using HMAC for securing IoT and privacy protection; In-depth analysis of the effect of address shuffling inside the entire network; Proposed approach based on the result analysis.
Alraja *et al.* [113]	2019	Proposed framework for IoT based healthcare system usability; User perception analysis towards the IoT based healthcare system usage, security, and privacy.
Hassija *et al.* [114]	2019	Comprehensive analysis of IoT based system application, security, and privacy analysis; Various technology integration in IoT networks is assessed, including security and privacy issues.
Rahman *et al.* [115]	2020	Integrating blockchain in IoT; Proposed SDN framework; Addressing the security and privacy of IoT data;
Mohanta *et al.* [116]	2020	Analyzing blockchain for IoT security and privacy; Analyzing IoT security threats; Result-oriented case study analysis for the integration factors.
Dedeoglu *et al.* [117]	2020	Comprehensive, result-oriented and in-depth analysis of blockchain-based IoT security issues challenges and research directions; Analyzing the opportunities and threats;
Hussain *et al.* [118]	2020	Analyzing the security attributes and threats of IoT; Feasibility analysis of various artificial intelligence-based techniques and models for threat prevention;
Sharma *et al.* [119]	2020	Mobile IoT architectural analysis; Security and privacy analysis in different layers and communication protocols; Recent security privacy and implementation challenges are discussed briefly.
Mohanty *et al.* [120]	2020	Blockchain-based model for IoT privacy and security in the smart home environment; Result analysis and performance comparison among the existing models.
Tewari *et al.* [121]	2020	Layered approach for threat and trust analysis in IoT; Integration issues related to various IoT devices.
Islam *et al.* [122]	2020	Threat analysis of IoT based home systems; Financial issues related to the home environment is discussed; Blockchain-based approach in leveraging the problems;

The above-mentioned table shows some of the recent literature related to IoT security and privacy. Apart from the mentioned points, the analysis can be depicted as follows-

- The IoT is studied extensively in recent times. Privacy and security issues are also discussed and analyzed in recent studies.
- IoT can be integrated with various other technologies. Researchers have made their approach to cloud computing and smart home-based techniques.
- Blockchain is one of the most promising technologies, and it is integrated with the internet of things. Blockchain can provide various facilities, for example, immutability, confidentiality, authenticity, and availability.
- IoT security and privacy issues can be addressed with blockchain technology. Though blockchain technology has several problems, such as scalability, interoperability, compliance issues, etc., the technology can be a potential white night for leveraging the security and privacy issues.
- Most recent studies related to IoT security and privacy involves blockchain. Scientists have been trying hard to find out various frameworks for addressing IoT security and privacy issues.
- Blockchain and IoT can be beneficial in potential research directions. If the application issues can be in-depth effectively, blockchain and IoT can be tools for developing smart and secure systems.
- There is a significant research gap in Mobile IoT device-related surveys and literature analysis. Extensive literature survey analysis can help analyze the implementation challenges, security, and privacy issue analysis, potentially finding potential research directions.

6. Challenges and Research Directions for the Future

From a privacy standpoint, blockchain application in the Internet of Things platforms and frameworks faces several obstacles. Researchers are incorporating blockchain into different IoT systems. This section addresses a few problems, open problems, and potential research paths from the perspective of confidentiality during the convergence of blockchain technology with numerous IoT implementations.

6.1 IoT in Industry

Due to its open and transparent existence, blockchain technologies in industrial IoT systems are growing. In a decentralized environment, for instance, in a production facility, IIoT detectors would be more efficient [123]. This is because, by updating the shared ledger at every stage, data can be spread to every single IIoT blockchain node. Many experiments have been carried out in previous literature to solve such privacy problems in IIoT systems, such as confidentiality and differential privacy, to maintain data integrity during industrial automation. However, before inclusion in the blockchain case, these methods need significant modifications. Therefore, such systems' privacy security is essential, and researchers should concentrate on protecting blockchain-based IIoT systems' privacy [124],[125].

6.2 Internet of Things for Farming

IoT based supply chain uses real-time monitoring of the production, manufacturing, shipment, housing, and distribution of agricultural goods. This traceability scheme aims to enhance farming and agrarian sector protection, supervision, cultivation, and processing practices. The monitoring and tracking processes in agriculture and agricultural IoT systems become more successful by using blockchain technologies. One such example is the leakage of any agricultural product's precise location and operation. Due to its diverse nature, intelligent contract security in blockchain-based IoT agriculture has enormous potential. Data leakage across the distribution cycle may be managed by writing successful codes based on secrecy. Future studies should propose combining privacy protection techniques in these systems by concentrating specifically on smart contracts and mixing strategies [126],[127].

6.3 Smart Cities

To further advance smart cities' ideas, researchers have begun combining blockchain with emerging smart city technology. Researchers have proposed that blockchain will remove multiple safety risks to smart cities due to its decentralized setting. Although blockchain is quite beneficial for smart communities, it often poses many privacy risks due to decentralization. Any hacker may enter the shared blockchain of a smart city and may attempt to acquire and infer sensitive details about smart city residents' personal lives and actions, resulting in significant privacy issues. Privacy security cannot only be grouped into a few predetermined domains in blockchain-based smart cities. However, for multiple smart city implementations, methods such as anonymization, smart contracts, and differential privacy can be used when the key prerequisite is to secure data sharing between different processes. Differential privacy is one of the possible choices, according to lightweight privacy protection in smart cities. It provides a reasonable guarantee of privacy, along with power over the utility of data as well [128],[129].

6.4 Crowd Sensing with Mobile Devices

A new sensing method called mobile crowdsensing has been introduced with the growing number of smart devices, exploiting smart device users' capacity, and gaining the advantage of using IoT technology for large-scale sensing. This transparency raises security issues for MCS apps. The crowd detector must provide clarity to MCS users while still transmitting data to the network in real-time. Blockchain-based crowdsensing systems need to guarantee that sensing by any effective privacy security process is anonymous and that no actual MCS user identities are exposed to adversaries. Using anonymization is one technique to protect the anonymity of MCS consumers. In this way, even though an adversary gets access to private data, the initial identities are not exposed. Noise in the data of MCS consumers using a differential privacy security approach may be another possible use. In a decentralized MCS environment, however, preserving the trade-off between precision and privacy can be difficult when users report their data in a real-time environment.

7. Conclusion

The article summarizes the interpretation of IoT architecture layers, the cooperation of IoT elements, and the applications of IoT. The internet has changed our way of living, shifting relations among people digitally in a couple of settings from intelligent life to social connections. IoT will probably apply another measure to this loop by empowering correspondence with and between smart items, subsequently prompting the vision of "whenever, wherever, whatever" communications

using any media. Security issues are growing with the growth of IoT devices in many business areas and human lives. Because of the restriction in assets, a broad scope of weaknesses has developed. The more significant part of these weaknesses can prompt framework disappointment in the workplace of the IoT.

Furthermore, this paper critically analyses recent pieces of literature related to IoT security and privacy issues. The recommended solution analyzed in this paper provides state of the art overview of current cybersecurity situations of IoT. Recent literature analysis also shows the research areas to work on in the future so that this technology can reach its epitome. There will be many technological challenges for a resource-constrained system such as IoT, as mentioned throughout the paper. Similarly, with the advent of new technological innovation, there needs to be some solutions that can address the challenges. Some of the recommendations are mentioned in the paper, and others are yet to be implemented in the future.

References

[1] Bartolomeo, M., 2014. Internet of things: Science fiction or business fact. *A Harvard Business Review Analytic Services Report, Tech. Rep*.

[2] Vermesan, O. and Friess, P. eds., 2013. *Internet of things: converging technologies for smart environments and integrated ecosystems*. River publishers.

[3] Santucci, G., 2010. The internet of things: Between the revolution of the internet and the metamorphosis of objects. *Vision and Challenges for Realising the Internet of Things*, pp.11-24.

[4] Mattern, F. and Floerkemeier, C., 2010. From the Internet of Computers to the Internet of Things. In *From active data management to event-based systems and more* (pp. 242-259). Springer, Berlin, Heidelberg.

[5] Kwon, D., Hodkiewicz, M.R., Fan, J., Shibutani, T. and Pecht, M.G., 2016. IoT-based prognostics and systems health management for industrial applications. *IEEE Access*, *4*, pp.3659-3670.

[6] Erlich, Y., 2015. A vision for ubiquitous sequencing. *Genome research*, *25*(10), pp.1411-1416.

[7] Wigmore, I., 2014. Internet of things (iot). *TechTarget*.

[8] WALDEN, I. and Noto La Diego, G., 2016. Contracting for the Internet of Things: Looking into the NEST. *European Journal of Law and Technology*.

[9] Kumar, N.M. and Mallick, P.K., 2018. The Internet of Things: Insights into the building blocks, component interactions, and architecture layers. *Procedia computer science*, *132*, pp.109-117.

[10] Catarinucci, L., De Donno, D., Mainetti, L., Palano, L., Patrono, L., Stefanizzi, M.L. and Tarricone, L., 2015. An IoT-aware architecture for smart healthcare systems. *IEEE internet of things journal*, *2*(6), pp.515-526.

[11] Srivastava, G., Parizi, R.M., Dehghantanha, A. and Choo, K.K.R., 2019, November. Data sharing and privacy for patient iot devices using blockchain. In *International Conference on Smart City and Informatization* (pp. 334-348). Springer, Singapore.

[12] Sakhnini, J., Karimipour, H., Dehghantanha, A., Parizi, R.M. and Srivastava, G., 2019. Security aspects of Internet of Things aided smart grids: A bibliometric survey. *Internet of things*, p.100111.

[13] Behera, T.M., Mohapatra, S.K., Samal, U.C., Khan, M.S., Daneshmand, M. and Gandomi, A.H., 2019. Residual energy-based cluster-head selection in WSNs for IoT application. *IEEE Internet of Things Journal*, *6*(3), pp.5132-5139.

[14] He, W., Yan, G. and Da Xu, L., 2014. Developing vehicular data cloud services in the IoT environment. *IEEE transactions on industrial informatics*, *10*(2), pp.1587-1595.

[15] Paranjothi, A., Khan, M.S., Zeadally, S., Pawar, A. and Hicks, D., 2019. GSTR: Secure multi-hop message dissemination in connected vehicles using social trust model. *Internet of Things*, *7*, p.100071.

[16] Ngu, A.H., Gutierrez, M., Metsis, V., Nepal, S. and Sheng, Q.Z., 2016. IoT middleware: A survey on issues and enabling technologies. *IEEE Internet of Things Journal*, *4*(1), pp.1-20.

[17] Qi, J., Yang, P., Min, G., Amft, O., Dong, F. and Xu, L., 2017. Advanced internet of things for personalised healthcare systems: A survey. *Pervasive and Mobile Computing*, *41*, pp.132-149.

[18] Santos, J., Rodrigues, J.J., Silva, B.M., Casal, J., Saleem, K. and Denisov, V., 2016. An IoT-based mobile gateway for intelligent personal assistants on mobile health environments. *Journal of Network and Computer Applications*, *71*, pp.194-204.

[19] Chen, J., Touati, C. and Zhu, Q., 2019. Optimal secure two-layer IoT network design. *IEEE Transactions on Control of Network Systems*, *7*(1), pp.398-409.

[20] Mahalle, P., Babar, S., Prasad, N.R. and Prasad, R., 2010, July. Identity management framework towards internet of things (IoT): Roadmap and key challenges. In *International Conference on Network Security and Applications* (pp. 430-439). Springer, Berlin, Heidelberg.

[21] Canedo, J. and Skjellum, A., 2016, December. Using machine learning to secure IoT systems. In *2016 14th annual conference on privacy, security and trust (PST)* (pp. 219-222). IEEE.

[22] Grassi, P.A., Garcia, M.E. and Fenton, J.L., 2017. DRAFT NIST Special Publication 800-63-3 Digital Identity Guidelines. *National Institute of Standards and Technology, Los Altos, CA*.

[23] HaddadPajouh, H., Dehghantanha, A., Parizi, R.M., Aledhari, M. and Karimipour, H., 2019. A survey on internet of things security: Requirements, challenges, and solutions. *Internet of Things*, p.100129.

[24] Koshizuka, N. and Sakamura, K., 2010. Ubiquitous ID: standards for ubiquitous computing and the internet of things. *IEEE Pervasive Computing*, *9*(4), pp.98-101.

[25] Taj-Eddin, I.A., Abou El-Seoud, M.S. and Elsofany, H., 2017, September. A Proposed Lightweight Cloud Security Framework to Secure Communications Between Internet of Things Devices. In *International Conference on Interactive Collaborative Learning* (pp. 517-525). Springer, Cham.

[26] Montenegro, G., Kushalnagar, N., Hui, J. and Culler, D., 2007. Transmission of IPv6 packets over IEEE 802.15. 4 networks. *Internet proposed standard RFC*, *4944*, p.130.

[27] Al-Fuqaha, A., Guizani, M., Mohammadi, M., Aledhari, M. and Ayyash, M., 2015. Internet of things: A survey on enabling technologies, protocols, and applications. *IEEE communications surveys & tutorials*, *17*(4), pp.2347-2376.

[28] Rushden, U., 2012. Belkin brings your home to your fingertips with WeMo Home Automation System. *Press Room Belkin*.

[29] Want, R., 2006. An introduction to RFID technology. *IEEE pervasive computing*, *5*(1), pp.25-33.

[30] Want, R., 2011. Near field communication. *IEEE Pervasive Computing*, *10*(3), pp.4-7.

[31] Kshetrimayum, R.S., 2009. An introduction to UWB communication systems. *Ieee Potentials*, *28*(2), pp.9-13.

[32] Ferro, E. and Potorti, F., 2005. Bluetooth and Wi-Fi wireless protocols: a survey and a comparison. *IEEE Wireless Communications*, *12*(1), pp.12-26.

[33] P. McDermott-Wells, "What is Bluetooth?" *IEEE Potentials*, 23(5), pp. 33–35, Jan. 2005.

[34] Khajenasiri, I., Estebsari, A., Verhelst, M. and Gielen, G., 2017. A review on Internet of Things solutions for intelligent energy control in buildings for smart city applications. *Energy Procedia*, *111*, pp.770-779.

[35] IEEE Standards Association, 2011. IEEE Std 802.15. 4-2011, IEEE standard for local and metropolitan area networks—part 15.4: Low-rate wireless personal area networks (LR-WPANs).

[36] Crosby, G.V. and Vafa, F., 2013, October. Wireless sensor networks and LTE-A network convergence. In *38th Annual IEEE conference on local computer networks* (pp. 731-734). IEEE.

[37] Ghosh, A., Ratasuk, R., Mondal, B., Mangalvedhe, N. and Thomas, T., 2010. LTE-advanced: next-generation wireless broadband technology. *IEEE wireless communications*, *17*(3), pp.10-22.

[38] Dunkels, A., Gronvall, B. and Voigt, T., 2004, November. Contiki-a lightweight and flexible operating system for tiny networked sensors. In *29th annual IEEE international conference on local computer networks* (pp. 455-462). IEEE.

[39] Levis, P., Madden, S., Polastre, J., Szewczyk, R., Whitehouse, K., Woo, A., Gay, D., Hill, J., Welsh, M., Brewer, E. and Culler, D., 2005. TinyOS: An operating system for sensor networks. In *Ambient intelligence* (pp. 115-148). Springer, Berlin, Heidelberg.

[40] [Cao, Q., Abdelzaher, T., Stankovic, J. and He, T., 2008, April. The liteos operating system: Towards unix-like abstractions for wireless sensor networks. In *2008 International Conference on Information Processing in Sensor Networks (ipsn 2008)* (pp. 233-244). Ieee.

[41] Baccelli, E., Hahm, O., Günes, M., Wählisch, M. and Schmidt, T.C., 2013, April. RIOT OS: Towards an OS for the Internet of Things. In *2013 IEEE conference on computer communications workshops (INFOCOM WKSHPS)* (pp. 79-80). IEEE.

[42] Open Auto Alliance. Available at: http://www. openautoalliance.net/. Accessed on Oct. 20, 2014.

[43] Xiao, L., Greenstein, L.J., Mandayam, N.B. and Trappe, W., 2009. Channel-based detection of sybil attacks in wireless networks. *IEEE Transactions on Information Forensics and Security*, *4*(3), pp.492-503.

[44] Xu, W., Trappe, W., Zhang, Y. and Wood, T., 2005, May. The feasibility of launching and detecting jamming attacks in wireless networks. In *Proceedings of the 6th ACM international symposium on Mobile ad hoc networking and computing* (pp. 46-57).

[45] Noubir, G. and Lin, G., 2003. Low-power DoS attacks in data wireless LANs and countermeasures. *ACM SIGMOBILE Mobile Computing and Communications Review*, *7*(3), pp.29-30.

[46] Chen, Y., Trappe, W. and Martin, R.P., 2007, June. Detecting and localizing wireless spoofing attacks. In *2007 4th Annual IEEE Communications Society Conference on Sensor, Mesh and Ad Hoc Communications and Networks* (pp. 193-202). IEEE.

[47] Chae, S.H., Choi, W., Lee, J.H. and Quek, T.Q., 2014. Enhanced secrecy in stochastic wireless networks: Artificial noise with secrecy protected zone. *IEEE Transactions on Information Forensics and Security*, *9*(10), pp.1617-1628.

[48] Hong, Y.W.P., Lan, P.C. and Kuo, C.C.J., 2013. Enhancing physical-layer secrecy in multiantenna wireless systems: An overview of signal processing approaches. *IEEE Signal Processing Magazine*, *30*(5), pp.29-40.

[49] OWASP, T. I. V. (2016). Available at: https://www. owasp. org/index. php.

[50] Zhang, K., Liang, X., Lu, R. and Shen, X., 2014. Sybil attacks and their defenses in the internet of things. *IEEE Internet of Things Journal*, *1*(5), pp.372-383.

[51] Wang, G., Mohanlal, M., Wilson, C., Wang, X., Metzger, M., Zheng, H. and Zhao, B.Y., 2012. Social turing tests: Crowdsourcing sybil detection. *arXiv preprint arXiv:1205.3856*.

[52] Riaz, R., Kim, K.H. and Ahmed, H.F., 2009, March. Security analysis survey and framework design for ip connected lowpans. In *2009 International Symposium on Autonomous Decentralized Systems* (pp. 1-6). IEEE.

[53] Dvir, A. and Buttyan, L., 2011, October. VeRA-version number and rank authentication in RPL. In *2011 IEEE Eighth International Conference on Mobile Ad-Hoc and Sensor Systems* (pp. 709-714). IEEE.

[54] Hummen, R., Hiller, J., Wirtz, H., Henze, M., Shafagh, H. and Wehrle, K., 2013, April. 6LoWPAN fragmentation attacks and mitigation mechanisms. In *Proceedings of the sixth ACM conference on Security and privacy in wireless and mobile networks* (pp. 55-66).

[55] Kim, H., 2008, August. Protection against packet fragmentation attacks at 6LoWPAN adaptation layer. In *2008 International Conference on Convergence and Hybrid Information Technology* (pp. 796-801). IEEE.

[56] Weekly, K. and Pister, K., 2012, October. Evaluating sinkhole defense techniques in RPL networks. In *2012 20th IEEE International Conference on Network Protocols (ICNP)* (pp. 1-6). IEEE.

[57] Ahmed, F. and Ko, Y.B., 2016. Mitigation of black hole attacks in routing protocol for low power and lossy networks. *Security and Communication Networks*, *9*(18), pp.5143-5154.

[58] Wazid, M., Das, A.K., Kumari, S. and Khan, M.K., 2016. Design of sinkhole node detection mechanism for hierarchical wireless sensor networks. *Security and Communication Networks*, *9*(17), pp.4596-4614.

[59] Peretti, G., Lakkundi, V. and Zorzi, M., 2015, January. BlinkToSCoAP: An end-to-end security framework for the Internet of Things. In *2015 7th International Conference on Communication Systems and Networks (COMSNETS)* (pp. 1-6). IEEE.

[60] Esposito, C., Castiglione, A., Tudorica, C.A. and Pop, F., 2017. Security and privacy for cloud-based data management in the health network service chain: a microservice approach. *IEEE Communications Magazine*, *55*(9), pp.102-108.

[61] Henze, M., Wolters, B., Matzutt, R., Zimmermann, T. and Wehrle, K., 2017, August. Distributed configuration, authorization and management in the cloud-based internet of things. In *2017 IEEE Trustcom/BigDataSE/ICESS* (pp. 185-192). IEEE.

[62] Conzon, D., Bolognesi, T., Brizzi, P., Lotito, A., Tomasi, R. and Spirito, M.A., 2012, July. The virtus middleware: An xmpp based architecture for secure iot communications. In *2012 21st International Conference on Computer Communications and Networks (ICCCN)* (pp. 1-6). IEEE.

[63] Liu, C.H., Yang, B. and Liu, T., 2014. Efficient naming, addressing and profile services in Internet-of-Things sensory environments. *Ad Hoc Networks*, *18*, pp.85-101.

[64] Brachmann, M., Keoh, S.L., Morchon, O.G. and Kumar, S.S., 2012, July. End-to-end transport security in the IP-based internet of things. In *2012 21st International Conference on Computer Communications and Networks (ICCCN)* (pp. 1-5). IEEE.

[65] Granjal, J., Monteiro, E. and Silva, J.S., 2013, June. Application-layer security for the WoT: Extending CoAP to support end-to-end message security for Internet-integrated sensing applications. In *International Conference on Wired/Wireless Internet Communication* (pp. 140-153). Springer, Berlin, Heidelberg.

[66] Sethi, M., Arkko, J. and Keränen, A., 2012, October. End-to-end security for sleepy smart object networks. In *37th Annual IEEE Conference on Local Computer Networks-Workshops* (pp. 964-972). IEEE.

[67] Xu, W., Trappe, W., Zhang, Y. and Wood, T., 2005, May. The feasibility of launching and detecting jamming attacks in wireless networks. In *Proceedings of the 6th ACM international symposium on Mobile ad hoc networking and computing* (pp. 46-57).

[68] Noubir, G. and Lin, G., 2003. Low-power DoS attacks in data wireless LANs and countermeasures. *ACM SIGMOBILE Mobile Computing and Communications Review*, *7*(3), pp.29-30.

[69] Xu, W., Wood, T., Trappe, W. and Zhang, Y., 2004, October. Channel surfing and spatial retreats: defenses against wireless denial of service. In *Proceedings of the 3rd ACM workshop on Wireless security* (pp. 80-89).

[70] Chae, S.H., Choi, W., Lee, J.H. and Quek, T.Q., 2014. Enhanced secrecy in stochastic wireless networks: Artificial noise with secrecy protected zone. *IEEE Transactions on Information Forensics and Security*, *9*(10), pp.1617-1628.

[71] Hong, Y.W.P., Lan, P.C. and Kuo, C.C.J., 2013. Enhancing physical-layer secrecy in multiantenna wireless systems: An overview of signal processing approaches. *IEEE Signal Processing Magazine*, *30*(5), pp.29-40.

[72] Pecorella, T., Brilli, L. and Mucchi, L., 2016. The role of physical layer security in IoT: A novel perspective. *Information*, *7*(3), p.49.

[73] Xiao, L., Greenstein, L.J., Mandayam, N.B. and Trappe, W., 2009. Channel-based detection of sybil attacks in wireless networks. *IEEE Transactions on Information Forensics and Security*, *4*(3), pp.492-503.

[74] Chen, Y., Trappe, W. and Martin, R.P., 2007, June. Detecting and localizing wireless spoofing attacks. In *2007 4th Annual IEEE Communications Society Conference on Sensor, Mesh and Ad Hoc Communications and Networks* (pp. 193-202). IEEE.

[75] Demirbas, M. and Song, Y., 2006, June. An RSSI-based scheme for sybil attack detection in wireless sensor networks. In *2006 International Symposium on a World of Wireless, Mobile and Multimedia Networks (WoWMoM'06)* (pp. 5-pp). ieee.

[76] Bhattasali, T. and Chaki, R., 2011, July. A survey of recent intrusion detection systems for wireless sensor network. In *International conference on network security and applications* (pp. 268-280). Springer, Berlin, Heidelberg.

[77] Riaz, R., Kim, K.H. and Ahmed, H.F., 2009, March. Security analysis survey and framework design for ip connected lowpans. In *2009 International Symposium on Autonomous Decentralized Systems* (pp. 1-6). IEEE.

[78] Harkanson, R. and Kim, Y., 2017, April. Applications of elliptic curve cryptography: A light introduction to elliptic curves and a survey of their applications. In *Proceedings of the 12th Annual Conference on Cyber and Information Security Research* (pp. 1-7).

[79] Eastlake, D., & Jones, P. 2001. US secure hash algorithm 1 (SHA1).

[80] Khan, M.A. and Salah, K., 2018. IoT security: Review, blockchain solutions, and open challenges. *Future Generation Computer Systems*, *82*, pp.395-411.

[81] Rivest, R.L., 1978. Shamir, a. and Adelman. *L." On Digital Signatures and Public Key*.

[82] Dvir, A. and Buttyan, L., 2011, October. VeRA-version number and rank authentication in RPL. In *2011 IEEE Eighth International Conference on Mobile Ad-Hoc and Sensor Systems* (pp. 709-714). IEEE.

[83] Li, F. and Xiong, P., 2013. Practical secure communication for integrating wireless sensor networks into the internet of things. *IEEE Sensors Journal*, *13*(10), pp.3677-3684.

[84] Zhou, J., Cao, Z., Dong, X. and Vasilakos, A.V., 2017. Security and privacy for cloud-based IoT:

Challenges. *IEEE Communications Magazine*, *55*(1), pp.26-33.

[85] Bohli, J.M., Skarmeta, A., Moreno, M.V., García, D. and Langendörfer, P., 2015, April. SMARTIE project: Secure IoT data management for smart cities. In *2015 International Conference on Recent Advances in Internet of Things (RIoT)* (pp. 1-6). IEEE.

[86] Pöhls, H.C., Angelakis, V., Suppan, S., Fischer, K., Oikonomou, G., Tragos, E.Z., Rodriguez, R.D. and Mouroutis, T., 2014, April. RERUM: Building a reliable IoT upon privacy-and security-enabled smart objects. In *2014 IEEE Wireless Communications and Networking Conference Workshops (WCNCW)* (pp. 122-127). IEEE.

[87] Khan, M.A. and Salah, K., 2018. IoT security: Review, blockchain solutions, and open challenges. *Future Generation Computer Systems*, *82*, pp.395-411.

[88] Pérez, S., Martínez, J.A., Skarmeta, A.F., Mateus, M., Almeida, B. and Maló, P., 2016, December. ARMOUR: Large-scale experiments for IoT security & trust. In *2016 IEEE 3rd World Forum on Internet of Things (WF-IoT)* (pp. 553-558). IEEE.

[89] Granjal, J., Monteiro, E. and Silva, J.S., 2013, June. Application-layer security for the WoT: Extending CoAP to support end-to-end message security for Internet-integrated sensing applications. In *International Conference on Wired/Wireless Internet Communication* (pp. 140-153). Springer, Berlin, Heidelberg.

[90] Brachmann, M., Keoh, S.L., Morchon, O.G. and Kumar, S.S., 2012, July. End-to-end transport security in the IP-based internet of things. In *2012 21st International Conference on Computer Communications and Networks (ICCCN)* (pp. 1-5). IEEE.

[91] Sethi, M., Arkko, J. and Keränen, A., 2012, October. End-to-end security for sleepy smart object networks. In *37th Annual IEEE Conference on Local Computer Networks-Workshops* (pp. 964-972). IEEE.

[92] Sethi, M., Arkko, J. and Keränen, A., 2012, October. End-to-end security for sleepy smart object networks. In *37th Annual IEEE Conference on Local Computer Networks-Workshops* (pp. 964-972). IEEE.

[93] Conzon, D., Bolognesi, T., Brizzi, P., Lotito, A., Tomasi, R. and Spirito, M.A., 2012, July. The virtus middleware: An xmpp based architecture for secure iot communications. In *2012 21st International Conference on Computer Communications and Networks (ICCCN)* (pp. 1-6). IEEE.

[94] Hall, B. and Henningsen, D.D., 2008. Social facilitation and human–computer interaction. *Computers in human behavior*, *24*(6), pp.2965-2971.

[95] Khan, M.A. and Salah, K., 2018. IoT security: Review, blockchain solutions, and open challenges. *Future Generation Computer Systems*, *82*, pp.395-411.

[96] Miller, D., 2018. Blockchain and the internet of things in the industrial sector. *IT professional*, *20*(3), pp.15-18.

[97] Dorri, A., Kanhere, S.S., Jurdak, R. and Gauravaram, P., 2017, March. Blockchain for IoT security and privacy: The case study of a smart home. In *2017 IEEE international conference on pervasive computing and communications workshops (PerCom workshops)* (pp. 618-623). IEEE.

[98] Fremantle, P., Aziz, B. and Kirkham, T., 2017, April. Enhancing IoT security and privacy with distributed ledgers-a position paper. In *IoTBDS 2017: 2nd Interantional Conference on Internet of Things, Big Data and Security* (pp. 344-349). SCITEPRESS–Science and Technology Publications.

[99] Oracevic, A., Dilek, S. and Ozdemir, S., 2017, May. Security in internet of things: A survey. In *2017 International Symposium on Networks, Computers and Communications (ISNCC)* (pp. 1-6). IEEE.

[100] Oh, S.R. and Kim, Y.G., 2017, February. Security requirements analysis for the IoT. In *2017 International Conference on Platform Technology and Service (PlatCon)* (pp. 1-6). IEEE.

[101] Ahemd, M.M., Shah, M.A. and Wahid, A., 2017, April. IoT security: A layered approach for attacks & defenses. In *2017 international conference on Communication Technologies (ComTech)* (pp. 104-110). IEEE.

[102] Ouaddah, A., Abou El Kalam, A. and Ouahman, A.A., 2017, March. Harnessing the power of blockchain technology to solve IoT security & privacy issues. In *ICC* (pp. 7-1).

[103] Salman, O., Elhajj, I., Chehab, A. and Kayssi, A., 2017, May. Software defined iot security framework. In *2017 Fourth International Conference on Software Defined Systems (SDS)* (pp. 75-80). IEEE.

[104] Miraz, M.H. and Ali, M., 2018, August. Blockchain enabled enhanced IoT ecosystem security. In *International Conference for Emerging Technologies in Computing* (pp. 38-46). Springer, Cham.

[105] Román-Castro, R., López, J. and Gritzalis, S., 2018. Evolution and trends in iot security. *Computer*, *51*(7), pp.16-25.

[106] Vorakulpipat, C., Rattanalerdnusorn, E., Thaenkaew, P. and Hai, H.D., 2018, February. Recent challenges, trends, and concerns related to IoT security: An evolutionary study. In *2018 20th International Conference on Advanced Communication Technology (ICACT)* (pp. 405-410). IEEE.

[107] Roy, S., Ashaduzzaman, M., Hassan, M. and Chowdhury, A.R., 2018, December. Blockchain for IoT security and management: current prospects, challenges and future directions. In *2018 5th International Conference on Networking, Systems and Security (NSysS)* (pp. 1-9). IEEE.

[108] Xiao, L., Wan, X., Lu, X., Zhang, Y. and Wu, D., 2018. IoT security techniques based on machine learning: How do IoT devices use AI to enhance security?. *IEEE Signal Processing Magazine*, *35*(5), pp.41-49.

[109] Stergiou, C., Psannis, K.E., Gupta, B.B. and Ishibashi, Y., 2018. Security, privacy & efficiency of sustainable cloud computing for big data & IoT. *Sustainable Computing: Informatics and Systems*, *19*, pp.174-184.

[110] Sollins, K.R., 2019. IoT big data security and privacy versus innovation. *IEEE Internet of Things Journal*, *6*(2), pp.1628-1635.

[111] Chaabouni, N., Mosbah, M., Zemmari, A., Sauvignac, C. and Faruki, P., 2019. Network intrusion detection for

IoT security based on learning techniques. *IEEE Communications Surveys & Tutorials*, *21*(3), pp.2671-2701.

[112] Nizzi, F., Pecorella, T., Esposito, F., Pierucci, L. and Fantacci, R., 2019. IoT security via address shuffling: the easy way. *IEEE Internet of Things Journal*, *6*(2), pp.3764-3774.

[113] Alraja, M.N., Farooque, M.M.J. and Khashab, B., 2019. The effect of security, privacy, familiarity, and trust on users' attitudes toward the use of the IoT-based healthcare: the mediation role of risk perception. *IEEE Access*, *7*, pp.111341-111354.

[114] Hassija, V., Chamola, V., Saxena, V., Jain, D., Goyal, P. and Sikdar, B., 2019. A survey on IoT security: application areas, security threats, and solution architectures. *IEEE Access*, *7*, pp.82721-82743.

[115] Rahman, A., Nasir, M.K., Rahman, Z., Mosavi, A., Shahab, S. and Minaei-Bidgoli, B., 2020. Distblockbuilding: A distributed blockchain-based sdn-iot network for smart building management. *IEEE Access*, *8*, pp.140008-140018.

[116] Mohanta, B. K., Jena, D., Ramasubbareddy, S., Daneshmand, M., & Gandomi, A. H. 2020. Addressing security and privacy issues of IoT using blockchain technology. *IEEE Internet of Things Journal*. doi: 10.1109/JIOT.2020.3008906

[117] Dedeoglu, V., Jurdak, R., Dorri, A., Lunardi, R.C., Michelin, R.A., Zorzo, A.F. and Kanhere, S.S., 2020. Blockchain technologies for iot. In *Advanced Applications of Blockchain Technology* (pp. 55-89). Springer, Singapore.

[118] Hussain, F., Hussain, R., Hassan, S.A. and Hossain, E., 2020. Machine learning in IoT security: current solutions and future challenges. *IEEE Communications Surveys & Tutorials*.

[119] Sharma, V., You, I., Andersson, K., Palmieri, F., Rehmani, M.H. and Lim, J., 2020. Security, privacy and trust for smart mobile-Internet of Things (M-IoT): A survey. *IEEE Access*, *8*, pp.167123-167163.

[120] Mohanty, S.N., Ramya, K.C., Rani, S.S., Gupta, D., Shankar, K., Lakshmanaprabu, S.K. and Khanna, A., 2020. An efficient Lightweight integrated Blockchain (ELIB) model for IoT security and privacy. *Future Generation Computer Systems*, *102*, pp.1027-1037.

[121] Tewari, A. and Gupta, B.B., 2020. Security, privacy and trust of different layers in Internet-of-Things (IoTs) framework. *Future generation computer systems*, *108*, pp.909-920.

[122] Islam, M.N. and Kundu, S., 2020. IoT security, privacy and trust in home-sharing economy via blockchain. In *Blockchain Cybersecurity, Trust and Privacy* (pp. 33-50). Springer, Cham.

[123] Barbosa, P., Brito, A. and Almeida, H., 2016. A technique to provide differential privacy for appliance usage in smart metering. *Information Sciences*, *370*, pp.355-367.

[124] Yin, C., Zhang, S., Xi, J. and Wang, J., 2017. An improved anonymity model for big data security based on clustering algorithm. *Concurrency and Computation: Practice and Experience*, *29*(7), p.e3902.

[125] Rodríguez, C.R.G., 2016, August. Using differential privacy for the Internet of Things. In *IFIP International Summer School on Privacy and Identity Management* (pp. 201-211). Springer, Cham.

[126] Ruiz-Garcia, L. and Lunadei, L., 2011. The role of RFID in agriculture: Applications, limitations and challenges. *Computers and Electronics in Agriculture*, *79*(1), pp.42-50.

[127] Tian, F., 2016, June. An agri-food supply chain traceability system for China based on RFID & blockchain technology. In *2016 13th international conference on service systems and service management (ICSSSM)* (pp. 1-6). IEEE.

[128] Lin, J., Yu, W., Zhang, N., Yang, X., Zhang, H. and Zhao, W., 2017. A survey on internet of things: Architecture, enabling technologies, security and privacy, and applications. *IEEE Internet of Things Journal*, *4*(5), pp.1125-1142.

[129] Biswas, K. and Muthukkumarasamy, V., 2016, December. Securing smart cities using blockchain technology. In *2016 IEEE 18th international conference on high performance computing and communications; IEEE 14th international conference on smart city; IEEE 2nd international conference on data science and systems (HPCC/SmartCity/DSS)* (pp. 1392-1393). IEEE.

SciEn
Journal of Engineering Advancements Vol. 01(04) 2020, pp 183-187 https://doi.org/10.38032/jea.2020.04.009

Friction and Wear Mechanisms of Cu/ta-C Coatings Under PAO-4 and PAO-4 with MoDTC Lubrication

Decelyne Elly Binjua[1], Seock-Sam Kim[1], Young-Jun Jang[2] and Jong-Kuk Kim[2]*

[1]Department of Mechanical Engineering, Universiti Malaysia Sabah, Malaysia
[2]Department of Extreme Environmental Coatings, Korea Institute of Materials Science, South Korea

Received: November 26, 2020, Revised: December 17, 2020, Accepted: December 17, 2020, Available Online: December 23, 2020

ABSTRACT

The tribological behavior of various types of DLC coatings in formulated and non-formulated lubricants are needed for proper usage of these coatings. In this research, the friction and wear mechanism of four different DLC coatings in poly-alpha-olefin type 4 (PAO-4) with and without MoDTC were investigated using ball-on-disc tribometer. One ta-C (tetrahedral amorphous carbon) and three Cu/ta-C (copper doped ta-C) with different sputter power of 50 W, 150 W, and 200 W coatings were deposited on silicon wafers by using FCVA (filtered cathodic vacuum arc) technique for this research. The results indicate that ta-C coating on silicon wafer has the lowest average friction coefficient (CoF) and better wear resistance than Cu/ta-C coating when lubricated under PAO-4 oil with MoDTC. Cu/ta-C with sputter powers of 150 W and 200 W exhibited the highest average friction coefficient under PAO-4 oil with MoDTC. Meanwhile, the average CoF for all samples were similar under PAO-4 base oil. In terms of wear, ta-C coating showed the highest wear rate under PAO-4 base oil then followed by Cu/ta-C with sputter power of 50 W. Nonetheless, Cu/ta-C with sputter powers of 150 W and 200 W exhibited significantly low wear rate under PAO-4 base oil compared to PAO-4 oil with MoDTC.

Keywords: Friction; Wear; Cu/ta-C coating; PAO-4; MoDTC; FCVA.

1. Introduction

In order to deliver greater wear resistance, coating materials with high hardness were developed to fulfil the demand for increased durability of mechanical components used in harsh environments. This type of coating has been demanded extensively for various engineering applications.

Diamond-like Carbon (DLC) coating is a coating that possesses properties of natural diamond with mechanical properties such as high wear resistance, high hardness, and a low coefficient of friction under dry conditions. DLC coatings are constructed by a network of different fractions of sp2 and sp3 hybridized C–C and C–H bonding and are usually amorphous [1].

Plasma Enhanced Chemical Vapour Deposition (PE-CVD) is an amorphous film used to coat a protective layer from gas state to solid state on a substrate. The deposition pressures influence the structures and properties of coatings. The average thickness of the coating increased as the deposition pressure increased. According to X. Wang et al. [2], in order to promptly deposit DLC coating, a pipeline is used directly as a deposition chamber by exciting carbon-containing source gas. DLC coating has excellent properties which is a good prospect in the field of inner protective coating. Application of coatings is one of the most widely used route in order to tailor wear performance, surface morphology, fatigue strength and adhesion of substrate material without altering bulk properties of the substrate.

Many coated DLC parts are used in bigger tribological system where steel-steel contacts still exist hence the coating performance under lubricated conditions becomes an important factor. DLC coating can be used for a variety of applications due to the modifications that can be done and its properties such as chemical inertness, infrared transparency, high electrical resistivity, high wear resistance and low friction coefficients that can be adjusted by choosing the right deposition method.

There are many deposition methods of DLC films. Filtered cathodic vacuum arc (FCVA) is one of the deposition processes used to deposit thin films for a variety of applications. This technique can filter the macroparticle during the deposition process by using the magnetic filters in order to produce tremendously high quality of ta-C coatings with 87% of sp3 bonding fraction. Hence, producing coatings with outstanding properties and are suitable to enhance the performance in corrosion and wear resistance [3].

However, the number of industrial utilisations of DLC films is limited due to their low toughness that causes the films to become brittle. Many have used metal doping to modify the microstructure of the DLC films to solve this problem. Copper is known to be a ductile metal and non-carbide former which can be used as the doping element to enhance the friction and wear mechanisms of DLC coatings under lubrication [4]. In this research, Cu was doped into ta-C films with different concentration by changing the sputter power.

Moreover, Molybdenum Dithiocarbamate or well known as MoDTC is a complex additive package that can be mixed into the base oil for better performance of lubricants.

Poly-alpha-olefin (PAO-4) base oil is one of the synthetic hydrocarbon liquids with low comparatively short molecular

*Corresponding Author Email Address: sskim@ums.edu.my

lengths and side branch densities that were established as high-performance base-stock oils for automotive and industrial applications. Thereby, this research paper aims to investigate ta-C and Cu/ta-C with different sputter power coatings on silicon wafer under PAO-4 oil with MoDTC and PAO-4 base oil lubrications.

2. System Design

In order to successfully execute the experiment, a set of systematic method is required to be set as a standard. The methods for data collection are included as well as the concepts and theories which underline the methods. The experiments procedures, concepts and theories are described in detail for further understanding on the experiment.

2.1 Deposition Process

In order to systematically study ta-C films under lubrication, one set of ta-C and three sets of Cu doped ta-C with different sputter power coated silicon wafer samples were designed. Three main deposition processes which are etching, sputtering and arc deposition were performed to fabricate the coated samples.

The silicon wafers undergo etching process by using the linear ion source (LIS) for 10 minutes to remove the impurities on the surface of the silicon wafers beforehand. Argon gas is used as the reactant gas with a flow of 18 sccm. The voltage supply used was 1.7kV which yielded a 260 mA of current.

After the etching process, it was then continued with the sputtering of Cu for 30 minutes to deposit a buffer layer on the surface of the substrate to enhance the adhesion strength of the coating layer. Argon gas was used as the reactant gas with a flow of 25sccm and a power supply of 250W.

Then, as for the coating layer, two types of coatings were designed which are ta-C and Cu doped ta-C coatings in this research. There were two processes involved in this coating process which are arc deposition and sputter processes. Both coatings have the same thickness which are 1μm but different deposition time. Arc deposition process was used to deposit the ta-C film on the substrates, meanwhile, arc deposition and sputter processes were used simultaneously to produce Cu doped ta-C film. The arc deposition process was conducted under duct bias voltage of 10 V with a reference current of 60 A in a 45°-bend magnetic FCVA system for both types of coatings.

For the Cu doped ta-C coating, it was conducted with argon gas as the source of reactant gas with a flow of 25 sccm. The power supply used varies for the Cu doped ta-C coating as there were three different samples designed. There are four samples that were designed with their own specific condition where one sample is for ta-C coating and the other three samples are for Cu/ta-C coating with variation of sputter power as shown in Table 1 below which reveals the coating layer structure of the substrate.

Table 1 The Type of ta-C and Cu Doped ta-C Coatings

Thickness	Sample #1	Sample #2	Sample #3	Sample #4
1 μm	ta-C	Cu/ta-C (50W)	Cu/ta-C (150W)	Cu/ta-C (200W)
0.3 μm	Cu Buffer Layer			
Silicon wafer (100)				

2.2 Tribological Test

The sliding friction test was carried out by using a ball-on-disk tribometer to determine the friction and wear properties of the coating film.

The counter specimen used was silicon nitride (Si3N4) ball of 4 mm radius. Prior to the experiments, the ball was cleaned in an ultrasonic bath using ethanol for 3 minutes to remove surface contaminants on the ball. The zig used to hold the silicon wafer was also cleaned by using ethanol. Then, the silicon wafer was attached to the zig with a glue.

Four types of samples with different deposition parameters were used for this experiment. The ball is reciprocated for 1 hour and 39 minutes against the sample with an applied load of 20 N, a linear speed of 84 mm/s and a stroke length of 4 mm at ambient temperature of 18-23 ℃ with humidity of 10-20 % for a total distance of 502654.82mm of 20000 cycles under two types of lubrications which are PAO-4 base oil and PAO-4 oil with MoDTC.

The coefficient of friction (CoF) was monitored as a function of the number of cycles. The results of friction coefficient were obtained by referring to the real time display of test information in computer software of tribometer. The average friction coefficient of each tested sample was computed and plotted in a graph for both lubrications. The wear rate for each tested sample was also recorded and plotted in a graph. Then, the images of the wear scar of the counterpart material and the wear track on the coating surface were observed by using confocal microscopy.

3. Results and Discussions

The results and discussions are presented in four subsections according to coating characterization, friction behavior, wear behavior and surface analysis.

3.1 Coating Characterization

The coating characterization was distinguished by comparing results from the previous study. Fig. 1 shows the Cu concentration and the average growth rate of the films as a function of the sputtering current of the magnetron sputtering unit. The Cu concentration increased with the sputtering current. In this research, the sputtering power was adjusted to control the Cu concentration in films. The sputtering current increased with the sputtering power, indicating that the Cu concentration increases when higher sputtering power is used.

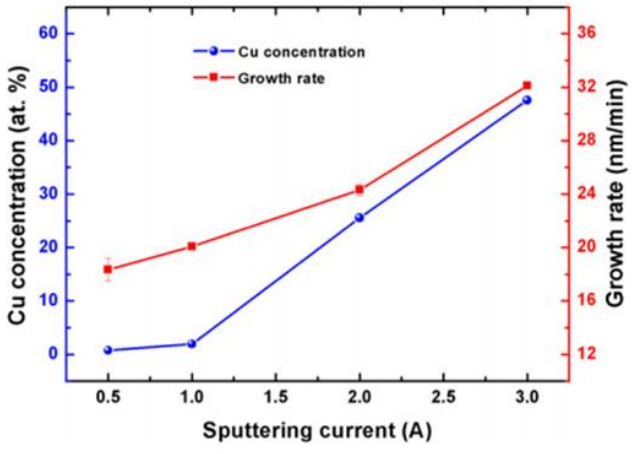

Fig. 1 Cu concentration and growth rate of the Cu-DLC films as a function of the sputtering current. (Source: [4])

Moreover, the residual stresses of the films were measured as a function of the Cu concentration, as shown in Fig. 2. Based on previous study, pure DLC film has higher residual stress which is about 2.7 GPa while the residual stress for Cu-DLC film is lower with 1.4 GPa when Cu 0.74 at.%. The residual stress of the films increases with increasing Cu concentration and starts to reduce when Cu concentration is 25.6 at.% which can be seen from Fig. 3. Thereby, it is believed that the residual stresses in this research study are similar to the previous study whereas it increases as the sputtering power increases.

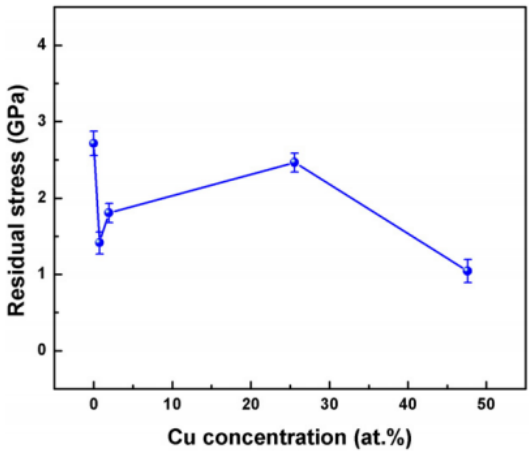

Fig. 2 Residual stress of the Cu-DLC films as a function of Cu concentration. (Source: [4])

The graph pattern of the film hardness and elastic modulus at different Cu concentrations were similar to the residual stress as both the mechanical properties and residual stress of the DLC films were highly dependent on the sp3-C bonding structures [4]. The film shows lower hardness compared to pure DLC at lower concentration of Cu. This result is homogenous to the previous research conducted by Hojun Ryu et al. [5], which showed that those N-doped ta-C films have lower hardness than that of non-doped ta-C film. Thus, it can be concluded that non-doped ta-C has higher hardness compared to Cu-doped ta-C in this study.

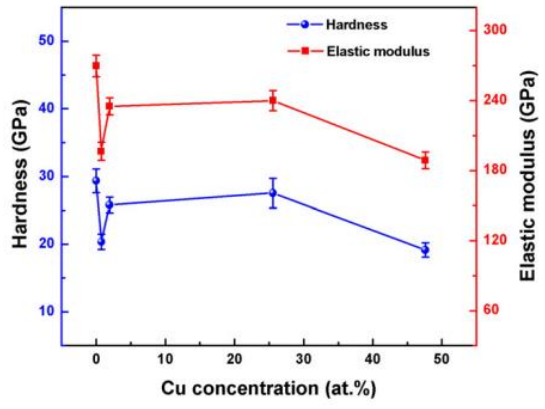

Fig. 3 Hardness and elastic modulus of the Cu-DLC films as a function of Cu concentration. (Source: Dai et al. 2015)

3.2 Frictional Behaviors Under PAO-4 Base Oil and PAO-4 Oil with MoDTC Lubrications

This sliding friction test was carried out by using ball-on-disc tribometer to determine the friction and wear properties of the coating film under two different types of lubrication which are PAO-4 base Oil and PAO-4 Oil with MoDTC.

Normally, PAO is known to have better lubricity hence the reduced friction coefficient. Moreover, the friction reduction might be due to the formation of MoDTC derived tribofilms MoS2 and surface graphitization [6], [7]. The addition of MoDTC further improve the friction performance. According to Zahid et al. [8] the surface energy is improved when DLC coatings are doped with metals as the chemical reactivity of the coating with lubricant is increased due to formation of active sites.

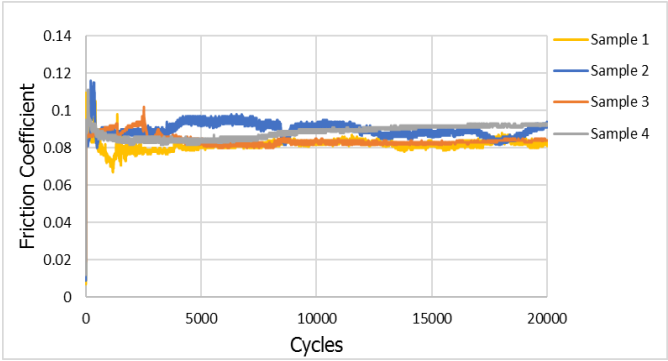

Fig. 4 Frictional behavior of ta-C and Cu-doped ta-C coatings under PAO-4 Base Oil

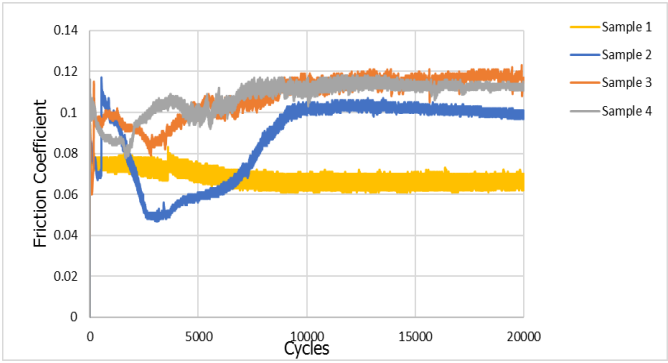

Fig. 5 Frictional behavior of different type of ta-C and Cu-doped ta-C coating under PAO-4 with MoDTC

Fig. 4 shows the behavior of the CoF for ta-C and Cu doped ta-C coating in PAO-4 base oil lubrication. In the case of ta-C coating, the coefficient of friction was the lowest and showed stable behavior, but it was confirmed that the coefficient of friction was lowered as the UBM (Unbalanced Magnetron) power for Cu doping increased. This is due to the high hardness characteristics of the ta-C coating film, and it is believed that the contact area is relatively smaller than that of Cu doping ta-C. The mechanical properties of the ta-C coating used in the experiment can be confirmed from the previous results [9]. In addition, the Cu-doped ta-C coating exhibits a high coefficient of friction behavior when contacting the mating material with the two materials ta-C and Cu during friction.

In addition, as shown in Fig. 5, when PAO-4 base oil with MoDTC was used, the ta-C coating still showed the lowest coefficient of friction, but the Cu doping ta-C showed a high friction behavior of 0.08 ~ 0.1 or more. However, it can be seen that the friction coefficient characteristics increase as the Cu sputter power increases.

The Cu sputter power of 50 W showed the lowest coefficient of friction among Cu-doped ta-C, which is believed to be due to the doping of a small amount of Cu compared to 150 W and 200 W.

3.3 Wear Behaviors Under PAO-4 Base Oil and PAO-4 Oil with MoDTC Lubrications

The wear behavior of disk and counter materials was investigated based on the analysis of frictional behavior of ta-C coating and Cu doped ta-C coatings. Fig. 6 and Fig. 7 show the amount of wear of the disk and the counter materials (Si3N4) used in the PAO-4 base oil and PAO-4 oil with MoDTC lubrications.

In the case of ta-C coating, the wear of disk and Si3N4 ball was highest in PAO environment. This is believed to be due to the simultaneous wear of the counterpart material and disk during friction due to the high hardness characteristics of the ta-C coating without the chemical effect of oil. In addition, it can be understood that carbon-based particles wear due to abrasion have a lubrication effect at the contact interface, so that the amount of wear is high, but the coefficient of friction is low.

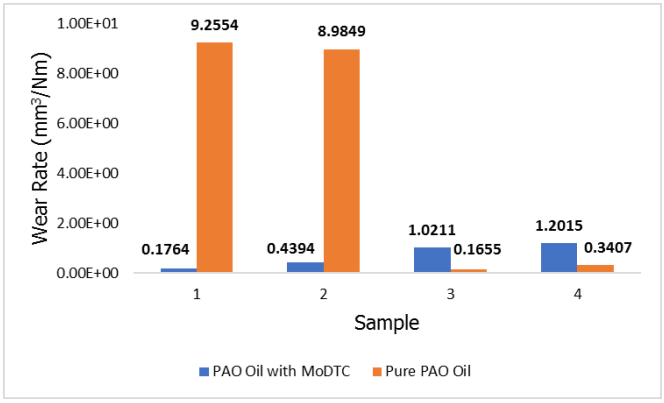

Fig. 6 To compare with wear rate of coatings under the PAO-4 base Oil and PAO-4 with MoDTC

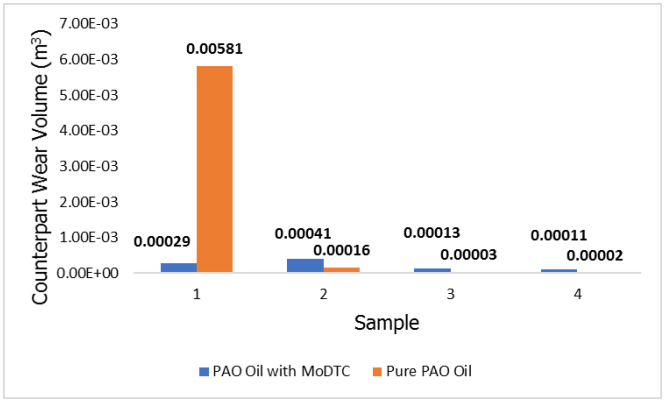

Fig. 7 To compare with wear volume of Counter materials (Si_3N_4 ball) under the PAO-4 base Oil and PAO-4 with MoDTC

However, in the case of Cu doped ta-C coatings, when the Cu sputtering power was 50 W, the disk wear decreased slightly, but at 100 W and 200 W, the wear of the counterpart material decreased sharply. This phenomenon shows that the coating with higher sputter power has better wear resistance when lubricated with PAO-4 base oil.

More interestingly, in the PAO-4 oil with MoDTC lubrication, low wear amount was observed in Cu doped ta-C coatings including ta-C coatings and counterpart materials. In addition, as the Cu sputtering power increases, the amount of disk wear increases, and the lowest disk wear behavior is seen in the general ta-C coating. This might be due to tribo-chemical reaction in Si3N4 that resulted in low wear under the boundary lubrication [10].

In this research, the addition of MoDTC in PAO-4 base oil showed positive effects on the wear performance. The wear rate in both ta-C/Si3N4 and Cu/ta-C/ Si3N4 contacts displayed similarly same behaviour as it resulted low wear under PAO oil with MoDTC lubrication. The wear rate for all types of DLCs in PAO oil with MoDTC are low suggesting that even with the presence of MoDTC, the wear rate is rather controlled by the nature of the DLC itself than the MoDTC [8].

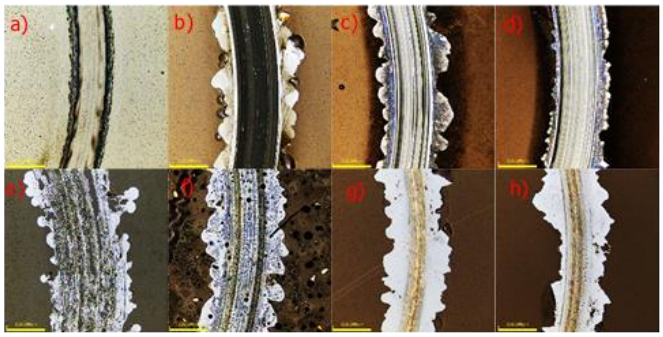

Fig. 8 Wear track of coatings for a) ta-C b) Cu-doped ta-C (50W) c) Cu-doped ta-C (150W) and d) Cu-doped ta-C (200W) under PAO-4 Oil with MoDTC and e) ta-C f) Cu-doped ta-C (50W) g) Cu-doped ta-C (150W) and h) Cu-doped ta-C (200W) under PAO-4 Base Oil

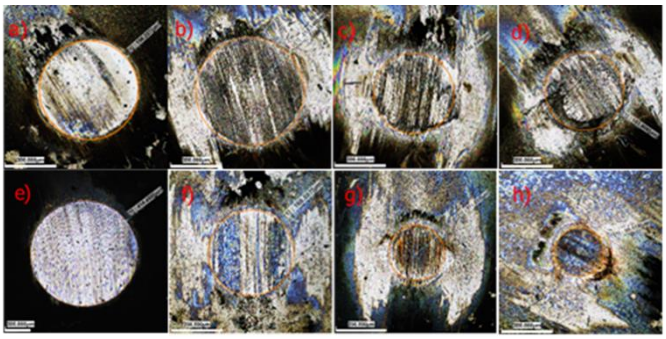

Fig. 9 Wear scar of the counterpart material for a) ta-C b) Cu-doped ta-C (50W) c) Cu-doped ta-C (150W) and d) Cu-doped ta-C (200W) under PAO-4 Oil with MoDTC and e) ta-C f) Cu-doped ta-C (50W) g) Cu-doped ta-C (150W) and h) Cu-doped ta-C (200W) under PAO-4 Base Oil

3.4 Surface Analysis

The wear track image (Fig. 8) on the coating surface and the wear scar of the counterpart material (Fig. 9) were observed by using the laser scanning confocal microscope. It can be observed that the wear tracks on the coating surface of all samples are severely damage when lubricated with pure PAO oil. The wear width of Sample 1 (ta-C coating) in pure PAO oil is significant due to abrasive wear. This evidence of abrasive wear can be evidence in the friction and wear phenomena of the ta-C coating as mentioned above.

Meanwhile, the wear track on the coating surface of Sample 1 (ta-C coating) is the smoothest when lubricated under PAO oil with MoDTC. This might be due to less formation of wear debris in ta-C coating than Cu/ta-C coating. In Fig. 10 and Fig. 11, the size of wear scar of the counterpart material reduced as the sputter power increased in Cu/ta-C/Si3N4 contacts for both types of lubrications. It can be observed that the size of wear scars of counterpart material for Samples 2 (Cu/ta-C, 50 W), 3 (Cu/ta-C, 100 W) and 4 (Cu/ta-C, 150 W) are smaller under pure PAO oil lubrication compared to PAO oil with MoDTC. This might be

due to the formation of tribo-film on the counterpart ball. However, it is the opposite in ta-C/Si3N4 contacts whereas size of wear scar of counterpart material is smaller under PAO oil with MoDTC lubrication compared to pure PAO oil.

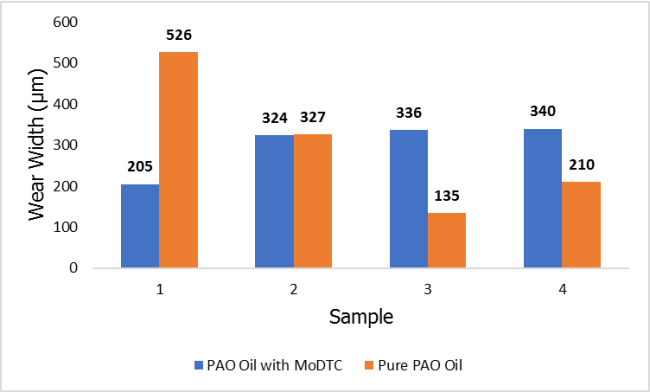

Fig. 10 Width of wear track of the coatings

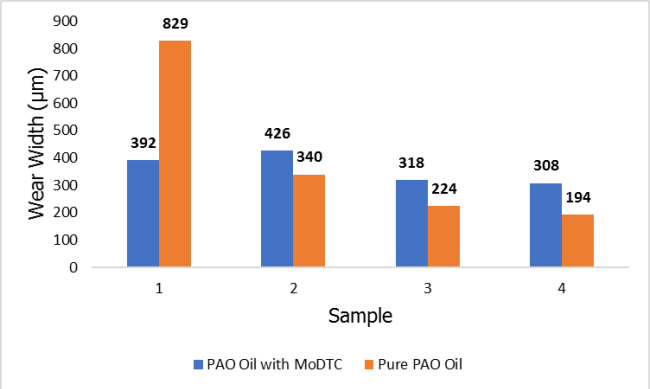

Fig. 11 Width of wear scar of the Si_3N_4 balls

4. Conclusion

In this research, silicon wafers were coated with ta-C and Cu/ta-C coating with different sputter power. The sputter powers of 50 W, 150 W and 200 W were used for the Cu/ta-C coatings. All samples were examined for its frictional and wear behaviour when lubricated with two types of lubrications which are PAO-4 base oil and PAO-4 oil with MoDTC.

The results show that:

i. Cu/ta-C coating with lower sputter power has smaller friction coefficient but ta-C coating has the smallest when lubricated under PAO-4 oil with MoDTC.

ii. Cu/ta-C coating with higher sputter power has better wear resistance under PAO-4 base oil lubrication.

iii. The size of wear scar of the counterpart material reduced as the sputter power increase in Cu/ta-C/Si3N4 contacts for both types of lubrications.

References

[1] Ren, Z., Qin, H., Dong, Y., Doll, G.L. and Ye, C., 2019. A boron-doped diamond like carbon coating with high hardness and low friction coefficient. Wear, 436, p.203031.

[2] Wang, X., Sui, X., Zhang, S., Yan, M., Yang, J., Hao, J. and Liu, W., 2019. Effect of deposition pressures on uniformity, mechanical and tribological properties of thick DLC coatings inside of a long pipe prepared by PECVD method. Surface and Coatings Technology, 375, pp.150-157.

[3] Ean, Y.C., Jang, Y.J., Kim, J.K., Hsien, W.L.Y., Siambun, N.J. and Kim, S.S., 2017. Effect of substrate bias on the tribological behavior of ta-C coating prepared by filtered cathodic vacuum arc. International Journal of Precision Engineering and Manufacturing, 18(5), pp.779-784..

[4] Dai, W., Wang, A. and Wang, Q., 2015. Microstructure and mechanical property of diamond-like carbon films with ductile copper incorporation. Surface and Coatings Technology, 272, pp.33-38.

[5] Jang, Y.J., Kang, Y.J., Kitazume, K., Umehara, N. and Kim, J., 2016. Mechanical and electrical properties of micron-thick nitrogen-doped tetrahedral amorphous carbon coatings. Diamond and Related Materials, 69, pp.121-126.

[6] Yazawa, S., Minami, I. and Prakash, B., 2014. Reducing friction and wear of tribological systems through hybrid tribofilm consisting of coating and lubricants. Lubricants, 2(2), pp.90-112.

[7] Vengudusamy, B., Green, J.H., Lamb, G.D. and Spikes, H.A., 2012. Behaviour of MoDTC in DLC/DLC and DLC/steel contacts. Tribology International, 54, pp.68-76.

[8] Zahid, R., Masjuki, H.H., Varman, M., Mufti, R.A., Kalam, M.A. and Gulzar, M., 2015. Effect of lubricant formulations on the tribological performance of self-mated doped DLC contacts: a review. Tribology Letters, 58(2), p.32.

[9] Lee, W.Y., Tokoroyama, T., Jang, Y.J. and Umehara, N., 2018. Effect of Substrate Bias and Temperature on Friction and Wear Properties for ta-C Coating Prepared under Different Substrate Bias Voltages with Filtered Cathodic Vacuum Arc Deposition. Tribology Online, 13(5), pp.241-247.

[10] Zeng, Q., Yu, F. and Dong, G., 2013. Superlubricity behaviors of Si3N4/DLC Films under PAO oil with nano boron nitride additive lubrication. Surface and interface analysis, 45(8), pp.1283-1290.

SciEn
Journal of Engineering Advancements Vol. 01(04) 2020, pp 188-194 https://doi.org/10.38032/jea.2020.04.010

Artificial Neural Network based COVID-19 Suspected Area Identification

Tanjima Akhter[1], Md. Ariful Islam[2], Saiful Islam[3]

[1] Department of Applied Mathematics, Noakhali Science & Technology University, Bangladesh
[2]Department of Robotics & Mechatronics Engineering, University of Dhaka, Bangladesh
[3]Department of Information and Communication Technology, Bangladesh University of Professionals, Bangladesh

Received: November 24, 2020, Revised: December 18, 2020, Accepted: December 19, 2020, Available Online: December 28, 2020

ABSTRACT

This paper deals with the symptoms based COVID-19 suspected area identification using an artificial neural network by which a country or region can be divided into red, yellow, and green zone representing the highly infected area, moderate infected area, and controlled or low infected area, respectively. At first, an online survey of twenty (20) patients was conducted based on the nine (09) major symptoms of COVID-19. Then, a model based on the fuzzy logic system was designed consisting of COVID-19 symptoms identification, fuzzification, rule evaluation, fuzzy inference mechanism, etc. for getting the data sets to be trained in neural networks. For different combinations of 09 symptoms, different rules were generated and evaluated for possible recommendations. Based on different rules, three possible outputs representing high infection probability, medium infection probability, and low infection probability were obtained using the Mamdani inference mechanism. These outputs were termed as red, yellow, and green zone separated by the crisp value of +1, 0, -1, respectively, and considered as target data to be trained in neural networks.

Keywords: Neural Network; COVID-19; Fuzzy Logic System; Mamdani Inference Mechanism.

1. Introduction

In Wuhan, China a novel corona virus named COVID-19 was discovered in early December 2019 and since then it has been spreading out rapidly throughout the world. Several viruses have appeared in the history of humanity since the beginning of civilization, COVID-19 is one of few which has been declared as 'Pandemic' throughout the world by WHO because of its infection nature. Nowadays, it becomes a major health concern which is causing several health issues in human beings. Till October 29, 2020, the number of confirmed cases is 44 million while the death toll reaches 1.17 million and the number of recovered cases is 29.8 million around the world [1]. COVID-19 has affected 216 countries and territories around the world [1]. Among all 216 countries USA, India, Brazil, Italy, Spain, Russia, the UK have been identified as the hotspot with the most confirmed cases and the infections are increasing exponentially. This is an alarming situation for the whole world and moreover, the situation is getting out of control for almost every country whether it's a rich or developing/poor one. It's affecting overall infrastructure, economic, social and other aspects of a country as to reduce the infection rate most of the country were compelled to declare a state of emergency and have locked down cities.

COVID-19 is a zoonotic type which can transmit the infection from animal to human but now infection is spreading from human to human and each infected human can infect more than two. In this way further infections may occur, and the infection rate has been identified as an exponential one [2]. Researchers and Scientists around the world were unable to find any specific treatment for COVID-19 so far but they are working hard and soul to find the vaccine for the prevention of this disease [2]. Several shreds of evidences predicted, Wuhan City, as the source of this outbreak and it has been identified as one of the significant role-playing places in the initial amplification of the outbreak.

The first identified case of COVID-19 subsequently named as SARS-COV-2 was reported by the official of Wuhan city, China in December 2019 [3].

Although COVID-19 causes mild illness for people with strong immunity, it may make some people very ill especially older people and people with pre-existing medical conditions appear to be more vulnerable and the disease can be fatal for them [4]. Fever, trouble breathing, chest pain, dry cough, diarrhea, sore throat, and headaches are known to be common symptoms of COVID-19. However, in some cases, it can cause pneumonia and kidney failure even no symptoms at all. People are dying every single day upon getting the infection. According to the study by Centers for Disease Control and Prevention (CDC) between two days to two weeks of exposure to the virus symptoms usually appear [5].

In processing huge data by analyzing computationally to reveal projection, prediction, and patterns, Artificial Neural Network has proven to be one of the efficient and time-consuming ones. It has a greater and enriching prospect not only in the engineering sector but also in the medical sector [6]. This study provides neural network-based logical decisions based on COVID-19 symptoms by which a country or region can be divided into red, yellow, and green zone representing highly infected, moderate infected, and controlled or low infected areas respectively. An algorithm based on neural network has proposed to give overall statistics of a country about low, medium, and high density of infected people. Three networks have generated to compare the proposed model and the Feed forward back propagation algorithm has implemented in these networks. The fuzzy logic output has trained into the neural network for which the threshold value of separating different places of a country can be categorized into three zones. MATLAB has used for testing algorithm and obtaining outcomes.

*Corresponding Author Email Address: arif_eeedu@yahoo.com Published by: SciEn Publishing Group

2. Methodology

In this paper, we propose a model using the artificial neural network by which the identification of COVID-19 suspected area based on COVID-19 symptoms can be realized easily. The flow chart of this model is shown in Fig. 1.

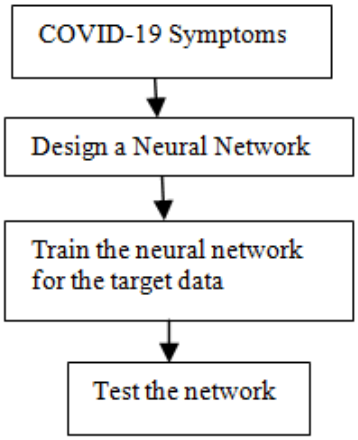

Fig. 1 Proposed algorithm for identification of danger zones of COVID-19

2.1 COVID-19 Symptoms

To train the neural network, we have generated data sets from the different combinations of COVID-19 symptoms. The major symptoms of COVID-19 are fever or body temperature (BT), dry cough (DC), trouble breathing (TB), chest pain (CP), diarrhea, sore throat (ST), and headache, etc. [7], [8]. If a person gets close contact to the infected person having these symptoms or travel to the infected area may become COVID-19 positive or negative. Based on these causes and symptoms of COVID-19, at first, an online survey of twenty (20) patients was conducted, recorded, and analysed. In most of the cases, patients having a severe level of breathing problems, chest pain, dry cough, and get close contact with the infected person were identified as COVID-19 positive while a few of them were resulted as COVID-19 negative despite having headache, fever, or sore throat. This survey information was implemented in the Mamdani inference system as shown in Fig. 2. Here, the symptoms level of COVID-19 was considered as linguistic variables and their corresponding possible output recommendations were recorded. Then, different fuzzy rules were inserted in the Mamdani inference system and evaluated for the possible recommendations depicted in Fig. 3.

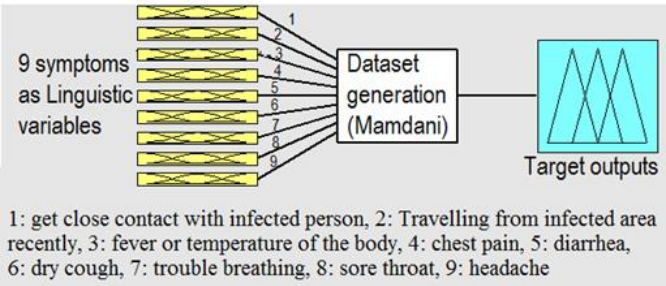

Fig. 2 Mamdani inference system for creating COVID-19 symptoms data set

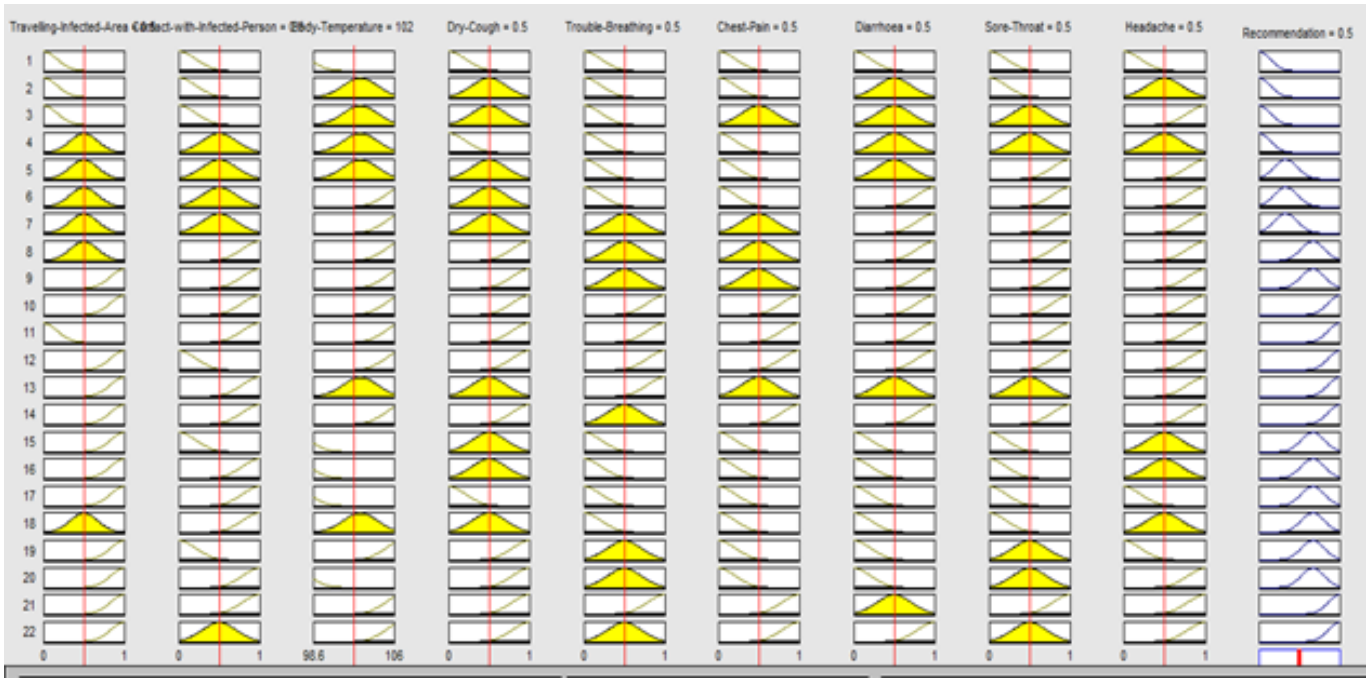

Fig. 3 Rule evaluation for possible recommendation

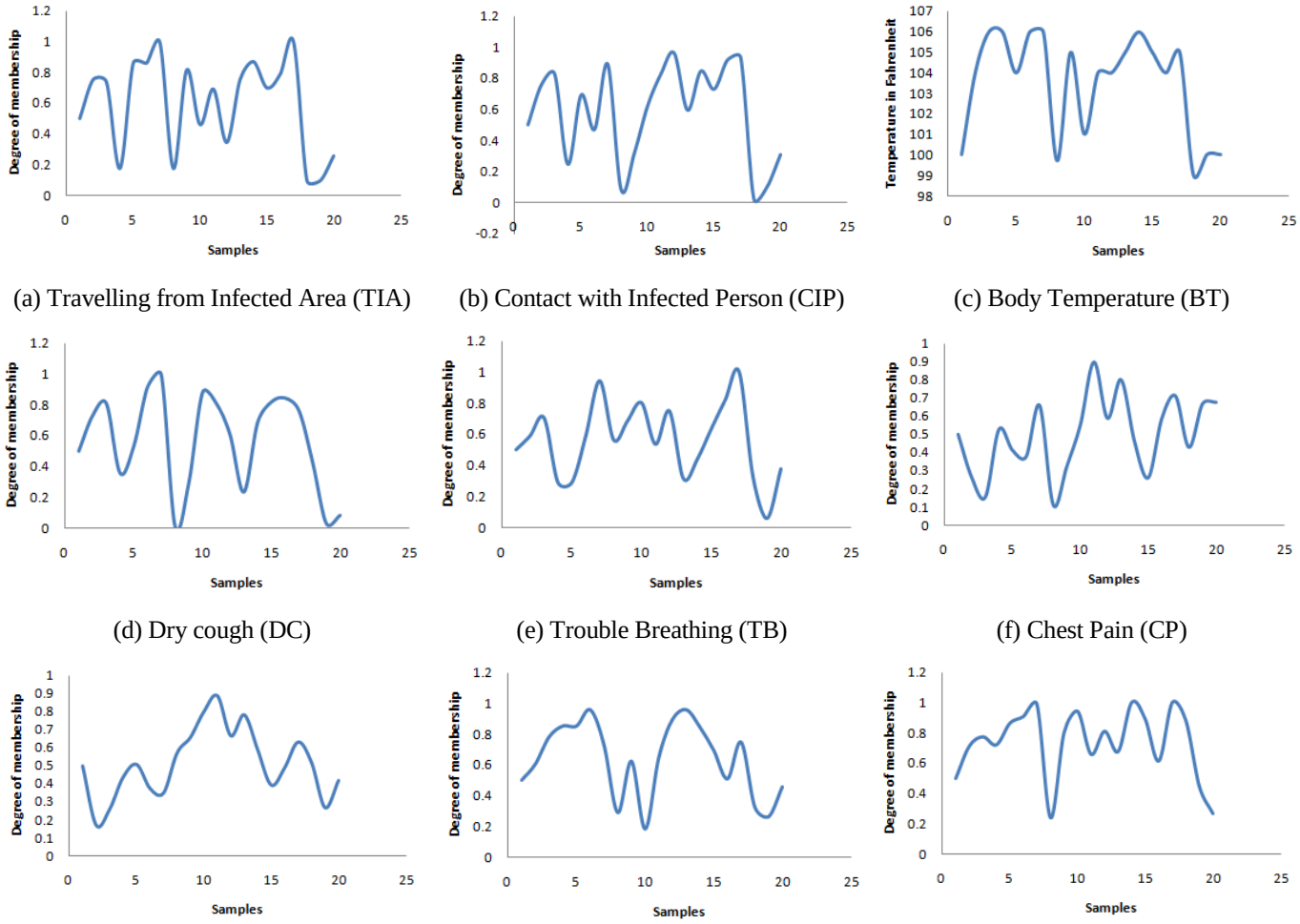

(a) Travelling from Infected Area (TIA) (b) Contact with Infected Person (CIP) (c) Body Temperature (BT)

(d) Dry cough (DC) (e) Trouble Breathing (TB) (f) Chest Pain (CP)

(g) Diarrhea (h) Sore Throat (ST) (i) Headache

Fig. 4 Different COVID-19 Symptoms provided from fuzzy logic system as training sets (a-i)

After that, all the 20 patient's data sets and their corresponding symptoms level were expressed in terms of the degree of membership illustrated in Fig. 4, and different outputs representing high, medium, and low infection probability were recorded. These output levels were separated by the crisp value of +1 (red zone), 0 (yellow zone), and -1 (green zone) as shown in Fig. 5 and considered as target data to be trained in neural networks.

2.2 Design a neural network

A neural network consists of a processing element with synaptic input connections and a single output. Usually, the inputs $x_1, x_2 \ldots x_3$ are multiplied by their respective numeric weights $w_1, w_2 \ldots w_n$ and the weighted sum of the input signals can be expressed as [9]:

$$net = (w_1.\ x_1 + w_2.\ x_2 + w_3.\ x_3 + \ldots\ldots + w_n.\ x_n) = (\sum_{i=1}^{n} w_i.\ x_i + b)$$

Here, b is the threshold value called bias which will always have the value of 1. The amplitude of the output of a neuron can be limited by a non-linear activation function, $f(.)$ as depicted in Fig. 6 [9].

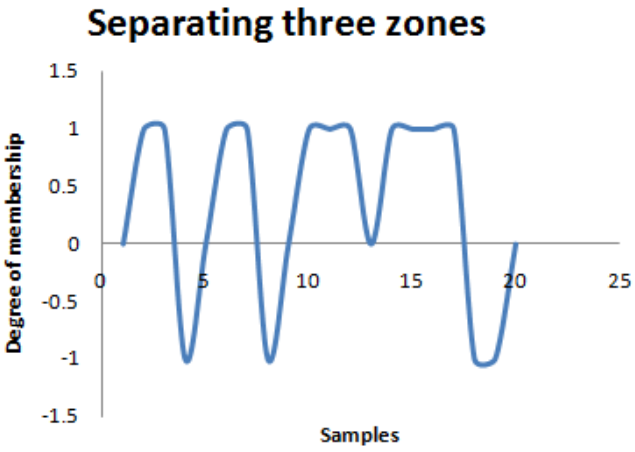

Fig. 5 Target samples or data

In a layered neural network, the neurons are organized in the form of layers. In the simplest form of a layered network, an input layer of source nodes is directly projected onto an output layer of neurons.

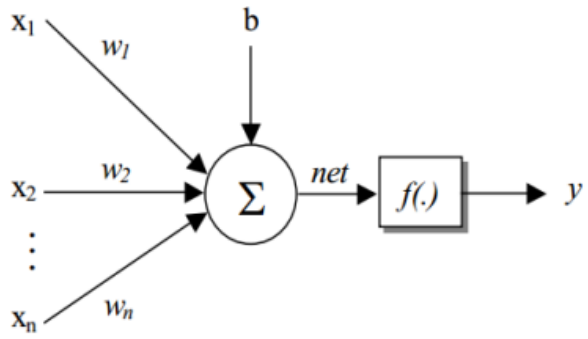

Fig. 6 Perceptron Model

This type of network is known as feedforward as only the forward connectivity of the neurons is considered [10]. Fig. 7 shows such a feedforward network where "single-layer" referring to the output layer of computation nodes (neurons) [9].

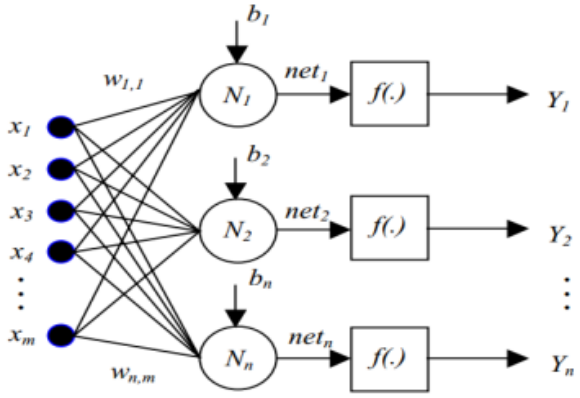

Fig. 7 Single layer feedforward network

Table 1 Rule insertion for zone separation

IF				
TIA	No	No	Yes	No
CIP	No	No	Yes	Yes
BT	Low	High	Medium	High
DC	No	Yes	Yes	Yes
TB	No	No	No	Yes
CP	No	No	No	Yes
Diarrhea	Sometimes	Sometimes	Sometimes	Sometimes
ST	No	Yes	No	Yes
Headache	Yes	Yes	Yes	Yes
THEN				
Target output	-1 (Green Zone)	0 (Yellow Zone)	1 (Red Zone)	1 (Red Zone)

*TIA= Recent travel from infected area, CIP= Close contact with infected person, BT= Body temperature, DC=Dry cough, TB= Trouble breathing, CP= Chest pain, ST= Sore throat.

The inputs of this network are the input vectors consisting different types of COVID-19 symptoms, weights of the network are the weight matrices, and biases are the bias vectors. The target data is output vectors consisting three different values -1, 0 and 1 representing green zone, yellow zone and red zone, respectively. Three networks such as zone_network1, zone_network2, and zone_network3 were generated with 10, 12 and 14 number of neurons respectively using the back-propagation algorithm as shown in Fig. 8. At first, the nine (09) major symptoms of COVID-19 was converted into linguistic variables and then, different IF----THEN rules were implemented in Mamdani fuzzy inference system listed in Table 1.

Thus, for different combination of major COVID-19 symptoms, different decisions were identified by experts.

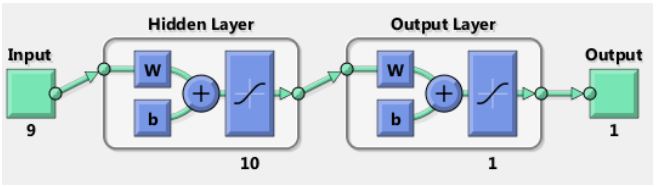

(a) zone_network1

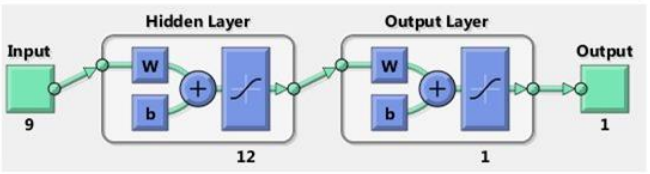

(b) zone_network2

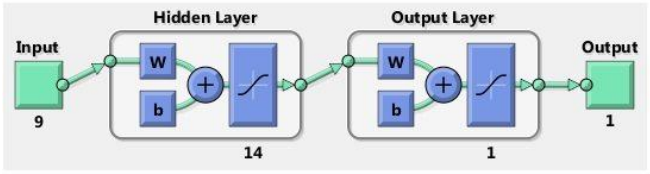

(c) zone_network3

Fig. 8 Network named zone network with 10, 12 and 14 neurons obtained during training process

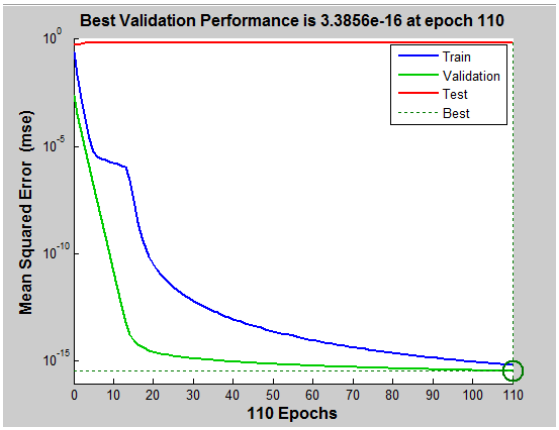

Fig. 9 Performance evaluation of training, validation and test sets in MATLAB

2.3 Train the neural network for the target data

The back-propagation algorithm trains the neural network by adjusting its weights [11]. The training process continues till the neural network continues to improve on the validation set. Each network accuracy was measured by test set and the performance was evaluated in terms of logarithmic mean squared error as depicted in Fig. 9. It is evident from Fig. 9 that the mean square error reduces quickly as the number of epoch's increases.

The algorithm and process information of this training process are listed in Table 2.

Table 2 Algorithm and process information of training

Algorithm and process information	
Data Division	Random
Training	Levenberg-Marquardt
Performance	Mean Squared Error (MSE)
Epoch	110 iterations
Time	0:00:04

2.4 Test the Network

In this step, the trained neural network was tested with real-world COVD-19 symptoms data set [12]. This testing estimates how well the neural network performs with the actual data set. The tested network generated outputs in the range of -1 to +1 as shown in Fig. 10. The value of nearly or exactly -1 indicates the state of low or no infected area whereas 0 defines the state of medium level of the infected area and +1 defines the state of the high infected area.

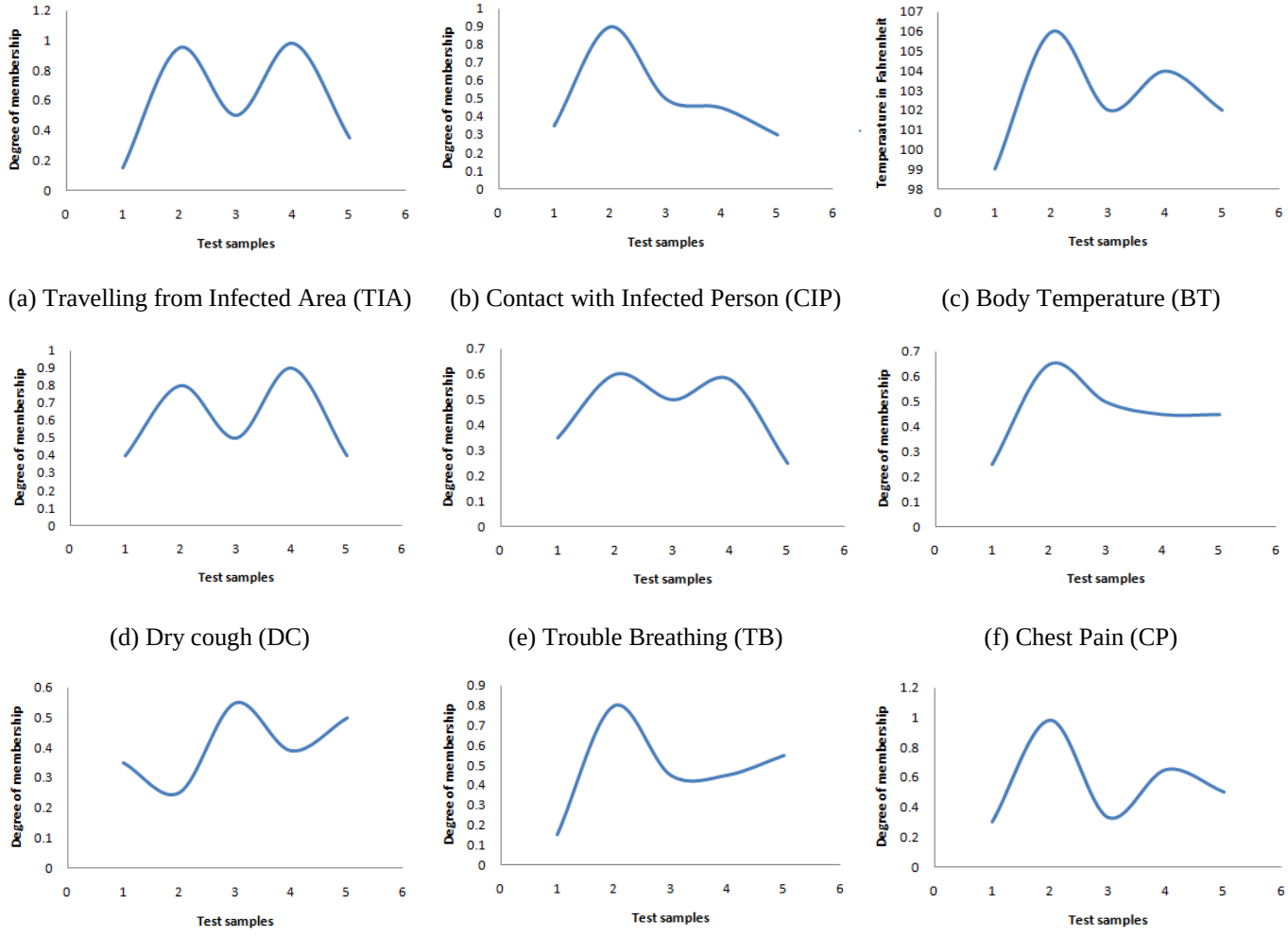

(a) Travelling from Infected Area (TIA) (b) Contact with Infected Person (CIP) (c) Body Temperature (BT)

(d) Dry cough (DC) (e) Trouble Breathing (TB) (f) Chest Pain (CP)

(g) Diarrhea (h) Sore Throat (ST) (i) Headache

Fig. 10 Different COVID-19 Symptoms provided from real world as testing sets (a-i)

3. Results and Discussion

In this work, different combinations of COVID-19 symptoms were used as linguistic variables of the fuzzy logic system and outputs provided by the experts considered as the target or desired outputs. The neural network was trained with these target outputs. If the network is satisfactorily trained, it is expected that any combinations of the test data or samples would like to follow the desired or target output. To validate this assumption, the neural network was tested by five (05) different combinations of COVID-19 symptoms provided from real-world patients and the predicted outputs of zone_network1, zone_network2, and zone_network3 were listed in Table 3-Table 5 respectively.

It can be seen from Table 3-Table 5 that the predicted output gets closer to the target output with the number of neurons. For instance, person-1 having COVID-19 symptoms resulted in a predicted output of -0.89 with 10 neurons, -0.92 with 12 neurons, and -0.96 with 14 neurons in zone_network1, zone_network2, and zone_network3, respectively.

This dependency on neurons is extensively studied in the Fig. 11 where it is obvious that the chances of getting authoritative desired output increases with the number of neurons at the cost of complexity.

Table 3 Predicted output with zone_network1

Symptoms	Person-1	Person-2	Person-3	Person-4	Person-5
TIA	0.25	0.45	0.6	0.15	0.9
CIP	0.34	0.35	0.6	0.14	0.9
BT	0.45	0.5	0.5	0.25	0.85
DC	0.23	0.45	0.55	0.23	0.75
TB	0.16	0.35	0.45	0.16	0.8
CP	0.1	0.1	0.45	0.15	0.75
Diarrhea	0.25	0.35	0.75	0.35	0.65
ST	0.2	0.45	0.5	0.4	0.8
Headache	0.1	0.45	0.35	0.4	0.8
Target output	-1	0	1	-1	1
Predicted output	-0.89	0.14	0.88	-0.86	0.93
Zone	Green	Yellow	Red	Green	Red

Table 4 Predicted output with zone_network2

Symptoms	Person-1	Person-2	Person-3	Person-4	Person-5
TIA	0.25	0.45	0.6	0.15	0.9
CIP	0.34	0.35	0.6	0.14	0.9
BT	0.45	0.5	0.5	0.25	0.85
DC	0.23	0.45	0.55	0.23	0.75
TB	0.16	0.35	0.45	0.16	0.8
CP	0.1	0.1	0.45	0.15	0.75
Diarrhea	0.25	0.35	0.75	0.35	0.65
ST	0.2	0.45	0.5	0.4	0.8
Headache	0.1	0.45	0.35	0.4	0.8
Target output	-1	0	1	-1	1
Predicted output	-0.92	0.08	0.91	-0.94	0.95
Zone	Green	Yellow	Red	Green	Red

Table 5 Predicted output with zone_network3

Symptoms	Person-1	Person-2	Person-3	Person-4	Person-5
TIA	0.25	0.45	0.6	0.15	0.9
CIP	0.34	0.35	0.6	0.14	0.9
BT	0.45	0.5	0.5	0.25	0.85
DC	0.23	0.45	0.55	0.23	0.75
TB	0.16	0.35	0.45	0.16	0.8
CP	0.1	0.1	0.45	0.15	0.75
Diarrhea	0.25	0.35	0.75	0.35	0.65
ST	0.2	0.45	0.5	0.4	0.8
Headache	0.1	0.45	0.35	0.4	0.8
Target output	-1	0	1	-1	1
Predicted output	-0.96	0.04	0.97	-0.98	0.98
Zone	Green	Yellow	Red	Green	Red

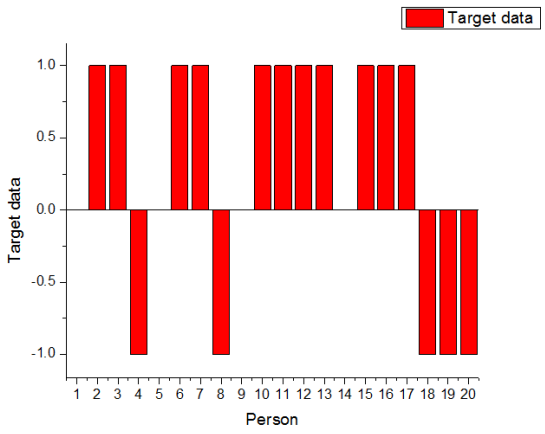

(a) Target data

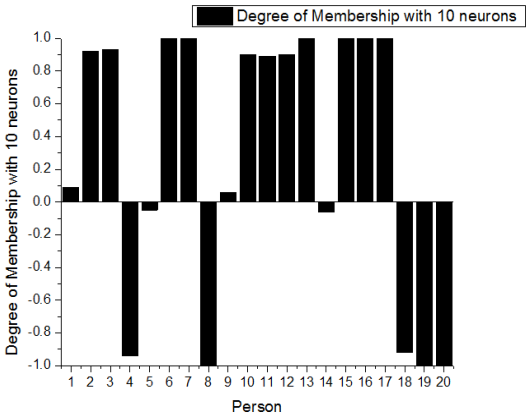

(b) 10 neurons

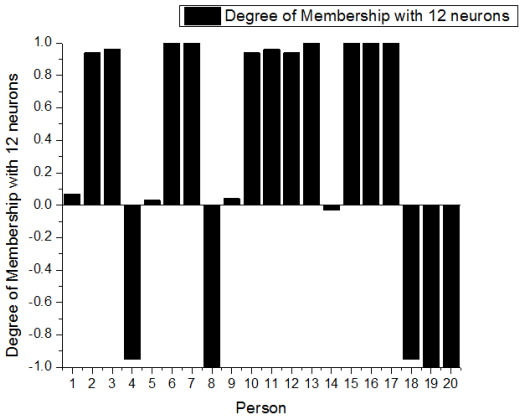

(c) 12 neurons

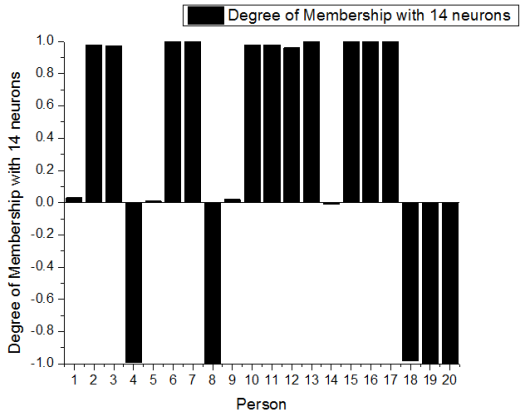

(d) 14 neurons

Fig. 11 Performance evaluation of actual and multilayer protocol output of COVID-19 symptoms

Thus, the fuzzy logic output was trained into the neural network in such a way that the threshold value of separating country into three zones: green, yellow, and red can be adapted according to miscellaneous symptoms situations of COVID-19.

4. Conclusion

For the last several months, the COVID-19 outbreak quickly surges worldwide. To control the COVID-19 infection cases government of many countries planned to imply zonal lockdown: red, yellow, and green in its territory based on the number of COVID-19 confirmed cases. Due to the lack of COVID-19 testing kit availability, social awareness, cost, or other reasons, the exact number of COVID-19 positive cases cannot be traced yet. Therefore, it would not be wise to divide such zones based on the infected number only. In this paper, we proposed an artificial neural network generated logical decisions based on COVID-19 symptoms by which a country or region can be divided into red, yellow, and green zone representing the highly infected areas, moderate-infected area, and controlled or low infected area, respectively. To train the neural network, the data sets were generated from the different combinations of COVID-19 symptoms. At first, an online survey of twenty (20) patients was conducted based on the nine (09) major symptoms of COVID-19. This survey information was implemented in the Mamdani inference system where these 09 symptoms were introduced as linguistic variables and their corresponding possible output recommendations were recorded. Then, different fuzzy rules were inserted in the Mamdani inference system and evaluated for possible recommendations. Based on these rules, three different outputs were generated representing highly infected area (red zone), moderately infected area (yellow zone), and controlled or low infected area (green zone), respectively. These outputs were considered as target data to be trained in neural networks. After the training, the neural network was tested by five (05) different combinations of COVID-19 symptoms provided from real-world patients. The accuracy of the predicted output gets closer to the target output with the number of neurons in the hidden layer.

References

[1] https://www.worldometers.info/coronavirus/?fbclid=IwAR2kywwEIfUIKzsE7bkKlKOHna_MR66fHZS0E_RAjrfhOtJchGxIxUgrf2o

[2] Dhiman, N. and Sharma, M.K., 2020. Fuzzy Logic Inference System for Identification and Prevention of Coronavirus (COVID-19). *International Journal of Innovative Technology and Exploring Engineering (IJITEE)*, 9(6), pp.1575-1580.

[3] https://www.who.int/docs/default-source/coronaviruse/situation-reports/20200423-sitrep-94-covid-19.pdf?sfvrsn=b8304bf0_2#:~:text=Retrospective%20investigations%20by%20 Chinese%20 authorities,%2C%20some%20did%20not, last accessed 2020/12/16.

[4] https://www.who.int/docs/default-source/coronaviruse/situation-reports/20200225-sitrep-36-covid-19.pdf?sfvrsn=2791b4e0_2#:~:text=Although%20for%20most%20people%20COVID,to%20be%20more%20vulnerable, last accessed 2020/12/16.

[5] Centers for Disease Control and Prevention | HealthData.gov, https://healthdata.gov/agencies/centers-disease-control-and-prevention, last accessed 2020/12/16.

[6] Tamang, S.K., Singh, P.D. and Datta, B., 2020. Forecasting of Covid-19 cases based on prediction using artificial neural network curve fitting technique. *Global Journal of Environmental Science and Management*, *6*(Special Issue (Covid-19)), pp.53-64.

[7] Coronavirus (COVID-19) Overview, https://www.webmd.com/lung/coronavirus, last accessed 2020/12/16.

[8] Larsen, J.R., Martin, M.R., Martin, J.D., Kuhn, P. and Hicks, J.B., 2020. Modeling the Onset of Symptoms of COVID-19. *Frontiers in public health*, *8*, p.473.

[9] Siddique, N. and Adeli, H., 2013. *Computational intelligence: synergies of fuzzy logic, neural networks and evolutionary computing*. John Wiley & Sons.

[10] Haykin, S., 2009. *Neural Networks and Learning Machines*, Prentice Hall, New York

[11] Hecht-Nielsen, R., 1992. Theory of the backpropagation neural network. In *Neural networks for perception* (pp. 65-93). Academic Press.

[12] Coronavirus Symptoms (COVID-19) - Worldometer, https://www.worldometers.info/coronavirus/coronavirus-symptoms/, last accessed 2020/12/18.

SciEn
Journal of Engineering Advancements Vol. 01(04) 2020, pp 195-198 https://doi.org/10.38032/jea.2020.04.011

Performance Evaluation of Tall Buildings using Optimized Tuned Mass Damper

*Mohammad Shamim Miah**

Department of Civil Engineering, International University of Business Agriculture and Technology, Dhaka 1230, Bangladesh

Received: November 21, 2020, Revised: December 19, 2020, Accepted: December 22, 2020, Available Online: December 30, 2020

ABSTRACT

This study investigates the performance of tall buildings using tuned mass damper (TMD) under dynamic loads such as harmonic loads, and the Loma Prieta Earthquake 1989 data. The numerical investigations are performed by considering a sixteen-storied dynamical system. To do this end, the aforementioned system is considered to be uncontrolled (meaning no damper is used) and a controlled case is assumed where a TMD is placed on the top floor. TMD performance mainly relies on the set of parameters (mass ratio, damping ratio, and stiffness). In reality, the tuning process of those parameters take serious effort and gets worse with the complicacy of the structure. Hence to obtain better performance of the TMD the damping ratio and the frequency of the TMD are optimized by using unconstrained derivative-free method. Finally, the uncontrolled and controlled performance of the sixteen-storied structure has been evaluated and compared. The results show that the dynamical response of the studied problem can be reduced significantly via the use of optimized parameters.

Keywords: Optimization; Vibration mitigation; TMD; Tall-buildings; Dynamic loads.

1. Introduction

The dynamic response of any buildings, bridges, towers, and power-plants are difficult to deal with due their complex phenomena. However, the safety of the aforementioned structures is not an option but must due to their importance in the society. Though there are many alternatives (passive, active, hybrid, etc.) available in existing literature [1]-[5] but still improvements are essential. The improvements of available alternatives are essential to fulfill the upcoming uncertain challenges and events such as gale thrust, and earthquake [5]. The tuned-mass damper (TMD) falls into the passive category. And TMD is one of the oldest vibration mitigation system and implemented to many existing structures [4]. For instance, the London Millennium Bridge, Tehran International Tower in Iran, Taipei 101 in Taiwan, Trump World Tower in USA, Tokyo Skytree, Burj Khalifa in UAE, and so on have adopted TMD to reduce unwanted vibration [6]. The performance of any TMD depends on the proper selection of its parameters. Many [7]-[12] have studied the role of TMD parameters such as mass ratio, stiffness, and damping have been reported their selection or tuning process. TMDs are widely used in various types of structures due to their simple structure and reasonable performance among other alternatives [11]. Typically, the performance of any TMD relies on the best selected parameters through tuning process. To tackle drawbacks of manual tuning process, [13]-[21] works have done the optimizing of TMDs properties using genetic algorithm. Initial works of modern TMD functionality was surfaced by Den Hartog [7]. Afterward, many [1],[11],[14] have developed different types of TMD.

Over the last few decays, many alternatives of TMD and its variations have been developed and implemented, such as active control systems, semi-active control systems, and hybrid control systems [1]-[6]. And early mentioned works have reported the superior performances of those controlling systems. However, there are underlying drawbacks of those controlling systems as most of the controlling technique (e.g., active) requires electric power, and that is quite difficult to ensure during an extreme event such as earthquake [2],[5]. And this is one of the most important issues about TMD that it does not require any electric power for its operation during an extreme event. Hence it can be operated even during an extreme event without putting much extra effort [4],[8],[11]. In general, the selection of TMD parameters take into a complicated situation when the structures are complex [15]. And when the structures are taller, the process gets harder to deal with; hence to overcome such issue optimization is preferable instead of manual tuning [19]. Therefore, an optimization will assist to overcome the drawbacks of sub-optimal tuning of parameters.

This study aims to evaluate the performance of TMD under earthquake and harmonic type dynamic loads. Additionally, the possibility of optimization of damping ratio and the frequency of the TMD has been investigated. In order to perform numerical analyses, the compact formulation of state-space is adopted. Additionally, the unconstrained derivative-free method was employed to perform the optimization. For numerical investigations, a sixteen-storied dynamical system is considered. Finally, the results of controlled and uncontrolled systems are compared.

2. Formulation and Description of the Problem

Usually, the dynamical systems are considered to be lumped-mass system and modeled as mass-spring-dashpot systems (see Fig. 1. And the dynamical systems are written into individual equation of motion by employing Newton's Second Law of classical mechanics. However, it is quite difficult to deal will several equations as each degree-of-freedom will provide an equation of motion. Hence in order to perform the investigations, those equations of motion need to bring into matrix-vector form. A dynamical system coupled with a TMD can be described as,

*Corresponding Author Email Address: mmshamim@iubat.edu Published by: SciEn Publishing Group

$$\underbrace{\begin{bmatrix} m_1 & 0 & 0 \\ 0 & \ddots & 0 \\ 0 & 0 & m_n \end{bmatrix}}_{M}\ddot{u}(t) + \underbrace{\begin{bmatrix} c_1+c_2 & -c_2 & 0 \\ -c_2 & \ddots & 0 \\ 0 & 0 & c_n \end{bmatrix}}_{C}\dot{u}(t) + \underbrace{\begin{bmatrix} k_1+k_2 & -k_2 & 0 \\ -k_2 & \ddots & 0 \\ 0 & 0 & k_n \end{bmatrix}}_{K}u(t) = -\Gamma\ddot{u}_g(t) + \Upsilon F(t) \quad (1)$$

where M represents the mass matrix $(n \times n)$, C is the damping matrix $(n \times n)$, K indicates the stiffness matrix $(n \times n)$, n is the number of degree-of-freedoms, $\ddot{u}$, $\dot{u}$, and u are the acceleration, velocity, and displacement vectors, respectively, and they have a size of $n \times 1$, t is the time vector, $\ddot{u}_g$ means the input disturbance, F is the TMD control force, Γ control the input excitation location, Υ locates the position of TMD. Note the second term on the right-hand side of the equation that will not be available if there is no control force applied to the system.

The free-body-diagrams of every degree of freedom (e.g., floor) are essential to derive the individual floor's equation of motion. Sample free-body-diagrams of the 1st, 5th, and top floor with TMD are depicted in Fig. 1 (b-d), respectively. And all of the equations are then complied into a compact form known as state-space formulation. The above-mentioned equation (Eq. (1)) can be further written into state-space form. The state-space formulation is accompanied with two main equations, (i) the system equation Eq. (2), and (ii) the observation equation Eq. (3). The system equation contains all the information related to consider dynamical system including input excitation and control force.

$$\dot{X}(t) = AX(t) + BU(t) \quad (2)$$

Where A is the system matrix, B indicates the input matrix, X is the state vector, and U contains the input excitation and control force information.

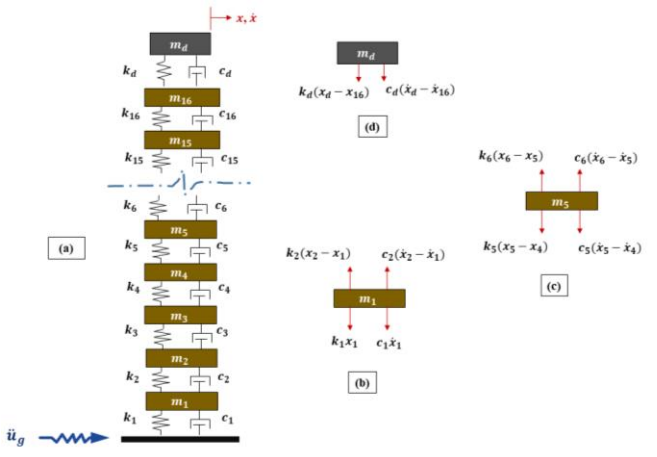

Fig. 1 The dynamical system: (a) the lumped-mass model, (b) free-body-diagram of 1st floor, (c) free-body-diagram of 5th floor, and (d) free-body-diagram of top floor.

While the observation equation describes about the information what ones want to measure or observe. Hence this equation needs to be modified as per the designer desire (based on what he/she wants to measure).

$$y(t) = CX(t) + DU(t) \quad (3)$$

where C is the output matrix, D indicates the feedthrough matrix, y is the output vector.

The parameters of the TMD has been tuned in a hybrid manner, more specifically, the mass ratio (μ) of the TMD is done through conventional procedure. The mass ratio of the TMD is defined as the ratio of the mass of the TMD to the targeted floor mass of the structure. While the frequency of the TMD has been defined as,

$$\omega_d = \delta \times \omega_n^{tar} \quad (4)$$

where ω_d is the frequency of the TMD, ω_n^{tar} is the targeted natural frequency of the structure, δ is the parameter needs to be tuned or determined to obtain an optimal frequency of the TMD. Further, the damping ratio of the TMD has been given by,

$$C_d = 2(\alpha\tau^{tmd})\omega_d \quad (5)$$

where α is a parameter links to the mass ratio of the TMD (but determined by the optimization algorithm), τ^{tmd} is the damping ratio of the TMD.

3. The Optimization Algorithm

A brief overview of the applied optimization algorithm is provided in this section. Assume the objective function of a problem is given by,

$$\min_x f(x) \to x \in \mathbb{R}^n$$

Then the iteration of the Nelder-Mead algorithm follows as shown below,

(i) Order: Order the $n+1$ vertices to satisfying the following rules

$$f(x_1) \le f(x_2) \le \ , \dots, \le f(x_{n+1})$$

(ii) Reflect: determine the reflection point x_r

$$f_r = f(x_r) = \bar{x} + \rho(\bar{x} - x_{n+1}) = (1+\rho)\bar{x} - \rho(x_{n+1}); \quad \bar{x} = \sum_{i=1}^{n} \frac{x_i}{n}$$

(iii) Expand: If $f_r < f_1$ determine the expansion point x_e

$$f_e = f(x_e) = \bar{x} + \chi\rho(\bar{x} - x_{n+1}) = (1+\rho\chi)\bar{x} - \rho\chi(x_{n+1})$$

If $f_e < f_r$ accept the expansion point x_e

(iv) Contract: if $f_r \ge f_n$ then perform a contraction between $\bar{x}$ and the better $x_{n+1}$and x_r

Outside: if $f_n \le f_r < f_{n+1}$ then calculate x_c, perform an outside contraction

$$f_c = f(x_c) = \bar{x} + \gamma(x_r - \bar{x}) = \bar{x} + \rho\gamma(\bar{x} - x_{n+1}) = (1+\rho\gamma)\bar{x} - \rho\gamma x_{n+1}$$

If $f_c \le f_r$ accept the contraction point x_c, and terminate the iteration; otherwise, go to perform a shrink.

Inside: if $f_r \ge f_{n+1}$ then calculate x_{cc}, perform an inside contraction

$$f_{cc} = f(x_{cc}) = \bar{x} - \gamma(\bar{x} - x_{n+1}) = (1-\gamma)\bar{x} + \gamma x_{n+1}$$

If $f_{cc} < f_{n+1}$ accept the contraction point x_{cc}, and terminate the iteration; otherwise, go to perform a shrink.

Perform a shrink step: Evaluate f_n at the n points

$v_i = x_1 + \sigma(x_i - x_1), i = 2, \dots, n+1$

Interested reader may obtain detail information about basic formulation of the employed optimization algorithm through [21].

4. Results and Discussion

The numerical investigations are performed by employing MATLAB and SIMULINK. It is mentioned that a sixteen-storied structure is considered for this study. And the response of the structure is evaluated subjected to harmonic type load and the Loma Prieta Earthquake 1989 data. The input excitations (a) Loma Prieta Earthquake 1989, and (b) harmonic loads are presented in Fig. 2. It is important to note that the input excitations are going to influence the output of the structure. That is the reason of choosing different excitations force to excite the selected system. The whole simulations are performed for both uncontrolled and controlled structure for earthquake and harmonic loads.

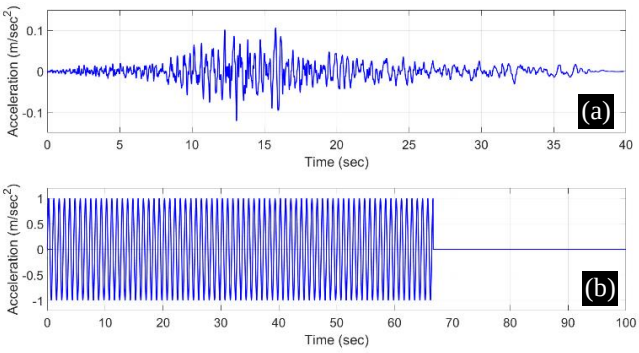

Fig. 2 The input excitations: (a) Loma Prieta Earthquake, and (b) harmonic loads.

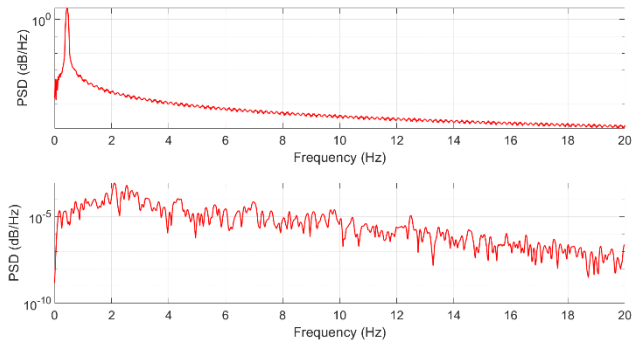

Fig. 3 The power spectral density of the input excitations.

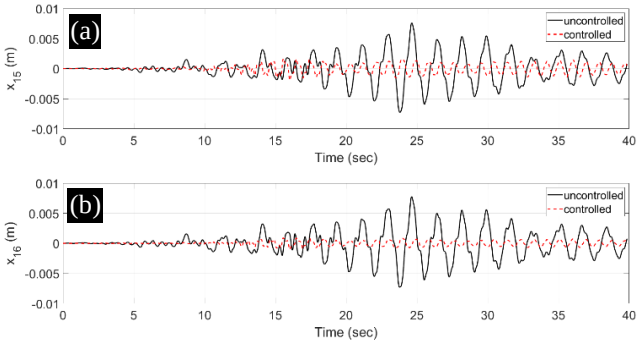

Fig. 4 Comparison of uncontrolled and controlled response of 15th and 16th floors under Loma Prieta earthquake.

The duration of the excitations 40 sec for earthquake and 100 sec for the harmonic load, also can be found in Fig. 2. In order to understand about the governing frequency (see the peaks) of the excitations, the power spectral density (PSD) of both input excitations are depicted in Fig. 3. The structure is assumed to have a mass in every floor of 50×10^3 kg and stiffness is assumed to have 70000×10^3 N/m, and the damping coefficients are assumed to 1.3334×10^3 N-s/m. It is mentioned earlier optimization was performed by adopting unconstrained derivative-free method.

Hence the simulations are performed using those optimized values of τ^{tmd} & δ instead of manual tuning. And the parameter α is assumed to be $0.04 \times m^{tar}$, where m^{tar} is considered to be modal mass of the targeted mode. However, that does not affect the uncontrolled structural response except the changes of input excitations e.g., earthquake, harmonic. To evaluate the performance of the optimized values of the TMD, the top two floors (x_{15} and x_{16}) displacements are compared for controlled and uncontrolled scenarios. Fig. 4 shows the comparison of the controlled (dotted red-line) and uncontrolled (black-line) displacements for the Loma Prieta 1989 earthquake data. It is visible that the response of the structure has been mitigated effectively.

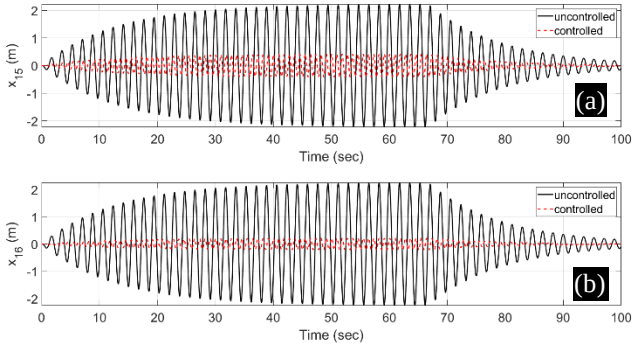

Fig. 5 Comparison of uncontrolled and controlled response of 15th and 16th floors subjected to harmonic load.

Afterward, the structure was hit by the harmonic load and the response of the uncontrolled and controlled structures are compared in Fig. 5. The dotted red line indicates the controlled response and the black line represents uncontrolled case. From the figure it can be stated that the vibration was reduced significantly.

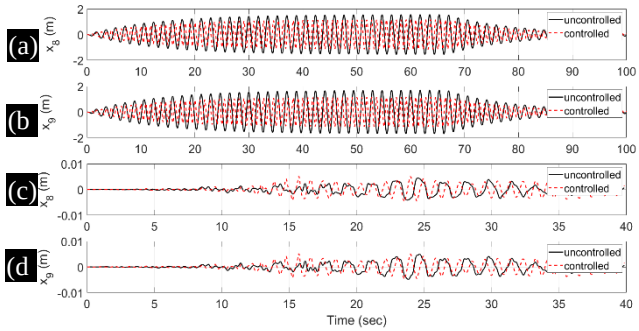

Fig. 6 The response of 8th and 9th floors subjected to harmonic load (a-b) and earthquake loads (c-d).

Furthermore, the maximum displacements of every floor have been evaluated and depicted in Fig. 5. The left figure (see Fig. 5 (a)) shows the output of the structures due to earthquake and the right figure (see Fig. 5 (b)) exhibits the response under harmonic load. The response of 8th and 9th floors are presented in Fig. 6 and it is visible that those floors are suffering with abrupt deformation. This phenomenon is also noticeable in Fig. 7.

It can be found that the maximum displacements of every floor have reduced for both earthquake and harmonic loads. It also visible in Fig. 7 (a) that the structure will reach in a position where it will face nonlinear/large deformation as a result structure may fail party/fully. Hence such situation will demand more safety to survive from extreme loads. However, the early mentioned situation also may occur even when harmonic type load hits the structure totally an unexpected way as shown in Fig. 7 (b).

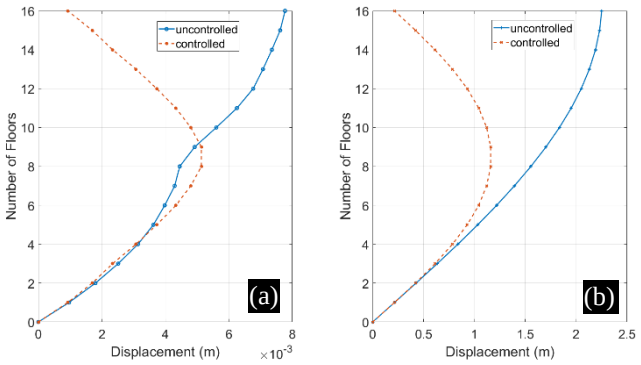

Fig. 7 The uncontrolled and controlled response of all of the floors subjected: (a) Loma Prieta earthquake, and (b) harmonic load.

5. Conclusion

The performance of a sixteen-storied dynamical system with and without TMD are investigated. Further, the frequency and the damping ratio of the TMD has been optimized to obtain better performance. An unconstrained derivative-free optimization method is used to perform the optimization. The outcome of the study shows that the optimization may be suitable for tall-buildings as complexities are not limited to the structure but also from input excitation and model descriptions. Hence to deal with such uncertain situation optimization of any tuning parameter such as mass ratio, damping ratio and stiffness of the TMD will perform better in comparison to sub-optimal/manual tuning. The future direction of this study will focus into the system identification to deal with more complex problems.

References

[1] Elias, S. and Matsagar, V., 2017. Research developments in vibration control of structures using passive tuned mass dampers. *Annual Reviews in Control*, 44, pp.129-156.

[2] Dyke, S.J., Spencer Jr, B.F., Belknap, A.E., Ferrell, K.J., Quast, P. and Sain, M.K., 1994, August. Absolute acceleration feedback control strategies for the active mass driver. *In Proc. First World Conference on Structural Control* (pp. 51-60).

[3] Chu, S.Y., Soong, T.T. and Reinhorn, A.M., 2005. Active, hybrid, and semi-active structural control: A design and implementation handbook. New York: *Wiley*.

[4] Miah, M.S., 2011. Dynamic Behavior of Bridge with New Innovative Type Spherical Elastomeric Bearing. *Kunsan National University*, Kunsan, South Korea, pp.1-122.

[5] Miah, M.S., Chatzi, E.N., Dertimanis, V.K. and Weber, F., 2017. Real-time experimental validation of a novel semi-active control scheme for vibration mitigation. *Structural Control and Health Monitoring*, 24(3), p.e1878.

[6] Wikipedia. Tuned mass damper, Available: https://en.wikipedia.org/wiki/Tuned_mass_damper (Accessed on 29 September 2020).

[7] Hartog, J. P. D. (1947). Mechnical vibrations, 3rd ed., *McGraw-Hil*, New York.

[8] Warburton, G.B., 1981. Optimum absorber parameters for minimizing vibration response. *Earthquake engineering & structural dynamics*, 9(3), pp.251-262.

[9] Tsai, H.C. and Lin, G.C., 1993. Optimum tuned-mass dampers for minimizing steady-state response of support-excited and damped systems. *Earthquake engineering & structural dynamics*, 22(11), pp.957-973.

[10] Sadek, F., Mohraz, B., Taylor, A.W. and Chung, R.M., 1997. A method of estimating the parameters of tuned mass dampers for seismic applications. *Earthquake Engineering & Structural Dynamics*, 26(6), pp.617-635.

[11] Miah, M.S., Miah, M. and Hossain, M., 2019. Development and Performance Evaluation of a Novel Translational Tuned Mass Damper. *In International Journal of Engineering Research in Africa* (Vol. 45, pp. 53-73). Trans Tech Publications Ltd.

[12] Murudi, M.M. and Mane, S.M., 2004, August. Seismic effectiveness of tuned mass damper (TMD) for different ground motion parameters. *In 13th World Conference on Earthquake Engineering*.

[13] Bekdaş, G. and Nigdeli, S.M., 2013. Mass ratio factor for optimum tuned mass damper strategies. *International Journal of Mechanical Sciences*, 71, pp.68-84.

[14] Qin, L., Yan, W.M., & Guo, S.B. (2011). Numerical Study of a New Variable Friction TMD. *Advanced Materials Research*, 243-249, 5450-5457.

[15] Farghaly, A.A. and Salem Ahmed, M., 2012. Optimum design of TMD system for tall buildings. *ISRN Civil Engineering*, 2012.

[16] Kang, Y.J. and Peng, L.Y., 2019. Optimisation Design and Damping Effect Analysis of Large Mass Ratio Tuned Mass Dampers. *Shock and Vibration*, 2019.

[17] Etedali, S. and Rakhshani, H., 2018. Optimum design of tuned mass dampers using multi-objective cuckoo search for buildings under seismic excitations. *Alexandria engineering journal*, 57(4), pp.3205-3218.

[18] Mohebbi, M. and Joghataie, A., 2012. Designing optimal tuned mass dampers for nonlinear frames by distributed genetic algorithms. *The Structural Design of Tall and Special Buildings*, 21(1), pp.57-76.

[19] Hervé Poh'sié, G., Chisari, C., Rinaldin, G., Fragiacomo, M., Amadio, C. and Ceccotti, A., 2016. Application of a translational tuned mass damper designed by means of genetic algorithms on a multistory cross-laminated timber building. *Journal of Structural Engineering*, 142(4), p.E4015008.

[20] Connor, J.J., 2003. Structural Motion Control (p. 220). *Pearson Education, Inc.*, New Jersey, USA.

[21] Banerjee, S. and Ghosh, A.D., 2020, September. Optimal Design of Tuned Mass Damper for Base-Excited Structures. *In IOP Conference Series: Materials Science and Engineering* (Vol. 936, No. 1, p. 012016). IOP Publishing.

[22] Lagarias, J.C., Reeds, J.A., Wright, M.H. and Wright, P.E., 1998. Convergence properties of the Nelder--Mead simplex method in low dimensions. *SIAM Journal on optimization*, 9(1), pp.112-147.

This page is left intentionally blank

Journal of Engineering Advancements (JEA)

DOI: https://doi.org/10.38032/jea

Indexed by:

Google Scholar Crossref

Scilit

Volume 01 Issue 04

DOI: https://doi.org/10.38032/jea.2020.04

Published by: SciEn Publishing Group

Website: www.scienpg.com